
THE UNIVERSITY
*of* EDINBURGH

# Toll-like receptor 2 orchestrates a novel tumour suppressor response in non-small cell lung cancer

Fraser Russell Millar


THE UNIVERSITY *of* EDINBURGH

Thesis submitted for the degree of Doctor of Philosophy (PhD)

The University of Edinburgh

2021

# Declaration

I declare that the work presented in this thesis is my own or that where research was carried out in collaboration with others, I have clearly acknowledged their contribution to the relevant experiments. This thesis has not been previously submitted for any degree or professional qualification.

Fraser Russell Millar, 2021

# Acknowledgements

Firstly, thank you to Juan Carlos for his supervision and friendship over the course of my PhD. You have helped turn a bumbling clinician into a half decent scientist and for that I am forever grateful. Thank you to Simon who has also been a great source of expertise and friendship throughout my fellowship, and to Margaret Frame for her help in selecting my project and her guidance and support throughout my time at the Institute of Genetics and Cancer. Thank you to the ECAT directors who first offered me my clinical research fellowship and have supported me to continue my clinical research career in Edinburgh. Thanks also to the many friends I have made at the Institute of Genetics and Cancer who each in their own way have helped contribute to this work, be that help with experiments or a sympathetic ear. Lastly, I would like to thank my family. To my son Keir, whose arrival during my PhD has helped give me perspective and purpose. To my parents whose unwavering support has been invaluable. And most importantly to my wife Jenna, who has been by my side supporting me throughout my whole career and without whom I would not have been able to complete this thesis.

# Abstract

Lung cancer is the most lethal cancer type worldwide, with a mortality rate greater than breast, colorectal and prostate cancer combined. Targeting early-stage disease is widely recognised to improve overall survival, however the mechanisms and components of the early tumour suppressor response in lung cancer are not fully elucidated. In this thesis I present data from human samples as well as genetically engineered mouse models (GEMMs) demonstrating that the previously identified senescence regulator TLR2 orchestrates a potent anti-tumour response in non-small cell lung cancer. Mechanistically, TLR2 regulates both cell intrinsic senescence-associated cell cycle arrest pathways and the proinflammatory senescence-associated secretory phenotype (SASP) that is integral in the immune surveillance of premalignant cells. TLR2 and the SASP are highly expressed in human lung cancer epithelium and correlate with clinical regression and improved survival. Importantly, pharmacological modulation of this pathway with a Tlr2 agonist significantly reduces lung tumour growth, highlighting a potential therapeutic target in early lung cancer.

# Lay Summary

Lung cancer kills more people than any other cancer. Early lung cancer is curable, however it is asymptomatic so patients rarely present with early-stage disease. Patients tend to present once symptoms have developed and invariably this is with advanced stage disease which is no longer curable. Therefore, understanding the biology of early lung cancer may allow us to develop new treatments and new ways of detecting lung cancer earlier. Cancer is driven by genetic mutations that cause cells to grow uncontrollably. When these mutations first happen, in order to try and stop cancer forming cells respond by stopping cell growth altogether and enter into a state called senescence. Senescent cells also release several chemicals and proteins that act as danger signals which also help defend against cancer formation. Senescent cells are present in early lung cancers in mice, however, are no longer present in late-stage cancers, suggesting that senescence acts as a barrier to cancer progression. Our group identified a protein called TLR2 that helps control senescence and the secretion of danger signals after cancer mutations occur in cells in culture. In this thesis I present data that shows that TLR2 also regulates senescence after cancer mutations occur in mice, and that this process prevents lung tumour growth. Most importantly, we also show that TLR2 is very important in human lung cancer where it correlates with improved survival. We have shown that by using a drug to activate TLR2 we can impair lung tumour growth in mice. We have therefore identified a possible new treatment for early lung cancer.

# Table of Contents

# List of figures

# List of tables

# List of abbreviations

| | |
|---|---|
| 3MR | Trimodality reporter |
| 7AAD | 7-amino-actinomycin D |
| AA | Arachidonic acid |
| AAH | Atypical adenomatous hyperplasia |
| AdenoCre | Ad5-CMV-Cre |
| AIM2 | Absent in melanoma 2 |
| AIS | Adenocarcinoma-in-situ |
| ALK | Anaplastic lymphoma kinase |
| AP-1 | Activator protein-1 |
| APR | Acute phase response |
| ARF | Alternate reading frame |
| A-SAA | Acute phase serum amyloid A protein |
| ASC | Apoptosis-associated speck like protein containing a CARD |
| AT2 | Alveolar type-2 |
| ATCC | American type culture collection |
| ATR | Ataxia telangectasia and Rad3 related protein |
| ATTAC | Apoptosis through targeted activation of Caspase 8 |
| BAC | Bioinformatic analysis core |
| BCL-2 | B-cell lymphoma 2 |
| Bp | Base pair |
| BSA | Bovine serum albumin |

| | |
|---|---|
| BTPNA | Bronchoscopic transparenchymal nodule access |
| CAD | Caspase-activated DNase |
| CARD | Caspase activation and recruitment domain |
| CAV1 | Caveolin-1 |
| CC10 | Clara cell 10-kDa |
| CCF | Cytoplasmic chromatin fragment |
| CCL2 | C-C motif chemokine ligand 2 |
| CD11b | Cluster of differentiation 11b |
| CD11c | Cluster of differentiation 11c |
| CD19 | Cluster of differentiation 19 |
| CD3 | Cluster of differentiation 3 |
| CD335 | Cluster of differentiation 335 |
| CD4 | Cluster of differentiation 4 |
| CD45 | Cluster of differentiation 45 |
| CD68 | Cluster of differentiation 68 |
| CD8 | Cluster of differentiation 8 |
| CDK | Cyclin-dependent kinase |
| CDK2 | Cyclin-dependent kinase 2 |
| CDK4 | Cyclin-dependent kinase 4 |
| CDK6 | Cyclin-dependent kinase 6 |
| cDNA | Complementary deoxyribonucleic acid |
| CEBPβ | CCAAT/enhancer-binding protein beta |
| cGAS | Cyclic GMP-AMP synthase |
| CHK1 | Checkpoint kinase 1 |

| | |
|---|---|
| CHK2 | Checkpoint kinase 2 |
| CI | Confidence interval |
| CK5 | Cytokeratin 5 |
| CK6 | Cytokeratin 6 |
| CLR | C-type lectin receptor |
| CMV | Cytomegalovirus |
| COPD | Chronic obstructive pulmonary disease |
| CRISPR | Clustered regularly interspaced short palindromic repeats |
| CT | Computed tomography |
| Ct | Cycle threshold |
| CT-PET | Computed tomography positron emission tomography |
| CTGF | Connective tissue growth factor |
| CXCL1 | C-X-C motif chemokine ligand 1 |
| CXCL12 | C-X-C motif chemokine ligand 12 |
| CXCR2 | C-X-C Motif chemokine receptor 2 |
| DAB | 3,3'-Diaminobenzidine |
| DAMP | Damage-associated molecular pattern |
| DAPI | 4',6-diamidino-2-phenylindole |
| Dcr2 | Decoy receptor 2 |
| DDR | DNA damage response |
| DEN | Diethylnitrosamine |
| DM2 | Diabetes mellitus type 2 |
| DMEM | Dulbecco's modified eagle's medium |
| DMSO | Dimethyl sulfoxide |

| | |
|---|---|
| DNA | Deoxyribonucleic acid |
| DNA-PK | DNA-dependent protein kinase |
| dNTP | Deoxyribonucleotide triphosphate |
| DPX | Distyrene, plasticizer and xylene |
| DSB | Double stranded breaks |
| dsDNA | Double stranded DNA |
| ECDF | Edinburgh Compute and Data facility |
| ECL | Enhanced chemiluminescence |
| ECM | Extracellular matrix |
| EDTA | Ethylenediaminetetraacetic acid |
| EGA | European genome-phenome archive |
| EGTA | Ethyl glycol-bis(b-aminoethyl ether)-N,N,N',N'-tetraacetic acid |
| EGF | Epidermal growth factor |
| EGFR | Epidermal growth factor receptor |
| EMT | Epithelial-to-mesenchymal transition |
| ER | Oestrogen receptor |
| EV | Empty vector |
| EV | Extracellular vesicles |
| FACS | Fluorescence activated cell sorting |
| FFPE | Formalin fixed, paraffin embedded |
| FGF | Fibroblast growth factor |
| FKBP | FK506-binding protein |
| FOXP3 | Forkhead box P3 |
| GAP | GTPase activating protein |

| | |
|---|---|
| GBM | Glioblastoma multiforme |
| G-CSF | Granulocyte colony stimulating factor |
| GDP | Guanosine diphosphate |
| GEF | Guanine nucleoside exchange factor |
| GEMM | Genetically engineered mouse model |
| GFP | Green fluorescent protein |
| GM-CSF | Granulocyte-monocyte colony stimulating factor |
| gRNA | Guide ribonucleic acid |
| GRO-α | Growth regulated oncogene α |
| GRO-β | Growth regulated oncogene β |
| GRO-γ | Growth regulated oncogene γ |
| GTP | Guanosine triphosphate |
| GWAS | Genome wide association study |
| H3K4me3 | Methylated histone 3 Lys 4 |
| H3K9ac | Acetylated histone 3 Lys 9 |
| H3K9me3 | Methylated histone 3 Lys 9 |
| HCC | Hepatocellular carcinoma |
| HER2 | Human epidermal growth factor receptor 2 |
| HGF | Hepatocyte growth factor |
| HLA | Human leukocyte antigen |
| HMGB1 | High-mobility-group box 1 |
| HRP | Horseradish peroxidase |
| HSV-TK | Herpes simplex virus 1 thymidine kinase |
| HTPU | Host and Tumour Profiling Unit |

| | |
|---|---|
| HTVI | Hydrodynamic tail vein injection |
| HUVEC | Human umbilical vein endothelial cell |
| ICAM | Intracellular adhesion molecule |
| IFN | Interferon |
| IHC | Immunohistochemistry |
| IKK | IκB kinase kinase |
| IL-1 | Interleukin 1 |
| IL-1R | Interleukin-1 receptor |
| IL-6 | Interleukin 6 |
| IL-7 | Interleukin 7 |
| IL-8 | Interleukin 8 |
| IL-17A | Interleukin 17A |
| IL-13 | Interleukin 13 |
| IL-15 | Interleukin 15 |
| IL1α | Interleukin-1 alpha |
| IL1β | Interleukin-1 beta |
| IPF | Idiopathic pulmonary fibrosis |
| IPN | Indeterminate pulmonary nodule |
| IRAK | IL-1 receptor-associated kinase |
| IRES | Internal ribosome entry site |
| IVIS | *In vivo* imaging system |
| Kb | Kilobase |
| KB | Kilobase |
| KO | Knockout |

| | |
|---|---|
| LB | Lysogeny broth |
| LDCT | Low dose computed tomography |
| LOH | Loss of heterozygosity |
| LPS | Lipopolysaccharide |
| LRR | Leucine rich repeat |
| LUAD | Lung adenocarcinoma |
| LUSC | Lung squamous carcinoma |
| Ly6C | Lymphocyte antigen 6C |
| Ly6G | Lymphocyte antigen 6G |
| MAPK | Mitogen-activated protein kinase |
| MCP | Monocyte chemoattractant protein |
| MDM2 | Mouse double minute 2 homolog |
| MEF | Mouse embryonic fibroblast |
| MEM | Minimum essential media |
| MES | 2-ethanesulfonic acid |
| MIA | Minimally invasive adenocarcinoma |
| MIP | Macrophage inflammatory protein |
| MIF | Macrophage migration inhibitory factor |
| MLL1 | Myeloid/lymphoid or mixed-lineage leukaemia 1 |
| MMP | Matrix metalloprotease |
| MOI | Multiplicity of infection |
| MPO | Myeloperoxidase |
| mTOR | Mechanistic target of rapamycin |
| MWA | Microwave ablation |

| | |
|---|---|
| NBF | Neutral buffered formalin |
| NEB | New England BioLabs |
| NF-κ | Nuclear factor kappa B |
| NK | Natural killer |
| NLR | Nucleoside-binding oligomerization domain-like receptor |
| NLRP3 | NLR family pyrin domain containing 3 |
| NOX4 | NADPH oxidase 4 |
| NOXA | Phorbol-12-myristate-13-acetate-induced protein 1 |
| ns | Non-significant |
| NSCLC | Non-small cell lung cancer |
| OIS | Oncogene-induced senescence |
| PAMP | Pathogen-associated molecular pattern |
| PAX2 | Paired box gene 2 |
| PET | Positron emission tomography |
| PBS | Phosphate buffered saline |
| PCA | Principal component analysis |
| PCR | Polymerase chain reaction |
| PD-L1 | Programmed death ligand-1 |
| PEI | Polyethylenimine |
| PFU | Plaque forming units |
| PGE2 | Prostaglandin E2 |
| PIN | Prostate intraepithelial neoplasia |
| PRR | Pattern recognition receptor |
| PUMA | p53-upregulated modulator of apoptosis |

| | |
|---|---|
| qPCR | Quantitative real time polymerase chain reaction |
| Rb | Retinoblastoma |
| REF | Rat embryonic fibroblast |
| RFA | Radiofrequency ablation |
| RFP | Red fluorescent protein |
| RGB | Red green blue |
| RhoA | Ras homolog family member A |
| rIL-1$\alpha$ | Recombinant interleukin 1 alpha |
| rIL-1$\beta$ | Recombinant interleukin 1 beta |
| RLR | Retinoic acid-inducible gene-1-like receptor |
| RNA | Ribonucleic acid |
| ROCK | Rho-associated protein kinase |
| ROI | Region of interest |
| ROR-$\gamma$T | RAR-related orphan receptor gamma |
| ROS | Reactive oxygen species |
| RPMI | Roswell Park Memorial Institute medium |
| RT | Reverse transcriptase |
| RTK | Receptor tyrosine kinase |
| RT-qPCR | Reverse transcription quantitative real-time polymerase chain reaction |
| SA-$\beta$-gal | Senescence-associated beta-galactosidase |
| SAA | Serum amyloid A |
| SABR | Stereotactic ablative radiotherapy |
| SAHF | Senescence-associated heterochromatin foci |

| | |
|---|---|
| SAMP | Senescence-accelerated mouse-prone |
| SASP | Senescence-associated secretory phenotype |
| SB13 | Sleeping beauty 13 |
| SBB | Sudan Black B |
| SCLC | Small cell lung cancer |
| SDS | Sodium dodecyl sulphate |
| SDS-PAGE | sodium dodecyl sulphate-polyacrylamide gel electrophoresis |
| shRNA | Short hairpin ribonucleic acid |
| Siglec F | Sialic acid-binding immunoglobulin-like lectin F |
| SOC | Super optimal broth |
| SPC | Surfactant protein C |
| STING | Stimulator of interferon genes |
| sTNFR | Soluble tumour necrosis factor |
| TAB | TAK1-binding protein |
| TAE | Tris-acetate-EDTA |
| TAK | TGF-β-activated kinase |
| TAM | Tumour associated macrophage |
| TBS | Tris-buffered saline |
| TCR | T-cell receptor |
| TERT | Telomerase reverse transcriptase |
| TGF-β | Transforming growth factor beta |
| TIMP-1 | Tissue inhibitor of metalloproteinase 1 |
| TIR | Toll-IL-1R homology |
| TKI | Tyrosine kinase inhibitor |

| | |
|---|---|
| TLR | Toll-like receptor |
| TLR2 | Toll-like receptor 2 |
| TLR3 | Toll-like receptor 3 |
| TLR4 | Toll-like receptor 4 |
| TNFα | Tumour necrosis factor alpha |
| TP53 | Tumour protein 53 |
| TRAF | TNF-α associated factor |
| TRAIL | Tumour necrosis factor-related apoptosis- inducing ligand |
| TRE | Tetracycline regulatory elements |
| Trp53 | Transformation-related protein 53 |
| TTF-1 | Thyroid transcription factor 1 |
| TU | Transduction units |
| UCL | University College London |
| UV | Ultraviolet |
| VEGF | Vascular endothelial growth factor |
| VSMC | Vascular smooth muscle cell |
| VSVG | Vesicular stomatitis virus G |
| WNT | Wingless/Integrated |
| WT | Wild type |

# 1: Introduction

## 1.1 Cellular senescence

### 1.1.1 Discovery of senescence

The observation that diploid human fibroblasts have a finite *in vitro* proliferative capacity was first made by Leonard Hayflick and Paul Moorhead more than 50 years ago (Hayflick and Moorhead, 1961). These non-dividing cells remained viable but were unable to proliferate despite the presence of nutrients and growth factors and ample space for clonal expansion. This phenomenon was named ‘cellular senescence’ and in this context has been shown to be mediated via attrition of telomeres after repeated cell divisions (Harley et al., 1990). This was in stark contrast to cancer cells that exhibited an indefinite capacity to proliferate. Soon after this discovery it was hypothesised that cellular senescence occurred *in vivo* and was what drove organismal aging. Furthermore, it was thought that senescence evolved to protect organisms from cancer. Many of these suggestions have since been proven correct (Baker et al., 2016; Campisi, 1997a, 2005; Dimri et al., 1995; Erusalimsky and Kurz, 2005; Herbig et al., 2006) and senescence has also since been shown to have wider physiological functions in embryogenesis and wound healing (Demaria et al., 2014; Munoz-Espin et al., 2013; Storer et al., 2013). Therefore, the understanding of senescence as an *in vitro* phenomenon limiting proliferation of diploid cells has since expanded to

include a wide variety of senescence phenotypes in both physiological and pathological contexts.

### 1.1.2 Induction of senescence

Cellular senescence is a terminal stress response induced by several stimuli and functions to remove damaged/stressed cells from the proliferating pool. Severe DNA damage anywhere in the genome (especially double stranded breaks – DSBs) can induce cellular senescence via the DNA damage response (DDR – discussed in detail in chapter 1.1.4) and subsequent activation of p53 (Di Leonardo et al., 1994; Herbig et al., 2004) and p16 (Beausejour et al., 2003; Jacobs and de Lange, 2004; Stein et al., 1999) tumour suppressor pathways (see chapter 1.1.4). This DNA damage can be mediated by ionizing radiation or chemotherapeutic drugs (so called 'therapy induced senescence') (Roninson, 2003; Schmitt et al., 2002) and telomere attrition following repeated cell divisions (so called 'replicative senescence') (Campisi, 1997b; Harley et al., 1990). Telomeres are repetitive stretches of DNA and associated proteins that cap the end of chromosomes and they function to protect chromosomes from fusion or degradation by DNA-repair processes (d'Adda di Fagagna et al., 2004). Standard DNA polymerases cannot fully replicate DNA ends, therefore cells lose 50-200 base pairs of telomeric DNA during each replication cycle (Harley et al., 1990), a phenomenon termed the 'end-replication problem' (Olovnikov, 1971). Human telomeres are around 10-15 kb in length, allowing several divisions before the end-replication problem occurs and dysfunctional

telomeres trigger senescence (Hemann et al., 2001; Martens et al., 2000). Dysfunctional telomeres activate the canonical DDR (d'Adda di Fagagna et al., 2003; Gire et al., 2004; Herbig et al., 2004; Takai et al., 2003) which enables cells to sense damaged DNA, undergo a growth arrest and activate DNA repair processes. Senescent cells characteristically have a persistent DDR response, leading to a stable growth arrest (Fumagalli et al., 2012; Rodier et al., 2011). The enzyme telomerase can circumvent the end-replication problem by catalysing the addition of telomeric DNA repeats to chromosome ends via the catalytic protein component telomerase reverse transcriptase (TERT) (Collins and Mitchell, 2002). Most normal cells do not express TERT and hence have a finite proliferative capacity (Masutomi et al., 2003). However, cancer cells and germ-line cells express TERT, rendering these cells immune from replicative senescence. Of note however, TERT expressing cells can still undergo senescence caused by non-telomeric DNA damage (Chen et al., 2001). Telomere attrition and replicative senescence is thought to explain the enhanced senescence response seen with aging, however pro-inflammatory cytokines (predominantly TNF-$\alpha$) produced by T-cells with dysfunctional mitochondrial metabolism (which recapitulates aging T-cells) can also induce systemic senescence in the absence of DNA damage (Desdin-Mico et al., 2020).

Oncogene activation also induces activation of the senescence response in normal diploid cells (so called ‘oncogene-induced senescence’ – see chapter 1.2.1) (Serrano et al., 1997). Enhanced mitogenic signalling caused by oncogene activation (or tumour suppressor loss) induces

senescence via the DDR owing to DNA damage caused by aberrant DNA replication (Bartkova et al., 2006; Di Micco et al., 2006) and increased mitochondrial production of reactive oxygen species (ROS) (Lee et al., 1999). Oncogene activation can also activate the INK4/ARF tumour suppressor locus via derepression of the polycomb group of transcriptional repressors (Barradas et al., 2009), thus inducing senescence. Furthermore, mitogenic signalling may directly induce senescence (Woo and Poon, 2004). Therefore oncogene-induced senescence a key tumour suppressor mechanism (Braig et al., 2005; Collado et al., 2005; Michaloglou et al., 2005).

Senescence can also be induced in response to repeated stimuli with anti-proliferative cytokines and ROS. Chronic interferon-β signalling can induce senescence via DNA damage caused by increased intracellular ROS (Moiseeva et al., 2006). The relevance of ROS as inducers of senescence is further highlighted by the fact that antioxidants delay or prevent senescence (Chen et al., 1995; Lee et al., 1999; Macip et al., 2002). Cells can also undergo stress induced senescence independently of DNA damage and the DDR. For example, chronic stimulation with transforming growth factor-β (TGF-β) can induce senescence by promoting p16-Rb signalling (Vijayachandra et al., 2003; Zhang and Cohen, 2004) and inadequate *in vitro* growth conditions (so called 'cell-culture stress') can also induce p16-dependent senescence with intact telomeres (Ramirez et al., 2001). Cellular senescence can also be induced in a paracrine manner, whereby secreted SASP factors from oncogene activated cells (including TGF-β family ligands, CCL2, CCL20 and VEGF) induce senescence in neighbouring normal cells

(Acosta et al., 2013). The so called ‘paracrine senescence’ response resembles full senescence, with evidence of DNA and oxidative damage, and activation of both p53-p21 and p16-Rb pathways (Acosta et al., 2013). Senescence can also be induced in the physiological setting (‘Physiological senescence’) whereby it plays a key role in embryogenesis and wound healing (Demaria et al., 2014; Munoz-Espin et al., 2013; Storer et al., 2013)(see chapter 1.1.6).

### 1.1.3 Features of senescence

While senescence can be induced by a variety of stimuli (as discussed above), several common characteristics of senescent cells exist that permits their identification *in vitro* and *in vivo*. The two main facets of senescence that underpin the tumour suppressor response are the growth arrest and the senescence-associated secretory phenotype (SASP). These features will be introduced here but a more detailed description of their regulatory mechanisms will be discussed in chapter 1.1.4 and 1.1.5 respectively.

#### 1.1.3.1 Growth arrest

Senescent cells are most well-known for exhibiting a robust cell cycle arrest, mediated via activation of p53-p21 and INK4/ARF tumour suppressor pathways (Chicas et al., 2010). This growth arrest was initially thought to be irreversible, owing to early *in vitro* observations (Kato et al., 1998; Zhu et al., 1998), however subsequent studies have highlighted escape mechanism that permit proliferation to continue. For example, inactivation of p53 or p16

(Beausejour et al., 2003; Dirac and Bernards, 2003) and components of the senescence associated secretory phenotype (see below) permit re-entry into the cell cycle (Coppe et al., 2008b; Kuilman et al., 2008). Escape from the senescence associated growth arrest is highly relevant *in vivo*, whereby clonal expansion of cells that have overcome senescence (for example via inactivating mutations of tumour suppressor genes) permits tumour progression (Milanovic et al., 2018).

#### 1.1.3.2 Senescence-associated secretory phenotype

Despite entering into a robust growth arrest, senescent cells remain highly metabolically active and secrete a variety of factors including cytokines, chemokines, growth factors and extracellular proteases (Coppe et al., 2010) (Acosta et al., 2013). These secreted factors are collectively termed the senescence-associated secretory phenotype (SASP) (Acosta et al., 2008; Coppe et al., 2008b; Kuilman et al., 2008). The SASP is composed of several families of soluble and insoluble factors (examples summarised in table 1.1) and can trigger a variety of cellular responses. For example, pro-inflammatory SASP chemokines can reinforce the senescence associated growth arrest in an autocrine manner signalling via the CXCR2 receptor (Acosta et al., 2008). Furthermore, multiple SASP components mediate paracrine signalling mechanisms to induce senescence in neighbouring cells (Acosta et al., 2013) and mediate the recruitment of immune cells which subsequently clear senescent cells (Kang et al., 2011; Xue et al., 2007). However, the SASP also exhibits tumour promoting effects (discussed in

detail in chapter 1.3.1) and can promote the proliferation of non-senescent tumour cells (Krtolica et al., 2001).

**Table 1.1**: SASP factor examples. Adapted from Coppe et al (Coppe et al., 2010).

| **Soluble factors** | | | | |
|---|---|---|---|---|
| *Interleukins* | *Chemokines* | *Other* | *Growth factors* | *Proteases* |
| **IL-1α, IL-1β** | IL-8 | GM-CSF | Amphiregulin | MMP-1 |
| **IL-6** | GRO-α, -β, -γ | G-CSF | Epiregulin | MMP-3 |
| IL-13 | MCP-2, -4 | IFN-γ | EGF | MMP-10 |
| IL-15 | MIP-1a, -3a | MIF | HGF | MMP-12 |
| IL-7 | HCC-4 | | VEGF | TIMP-1 |
| **Shed receptors or ligands** | | | | |
| ICAM-1, -3 | | | | |
| sTNFR1, -2 | | | | |
| TRAIL-R3 | | | | |
| Fas | | | | |
| EGF-R | | | | |
| **Non-protein soluble factors** | | | | |
| PGE2 | | | | |
| Nitric oxide | | | | |
| Reactive oxygen species | | | | |
| **Insoluble factors (ECM)** | | | | |
| Fibronectin | | | | |
| Collagens | | | | |
| Laminin | | | | |

While many SASP factors are conserved, there exists significant heterogeneity in SASP factors expression depending on cell type and senescence inducer (Basisty et al., 2020; Coppe et al., 2010). For example, cells induced to senesce via oncogenic RAS express a SASP rich in interleukins (such as IL-1$\beta$ and IL-6) and other pro-inflammatory mediators (such as GM-CSF and GRO$\alpha$), when compared with cells induced to senesce via replicative exhaustion or irradiation (Coppe et al., 2008b; Rodier et al., 2009). Furthermore, overexpression of $p16^{INK4a}$ induces several hallmarks of senescence, but does not induce expression of the SASP as seen with other senescence inducers (Coppe et al., 2010). More recently, proteomic analysis of senescence-associated secretomes from human primary fibroblasts induced to senesce by oncogenic RAS, irradiation and drug induced senescence revealed that only 150 proteins are commonly overexpressed in all three conditions (out of a total of 1,091) (Basisty et al., 2020). Thus, the majority of SASP components in these *in vitro* assays were heterogenous and not common amongst different senescence inducers. The same study compared the SASP in irradiation treated fibroblasts and renal epithelial cells and again found that significant heterogeneity exists. The secretome of irradiated fibroblasts and epithelial cells was distinct, with less than 25% of secreted factors overlapping between cell types. However, the most striking observation was that the overall magnitude of increased expression was significantly less in epithelial cells, suggesting that different cell types not only secrete different components but the capacity for upregulation of SASP factors is distinct (Basisty et al., 2020).

#### 1.1.3.3 Resistance to apoptosis

Another common feature of senescent cells is a resistance to undergo programmed cell death (apoptosis) (Childs et al., 2014). While apoptosis and senescence may seem like opposing entities, the stress stimuli triggering these cell fate responses are often the same, albeit at different levels (Vousden and Lane, 2007). For example, the administration of DNA damaging agents (for example chemotherapeutic agents, irradiation or reactive oxygen species) at high doses induce apoptosis in cultured cells, whereas lower doses induce senescence (Chen and Ames, 1994; Chen et al., 2000a; Debacq-Chainiaux et al., 2005; Probin et al., 2006; Song et al., 2005). Pro-senescence stimuli induce increases in total p53 levels to a lesser extent than apoptotic stimuli. This leads to lower levels of pro-apoptotic p53-upregulated modulator of apoptosis (PUMA) and NOXA, and higher levels of BCL-2 family proteins (Tavana et al., 2010a). BCL-2 proteins are overexpressed in senescent cells and inhibit mitochondrial outer membrane polarization and apoptosis (Yosef et al., 2016). On top of differences in total p53 protein levels, post-translational modification of p53 also occurs distinctively in apoptosis and senescence (Webley et al., 2000). For example, point mutations involving individual acetylation sites in p53 can influence the choice to apoptose or senesce (Li et al., 2012), suggesting that post translational modifications play in integral role in cell fate decisions. Furthermore, mutations affecting the quaternary structure of p53 affects a cells ability to undergo apoptosis but have no bearing on its ability to senesce (Schlereth et al., 2010; Timofeev et al., 2013). p21 (which is typically

upregulated in senescence) can block apoptosis (Hayward et al., 2003; Zhang et al., 2011a) and may also inhibit caspase 3 directly (Tang et al., 2006). Developmental senescence and subsequent immune clearance is impaired in p21 deficient mice, however this is partially rescued by increased apoptosis (Munoz-Espin et al., 2013), suggesting that p21 functions to oppose apoptosis and promote senescence in this context. Lastly, blocking apoptosis (for example with caspase inhibitors) can also induce cellular senescence (Rebbaa et al., 2003; Zhang et al., 2005). Thus, the decision to undergo apoptosis versus senescence is complex and dictated by several factors.

#### 1.1.3.4 Morphological changes

The morphological changes associated with senescence can be striking and are often used to preliminarily identify whether cells have undergone senescence *in vitro*. Senescent cells typically undergo characteristic morphological changes which involve a large, flattened appearance and can often become multinucleated or exhibit vacuolisation (Denoyelle et al., 2006; Serrano et al., 1997). There can be some differences based on the senescence trigger and cell type. For example, $HRAS^{G12V}$ induced senescent fibroblasts (the first described oncogene-induced senescence model) exhibit the aforementioned appearance (Serrano et al., 1997), whereas $BRAF^{V600E}$ induced senescent melanocytes have a more spindle shaped morphology (Michaloglou et al., 2005). The mechanism underlying these morphological changes are unclear but previous reports

have shown enhancement of actin stress fibres and redistribution of focal adhesion proteins in cells induced to senesce due to oxidative damage (Chen et al., 2000b) which may explain this phenomenon.

#### 1.1.3.5 Chromatic reorganisation

Altered chromatin architecture is a key feature of senescence (Adams, 2007). Epigenetic regulation is a key mechanism regulating expression of the of the *INK4/ARF* locus (discussed in detail in chapter 1.1.4) and thus chromatin reorganisation is a key step regulating senescence. DNA staining of senescent cells reveals punctate nuclear staining, representing so called senescence-associated heterochromatin foci (SAHF) (Narita et al., 2003). These foci of epigenetically silenced DNA loci are enriched in methylated histone 3 Lys 9 (H3K9me3 - catalysed by the histone methyltransferase Suv39h1), whereas euchromatin markers such as acetylated histone 3 Lys 9 (H3K9ac) and methylated histone 3 Lys 4 (H3K4me3) are excluded from SAHF. Thus, the formation of SAHF (mediated by p16-Rb signalling) function to silence parts of the genome involved in cell cycle progression (such as E2F target gene promoter regions), reinforcing the cell cycle arrest (Narita et al., 2003).

#### 1.1.3.6 Senescence biomarkers

Senescent cells undergo an expansion of their lysosomal compartments, giving rise to increased activity of lysosomal β-galactosidase (Kurz et al., 2000). While non-senescent cells also express lysosomal β-

galactosidase, detection in this setting requires an optimal pH of 4, whereas detection in senescent cells can be performed at a suboptimal pH of 6 (Lee et al., 2006). Therefore, detection of so-called senescence-associated β-galactosidase (SA-β-gal) is often used as a biomarker of senescence (Debacq-Chainiaux et al., 2009; Dimri et al., 1995). Currently, *in vivo* detection of SA-β-gal requires snap frozen tissue in order to preserve enzymatic activity (Debacq-Chainiaux et al., 2009). Therefore, this method cannot be used for archival formalin-fixed paraffin embedded samples. Sudan-black-B (SBB) staining of lipofuscin seeks to overcome this drawback of SA-β-gal mediated detection of senescent cells (Georgakopoulou et al., 2013). Lipofuscin is an aggregate of oxidised proteins that accumulate in senescent cells (Jung et al., 2007) and SBB is a lipophilic histochemical stain that can be used to identify lipofuscin *in vitro* and *in vivo* (Georgakopoulou et al., 2013). Due to the complexities of senescence, a universal senescence biomarker is yet to be identified. Therefore, a consensus approach involves identifying multiple characteristics of senescence (as discussed in this section) in order to reliably identify senescent cells *in vitro* and *in vivo* (Gonzalez-Gualda et al., 2021).

Degradable inorganic nanoparticles allowing selective release of encapsulated cargoes have been utilised in an attempt to detect SA-β-gal expressing senescent cells *in vivo* (Karlsson et al., 2018). For example, galacto-oligosaccharide encapsulated nanoparticles permit controllable release of contrast dye, fluorescent senoprobes (Lozano-Torres et al., 2017; Wang et al., 2019) and PET probes (Ou et al., 2021) following exposure to

high levels of β-galactosidase (Aznar et al., 2016), as seen in senescent cells. These techniques would conceivably allow the detection of senescent premalignant lesions via non-invasive imaging modalities. Liquid biopsy approaches have also been proposed as a means to detect the presence of senescent cells in a non-invasive manner. Analysis of circulating cell free DNA, extracellular vesicles (EVs) (Kustanovich et al., 2019) and SASP factors (Basisty et al., 2020; Schafer et al., 2020) have shown promise in early preclinical studies. While these techniques are yet to be translated into clinical practice, the reliable detection of senescent cells would provide robust methods to improve the early detection of cancer and stratify patients at higher risk for developing invasive malignancies, allowing heightened targeting of such patients with screening techniques.

### 1.1.4 Mechanisms of the senescence growth arrest

The many stimuli that induce senescence signal through various pathways, many of which converge on the activation of cyclin-dependent kinase (CDK) inhibitors (Munoz-Espin and Serrano, 2014). The activation of CDK inhibitors results in hypo-phosphorylation of Rb and subsequent proliferative arrest (Chicas et al., 2010) (summarised in Figure 1.1). The two main pathways culminating in this arrest are the p53-p21 and INK4/ARF pathways. DNA damage (double or single stranded breaks) results in the phosphorylation of H2Ax by members of the PI3 kinase family (notably ATM, ATR and DNA-PK) thus forming γH2Ax which is deposited in chromatin regions flanking the DNA break lesion (Dickey et al., 2009). γH2Ax deposition

subsequently activates a kinase cascade involving ATM-CHK2 or ATR-CHK1 (for double stranded breaks or single stranded breaks respectively) (d'Adda di Fagagna, 2008; Fumagalli et al., 2012). This cascade culminates in p53 activation that in turn induces the transcription of the CDK inhibitor p21 (a product of the *CDKN1A* gene). p21 in turn inhibits Rb phosphorylation indirectly via inhibition of CDK2 (Brugarolas et al., 1998). The *INK4/ARF* locus includes the *CDKN2A* gene that encodes the tumour suppressors $p16^{INK4a}$ and ARF (alternate reading frame), and the *CDKN2B* gene that encodes the tumour suppressor $p15^{INK4b}$. $p16^{INK4a}$ and $p15^{INK4b}$ are CDK inhibitors that inhibit CDK4/6 activity resulting in hypo-phosphorylation of Rb. Crossover between p53 and products of the *INK4/ARF* locus exists, whereby the induction of ARF degrades the ubiquitin ligase MDM2, which itself is a negative regulator of p53 activity, thus contributes to increased levels of p53 (Zhang et al., 1998). Furthermore, p53 can regulate ARF expression through a negative feedback loop (Harris and Levine, 2005). The *INK4/ARF* locus is typically epigenetically silenced in young cells via polycomb protein mediated methylation of H3K27 (Bracken et al., 2007). Disruption of this process (for example during aging (Krishnamurthy et al., 2004) or oncogene activation (Barradas et al., 2009)) leads to derepression of the *INK4/ARF* locus and cellular senescence (Barradas et al., 2009; Jacobs et al., 1999).

**Figure 1.1: Senescence associated growth arrest pathways.** Schematic summarising the two main pathways mediating the senescence associated growth arrest.

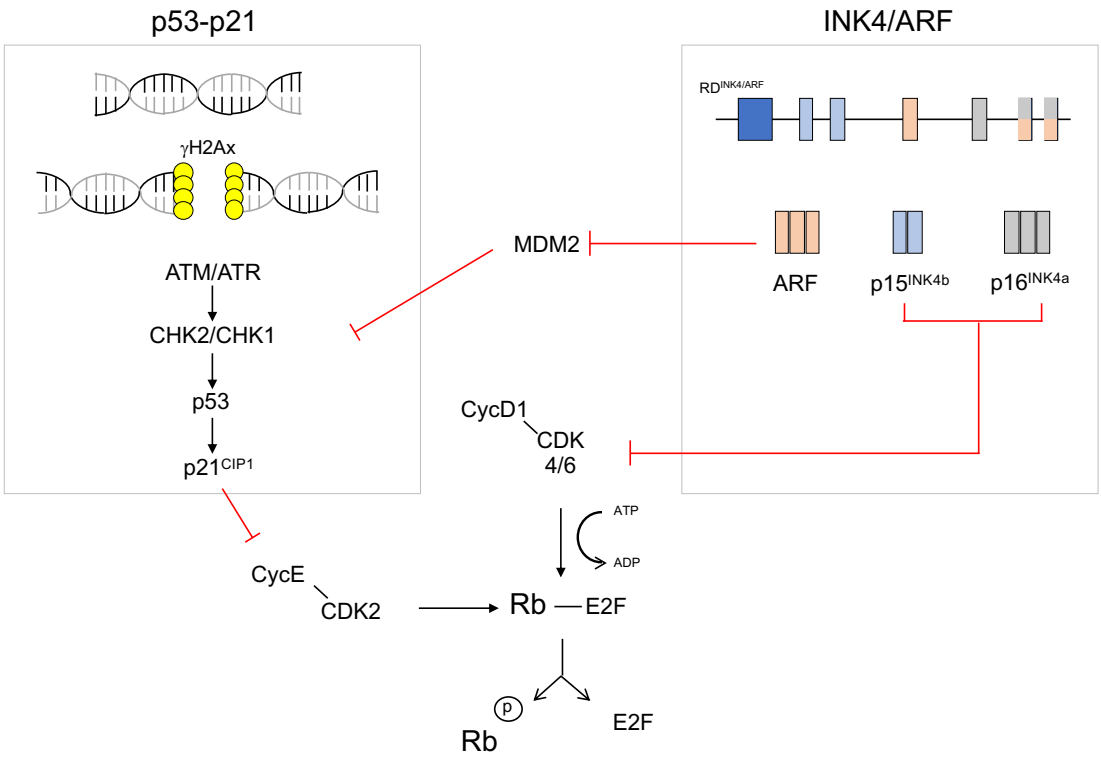


### 1.1.5 Mechanisms of SASP expression

The specific combination of factors secreted by senescent cells is dependent on the context (including the senescence inducer and cell type), however many of the regulatory mechanisms are shared (Faget et al., 2019) (summarised in Figure 1.2). The key transcription factors regulating SASP expression are Nuclear factor κB (NF-κB) and CCAAT/enhancer-binding protein β (CEBPβ) (Acosta et al., 2008; Kuilman et al., 2008). The molecular events leading up to NF-κB and/or CEBPβ activation are complex and poorly defined. DNA damage can induce expression of the SASP via these

pathways (Rodier et al., 2009) and recently it has been shown that SASP expression is triggered by cytoplasmic chromatin fragments (CCFs) released during forms of senescence associated with DNA damage (including replicative, therapy induced and oncogene induced senescence) (Dou et al., 2017; Gluck et al., 2017). However, CCF release was also observed following application of non-genotoxic senescence inducers such as direct CDK4/6 inhibitors (palbocilib), suggesting that this mechanism of SASP induction is not reliant on DNA damage (Gluck et al., 2017). CCF release engages the cytosolic DNA sensing cGAS/STING pathway leading to secretion of a pro-inflammatory SASP (Dou et al., 2017; Gluck et al., 2017) (discussed in detail in chapter 1.4). Another key regulator of the SASP is p38 MAPK which is activated independently of the DNA damage response and functions to increase the transcriptional activity of NF-κB (Freund et al., 2011). Additional regulators exist including mTOR (Herranz et al., 2015; Laberge et al., 2015), GATA4 (Kang et al., 2015) and MLL1 (Capell et al., 2016). Different components of the SASP can have different upstream regulators. For example, IL-1 signalling mediated by the canonical NLRP3 inflammasome regulates the pro-inflammatory arm of the SASP (Acosta et al., 2013) (discussed in detail in chapter 1.4), whereas Notch signalling regulates a TGF-β rich SASP (Hoare et al., 2016). More recently, our group identified Toll-like receptor 2 (TLR2) as a novel regulator of the SASP during OIS, signalling via acute phase serum amyloid A (A-SAA) proteins (discussed in detail in chapter 1.4) (Hari et al., 2019).

While the senescence growth arrest is dependent on the activation of tumour suppressor pathways (see chapter 1.1.4), this is not the case for the SASP. $p16^{INK4A}$ expression is sufficient to induce the growth arrest (Chicas et al., 2010), however it is not required to induce the SASP (Coppe et al., 2010). Similarly, p53 is required for the DNA damage induced growth arrest (d'Adda di Fagagna, 2008), but not the SASP. In fact, p53 has been shown to restrain expression of the SASP; cells lacking p53 secrete markedly higher levels of most SASP factors (Coppe et al., 2008b). Thus, regulation of the SASP can be mediated via DNA damage and DNA damage independent mechanisms and is not reliant on growth arrest pathways.

**Figure 1.2: SASP regulation.** Schematic summarising the main regulatory pathways involved in the SASP.

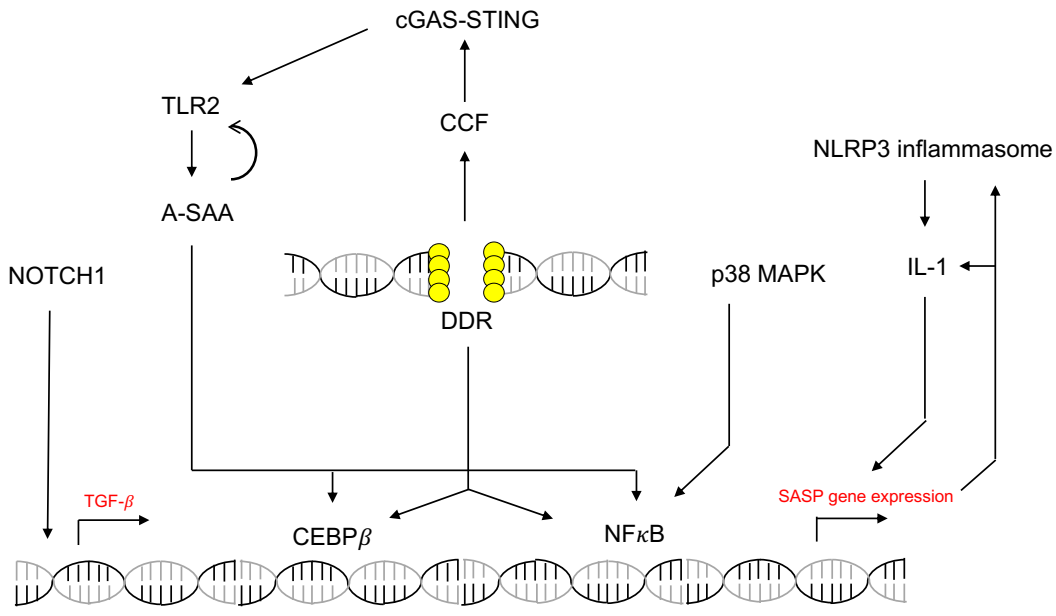

### 1.1.6 Senescence in development and physiology

While senescence is mainly thought of as a cellular response to stress or damage, it has also been shown to be integral to several physiological and developmental processes. Indeed, oncogenes and tumour suppressor genes evolved not to limit cancer progression but to control developmental process and maintain tissue homeostasis (Jain and Barton, 2018). Senescent fibroblasts and endothelial cells appear early following cutaneous wounding where they induce myofibroblast differentiation (via secretion of platelet-derived growth factor AA), thus facilitating wound closure (Demaria et al., 2014). Senescence has also been observed during embryological development of several organisms including mice (Munoz-Espin et al., 2013; Storer et al., 2013) and humans (Munoz-Espin et al., 2013), suggesting that it is common throughout the developing embryo and evolutionarily conserved across species. Senescent cells have been identified in a variety of developing structures including the neural tube, regressing interdigital webs, the apical ectodermal ridge of the limbs, mesonephric tubules and the endolymphatic sac of the inner ear (Munoz-Espin et al., 2013; Storer et al., 2013). Senescence in these contexts does not involve DNA damage, as markers of DNA damage and the DDR are notably absent, but heavily involve the CDK inhibitor p21 as demonstrated by a marked impairment of developmental senescence in *Cdkn1a* null embryos (Munoz-Espin et al., 2013; Storer et al., 2013). Transcriptional profiles of senescent cells in embryos are reminiscent of developmental pathways including TGF-β, WNT and Hedgehog signalling. They also include a SASP similar to other forms of

senescence with the notable addition of fibroblast growth factor 4 and 8 (FGF4 and FGF8) (Munoz-Espin et al., 2013; Storer et al., 2013). Clearance of senescent cells by macrophages occurs in the developing mesonephros and the apical ectodermal ridge of limbs, which also appears to be dependent on intact p21 activity (Munoz-Espin et al., 2013). While defects in developmental senescence can be partially overcome by apoptosis and late clearance by macrophages, impaired p21 dependent senescence can result in morphological defects (Munoz-Espin et al., 2013). Senescence is also integral to the maturation programmes of several cell types including megakaryocytes (Besancenot et al., 2010) and placental syncytiotrophoblasts (Chuprin et al., 2013). In the case of megakaryocytes, senescence is again dependent on p21, and impaired p21 expression is characteristic of primary myelofibrosis which is a myeloproliferative disorder characterised by impaired megakaryocyte senescence (Besancenot et al., 2010). Syncytiotrophoblast senescence is less reliant on p21 activity and is associated with DDR markers, p16 and p53 expression (Chuprin et al., 2013).

### 1.1.7 Senescence in disease

Senescent cells are also heavily involved in several pathological settings, whereby they can exhibit both beneficial and detrimental effects on disease progression (Munoz-Espin and Serrano, 2014). The most well studied disease associated with senescence is cancer (Collado and Serrano, 2010), which will be discussed in detail below (in chapter 1.2). Senescence

has been shown to have beneficial effects in several fibrotic diseases including liver fibrosis (Krizhanovsky et al., 2008; Wiemann et al., 2002), skin fibrosis (Jun and Lau, 2010a, b), post obstructive renal fibrosis (Wolstein et al., 2010) and post infarction cardiac fibrosis (Zhu et al., 2013). In these contexts, senescence of scar producing myofibroblasts prevents excessive myofibroblast proliferation and scar formation. Furthermore, senescent myofibroblasts secrete a SASP, mediating immune clearance of senescent cells and partial elimination of scar tissue. Senescence is also associated with idiopathic pulmonary fibrosis (IPF), a disease characterised by progressive lung fibrosis involving alveolar and interstitial cells resulting in loss of gas exchange capacity. Senescence markers are expressed in alveolar, bronchial and interstitial cells in mouse models of IPF and IPF patients (Aoshiba et al., 2013; Aoshiba et al., 2003; Minagawa et al., 2011) and senescence is thought to have a detrimental function in this context. Impaired senescence and SASP expression via loss of caveolin-1 (CAV1) protects mice from bleomycin induced lung fibrosis (Shivshankar et al., 2012) and pharmacological inhibition of the ROS generator NOX4 decreases p16 and p21 expression and reverses bleomycin induced lung fibrosis in mice (Hecker et al., 2014). IPF is an independent risk factor for the development of lung cancer (Wells and Mannino, 1996) and there are multiple cellular processes that connect lung fibrosis with cancer including increased proliferation, inflammation and tissue invasion (Ballester et al., 2019). Conceivably, the SASP produced by senescent fibroblasts in IPF could

promote malignant growth (as discussed in chapter 1.3.1), however this has not yet been proven.

Pulmonary artery smooth muscle cell senescence has been demonstrated in patients with chronic obstructive pulmonary disease (COPD) (Noureddine et al., 2011) and mouse models have shown that impairment of senescence (via disruption of *Trp53* or *Cdkn1a* expression) worsens pulmonary hypertension (Mizuno et al., 2011). Furthermore, exposure of mice to cigarette smoke (the main cause of COPD) induces senescence in alveolar epithelial cells (Tsuji et al., 2004) and alveolar cells from COPD patients express high levels of p16 and NF-κB (Tsuji et al., 2010).

Senescence is also integral during atherosclerotic plaque formation, whereby vascular smooth muscle cells (VSMCs) undergo senescence after a period of proliferation during plaque formation (Wang and Bennett, 2012). VSMC senescence involves SASP expression and induces paracrine senescence in neighbouring cell types, thus limiting plaque growth (Wang and Bennett, 2012). Mouse models with impaired senescence have an increased susceptibility to atherosclerosis (Diez-Juan and Andres, 2001; Gonzalez-Navarro et al., 2010; Khanna, 2009; Mercer et al., 2005) and activation of senescence is protective against plaque formation (Sanz-Gonzalez et al., 2007). Furthermore, several genome wide association studies (GWAS) have identified polymorphisms in the *CDKN2A/CDKN2B* loci that are pro-atherosclerotic, inferring that these loci are protective against plaque formation (Jeck et al., 2012; Liu et al., 2009). Moreover, deletion of homologous regions in mouse models impairs expression of *Cdkn2a*/*Cdkn2b*

and worsens mortality after a high fat/cholesterol diet (Visel et al., 2010), confirming the importance of senescence in limiting atherosclerotic plaque formation.

In both humans and mice adipose tissue upregulates p53-p21 signalling, expresses senescence markers and a SASP (Tchkonia et al., 2010). Senescence may contribute to the adverse effect of obesity as tissue specific deletion of *Trp53* protects mice from insulin resistance induced by excessive calorific intake (Minamino et al., 2009). Chronic high fat diet in mice also induces senescence in pancreatic β cells (Sone and Kagawa, 2005) and is associated with models of type 2 diabetes melliltus (DM2) (Chesnokova et al., 2009; Tavana et al., 2010b; Wang et al., 2003). Further data linking senescence to DM2 is found in GWAS studies linking polymorphisms close to the *CDKN2A/CDKN2B* loci that are linked to DM2 susceptibility (Doria et al., 2008; Jeck et al., 2012).

Sarcopenia (loss of muscle mass) is a key aging associated pathology and senescence of satellite cells (muscle stem cell progenitors) has been shown to be a key mediator of this process (Sousa-Victor et al., 2014). Another aging associated pathology is cataract formation. Elimination of senescent cells lessens cataract formation in mouse models (Baker et al., 2011), indicating that senescence plays a key role in this process. Senescence is also potentially involved in several other diseases including aneurysmal disease (Fukazawa et al., 2007), glaucoma (Liton et al., 2005), Alzheimer's disease (Bhat et al., 2012), Parkinsons disease (Chinta et al.,

2013), osteoarthritis (Price et al., 2002), and macular degeneration (Zhu et al., 2009).

### 1.1.8 Senescence and aging

Aging is characterised by gradual functional decline involving multiple organ systems, and as a result aging is a major risk factor for several of the diseases discussed in chapter 1.1.7 (McHugh and Gil, 2018). Senescent cells accumulate in aged tissues (Burd et al., 2013; Dimri et al., 1995; Jeyapalan et al., 2007) where they can lead to natural features of aging including sarcopenia, lipodystrophy and cataracts (Baker et al., 2008; Hanks et al., 2004). The regenerative capacity of multiple tissue types decreases with aging, and this occurs in conjunction with increased evidence of stem cell senescence (Chang et al., 2016; Loeser, 2009; Molofsky et al., 2006; Raggi and Berardi, 2012; Tchkonia et al., 2010). Furthermore, SASP expression from accumulated senescent cells further contribute to the aging phenotype via chronic low-level inflammation (McHugh and Gil, 2018; Tilstra et al., 2012) (so called ‘inflammaging’ (Franceschi and Campisi, 2014)). While the SASP functions to mediate the clearance of senescent cells in healthy tissues (Kang et al., 2011), in aged individuals immune dysfunction occurs which limits this (so called ‘immunosenescence’ (Lian et al., 2020)) leading to further accumulation of senescent cells and perpetuating chronic inflammation via SASP expression (McHugh and Gil, 2018). Studies involving transgenic mouse models that allow the selective removal of senescent cells (which will be discussed in detail below in chapter 1.5.2)

have shown that removing senescent cells blunts the development of age related diseases (Baker et al., 2016; Baker et al., 2011) and extends median lifespan (Baker et al., 2016), confirming that senescence at least contributes to the aging phenotype. The identification of pharmacological agents that selective kill senescent cells (so called 'senolytics') (Fuhrmann-Stroissnigg et al., 2017; Guerrero et al., 2019; Triana-Martinez et al., 2019; Yosef et al., 2016; Zhu et al., 2016; Zhu et al., 2015) has prompted interest in developing therapies to limit the negative effects of aging. However, studies have yet to show that pharmacological clearance of senescent cells impairs the onset of age-related pathologies or extends healthy lifespan. Nonetheless this area of research holds significant promise.

## 1.2 Senescence in cancer

### 1.2.1 Oncogene induced senescence

The first evidence demonstrating oncogenic signalling can induce senescence was uncovered in 1986 following viral transformation of human fibroblasts with oncogenic *KRAS* (O'Brien et al., 1986). This led to a phenotype similar to that first described by Hayflick and colleagues and led to the discovery of oncogene-induced senescence (OIS). Subsequent to this, forced expression of oncogenic *HRAS* (*HRAS*$^{G12V}$) mirrored this phenotype, confirming that oncogene activation induces cellular senescence (Serrano et al., 1997). As alluded to above, senescence in the context of oncogene activation is mediated via the DDR owing to aberrant DNA replication

(Bartkova et al., 2006; Di Micco et al., 2006), increased mitochondrial ROS production (Lee et al., 1999) and direct derepression of the *CDKN2A* locus (Barradas et al., 2009). This leads to the upregulation of the *CDKN2A* locus thus activating both INK4/ARF and p53-p21 tumour suppressor pathways (discussed in detail in chapter 1.1.4) (Serrano et al., 1997).

### 1.2.2 Oncogene induced senescence *in vivo*

While initially described *in vitro*, the occurrence of OIS *in vivo* was first reported by studies showing the expression of senescence markers in pre-malignant tumours (with a lack of expression in their malignant counterparts) (Braig et al., 2005; Chen et al., 2005; Collado et al., 2005; Lazzerini Denchi et al., 2005; Michaloglou et al., 2005). The number of genes which have been shown to induce senescence *in vivo* when mutated is increasing and is summarised in table 1.1 (Collado and Serrano, 2010). Oncogenic *Kras* ($Kras^{G12V}$) expression has been shown to induce senescence in early mouse lung and pancreatic premalignancies, detected via SA-β-gal expression, tumour suppressor pathway activation and the presence of SAHF that were all notably absent in adjacent malignant lesions (Collado et al., 2005). Other Ras family member can also induce senescence *in vivo*. For example, transgenic expression of oncogenic *Nras* ($Nras^{G12D}$) in lymphoid tissue significantly increases the susceptibility of lymphocytes to therapy-induced senescence (Braig et al., 2005) and mammary gland expression of $Hras^{G12V}$ induces OIS when expressed at high levels (Sarkisian et al., 2007). Subsequent studies demonstrated that this response is not restricted to

oncogenic *Ras* activation. OIS has been observed in lung tumours and melanocytic naevi induced by endogenous $Braf^{V600E}$ expression (Dankort et al., 2007; Dhomen et al., 2009) and chemically induced skin papillomas were also found to express senescence markers (Collado et al., 2005). *Myc* activation also induces senescence in pancreatic cancer and lymphoma mouse models (Campaner et al., 2010). Furthermore, E2F transcription factor activation (for example the inducible *E2f3* transgene) induces proliferation, swiftly followed by OIS in the mouse pituitary gland (Lazzerini Denchi et al., 2005). The name oncogene-induced senescence is actually a misnomer, as loss of tumour suppressor genes can cause similar activation of the OIS response via aberrant DNA replication. Prostate specific deletion of the tumour suppressor *Pten* leads to the formation of prostate intraepithelial neoplasia (PIN) lesions which exhibit features of OIS (Chen et al., 2005) and loss of the tumour suppressor *Vhl* in the murine kidney similarly leads to OIS (Young et al., 2008). Overall, OIS has moved from an observed *in vitro* phenomenon to a widespread process in several mouse models of pre-malignancy. The lack of expression of such markers in adjacent malignant lesions, and the accelerated tumourigenesis observed following genetic deletion of key senescence associated tumour suppressor pathways (Beck et al., 2020) has led to the recognition that OIS is a key tumour suppressor mechanism *in vivo*.

**Table 1.2**: Genes involved in oncogene-induced senescence *in vivo*. Adapted from Collado et al (Collado and Serrano, 2010).

| Gene | Tissue |
|---|---|
| ***Oncogenes*** | |
| *Hras*$^{G12V}$ | Mammary, bladder and skin tumours |
| *Kras*$^{G12V}$ | Lung and pancreatic preneoplasia |
| *Nras*$^{G12D}$ | Lymphoproliferative disorders |
| *Braf*$^{V600E}$ | Melanocytic naevi, lung tumours |
| *Rheb* | Prostate intraepithelial neoplasia |
| *E2f3* | Pituitary hyperplasia |
| *Akt1* | Prostate intraepithelial neoplasia |
| *β-catenin* | Thymus preneoplasia |
| ***Tumour suppressor genes*** | |
| *Pten* | Prostate intraepithelial neoplasia |
| *Rb* | Thyroid adenoma |
| *Vhl* | Renal cancer |
| *p53* | Sarcoma, liver carcinoma |

### 1.2.3 Oncogene induced senescence in human tumours

The observation of OIS *in vivo* has not been restricted to mouse models and there are examples of human tumours which exhibit evidence of OIS (summarised in table 1.2). The first reports of OIS in human tumours was that of melanocyte senescence associated with oncogenic *BRAF*$^{V600E}$ (Michaloglou et al., 2005). Human PIN lesions (Acosta et al., 2008; Chen et al., 2005) and pre-malignant colonic adenomas (Bartkova et al., 2006;

Kuilman et al., 2008) also exhibit features of senescence. Inherited or spontaneous loss of the tumour suppressor *NF1* results in in a condition called neurofibromatosis. *NF1* encodes a RAS GTPase-activating protein (GAP) (see chapter 1.6.7), thus loss of *NF1* results in RAS overactivation and the formation of cutaneous pre-malignant tumours called neurofibromas that undergo senescence (Courtois-Cox et al., 2006). These examples suggest that OIS is also an important process limiting malignant progression in human cancer.

**Table 1.3**: Genes involved in oncogene-induced senescence in humans. Adjusted from Collado et al (Collado and Serrano, 2010).

| Gene | Tissue |
|---|---|
| ***Oncogenes*** | |
| *BRAFV600E* | Melanocytic naevia |
| *NF1* | Neurofibromas |
| *Not determined* | Colonic adenomas |
| *Not determined* | Prostate intraepithelial neoplasia |

## 1.3 The SASP in cancer

The SASP is a non-cell autonomous effector of senescence, with important functions in both physiological and pathological settings (Munoz-Espin and Serrano, 2014). The mechanisms of SASP induction following oncogene activation are discussed in detail in chapter 1.1.5 and involve both DNA damage and DNA damage independent mechanisms converging on

activation of downstream effectors such as NF-κB, C/EBPβ and p38MAPK. The effect of the SASP on tumourigenesis is complex and context dependent, including both pro- and anti-tumourorigenic functions (Faget et al., 2019).

### 1.3.1 Pro-tumourigenic effects of the SASP

SASP factors have been shown to aid malignant progression via a variety of mechanisms. Direct co-culture with senescent fibroblasts, or the addition of conditioned media from senescent fibroblasts promotes the growth of prostate cancer cells (Bavik et al., 2006) and immortalised keratinocytes *in vitro* (Coppe et al., 2008a) confirming paracrine induction of proliferation by secreted factors. Furthermore, senescent fibroblasts also promote proliferation in immortalised ovarian cancer cell lines and organoid models (Lawrenson et al., 2010). The tumour promoting effects of the SASP are further highlighted by *in vivo* studies demonstrating marked tumour growth following subcutaneous co-injection of senescent fibroblasts with human breast cancer cell lines, an effect shown to be due to secreted factors (Krtolica et al., 2001). Subsequent studies revealed that this growth promoting effect was impaired by inhibition of matrix-metalloproteases (MMPs), highlighting MMPs as key tumour promoting SASP factors (Liu and Hornsby, 2007). Senescent fibroblasts also promote epithelial-to-mesenchymal transition (EMT) in pre-malignant mammary epithelial cells, promoting invasion and full transformation to malignancy, a function primarily mediated by MMP-3 (Parrinello et al., 2005). IL-6 (a key pro-inflammatory

SASP factor) has been shown to accelerate *in vivo* tumour growth in models of skin (Lederle et al., 2011), breast (Di et al., 2014; Hartman et al., 2013), prostate (Rojas et al., 2011) and lung cancer (Song et al., 2011) and CXCL1 stimulates tumour growth in oesophageal cancer models (Wang et al., 2006). It must be noted that the promotion of proliferation by the SASP seems to only occur with immortalised cancer cell lines (Krtolica et al., 2001) suggesting that these proliferation promoting effects require defective tumour suppressor pathways. Therefore, bystander senescence and SASP expression (in for example aged tissues) may promote growth of neighbouring transformed pre-malignant or malignant cells but is less likely to promote malignant transformation in normal diploid cells. As well as promoting proliferation, the SASP can promote metastasis. Tumours derived from subcutaneously implanted transformed epithelial cells exhibit increased vascular invasion mediated by secretion of vascular endothelial growth factor (VEGF) by co-injected senescent fibroblasts (Coppe et al., 2006). Furthermore, another SASP factor CTGF promotes vascular invasion of tumours in a mouse model of prostate cancer (Yang et al., 2005). Enhanced tumour cell migration in breast cancer cell lines is observed and is mediated by inhibition of RhoA/ROCK signalling by senescent stromal cells (Aifuwa et al., 2015) and secretion of the SASP factor Chemerin increases cell migration in cutaneous squamous cell carcinoma models (Farsam et al., 2016). Senescence induction in breast cancer cells via constitutive expression of the tyrosine kinase receptor HER2 promotes the secretion of SASP factors and subsequent metastasis of neighbouring non-senescent

breast cancer cells *in vivo* (Angelini et al., 2013). Similarly, senescent cells at the invasive border of murine papillary thyroid cancers increases invasion of senescent and non-senescent tumour cells via CXCL12 signalling (Kim et al., 2017). IL6 secreted from senescent stromal osteoblasts facilitates breast tumour cell seeding in bone via direct stimulation of local osteoclastogenesis (Luo et al., 2016) and endothelial cell senescence mediated by *Notch1* promotes lung metastasis of B16F10 melanoma cells via expression of vascular cell adhesion proteins (Wieland et al., 2017). Thus, the SASP can also prime the metastatic niche, further promoting tumour metastasis. The SASP can also permit an immunosuppressive environment, allowing progression of tumour growth. It has been proposed that continuous immune stimulation via the SASP may increase tumour immunoediting, thus increasing the malignant potential of senescent or neighbouring non-senescent tumour cells (Velarde et al., 2013). Furthermore, CCL2 secreted from senescent stromal cells promotes the recruitment of myeloid derived suppressor cells that impair NK cell mediated tumour clearance in mouse liver cancer models, and the presence of senescent tumour stroma is associated with poorer survival in human liver cancer (Eggert et al., 2016). The SASP related immune infiltration can also promote tumour growth via disruption of the senescence growth arrest (Di Mitri et al., 2014). Mechanistically, interleukin-1 receptor antagonist (IL-1RA) secreted from $CD11b^{+}Gr\text{-}1^{+}$ myeloid cells antagonises senescence in *Pten* null murine prostate intraepithelial neoplasia (PIN), and adoptive transfer of *Il1ra* knockout myeloid cells enhanced PIN senescence (Di Mitri et al., 2014).

Another study by the same group highlighted that CXCL2, a key component of the SASP in *Pten* null prostate lesions, polarises CXCR2 expressing tumour associated macrophages (TAMs) towards an anti-inflammatory pro-tumour phenotype (Di Mitri et al., 2019). Pharmacological blockade of CXCR2 reverts these macrophages to a pro-inflammatory phenotype and transfer of CXCR2 knockout monocytes enhances senescence and impairs tumour growth in *Pten*$^{-/-}$*Trp53*$^{-/-}$ prostate tumours (Di Mitri et al., 2019). Knockdown of PTBP1 which regulates the SASP (via alternative splicing of *EXOC7*) but not the growth arrest was shown to prevent the tumour promoting effects of the SASP (Georgilis et al., 2018), highlighting the SASP as a potential therapeutic target in anti-cancer treatment. Furthermore, inhibition of MTOR (a key SASP regulator) also suppresses SASP expression at both the transcriptional (IL6) and translational (IL1A) level, and pre-treatment of senescent fibroblasts with Rapamycin (an MTOR inhibitor) suppresses the tumour promoting effects following cutaneous co-implantation with malignant PC3 prostate cancer cells (Laberge et al., 2015). Thus, the pro-tumourigenic effects of the SASP are numerous and wide ranging. However, it must be pointed out once more that these studies almost exclusively use transformed cells either *in vitro* or *in vivo* with mouse implantation models, and no studies to date have demonstrated an ability of the SASP to transform normal diploid cells. This point is further reinforced in studies by Pribluda et al whereby *CKIα* loss in the gut epithelium triggers extensive Wnt activation, induction of the DDR and activation of p53-p21 dependent senescence that prevents the formation of overt colonic tumours

(Pribluda et al., 2013). This senescence response is associated with a pro-inflammatory SASP that in the context of intact p53-p21 signalling functions to reinforce the growth arrest and prevent tumour invasion. On the contrary, when p53 is ablated or mutated, this SASP induces tumour cell hyperproliferation and invasion resulting in the formation of colonic adenocarcinomas (Pribluda et al., 2013). One potential piece of data that argues against this is from studies examining mouse models of adamantinomatous craniopharyngioma, whereby oncogenic β-catenin expressing embryonic pituitary stem cells undergo senescence and express a SASP that can induce transformation in neighbouring non-mutated cells (Gonzalez-Meljem et al., 2017). However, this model involves embryonic tissue of only 18.5 days post coitum and does not demonstrate the ability of the SASP to transform differentiated diploid cells. Thus, the SASP is able to promote the growth of transformed cells, cells with impaired senescence-associated growth arrest pathways or embryonic stem cells, but the premise of SASP mediated tumour initiation/promotion in normal cells has yet to be established.

### 1.3.2 Anti-tumourigenic effects of the SASP

The anti-tumourigenic effects of the SASP constitute the major non-cell autonomous tumour suppressor functions of OIS. Initial studies to characterise the function of secreted factors from senescent cells identified the chemokine receptor CXCR2 as a key regulator of the growth arrest in OIS (Acosta et al., 2008; Kuilman et al., 2008). Cells undergoing OIS secrete

multiple factors that act as CXCR2 ligands and function to reinforce the senescence associated growth arrest in an autocrine manner. CXCR2 expression is increased in preneoplastic tissues *in vivo*, suggesting a tumour suppressor function for this SASP signalling pathway (Acosta et al., 2008). Subsequently, expression of the SASP was shown to be controlled by canonical inflammasome/IL-1 signalling which activates a diverse cytokine cascade that can induce senescence and growth arrest in neighbouring normal cells (so called 'paracrine senescence') (Acosta et al., 2013). This function was also observed *in vivo* further suggesting a tumour suppressor function for the SASP. Immune surveillance of malignant tissues has long been known to limit tumour progression. Using conditional RNA interference approaches, reactivation of the senescence program via derepression of p53 activity induced a robust growth arrest and expression of the SASP *in vitro* (Xue et al., 2007). *In vivo* however the SASP induced the activation of a robust innate immune response that targeted senescent tumour cells resulting in tumour regression (Xue et al., 2007). This was the first study to highlight a potential tumour suppressor link between senescence and the immune system. Further delineation of this process revealed that senescence induced by oncogene activation leads to expression of pro-inflammatory SASP factors, which orchestrate an adaptive immune response termed 'senescence surveillance' (Kang et al., 2011). Forced expression of oncogenic *Nras* ($Nras^{G12V}$) in otherwise normal murine hepatocytes induces OIS and the secretion of a wide ranging pro-inflammatory SASP. These cells are then subject to immune mediated clearance, a process dependent on

$CD4^+$ T-cells which regulate the recruitment of monocytes/macrophages that clear senescent hepatocytes (Kang et al., 2011). Importantly, impairment of senescence surveillance results in the development of invasive hepatocellular carcinomas (HCCs) further highlighting the important tumour suppressor function of SASP-immune cell communication. Key to these studies was the fact that the models involved were non-transformed cell lines or tissues, further suggesting that the tumour promoting functions of the SASP require disassembly of senescence-associated tumour suppressor pathways. Further studies highlighting that the SASP can promote an anti-tumour immune environment were performed by Lujambio et al (Lujambio et al., 2013), whereby it was shown that p53 expressing senescent hepatic stellate cells release SASP factors that polarise macrophages towards an inflammatory anti-tumour phenotype, whereas p53 deficient stellate cells release factors that promote the polarisation of macrophages into a tumour promoting phenotype capable of enhancing the proliferation of premalignant hepatocytes (Lujambio et al., 2013). Impairment of the SASP in pancreatic ductal adenocarcinoma (PDAC) lesions via inactivation of *RelA* accelerates PDAC lesion formation, and this was found to be mediated by loss of OIS promoting CXCL1-CXCR2 signalling (Lesina et al., 2016). Following genetic inactivation of OIS in these lesions via *Trp53* loss, RelA then functioned to promote tumour growth (Lesina et al., 2016), further highlighting that the SASP is capable of promoting tumour growth but only in the context of impaired senescence mechanisms. Lastly, the anti-tumour effects of the SASP are not restrained to solid tumours. A robust DDR followed by the

expression of pro-inflammatory regulators enhance senescence and prevent leukaemic transformation in *MLL-ENL* induced myeloid leukaemia models (Takacova et al., 2012). Thus, the SASP has wide ranging anti-tumour properties and functions as a key non-cell autonomous tumour suppressor mechanism.

## 1.4 Innate immune signalling and senescence

### 1.4.1 Innate immune sensors

The innate immune system is a major contributor to inflammation induced by tissue damage or infection (Akira et al., 2006). Innate pattern recognition receptors (PRRs) are present not just on innate immune cells but are widely expressed on epithelial cells, endothelial cells and fibroblasts alike (Kawasaki and Kawai, 2014; Takeuchi and Akira, 2010). PRRs function to sense the presence of microorganisms via the recognition of so-called pathogen-associated molecular patterns (PAMPs) and sense the presence of tissue damage via the recognition of damage-associated molecular patterns (DAMPs) (Takeuchi and Akira, 2010). Four classical PRR families have been described including transmembrane Toll-like receptors (TLRs) and C-type lectin receptors (CLRs), and cytoplasmic Retinoic acid-inducible gene (RIG)-I-like receptors (RLRs) and NOD-like receptors (NLRs). cGAS-STING DNA sensing, inflammasome activation and TLRs are key innate immune sensing pathways with recognised roles in senescence and cancer so will also be discussed in this section.

#### 1.4.1.1 cGAS-STING

cGAS is a cytoplasmic PRR that functions to recognise double-stranded DNA (dsDNA) (Sun et al., 2013). Upon binding with dsDNA, cGAS synthesises the second messenger 2'3'cyclic GMP-AMP (cGAMP) which engages STING (synthase linked to stimulator of interferon genes) (Ablasser et al., 2013) and subsequently leads to the expression of type 1 interferons (Sun et al., 2013). Exogenous sources of dsDNA (for example from microorganisms) can therefore provoke necessary inflammatory responses to help control microbial infections (Ishikawa and Barber, 2008). However, endogenous sources of dsDNA can also contribute to cGAS-STING activation. For example, altered DNA metabolism due to genetic defects (Crow and Manel, 2015; Gao et al., 2015; Gray et al., 2015) and stress induced mitochondrial outer membrane polarisation (MOMP) can provide endogenous sources of nucleic acids which activate cGAS-STING signalling. Stress induced MOMP can occur in a minority of mitochondria (so called 'minority MOMP') (Ichim et al., 2015) which is insufficient to trigger apoptosis but can result in genomic instability, caspase-activated DNase (CAD) dependent DNA damage and mitochondrial DNA release (Riley et al., 2018), which can in turn activate cGAS-STING signalling (Bock and Tait, 2020; West et al., 2015). Lastly, cytoplasmic DNA (so called cytoplasmic chromatin fragments – CCF) released during senescence can also activate cGAS-STING signalling (See chapter 1.4.2) (Dou et al., 2017; Gluck et al., 2017).

#### 1.4.1.2 Inflammasome activation

Inflammasomes are multimeric signalling complexes that function to regulate pro-IL1β/pro-IL18 cleavage by activated Caspase-1 (Figure 1.3) (Howard et al., 1991; Martinon et al., 2002). Activation of inflammasomes is a key function of the innate immune response to pathogens and tissue damage and this process involves several PRRs which have roles as components of the inflammasome (including NLRs) and primers of inflammasome activation (TLRs) (Guo et al., 2015). The typical priming event prior to canonical inflammasome activation is LPS binding to TLR4 with subsequent NF-κB signalling activation and upregulation of inflammasome scaffolding proteins and pro-IL1β. Once primed, inflammasome activation occurs in response to direct binding/sensing of stimuli by inflammasome components (for example NLRs or AIM2) which subsequently coalesce with other inflammasome components such as apoptosis-associated speck like protein containing a CARD (ASC) to recruit and activate pro-Caspase 1 through CARD-CARD interactions (Martinon et al., 2002; Srinivasula et al., 2002) and subsequent autoproteolytic cleavage (Yang et al., 1998). The resulting cleavage of pro-IL-1β/pro-IL-18 by active Caspase-1 then results in activation of IL-1β/IL-18 signalling which mediate the downstream effects of inflammasome activation.

**Figure 1.3: Inflammasome priming and activation.** Schematic showing the main mechanisms mediating inflammasome priming and activation.

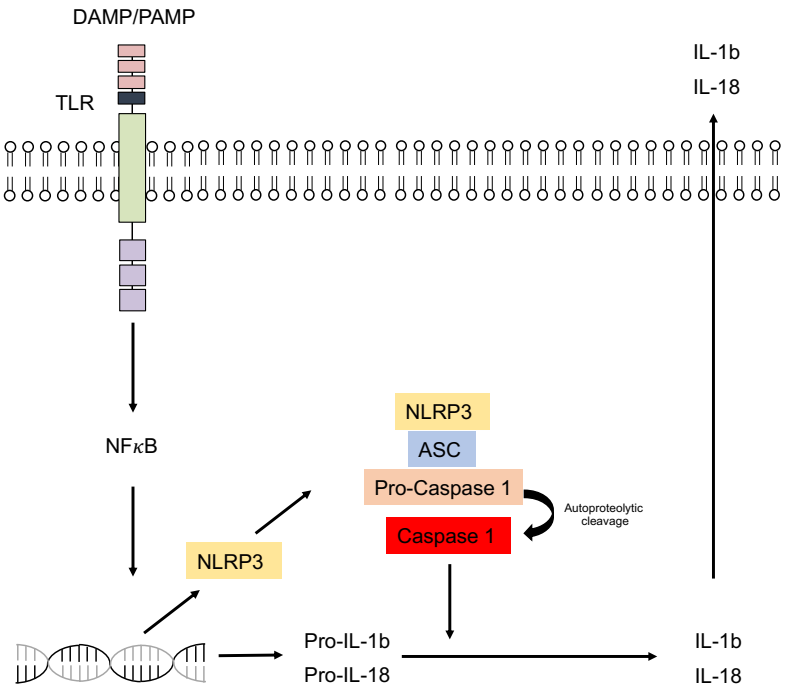


### 1.4.1.3 Toll-like receptors

TLRs are perhaps the most well-characterised PRR family and 10 different TLRs have been described in humans. The localisation of different TLRs is tailored to the type of ligand they recognise. For example, cell membrane TLRs (1, 2, 4, 5, 6 and 10) bind lipids and proteins, whereas cytoplasmic/endosomal TLRs (3, 7, 8 and 9) bind nucleic acids (Rakoff-Nahoum and Medzhitov, 2009). More specifically, lipopolysaccharide (a major component of the gram-negative bacterial cell wall) is the main ligand for TLR4, whereas endolysosomal TLR3 senses the presence of viral dsRNA (Takeuchi and Akira, 2010). The common TLR structure contains three main parts: 1. N-terminal leucine rich repeats (LRRs), 2. A transmembrane region

and 3. A cytoplasmic Toll-IL-1R homology (TIR) domain (Jezierska et al., 2011) (see Figure 1.3).

**Figure 1.4: Toll-like receptor structure.** Schematic representation of the common structure of Toll-like receptors.

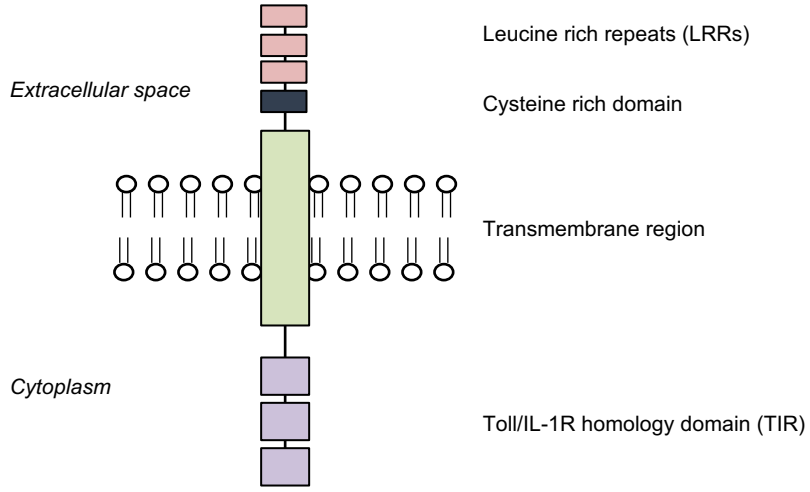


Signalling downstream of TLR activation is complex. While several common features exist, receptor activation and downstream signalling does differ between TLR subtypes (Akira et al., 2006). For the purpose of this section TLR2 signalling will be described in detail (see Figure 1.4). TLR2 senses various microorganismal lipoproteins including those from bacteria (for example lipoteichoic acid, peptidoglycan and lipopeptides), mycoplasma (diacyl lipoproteins), fungi (glucuronoxylomannan and phospholipomannan) and viruses (glycoprotein B and hepatitis B/C proteins) (Oliveira-Nascimento et al., 2012; Takeuchi and Akira, 2010). Upon ligand binding to TLR2 it forms a heterodimer with either TLR1 or TLR6, or the less well studied TLR10 (Oliveira-Nascimento et al., 2012). TLR1/2 complexes recognise triacyl

lipoproteins whereas TLR6/TLR2 complexes recognise diacyl lipoproteins (Oliveira-Nascimento et al., 2012; Takeuchi and Akira, 2010). Subsequent signalling is mostly mediated via the common adaptor molecule MyD88 which is recruited to the TLR complex. The binding of MyD88 promotes the binding of IL-1 receptor-associated kinase (IRAK) 4 and 1 with TNF-$\alpha$ associated factor 6 (TRAF6). The IRAK-TRAF6 complex dissociates from the TLR and interacts with a complex formed by TGF-$\beta$-activated kinase (TAK1), TAK1-binding protein-1 (TAB1) and TAB2. Cytoplasmic TAK1 activation leads to the activation of I$\kappa$B kinase kinases (IKKs) that phosphorylate I$\kappa$B leading to their degradation. The degradation of I$\kappa$B releases NF-$\kappa$B, which then translocates to the nucleus where it induces the transcription of several inflammatory cytokine/chemokines (Jezierska et al., 2011). Similarly, TAK1 also activates MAPK cascades leading to the activation of AP-1 which contributes to further cytokine expression (Takeuchi and Akira, 2010).

**Figure 1.5: Toll-like receptor 2 (TLR2) signalling.** TLR2 signalling is dependent on the adaptor protein MyD88 and converges on activation of the transcription factors NF-κB and MAPK.

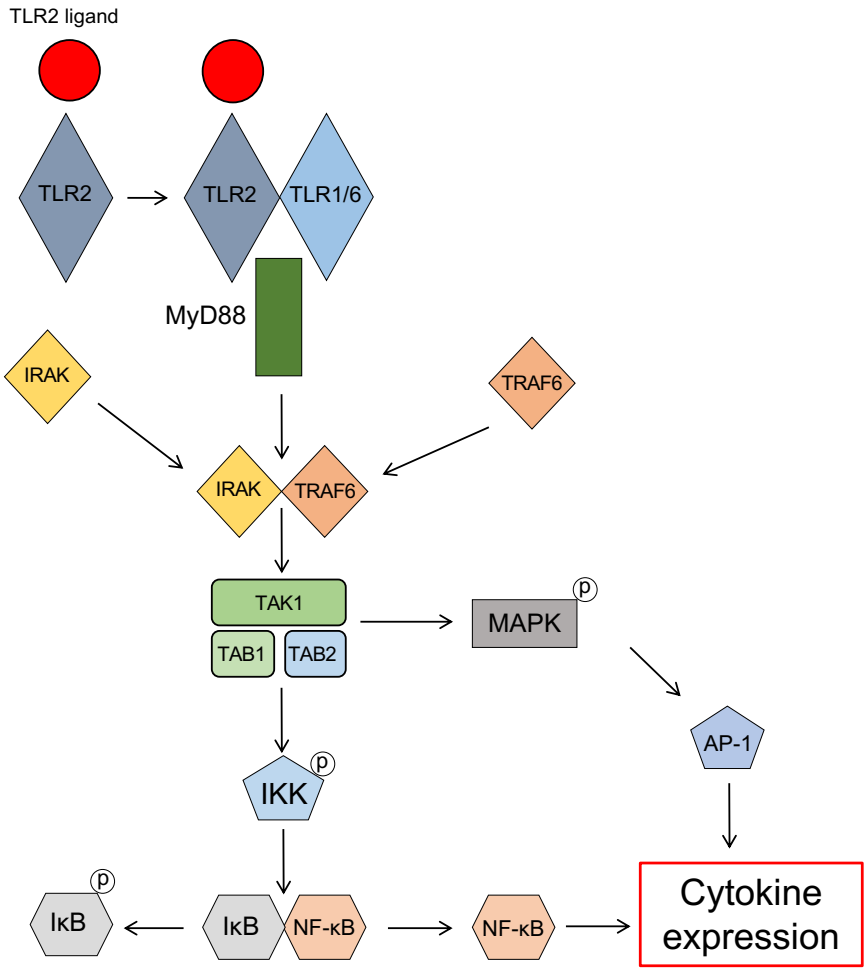


### 1.4.2 Innate immune sensors in senescence

The primary evolutionary role of innate immune sensors is as our first line of defence against microbial infections. However, cellular stress of any source also leads to their activation and therefore serendipitously innate immune sensors appear to play a key role in the senescence response.

#### 1.4.2.1 cGAS-STING and senescence

During senescence chromatin is release into the cytoplasm due to aberrant DNA replication (Dou et al., 2015; Ivanov et al., 2013) and downregulation of DNase2 and the exonuclease TREX1 during senescence leads to further cytoplasmic accumulation of nuclear DNA (Takahashi et al., 2018). These cytoplasmic chromatin fragments (CCFs) and DNA are sensed by cGAS via topoisomerase 1-DNA covalent cleavage complex (TOP1cc) (Zhao et al., 2020), subsequently activating cGAS-STING signalling that in turn regulates expression of the SASP (Dou et al., 2017; Gluck et al., 2017; Takahashi et al., 2018). Furthermore, cGAS regulates senescence itself, as irradiation induced expression of *Cdkn2a* was markedly impaired in *cGAS* and *STING* deficient mice and exogenously expressed oncogenic *Nras* ($Nras^{G12V}$) induced expression of SA-β-gal to a lesser extent in *cGAS* null mice (Gluck et al., 2017). *cGAS* (Gluck et al., 2017) and *STING* deficient mice (Dou et al., 2017) have impaired immune surveillance of $Nras^{G12V}$ expressing senescent hepatocytes, resulting in the formation of invasive hepatocellular carcinomas (Dou et al., 2017). Thus, cGAS-STING signalling is an integral regulator of OIS and the SASP in the context of DNA damage and genomic instability and therefore constitutes a potent tumour suppressor mechanism. However, these studies examining immune surveillance used global KO cGAS/STING mice, therefore cGAS/STING loss in immune cell populations cannot be excluded as a contributing factor to the observed phenotype. cGAS-STING DNA sensing has also been shown to be integral in other forms of senescence. The activation of retrotransposable elements

(RTEs) with aging and replicative senescence induces the expression of senescence and interferon-1 (IFN-1) signalling, a response that is dependent on cGAS-STING mediated sensing of LINE-1 cDNA (the only human RTE capable of autonomous retrotransposition) (De Cecco et al., 2019). Other intracellular DNA sensors may also contribute to the senescence response. Knockdown of the DNA sensor gamma-interferon-inducible protein 16 (IFI16) (Unterholzner et al., 2010) also delays the onset of cellular senescence in human diploid fibroblasts (Duan et al., 2011).

#### 1.4.2.2 Inflammasome signalling and senescence

It has been shown that inflammasome mediated IL-1 signalling controls the SASP, whereby IL-1$\alpha$/IL-1$\beta$ signalling via IL-1 receptor (IL-1R) triggers additional amplifying feedback loops involving other pro-inflammatory SASP components (Acosta et al., 2013). IL-1$\beta$ signalling via the canonical inflammasome has also recently been implicated in mediating the radiation induced anti-tumour immune response (Han et al., 2021). These data further supported the theory that PRRs are involved in OIS and the SASP and anti-tumour responses more generally. However, the mechanisms regulating inflammasome priming in OIS were as yet unclear. Subsequently, the Acosta lab characterised a precise role for immune sensing via TLR2 in the regulation of oncogene-induced senescence (OIS) and expression of the SASP (Hari et al., 2019), suggesting that TLR2 is involved in inflammasome priming in the context of OIS (see section 1.4.2.3).

#### 1.4.2.3 Toll-like receptors and senescence

The first report of TLR2 being involved in senescence in the context of cancer came from Lin et al (Lin et al., 2013) who observed that genetic deletion of *Tlr2* increases sensitivity of mice to tumour formation in diethylnitrosamine (DEN) induced hepatocellular carcinoma models. This was associated with impaired p21 and p16 dependent senescence and impaired pro-inflammatory signalling pathway activation (including NF-κB/MAPK signalling and reduced TNF-α, IFN-γ, IL-1α, IL-1β, IL-6 and Cxcl-2 expression). *Tlr2* null liver tumours also had significantly reduced infiltration of $F4/80^+$ macrophages (Lin et al., 2013), however it was not determined whether this represented impaired recruitment of circulating monocytes or tissues resident macrophage populations.

The Acosta lab subsequently confirmed TLR2 as a key regulator of senescence. Using human diploid fibroblasts retrovirally transduced with an inducible oncogenic *RAS* transgene (ER:RAS IMR-90 cells, see chapter 1.5.1), it was observed that *TLR2* expression increased following oncogene activation, and this was necessary for the senescence associated growth arrest and expression of the SASP. Furthermore, acute-phase serum amyloid A 1 and 2 (A-SAA1/2) proteins were identified as key senescence-associated DAMPs that are sensed by TLR2 after oncogenic stress and regulate the SASP via TLR2 (Hari et al., 2019). This process was downstream of cGAS-STING signalling, as knockdown of cGAS or STING strongly impaired transcriptional activation of *TLR2* and *SAA* during OIS, and activation of cGAS-STING signalling induced *TLR2* and *SAA* expression

(Hari et al., 2019). TLR2 has also been shown to regulate senescence in other contexts including replicative senescence and therapy-induced senescence (Hari et al., 2019) and has recently been shown to regulate senescence and SASP expression in degenerating human intervertebral disc cells from chronic back pain patients (Mannarino et al., 2021). Furthermore, *Tlr2* has been shown to regulate tubular epithelial cell senescence in *Glis2* knockout mouse models of nephronophthisis (Jin et al., 2020) and in renal injury models (Jin et al., 2019b). Therefore, several studies have identified TLR2 as a regulator of senescence, both in malignant and non-malignant contexts.

Other TLR's have also been linked to senescence. The chromatin binding factor high mobility group box 1 (HMGB1) is predominantly a nuclear protein, however senescent cells actively transport nuclear HMGB1 and release it into the extracellular space where it can stimulate IL-6 expression via TLR4 (Davalos et al., 2013), suggesting TLR4 stimulation is also required for optimal SASP expression. Furthermore, repeated lipopolysaccharide (LPS) stimulation of TLR4 can induce activation of p53-p21 signalling and enhance SA-β-gal expression in dental pulp stem cells (DPSCs) (Feng et al., 2018). RIG-1 regulates the expression of IL-6 and IL-8 in senescent human umbilical vein endothelial cells (HUVECs), signalling via the ataxia telangiectasia mutated – interferon regulatory factor 1 (ATM-IRF1) pathway (Liu et al., 2011), suggesting a regulatory role for RLRs in expression of the SASP.

### 1.4.3 Toll-like receptors in cancer

High pan TLR expression is associated with improved overall survival in human lung cancer (Bauer et al., 2017) and Tlr4 deficiency promotes lung tumour development in mouse models of lung adenocarcinoma (Bauer et al., 2005). Furthermore, several TLR agonist have been shown to have protective effects in various malignant contexts in both mice and humans (Ghochikyan et al., 2014; Smith et al., 2014; Wang et al., 2015; Wang et al., 2010; Weihrauch et al., 2015; Zhang et al., 2011b). Attenuated Bacillus Calmette-Guerin (BCG), first developed as a tuberculosis vaccine, is a TLR2/TLR4 ligand that is approved for the treatment of bladder cancer (Morales et al., 1976) and the TLR7 agonist Imiquimod is an approved therapy for skin basal cell carcinomas (Bubna, 2015). The mechanisms of action are not fully understood but involve both cell intrinsic effects (for example due to infection by BCG (Fuge et al., 2015), or induction of apoptosis by imiquimod (Bubna, 2015)) and by boosting the anti-tumour immune response (Bubna, 2015; Fuge et al., 2015). However, several TLRs have also been associated with worse outcomes in cancer (Urban-Wojciuk et al., 2019). Altered localisation and over activation of cell membrane TLRs (including 2, 4 and 5) leads to chronic inflammation and tumour progression in oesophageal and oral malignancies (Jouhi et al., 2014). Therefore, the precise function of TLRs is wide ranging and dependent of both TLR and tumour subtype. More specifically, Tlr2 activity has been shown to mediate tumour regression in mouse models of cancer. Tlr2 signalling is integral to an effective anti-tumour immune response in mouse models of glioblastoma

multiforme (GBM) (Curtin et al., 2009). High-mobility-group box 1 (HMGB1) released from necrotic tumour cells acts as a Tlr2 ligand in GBM infiltrated bone marrow derived dendritic cells, thus activating a robust anti-tumour response. A synthetic bacterial lipoprotein and TLR1/TLR2 agonist was also shown to induce tumour regression in subcutaneous tumour implantation models using lung, melanoma and leukaemia cancer cell lines, an effect shown to be mediated via reduced activity of regulatory T-cells and enhanced activity of cytotoxic T-cells (Zhang et al., 2011b). TLR ligands (including those of TLR2) used in conjunction with interferons have been shown to induce M1 polarization of macrophages boosting their anti-tumour response *in vitro* (Muller et al., 2017; Müller et al., 2018). Besides activation of anti-tumour immune responses, cell autonomous functions also appear to be important. *Tlr2* null mice develop significantly more and larger colorectal tumours in colitis induced colorectal cancer with an associated dysregulated epithelial immune response (Lowe et al., 2010). These tumours develop earlier and grow larger, suggesting that both initial barriers to malignant transformation and growth restriction mechanisms are impaired. Dysregulated OIS may well explain this effect. While multiple TLRs have been shown to have a role in lung cancer, no such defined role has yet been described for TLR2 (Yang et al., 2014).

## 1.5 Models of senescence

### 1.5.1 *In vitro* models of senescence

Serial passaging of non-transformed cells was the model system first used to discover and describe senescence (Hayflick and Moorhead, 1961), and this approach is used to this day to study replicative senescence in a variety of non-transformed cell types. *In vitro* systems provide easy means to study tumour suppressor activation via traditional cellular biology techniques. Furthermore, study of conditioned media allows the analysis of secreted factors following the induction of senescence. Culture of cell lines can be used to study other forms of senescence including senescence induced by DNA damaging agents (such as etoposide), radiation or oxidative stress. Furthermore, non-genotoxic inducers such as CDK4/6 inhibitors (Palbociclib) or MDM2 inhibitors (Nutlin3a) can also be easily applied to induce senescence in this setting. Viral transduction of oncogenic *KRAS* in human fibroblasts was the first model used to describe and study OIS (O'Brien et al., 1986). Subsequent models involving retroviral transduction of an activated *HRAS* allele ($HRAS^{GV12}$) into primary human diploid fibroblasts (IMR90) and murine and rat cell lines were developed to further characterise OIS and the SASP (Coppe et al., 2008b; Serrano et al., 1997). An *in vitro* model allowing conditional activation of $HRAS^{G12V}$ in IMR90 fibroblasts was subsequently developed allowing further refinement of *RAS* induced senescence models (Innes and Gil, 2019). This was achieved by retrovirally infecting IMR90 fibroblasts with a tamoxifen inducible oncogenic $HRAS^{G12V}$ construct (ER:RAS), therefore allowing temporal control of oncogene activation in

otherwise non-transformed normal cells. These cells recapitulate several classical aspects of senescence including a robust growth arrest mediated by INK4/ARF and p53-p21 pathways, and secretion of a pro-inflammatory SASP (Innes and Gil, 2019). Similar to the models first described by Seranno and colleagues (Serrano et al., 1997), ER:RAS IMR90 fibroblasts have also used to characterise the SASP and other features of OIS (Acosta et al., 2013; Acosta et al., 2008; Barradas et al., 2009). As discussed in chapter 1.3.1 senescent fibroblasts (induced by a variety of methods described above) have been used to study the effect of the SASP in tumour development, both *in vitro* and *in vivo* (Bavik et al., 2006; Coppe et al., 2008a; Coppe et al., 2006; Krtolica et al., 2001; Lawrenson et al., 2010; Parrinello et al., 2005). While this approach offers significant mechanistic insight into the function of pro-inflammatory signalling in tumour progression, it offers little physiological relevance for the function of the SASP at the inception of malignant transformation.

Historically, fibroblast cell models have mostly been used to study senescence *in vitro* (Hayflick and Moorhead, 1961; Serrano et al., 1997), however epithelial cell lines have also been used to study the role of senescence in different disease contexts including chronic kidney disease (Small et al., 2012) and pulmonary fibrosis (Minagawa et al., 2011) and epithelial cancer cell lines are frequently used to study therapy induced senescence (Ewald et al., 2010).

### 1.5.2 *In vivo* models of senescence

Senescence prone mice (so called senescence-accelerated mouse-prone – SAMP models) are often used to study senescence and aging phenotypes *in vivo* (Beck et al., 2020). SAMP mice develop several age-associated pathologies including neurological deficits with pathological hallmarks akin to Alzheimer's disease (Morley et al., 2012) (such as astrogliosis, neurodegeneration (Karasawa et al., 1997) and hyperphosphorylation of tau (Canudas et al., 2005)), osteoporosis (Silva et al., 2002), retinal degeneration (Feng et al., 2016) and myocardial fibrosis (Karuppagounder et al., 2017) amongst others. These models are used to study organismal senescence/aging rather than cellular senescence itself. While organismal aging is associated with increased cellular senescence in several cell types, the two processes are not mutually inclusive (Beck et al., 2020).

As discussed in detail in chapter 1.2.2 several cancer mouse models exhibit senescence in pre-malignant tumours, permitting the study of OIS *in vivo*. For example, prostate specific ablation of the tumour suppressor *Pten* results in pre-malignant prostatic lesions that have been used to study senescence in early prostate cancer (Chen et al., 2005) and oncogenic *Kras* activation has been used to study senescence in lung and pancreatic premalignancies (Collado et al., 2005). Other methods of inducing oncogene activation exist that do not require the formation of overt tumours to induce senescence. One such model is ectopic expression of oncogenic *Nras* ($Nras^{G12V}$) via hydrodynamic delivery of $Nras^{G12V}$ expressing transposable

elements into mouse hepatocytes (Carlson et al., 2005). With intact tumour suppressor pathways, these hepatocytes exhibit key features of senescence and express a SASP within six days of oncogene delivery. Therefore, this model has been used extensively to study regulators of OIS and the SASP (Dou et al., 2017; Gluck et al., 2017; Goncalves et al., 2021; Kang et al., 2011).

Mice lacking key mediators of senescence such as p16, p53 or p21 have also been used to study the role of senescence *in vivo*, both in malignant and non-malignant settings. For example, p53 or p21 null mice have been used to identify critical roles for these pathways in physiological/developmental senescence and in the promotion of premature ageing (Benson et al., 2009; Munoz-Espin et al., 2013; Varela et al., 2005; Xu et al., 1998) and p16 knockout mice have also been used to study the role of senescence in post-ischaemic renal fibrosis (Lee et al., 2012a).

The $p16^{LUC}$ mouse model developed by the Sharpless lab permitted the longitudinal tracking of senescent cell accumulation with aging and several forms of preneoplasia (Burd et al., 2013). This was achieved by knocking in a firefly luciferase construct targeted to the translational start site of the endogenous p16 locus, therefore allowing longitudinal tracking of p16 expression *in vivo* by bioluminescence imaging. Moreover, other models have been developed to allow not only the tracking of senescent cells *in vivo* but also to allow selective removal of senescent cells to study how this affects disease trajectory. The p16-3MR mouse model is one such model which has been used to characterise the role of senescent cells in wound

healing (Demaria et al., 2014). The 3MR (trimodality reporter) fusion protein contains functional synthetic luciferase, red fluorescent protein (RFP) and truncated herpes simplex virus 1 thymidine kinase (HSV-TK) and is driven by the p16 promoter. Therefore, senescent p16 expressing cells in the p16-3MR mouse also express luciferase (allowing *in vivo* bioluminescence imaging of senescence), RFP (allowing sorting senescent cells from tissues) and HSV-TK (allowing selective killing by the administration of the HSV-TK high affinity nucleoside analogue ganciclovir) (Demaria et al., 2014). The *INK-ATTAC* transgenic mouse also permits selective removal of p16 expressing senescent cells (Baker et al., 2011). Caspase 8 is a key mediator of the extrinsic apoptosis pathway and the ATTAC construct (targeted apoptosis through activation of caspase 8) expresses a membrane bound FK506-binding protein-Caspase 8 (FKBP-Casp8) fusion protein tagged with green fluorescent protein (GFP) (Baker et al., 2011). The administration of a synthetic drug (AP20187) induces dimerization and subsequent activation of membrane bound FKBP-Casp8 and therefore induces apoptosis. This construct is also driven by the p16 promoter, allowing identification/sorting of senescent cells via GFP expression and selective killing via administration of AP20187 (Baker et al., 2011). This mouse model was used to show that clearance of p16 expressing senescent cells delays the onset of several age associated pathologies and increases median lifespan (Baker et al., 2016; Baker et al., 2011).

Due to the wide range of contexts where senescence is important, a wide range of models are required to study senescence *in vivo*. Several such

models are available and have significantly advanced the understanding of senescence in several non-malignant and malignant disease processes.

## 1.6 Lung cancer

### 1.6.1 Clinical background

Lung cancer is the most lethal cancer type worldwide, with a mortality rate greater than breast, colorectal and prostate cancer combined (Siegel et al., 2020). Non-small cell lung cancer (NSCLC) is the predominant subtype, accounting for approximately 88% of cases, whereas the more aggressive small cell lung cancer (SCLC) accounts for the remainder of cases (Physicians, 2016). The differentiation between these two main subtypes is of immense importance when considering treatment options (as discussed in chapter 1.6.6). Lung adenocarcinoma (LUAD) and lung squamous carcinoma (LUSC) are the most common histological subtypes of NSCLC (Molina et al., 2008) and histological distinction between these subtypes has traditionally been the mainstay of deciding appropriate treatment options (see table 1.3). While distinction between LUAD and LUSC is still very important, due to recent advances in immunotherapy and targeted therapies against identifiable driver oncogenes (for example *EGFR* mutations or translocated *ALK*), the molecular characterisation of lung tumours has become increasingly important when deciding optimal treatment regimens (Camidge et al., 2012; Gandhi et al., 2018; Mok et al., 2009; Reck et al., 2016). All major subtypes of lung cancer are associated with cigarette smoking,

however this causative relationship is stronger with LUSC and SCLC than with LUAD. LUAD is therefore the most common lung cancer in never smokers (Sun et al., 2007) which is most common in women and in East Asia. The reason for this is unclear however is thought to be associated with environmental exposures (second hand smoke, pollution, occupational exposures) and due to inherited genetic factors (Alberg et al., 2013; Hackshaw et al., 1997; Vineis et al., 2005). Early-stage NSCLC is amenable to curative treatment with surgery with/without adjuvant therapy. As a result, early-stage disease is associated with a favourable 5-year survival rate of over 50% (Goldstraw et al., 2016). However, due to the asymptomatic nature of early-stage disease, the majority of patients present with advanced-stage disease no longer suitable for surgical resection resulting in a 5-year survival rate of just 6% (Goldstraw et al., 2016). The recent advances outlined above have improved outcomes in a small subset of NSCLC patients (Camidge et al., 2012; Gandhi et al., 2018; Mok et al., 2009; Reck et al., 2016). However, due to the low frequency of targetable mutations and the inevitable emergence of resistance and disease relapse, overall outcomes are still very poor. Therefore, to improve overall lung cancer survival, it is clear that we must understand and target early-stage disease.

**Table 1.4**: Pathological features of the two main subtypes of non-small cell lung cancer: lung adenocarcinoma and lung squamous carcinoma.

| Subtype | Adenocarcinoma | Squamous carcinoma |
|---|---|---|
| **Cell of origin** | AT2 cells, club cells | Airway basal cells |
| **Pathology** | Acinar/tubular structure<br>Mucin production | Keratinisation<br>Intercellular bridges |
| **Histological markers** | TTF-1 +/- Napsin A | p40, CK5/6, p63 |
| **Location** | Peripheral>central | Central>peripheral |

### 1.6.2 Biology of non-small cell lung cancer

The most common genetic mutations in NSCLC are summarised in table 1.4. *KRAS* mutations are the most frequently mutated oncogene in LUAD (Cancer Genome Atlas Research, 2014) and are present across all stages of disease suggesting their importance as early drivers of malignant transformation as well as progression (Chen et al., 2019). *TP53* mutations are also common in LUAD (Cancer Genome Atlas Research, 2014) and tend to occur in more advanced lesions (Chen et al., 2019), suggesting that mutation in *TP53* is an important step during lesion progression to invasion. *EGFR* mutational frequency differs significantly depending on region and ethnicity and is currently the most common activating oncogene in East Asia (Gazdar, 2014). Mutations in *EGFR* and *KRAS* tend to be mutually exclusive as they are involved in the same signalling pathway, however they can co-exist and *KRAS* mutations may cause resistance to EGFR inhibitors (Pao et

al., 2005). Tumours driven by targetable point mutations affecting genes such as *EGFR*, *ROS1* or *ALK* rearrangements tend to have lower genetic diversity as these tend to occur in non/light smokers. On the contrary, tumours in smokers tends to have a significantly greater mutations load and be driven by non-targetable mutations such as those in *KRAS* or *TP53* (Cancer Genome Atlas Research, 2014; Ding et al., 2008). Unlike in LUAD, targetable point mutations rarely occur in LUSC (Reck and Rabe, 2017). Similarly, *KRAS* mutations are rare in LUSC and LUSC lesions are commonly driven by mutations in *TP53* and *CDKN2A* (Cancer Genome Atlas Research, 2012; Teixeira et al., 2019). In LUSC, *CDKN2A* can be inactivated by a variety of mechanisms including epigenetic silencing, homozygous deletion, inactivating mutations and exon skipping (Herbst et al., 2018)

**Table 1.5**: Main genetic mutations found in lung adenocarcinoma and lung squamous carcinoma. Data from Herbst et al (Herbst et al., 2018).

| | **Adenocarcinoma** | **Squamous carcinoma** |
|---|---|---|
| **Oncogenes** | KRAS (32%), EGFR (27%) | KRAS (3%), EGFR (<9%) |
| **Tumour suppressor genes** | TP53 (46%), KEAP1 (19%), STK11 (17%), NF1 (11%) | TP53 (90%), CDKN2A (70%) |

Lung cancer is a genetically heterogenous disease with complex biology. Tumours are typically composed of different subpopulations of cells

resulting in intra-tumoural heterogeneity (Herbst et al., 2018; Zhang et al., 2014). Large subclonal fractions are what underlie the almost inevitable relapse after the use of targeted therapies which only target the dominant subclone (Engelman et al., 2007; Turke et al., 2010), but also account for increased relapse after surgery (Zhang et al., 2014) suggesting that subclonal diversity also drives early metastasis during tumour development.

### 1.6.3 Early-stage NSCLC pathobiology

LUSC lesions are believed to originate from large airway basal cells (Hynds and Janes, 2017), therefore typically (but certainly not exclusively) arise from the large airways where they were previously thought to undergo stepwise progression from mild/moderate dysplasia to severe dysplasia/carcinoma-in-situ prior to forming invasive cancer (Figure 1.5) (Nicholson et al., 2001).

**Figure 1.6**: **Lung squamous carcinogenesis.** Figure demonstrating the previously assumed linear stepwise progression of preinvasive lung squamous carcinoma lesions to invasive malignancy.

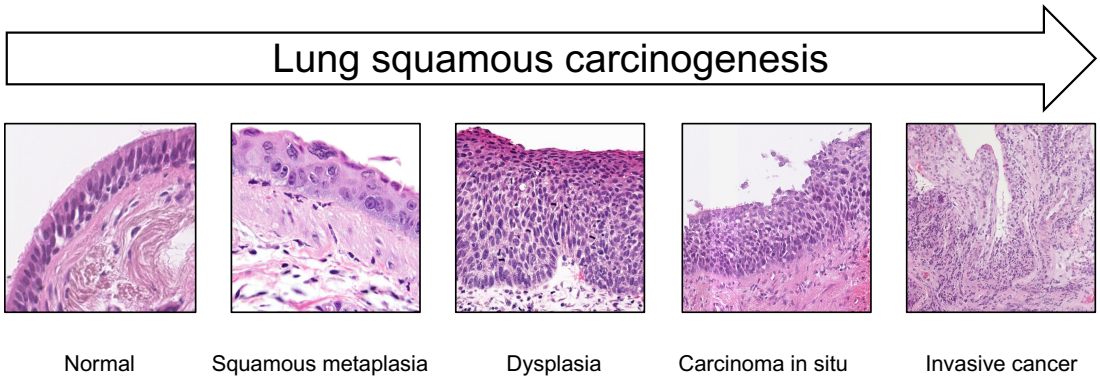

The often-proximal location of preinvasive LUSC lesions makes this process easy to study as these lesions are amenable to repeated bronchoscopic surveillance and biopsy (Teixeira et al., 2019). While LUSC lesion progression was initially defined as a linear, one way process (Figure 1.5), longitudinal follow up revealed that not all preinvasive LUSC lesions progress to invasive cancer, and in fact up to one third regress back to normal epithelium (Figure 1.6) (Jeremy George et al., 2007).

**Figure 1.7**: **Lung squamous cell cancer progression and regression.** Only 50% of squamous carcinoma in situ lesions progress to invasive cancer, and up to 30% regress back to normal epithelium.

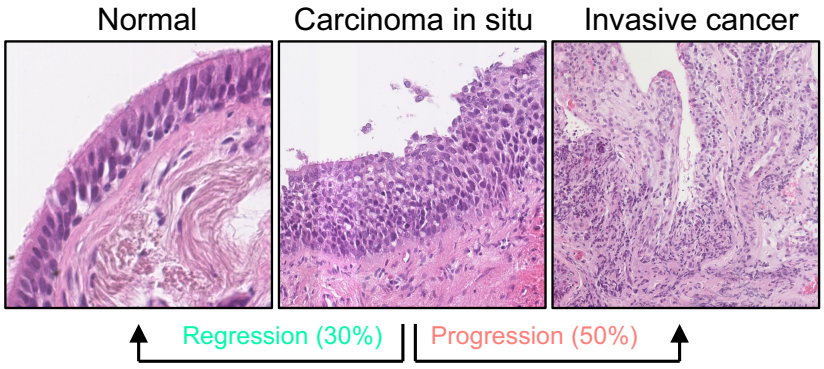


The progression of preinvasive LUAD is less well studied, as these lesions are typically found at the lung periphery owing to the peripherally situated cells of origin (AT2 cells or club cells (Ferone et al., 2020)). It has been proposed that LUAD lesions evolve from areas of atypical adenomatous hyperplasia (AAH) which progress to adenocarcinoma-in-situ (AIS), then to minimally invasive adenocarcinoma (MIA) then eventually invasive LUAD (Figure 1.7) (Lee et al., 2012b).

**Figure 1.8**: **Lung adenocarcinoma carcinogenesis.** Lung adenocarcinoma lesions progress from adenocarcinoma in situ (AIS), to minimally invasive adenocarcinoma (MIA) then finally invasive lung adenocarcinoma (LUAD). Key pathological features of these lesions are outlined below.

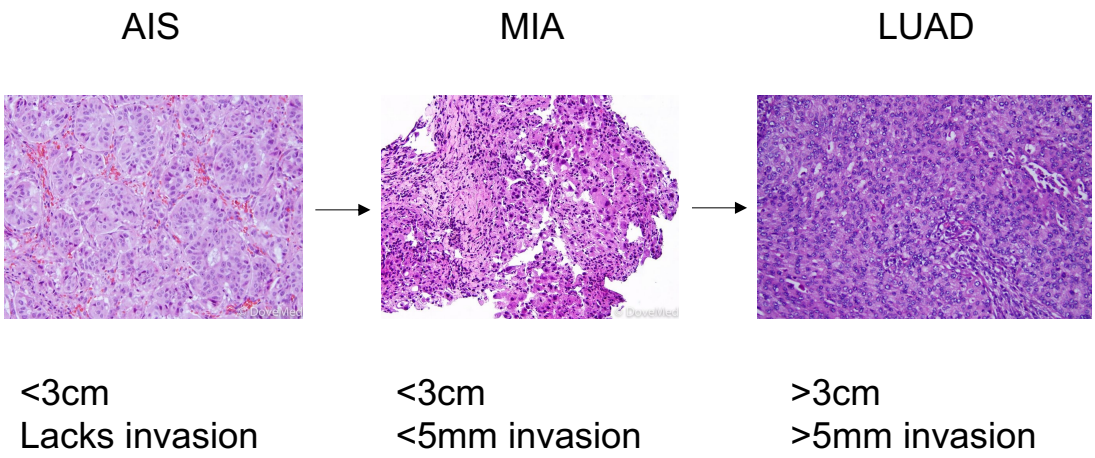


These lesions are asymptomatic and typically are detected incidentally as a solitary pulmonary nodule on computed tomography (CT) scans (Hiramatsu et al., 2008). However, surgical resection is often not indicated in the first instance as this appearance can represent several other benign pathologies (such as infection or inflammation). Furthermore, the diagnostic yield of biopsy is low in small nodules, especially in those with predominant sub-solid components (Chen et al., 2018). Therefore, the management of these LUAD precursor lesions is complex, mediated not least by the inability to reliably define their existence.

### 1.6.4 Non-small cell lung cancer and immune surveillance

Immune surveillance is rife in preinvasive LUSC lesions. Immune sensing involving T-cells and myeloid cells peaks in high grade preinvasive LUSC lesions, and activation of immunosuppressive signatures promote invasion via immune escape mechanisms (Mascaux et al., 2019). Furthermore, clinical regression of LUSC lesions has been shown to be, at least in part, mediated via $CD8^+$ T-cell mediated immune surveillance (Pennycuick et al., 2020).

Immune surveillance also occurs early in LUAD lesions prior to invasion (Zhang et al., 2019). Human leukocyte antigen (HLA) loss of heterozygosity (LOH) is a potential immune escape mechanism in lung cancer (McGranahan et al., 2017) and HLA LOH (predominantly involving chromosome 6p) is observed at increasing frequency in advanced LUAD in comparison to precursor lesions (Chen et al., 2019), suggesting that HLA LOH and subsequent immune evasion promotes LUAD progression. Protein altering mutations create neoantigens, which are recognised by T-cells. Thus, a high neoantigen burden in advanced LUAD is associated with a T-cell rich inflamed tumour microenvironment (Herbst et al., 2018) and can confer susceptibility to immune checkpoint inhibition (McGranahan et al., 2016). In LUAD, macrophages make up the majority of the tumour immune infiltrate (Conway et al., 2016). The effect these have on tumour progression are unclear, with some studies linking high macrophage infiltration to poorer survival (Arenberg et al., 2000; Chen et al., 2003) and some showing no association with survival (Toomey et al., 2003). Subsequent studies

examining the abundance of macrophages within tumour islets (as opposed to stromal macrophages) found that increased abundance was associated with improved survival (Dai et al., 2010; Kim et al., 2008; Welsh et al., 2005). Thus, the tumour microenvironment of NSCLC is complex and its precise role in lung tumourigenesis is poorly defined.

### 1.6.5 Early diagnosis

The early diagnosis of lung cancer offers the best chance of cure and long term favourable clinical outcomes. Due to the difficulty in diagnosing malignant pulmonary nodules, current British Thoracic Society guidelines advocate CT surveillance for indeterminate pulmonary nodules (IPNs) that lack classic features of benign disease (for example calcification or peri-fissural location) and are too small for further evaluation with positron emission tomography (PET) scanning +/- biopsy (<8mm diameter or <300$mm^3$ volume) (Callister et al., 2015). This approach aims to monitor IPNs over time, with any observed growth prompting further investigation and surgical intervention. Pulmonary nodules are asymptomatic therefore patients with IPNs who end up undergoing CT surveillance are classically identified incidentally, leaving the vast majority of lung cancer patients to be diagnosed after symptom onset when curative treatment is often no longer available. This prompts the question: would screening at risk patients with CT scans help improve early detection and reduce overall lung cancer mortality? While the answer seems straightforward, it must be noted that national CT screening would require vast resources in terms of CT scanners, radiologists

and multi-disciplinary team follow up. Nonetheless, two large multicentre randomised clinical trials have demonstrated a clear mortality benefit with the use of low dose computed tomography (LDCT) screening in patients at high risk of lung cancer (de Koning et al., 2020; National Lung Screening Trial Research et al., 2011), prompting calls for LCDT screening to be implemented in the UK. Off the back of this, several implementation trials are already underway (Crosbie et al., 2019; Crosbie et al., 2020; Ruparel et al., 2020) and LDCT screening for lung cancer is likely to become standard practice in the UK within the next decade. This approach is not without its drawbacks; initial trials showed LDCT screening to have a high false positive rate, however this has since been improved with individual risk prediction models and standardised lung nodule follow up protocols. Nonetheless, false positives remain problematic and result in significant anxiety and potentially dangerous investigations in healthy patients. Furthermore, risk prediction tools used to assess an individual's suitability for screening can underestimate risk in certain patient demographics (Lebrett et al., 2020) and it has been reported that only one third of new lung cancer patients would have met eligibility criteria for LDCT screening (Wu et al., 2016). Therefore, further measures such as biomarkers could improve screening population selection and aid in the stratification of IPNs, greatly improving the efficacy of LDCT lung cancer screening.

### 1.6.6 Current treatment options

The most cost-effective intervention to improve lung cancer mortality is to eradicate the use of tobacco products, and this remains a key goal in the global fight against cancer. Policy measures that range from public health messaging, curbs on advertisements/branding and increased taxation go some way to prevents tobacco use. Furthermore, targeting nicotine addiction with replacement therapy, via e-cigarettes (Shahab et al., 2017) or through pharmacological administration of partial agonists of the nicotinic acetylcholine receptor (Hays and Ebbert, 2008) can help reduce tobacco use. Despite all this, the use of tobacco products is still high (and increasing in some developing countries) therefore lung cancer remains a significant burden on global health services. The main treatment options for SCLC and NSCLC are summarised in table 1.5. In the case of SCLC, platinum-based chemotherapy is the mainstay of treatment owing to the classically high mitotic index of small cell tumours and resultant sensitivity to chemotherapeutic agents (Murray and Turrisi, 2006; Socinski and Bogart, 2007). This can be in in conjunction with radiotherapy (Turrisi et al., 1999), however surgery is rarely a viable option (with the exception of very early-stage disease (Seidenfeld et al., 2006)). Relapse is common, making SCLC an aggressive, hard to treat lung malignancy with poor clinical outcomes. With regards to NSCLC, the mainstay of curative treatment is surgical resection, and this can be in conjunction with adjuvant chemotherapy or radiotherapy depending on tumour stage. The treatment of NSCLC has evolved from empirical use of chemotherapeutic agents and radiotherapy

towards personalised medicine, whereby treatment options are tailored to the genetic alterations and programmed death ligand-1 (PD-L1) status of a patient's tumour (Herbst et al., 2018). The identification of driver oncogenes has transformed the treatment of advanced LUAD (Camidge et al., 2012; Mok et al., 2009). For example, activating mutations in tyrosine kinase receptors including *EGFR*, *ALK* and *ROS1* (amongst others) can be targeted with tyrosine kinase inhibitors (TKIs) (Herbst et al., 2018). While actionable driver mutations are rarely detected in LUSC, precluding the use of TKIs in this context (Reck and Rabe, 2017), immunotherapy is often used in LUSC and LUAD dependent on tumour PD-L1 status (Herbst et al., 2018). PD-L1 is expressed by tumour cells and functions to dampen the tumour associated immune response by interacting with PD-L1 receptors on T-cells (Iwai et al., 2002). Blocking this interaction with antibodies (such as Pembrolizumab or Nivolumab) helps restore T-cell mediated antitumour immunity (Garon et al., 2015; Herbst et al., 2014; Topalian et al., 2012). These therapies are now a mainstay of treatment for advanced NSCLC.

**Table 1.6**: Table summarising treatment options of the two main subtypes of non-small cell lung cancer.

| Subtype | Small cell | Adenocarcinoma | Squamous carcinoma |
|---|---|---|---|
| **Surgery** | Rarely | Yes | Yes |
| **Chemotherapy** | Yes | Yes | Yes |
| **Radiotherapy** | Yes | Yes | Yes |
| **Targeted therapies** | No | Yes | No |
| **Immunotherapies** | No | Yes | Yes |

While surgical resection is the mainstay of early lung cancer treatment (Howington et al., 2013), certain patients are unable to undergo invasive surgery due to poor lung function, other medical co-morbidities or advanced age (Powell et al., 2013). For these patients less invasive therapies are required. Stereotactic ablative radiotherapy (SABR) has been shown to be effective for stage 1 lung cancer patients unable to undergo curative surgery (Ricardi et al., 2015) but this can also be met with significant side effects and is not suitable for centrally located tumours due to radiation associated damage to essential mediastinal structures. A potential role for local ablative therapies has emerged including percutaneous radiofrequency ablation (RFA), microwave ablation (MWA) and cryoablation (Hinshaw et al., 2014; Palussiere et al., 2017; Zhao et al., 2018). These approaches, while showing reasonable efficacy in the short term, are associated with poor long-term outcomes (Donington et al., 2012). Furthermore, pneumothorax rates (air leak into the pleural space due to lung rupture) are high (Li et al., 2018; Zhao

et al., 2018) which can be serious given that these techniques are reserved for multimorbid patents not fit for surgical intervention. Technical advances in bronchoscopy (including electromagnetic navigational bronchoscopy (Folch et al., 2019) and radial endobronchial ultrasound (radial EBUS) (Eberhardt et al., 2007; Steinfort et al., 2016)) has markedly improved bronchoscopic access to peripheral lung lesions, and up and coming technologies may even permit access to non-airway based lesions via bronchoscopic transparenchymal nodule access (BPTNA) bronchoscopy (Herth et al., 2015). Furthermore, the development of novel endobronchial optical fibre-based imaging technologies capable of differentiating between benign and malignant pulmonary nodules would add further diagnostic accuracy (Fernandes et al., 2021). This opens up wide possibilities in bronchoscopic ablation of early-stage lung cancer lesions, many of which are already under evaluation (Steinfort and Herth, 2020).

### 1.6.7 Modelling NSCLC in mice

The molecular characterisation of human lung cancer has identified a wide range of mutations associated with human disease (Cancer Genome Atlas Research, 2012, 2014). Yet the majority of our understanding of what drives lung tumour initiation has come from the study of genetically engineered mouse models (GEMMs) (Ferone et al., 2020). GEMMs allow for the highly reproducible development of lung tumours owing to controlled environmental conditions and spatial and temporal control of oncogene activation/tumour suppressor inhibition (Kwon and Berns, 2013).

Furthermore, GEMMs can provide reproducible phenotypic readout when genetic mutations of interest are introduced into specific cell lineages. In the case of human LUAD, the most frequently mutated oncogene is *KRAS* (Cancer Genome Atlas Research, 2014). *KRAS* belongs to the *RAS* superfamily of small GTPases (Wennerberg et al., 2005) and under physiological conditions is involved in signal transduction events regulating cell proliferation and survival including MAPK/ERK and PI3K pathways. The activity state of KRAS is dictated by high affinity binding to either GDP (inactive) or GTP (active). GTP binding is instigated following binding of growth factors to upstream receptors (for example EGFR) resulting in KRAS activation. Intrinsic enzymatic activity (resulting in terminal phosphate cleavage and conversion to GDP) and the activity of GTPase activating proteins (GAPs) result in inactivation of KRAS. Subsequently, inactive KRAS can bind to guanine nucleoside exchange factor (GEF) proteins, forcing the release of GDP, allowing subsequent binding to GTP and KRAS reactivation (Figure 1.8).

**Figure 1.9: RAS signalling.** Diagrammatic representation of the RAS signalling pathway.

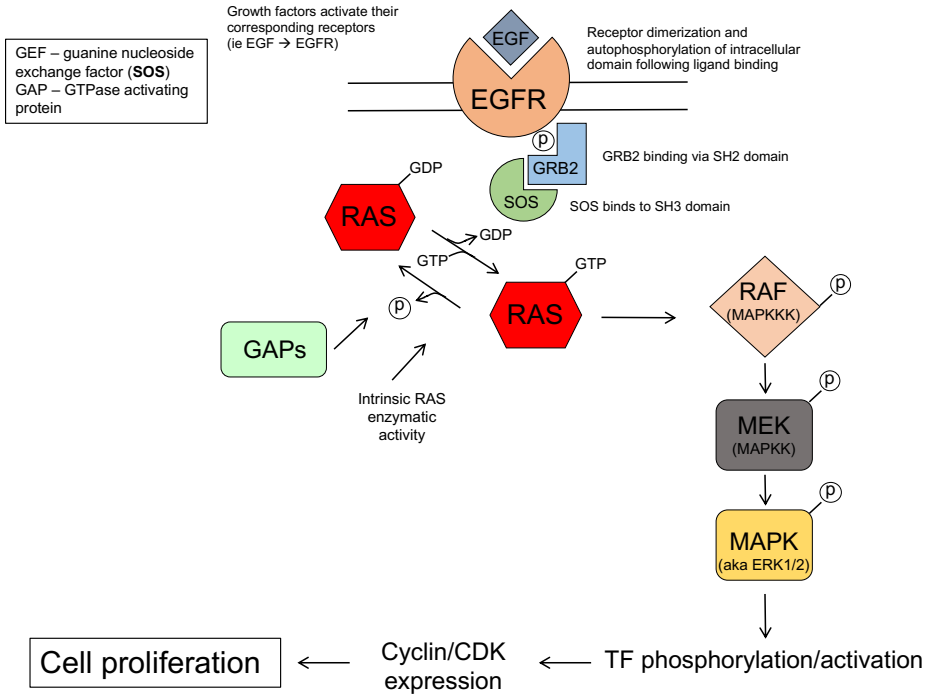


The most frequently observed point mutations in oncogenic *KRAS* involve codons 12 and 13 and result in reduced intrinsic enzymatic activity and therefore constitutive activation of KRAS signalling (Stolze et al., 2015). Thus, several GEMMs have been developed involving mutant $Kras^{G12D}$ or $Kras^{G12V}$ (amino acid substitution of glycine (G) at position 12 by an aspartic acid (D) or valine (V) respectively) in order to model human LUAD. The Jacks laboratory were integral in the generation of such models, with early models involving spontaneous whole animal activation of $Kras^{G12V}$ resulting in the formation of early onset lung tumours (Johnson et al., 2001). Subsequently the more widely used *LoxP-STOP-LoxP-*$Kras^{G12D}$ (hereafter $Kras^{LSL\text{-}G12D/+}$) was developed (Jackson et al., 2001) allowing lung specific

activation of *Kras*$^{G12D}$ following intranasal or intratracheal delivery of Cre-recombinase expressing viruses (Figure 1.9).

**Figure 1.10: The *Kras*$^{LSL\text{-}G12D}$ allele.** The *Kras*$^{LSL\text{-}G12D}$ allele consists of a STOP codon flanked by loxP sites upstream of the oncogenic *Kras*$^{G12D}$ allele. Following exposure to Cre-recombinase expressing viruses the STOP codon is removed resulting in constitutive activation of mutant *Kras*$^{G12D}$ signaling.

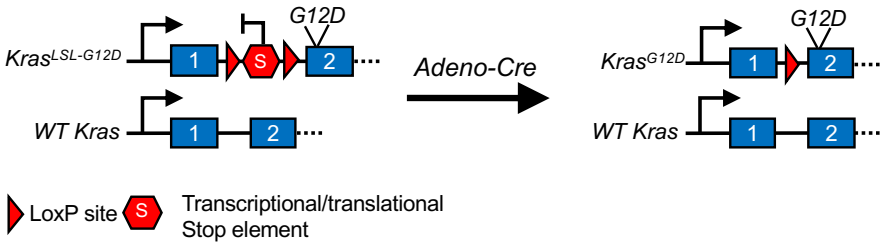


The most commonly used virus is an adenovirus expressing Cre under control of a constitutive CMV promoter (Ad5-CMV-Cre), however adenoviruses expressing Cre under the control of cell type specific promoters (for example the SPC promoter for AT2 cell and CC10 promoter for club cell specific *Kras*$^{G12D}$ activation) can further tailor this model and allow inferences to be made regarding the likely cell of origin of LUAD (Ferone et al., 2020; Jackson et al., 2001). Similar results can be obtained using Cre expressing lentiviruses (DuPage et al., 2009) and furthermore specific lentiviral constructs have been generated allowing the co-delivery of Cre and CRISPR/Cas9 machinery (allowing concurrent gene editing and somatic activation of *Kras*$^{G12D}$) (Sanchez-Rivera et al., 2014), and the delivery of T-cell antigens to heighten tumour immune responses (DuPage et al., 2011). The *Kras*$^{LSL\text{-}G12D}$ allele forms the basis of most GEMMs of LUAD and has

been used in conjunction with several other conditional alleles. For example, conditional mutant *Trp53* alleles are frequently used, either as homozygous 'floxed' alleles (*Trp53*$^{fl/fl}$ - LoxP sites flanking part of the coding sequence of the *Trp53* gene resulting in genetic inactivation of Trp53 signalling after exposure to Cre recombinase) or heterozygous LoxP-STOP-LoxP-*Trp53* point mutations that are found in inherited human diseases with high predisposition to tumour development (*Trp53*$^{R270H/+}$ and *Trp53*$^{R172H/+}$) (Olive et al., 2004). When the *Trp53*$^{fl/fl}$ allele is used in conjunction with the *Kras*$^{LSL-G12D}$ allele (*Kras*$^{LSL-G12D/+}$;*Trp53*$^{fl/fl}$) this is often referred to as the 'KP' mouse (see Figure 1.10).

**Figure 1.11: The 'KP' mouse model.** *Kras*$^{LSL-G12D/+}$;*Trp53*$^{fl/fl}$ mice not only harbour the *Kras*$^{LSL-G12D}$ allele but also loxP sites flanking the *Trp53* allele. Following exposure to Cre-recombinase the STOP codon is removed resulting in constitutive activation of mutant *Kras*$^{G12D}$ signaling and loss of *Trp53*.

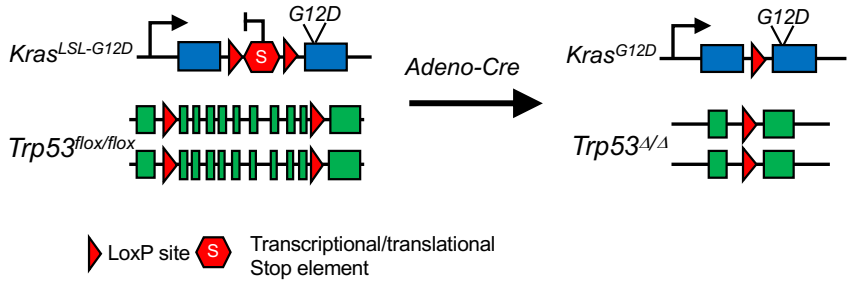


Interestingly, GEMMs with *Trp53* point mutations give rise to more advanced LUAD than those with *Trp53*$^{fl/fl}$ suggesting that these 'humanised' mutations have a greater impact on LUAD progression (Lang et al., 2004; Olive et al., 2004). Viral delivery of Cre-recombinase is not the sole method

of genetic activation (or inactivation) used in lung cancer GEMMs. Transgenic Cre-recombinase expression controlled by oestrogen receptor (ER) tagged tissue specific promoters (for example *SPC*$^{CreER}$) allow tissue specific genetic recombination following the addition of Tamoxifen (Lin et al., 2012). Furthermore, the tet-on/off system whereby alleles harbour tetracycline regulatory elements (TRE) that can either switch downstream gene expression on or off following stimulation with tetracycline derivatives (such as doxycycline) (Das et al., 2016), are also widely used. Similar GEMMs to those discussed above have been developed either separately or in conjunction with oncogenic *Kras* to study other genetic drivers of lung cancer, including *Pten* (Iwanaga et al., 2008; Yanagi et al., 2007), *EGFR* (Ji et al., 2006; Politi et al., 2006), *Braf* (Ji et al., 2007), *Rac1* (Kissil et al., 2007), *PI3K* (Engelman et al., 2008) and *Lkb1* (Nagaraj et al., 2017).

*KRAS* mutations are essentially absent in LUSC (Cancer Genome Atlas Research, 2012) therefore the above GEMMs are not suitable for modelling human LUSC. Overall GEMMs recapitulating human LUSC are less well developed than their LUAD counterparts. Nonetheless, GEMMs targeting LUSC associated driver mutations such as *Ikk*$\alpha$ (Xiao et al., 2013), *Sox2* (Ferone et al., 2016) and *Nkx2* (Camolotto et al., 2018) have been developed. Furthermore, LUSC formation can also be induced by topical application of chemical carcinogens such as intratracheal delivery of methyl carbamate (Nettesheim and Hammons, 1971) or cutaneous application of N-nitroso-methyl-bis-chloroethylurea or N-nitroso-methyl-tris-chloroethylurea (Rehm and Kelloff, 1991; Wang et al., 2004).

## 1.7 Thesis aims

OIS has been shown to be a key tumour suppressor mechanism *in vivo* including in models of early-stage lung cancer. The precise mechanisms regulating OIS and the SASP are not fully understood. However emerging evidence points to innate immune sensors, in particular TLR2, as regulators of this process. This thesis aims to build on existing *in vitro* evidence around the role of TLR2 as a regulator of this process and pursue the following three aims:

1. To investigate the role of *Tlr2* in the regulation of OIS and the SASP *in vivo*.
2. To determine whether TLR2 signalling is active in human NSCLC and whether it has a tumour suppressor function in this context.
3. To investigate the mechanism of *Tlr2* mediated tumour suppression in NSCLC using genetically engineered mouse models.

# 2 : Materials and Methods

## 2.1 *In vitro* experiments

### 2.1.1 Cell culture

Mouse embryonic fibroblasts (MEFs) and 293T cell lines were acquired from colleagues at the Institute of Genetics and Cancer (University of Edinburgh). 293T cells were cultured in Dulbecco's Modified Eagle's Medium – High glucose (DMEM; Sigma D5796) supplemented with 10% fetal calf serum and 1% antibiotic-antimycotic solution (Thermo Fisher, 15240062). MEFs were cultured in Dulbecco's Modified Eagle's Medium – High glucose/high pyruvate (Sigma 200092) supplemented with 10% fetal calf serum, 1% antibiotic-antimycotic solution (Thermo Fisher, 15240062) and 1% L-glutamine (Sigma, G7513). All cell lines were incubated in a 37$^{o}$C tissue culture incubator at 5% $CO_2$. Regular incubator decontamination was performed, and regular mycoplasma testing was performed on all cell lines. For passaging, cells were washed twice with phosphate buffered saline (PBS) and detached using 1ml of 0.05% trypsin (Thermo Fisher 25300-054). To allow full detachment, cells in trypsin solution were placed back into an incubator for up to 5 minutes, followed by neutralisation of trypsin with 9mls of serum containing media. A homogenous cell solution was obtained by repeated aspiration with a stripette prior to pelleting using a centrifuge at 1000rpm for 5 minutes. The cell pellet was resuspended in fresh media and cells were plated at a ratio between 1:4 to 1:8 of the original density. Cells

were frozen in 1ml of cell freezing media (normal cell culture media supplemented with 10% DMSO) in cryotubes on dry ice prior to storage at -80$^{o}$C or long-term storage in liquid nitrogen. Cells were thawed rapidly at 37$^{o}$C prior to resuspension into 9ml of normal cell culture media and centrifugation at 1000rpm for 5 minutes. Media/DMSO was discarded using an aspirator pipette and the cell pellet was resuspended and incubated as described above.

### 2.1.2 Western blotting

Cells were split and pelleted as described above and were resuspended in 1ml of cold PBS in a microcentrifuge tube prior to centrifuging at 10,000rpm for 5 minutes. PBS was aspirated and washed cell pellets were resuspended in between 50-200ul of a 1 x cell lysis buffer (20mM Tris-HCl (pH 7.5), 150mM NaCl, 1mM $Na_2EDTA$, 1mM EGTA, 1% triton, 2.5mM sodium pyrophosphate, 1mM $\beta$-glycerophosphate, 1mM $Na_3VO_4$, 1$\mu$g/ml leupeptin) (Cell signalling, 9803S) supplemented with cOmplete$^{TM}$ EDTA-free protease inhibitor cocktail solution (1 tablet per 10ml of cell extract, Roche, 04693159001). Samples were placed on ice for 10 minutes then centrifuged at 14,000rpm for 10 minutes at 4$^{o}$C. The supernatant was aspirated and placed in a new microcentrifuge tube on ice. Protein quantification was performed using a Bradford assay. Stock Bradford reagent (Biorad, 500-0006) was diluted at a ratio of 1:5 in $dH_2O$ to achieve an appropriate working concentration. Protein lysates were diluted 1:10 in cell lysis buffer. 2ul of bovine serum albumin (BSA) protein standards (Thermo

Fisher, 23208) and 2ul of diluted protein lysates were added to a 96-well plate in triplicate, prior to the addition of 198ul of working concentration Bradford reagent using a multichannel manual pipette. Absorbance at 595nm was measured using a multimode plate reader (TECAN Spark® 20M). Standard curve calculation was performed using linear regression and the resulting regression formula was used to calculate the sample protein concentration. The volume of sample with the required protein quantity (10-20μg) was calculated and mixed with equal volume of 2X Laemmli loading buffer (Alfa Aesar, J61042) and cell lysis buffer to make a final volume of 15-30ul (depending on gel size). The SDS-PAGE (sodium dodecyl sulphate-polyacrylamide gel electrophoresis) method was used to perform Western blotting experiments. Precast polyacrylamide Tris-Glycine gels were selected based on appropriate gel polyacrylamide percentages to achieve optimal separation of the target protein (based on target protein size). When there were multiple proteins were of interest, polyacrylamide percentage gradient gels were selected to achieve optimal separation of multiple proteins. Gels were opened, combs removed, wells carefully washed in $dH_2O$ and secured in place in a gel tank. The central chamber was filled with 1X SDS running buffer (NuPAGE™ MES SDS running buffer: 1M MES, 1M Tris base, 69.3mM SDS, 20.5mM EDTA, pH 7.3) to ensure there was no leak surrounding the gel. Samples were loaded carefully alongside 5ul of a colour pre-stained broad range protein standard ladder (NEB, P7719). Samples were then subjected to electrophoresis at 100-150V for 1-2 hours, until the loading dye reached the bottom of the gel and the protein ladder was fully

expanded. Following this, the gel was removed from the tank and the plastic cassette and placed in a tray with SDS running buffer. Semi-dry protein transfer was performed using the iBlot system (Invitrogen) to transfer gels onto a nitrocellulose membrane. The bottom anode component of the transfer stack (Invitrogen, IB301002) was placed in the iBlot and the gel was placed onto the nitrocellulose membrane. Transfer paper soaked in $dH_2O$ was placed on top of the gel followed by the top cathode component of the transfer stack. A blotting roller was used to remove bubbles and the sponge was placed in the lid of the iBlot. The iBlot was closed and Program P3 (20V for 7 minutes) was used to transfer all proteins. When the transfer was complete the stack was disassembled, and the membrane was cut to an appropriate size. Blocking was performed in TBS + 5% non-fat milk for 1 hour at room temperature prior to incubation in primary antibodies diluted in blocking buffer overnight at 4$^{o}$C on a rocker (see table 2.1 for primary antibody details). After three 10-minute washes with TBS + 0.1% tween the membranes were incubated with appropriate HRP-conjugated secondary antibodies (see table 2.1 for secondary antibody details) in blocking buffer for 1 hour at room temperature. Membranes were then washed a further three times for 10 minutes each prior to the addition of Enhanced Chemiluminescence (ECL) solution. Equal volume of ECL solution A + B were mixed and added to membrane that was placed within a plastic sleeve in an exposure cassette. They were incubated for 5 minutes prior to timed exposure with X-ray film and developed using an X-ray film processor.

**Table 2.1:** Antibodies used in western blotting

| REAGENT or RESOURCE | SOURCE | IDENTIFIER | DILUTION |
|---|---|---|---|
| **Mouse anti-TLR2** | Abcam | Ab108998 | 1:500 |
| **Anti-mouse HRP** | Sigma | A2554 | 1:10,000 |
| **Anti-β-actin-HRP** | Sigma | A3854 | 1:80,000 |

### 2.1.3 RNA extraction from cell pellets

RNA extraction from cell pellets was performed using the RNeasy plus mini kit according to manufacturer's instructions (Qiagen, 74134). Cell pellets were prepared as detailed above. 600ul of guanidine isothiocycanate containing lysis buffer (RLT buffer) was added to cell pellets and resuspended using a pipette. The contents were then added to a biopolymer-shredding spin-column (QIAshredder column, Qiagen, 79654) and centrifuged at 13,000rpm for 2 minutes to homogenise the tissue. Homogenised tissue was then placed into a gDNA eliminator spin column to remove DNA contaminants and centrifuged at 10,000rpm for 30 seconds. 600ul of 70% ethanol was added to the flowthrough and mixed with a pipette. Sample/ethanol mix was transferred into an RNeasy spin column and centrifuged for 10,000rpm for 15 seconds. The flowthrough was then discarded. 700ul of a guanidine salt/ethanol containing wash buffer (RW1 buffer) was added and centrifuged at 10,000rpm for 15 seconds to remove non-RNA biomolecules (for example carbohydrates, proteins and fatty acids). The flowthrough was again discarded. The sample was then washed with

500ul of a mild washing buffer (RPE buffer), centrifuged at 10,000rpm for 15 seconds to remove trace salts left from buffers used in previous steps. The flowthrough was again discarded. This last step was repeated then the RNeasy spin column was centrifuged for 1 minute to dry the column membrane. RNA elution was performed by the addition of 30-50ul RNAse free $H_2O$ directly onto the column membrane and placing the column in a fresh microcentrifuge tube to collect the eluate. The column/tube was then centrifuged at 10,000rpm for 1 minute. Sample quantification was then performed using a nanodrop 2000C, using RNase free water as the blank standard.

### 2.1.4 Reverse transcription quantitative real-time polymerase chain reaction (RT-qPCR)

cDNA was produced by reverse transcription of isolated RNA. 1ug of RNA was diluted to equal volumes in RNAse free water and mixed with 8ul of a reverse transcriptase (RT) containing mastermix (qScript cDNA SuperMix (Quantabio, 95048) containing qScript reverse transcriptase, reaction buffer with molecular grade $MgCl_2$, deoxyribonucleotide triphosphates (dNTPs), recombinant ribonuclease inhibitor protein, oligo(dT) primers and enzyme stabilizers). No RT controls consisted of RNA and RNAse free water only. These samples were briefly centrifuged and underwent cDNA synthesis using an Agilent SureCycler 8800 using the following cDNA synthesis programme:

5 min 25°C → 30 min 42°C → 5 min 85°C → ∞ 4°C

RT-qPCR primers were designed by myself, Dr Priya Hari and Dr Andrea Quintanilla using the NCBI 'Pick primers' tool (https://www.ncbi.nlm.nih.gov/tools/primer-blast/) (see table 2.2 for primer sequences), synthesised by Sigma and stored at -20°C at a stock concentration of 100uM. A Taq-polymerase containing mastermix was prepared consisting of SYBR Select (1X; Thermo Fisher, 4472908, containing AmpliTaq™ DNA polymerase, dNTPs and SYBR™ GreenER™ dye), forward primer (100nM), reverse primer (100nM) and RNase-free $H_2O$. 3.5ul of cDNA from each sample was added to a separate PCR tubes and then 66.5ul of the mastermix was added to each tube followed by vortexing and brief centrifugation. 20ul of the cDNA/mastermix was aliquoted into wells of an RNase-free 96 well plate (Star Lab, E1403-7700) in triplicate and centrifuged at 1600rpm for 5 minutes. qPCR was performed on the Applied Biosystems Plus Real-Time PCR system, using the following programme:

10 min 95°C → x40 cycles:

Denaturation 15s 95°C

Annealing 30s 60°C

Extension 15s 72°C

→15s 95°C

Using the StepOne software, a threshold cycle (Ct) was manually defined in the mid-linear phase of amplification and the mean Ct value was calculated from the triplicate wells. The relative expression of target genes was calculated by normalising to β actin using the formula $2^{-\Delta Ct}$.

**Table 2.2:** qPCR primer sequences

| Gene | Forward/Reverse | Target sequence |
|---|---|---|
| Tlr2 | Forward | CTAGAAGTGGAAAAGATGTCG |
| | Reverse | TAGCATCCTCTGAGATTTGAC |
| IL-1b | Forward | CCAAAAGATGAAGGGCTGCT |
| | Reverse | TCATCAGGACAGCCCAGGTC |
| IL-1a | Forward | AGGAGAGCCGGGTGACAGTA |
| | Reverse | TCAGAATCTTCCCGTTGCTTG |
| IL-6 | Forward | CAAGAAAGACAAAGCCAGAGTC |
| | Reverse | GAAATTGGGGTAGGAAGGAC |
| Arf | Forward | GCCGCACCGGAATCCT |
| | Reverse | TTGAGCAGAAGAGCTGCTACGT |
| Dcr2 | Forward | AGCTAACCCAGCCCATAATCGTC |
| | Reverse | AGTTCCCTTCTGACAGGTACTGGC |
| Cdkn1a (p21) | Forward | GTTCCGCACAGGAGCAAAGT |
| | Reverse | ACGGCGCAACTGCTCAC |
| β actin | Forward | TGTTACCAACTGGGACGACA |
| | Reverse | GGGGTGTTGAAGGTCTCAAA |

## 2.2 Hydrodynamic tail vein injection (HTVI) model

### 2.2.1 Plasmid preparation

Large quantities of transposon and transposase expressing plasmid was required to perform the HTVI technique, therefore plasmids were prepared using a Qiagen HiSpeed Plasmid Maxi kit according to manufacturer's instructions (Qiagen, 12663). Glycerol stocks were thawed, and small bacterial stabs were added to 150-250ml L-broth in a canonical flask supplemented with appropriate antibiotics at a dilution of 1:1000. These were incubated overnight in a shaking incubator at 37°C. Bacterial cells were harvested by centrifugation at 6000 *x g* for 15 minutes at 4°C. The bacterial pellet was resuspended in 10ml of resuspension buffer (buffer P1: 50mM TrisHCl pH 8.0, 10mM EDTA, 100μg/ml RNase A), prior to adding 10ml of lysis buffer (buffer P2: 200mM NaOH, 1% sodium dodecyl sulphate (SDS)). The solutions were mixed by repeated inversion and incubated at room temperature for 5 minutes. 10ml of chilled neutralisation buffer (buffer S3: 3.0M potassium acetate, pH 5.5) was added and mixed by repeated inversion. The lysate solution was transferred to a QIAfilter cartridge and incubated at room temperature for 10 minutes. During this incubation a HiSpeed Qiagen-tip was placed over an empty beaker and equilibrated with 10ml of equilibration buffer (buffer QBT: 750mM NaCl, 50mM 3-(N-morpholino)propane sulfonic acid (MOPS), pH 7.0, 15% isopropanol, 0.15% Triton X-100). The lysate was then added to the HiSpeed Qiagen-tip by inserting a syringe plunger into the QIAfilter cartridge over the HiSpeed Qiagen-tip. The lysate was allowed to enter the Qiagen-tip by gravity flow.

After the lysate had entered the resin of the HiSpeed Qiagen-tip the tip was washed with 60ml of wash buffer (buffer QC: 1.0M NaCl, 50mM MOPS, pH 7.0, 15% isopropanol). Plasmid DNA was eluted from the Qiagen-tip with 15ml of elution buffer (buffer QF: 1.25M NaCl, 50mM Tris-Cl, pH 8.5, 15% isopropanol) into a new falcon. 10.5ml of isopropanolol was added to the eluate and this was incubated for 5 minutes at room temperature to precipitate the DNA. The plunger was removed from a 30ml syringe and a QIAprecipitator module was attached to the syringe outlet nozzle. The eluate-isopropanolol mixture was added to the syringe and the plunger was replaced to force the mixture through the QIAprecipitator module under constant pressure, over a waste beaker. The plunger was again removed and 2ml 70% ethanol was added to the syringe, prior to re-inserting the plunger under constant pressure, to wash the DNA. The QIAprecipitator module was removed, and the plunger was pulled out. The QIAprecipitator module was reattached, and the plunger inserted to force air through the QIAprecipitor module. This was repeated several times to dry the module membrane. The plunger was removed from a 5ml syringe and the QIAprecipitator module was attached to the outlet nozzle and held over a 1.5ml microcentrifuge tube. 1ml of DNA solubilising buffer (buffer TE: 10mM Tris-Cl, pH 8.0, 1mM EDTA) was added to the syringe and the plunger inserted under constant pressure to elute the DNA into the 1.5ml microcentrifuge tube. The QIAprecipitator was removed then the plunger removed, and the QIAprecipitator reattached. The eluate was transferred from the tube back into the syringe using a pipette and the plunger re-

inserted for a second time over the same microcentrifuge tube, to ensure complete elution of plasmid DNA. DNA quantification was performed using a nanodrop 2000C, using buffer TE as the blank standard. Samples were then stored at -20$^{o}$C.

### 2.2.2 HTVI technique

Oncogenic *Nras* (pT3-*NRas*$^{G12V}$-IRES-GFP), effector loop mutant (pT3-NRas$^{G12V/D38A}$-IRES-GFP) and transposase expressing plasmids (CMV-SB13) were received from the Scott Lowe lab and transformed into NEB Stable Competent E. coli (NEB, C3040I). Plasmids were prepared with a maxi prep as detailed above. Mice of male or female sex over the age of 6 weeks were included in this study. Each mouse received 20ug of *Nras* transposon expressing plasmid and 6ug of transposase expressing plasmid, diluted in 0.9% NaCl to 10% of the animal's body weight (max 2.5ml). Mice were warmed in a heat box to encourage vasodilation and the appropriate volume of plasmid solution was injected into the lateral tail vein over 10 seconds. The large volume/speed of injection causes congestion of the right heart and subsequent reflux of plasmid rich solution down the hepatic vein and into the liver (see Figure 2.1). The high pressure causes endothelial damage and subsequent uptake of plasmid into hepatocytes. The transposase plasmid is transiently expressed, and the enzyme transposase targets the inverted repeat sequences that flank the transposon constructs and randomly inserts these constructs into the hepatocyte genome (see

Figure 2.2). This results in stable expression of transposon constructs within hepatocytes.

**Figure 2.1: Hydrodynamic tail vein injection technique.** The large volume/speed hydrodynamic tail vein injection causes right heart congestion and reflux of plasmid rich solution into the hepatic vasculature.

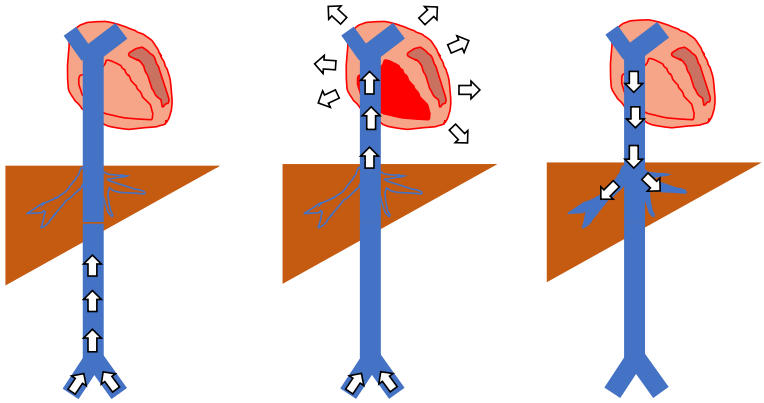

**Figure 2.2: Transposon and transposase constructs.** Transposon constructs are flanked with inverted repeats (IR) that are targeted by the transposase enzyme and randomly inserted into the murine hepatocyte genome.

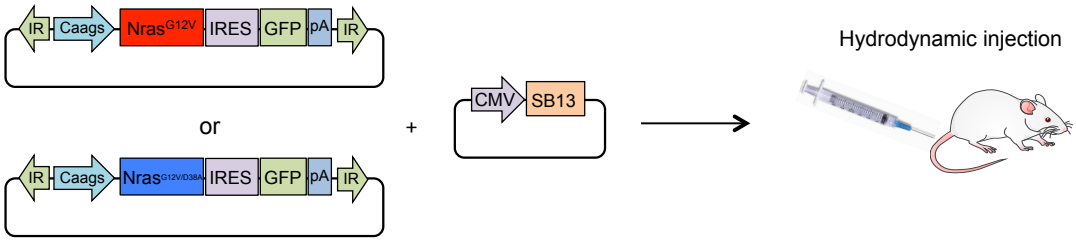


### 2.2.3 Tissue dissection and histology

Six days after HTVI, mice were culled humanely by cervical dislocation and exsanguination. The abdomens were opened and 1ml of sterile PBS was infused into the inferior vena cava, prior to laceration of the

splenic vein, to flush the liver of blood. Following this, the liver was dissected, and posterior lobes were snap frozen for RNA extraction. Large anterior lobes were placed immediately in 10% neutral buffered formalin (NBF) and incubated at room temperature overnight. The next day NBF was removed and replaced with 70% ethanol and samples were processed in a tissue processor the following day using graded ethanol, xylene and pressurised wax steps. Processed samples were then embedded in paraffin onto cutting blocks.

### 2.2.4 Immunohistochemistry

3-5um sections were cut onto positively charged microscope slides (Superfrost Plus, 10149870) from formalin fixed, paraffin embedded (FFPE) samples using a microtome, and incubated in a 60$^{o}$C oven for a minimum of 2 hours. Slides were de-waxed with two 5-minute incubations in xylene, then rehydrated with ethanol of decreasing concentrations (100%, 90%, 70%, 50%) for 1 minute each, followed by 5 minutes in d$H_2O$. For all primary antibodies (except F4/80) antigen retrieval was performed by immersing rehydrated slides in 10mM sodium citrate solution (pH6) and boiling in a microwave for 10 minutes. For F4/80 staining antigen retrieval was performed using proteinase K (20ug/ml in TE buffer (500mM Tris-HCl (pH 7.5), 1mM EDTA (pH 8.0), 5mM $CaCl_2$, 0.5% Triton X-100 pH 7.5)). Slides were then cooled under running water prior to blocking with 3% $H_2O_2$ solution for 10 minutes at room temperature. Slides were washed in PBS and mounted onto sequenza racks (Thermo Fisher, 73310017). Due to the use of

biotinylated secondary antibodies, endogenous biotin blocking was required. To do this, three drops of an avidin solution (Biolegend, SIG-31126) was applied to each slide and incubated for 15 minutes at room temperature. This was followed by three 5 minutes washes with PBS. Leftover avidin was then removed by applying three drops of biotin solution (Biolegend, SIG-31126) which binds any unbound avidin. This was again incubated for 15 minutes at room temperature, followed by three 5-minute PBS washes to remove all avidin and biotin. Three drops of a serum-free 0.5% Casein protein block (Abcam, ab64226) were added to each slide and incubated for 30 minutes at room temperature. During the incubation, primary antibody was diluted in a 0.05mol/L Tris-HCl 0.1% tween antibody diluent (Dako, S3022) at appropriate concentration (see table 2.3 for primary antibody details). After the blocking step, 120ul of primary antibody solution was added and incubated either for 1 hour at room temperature, or overnight at 4$^{o}$C. Following this, samples were washed three times with PBS for 5 minutes and biotinylated secondary antibody was diluted in antibody diluent and added to each sample (see table 2.3 for secondary antibody details) and incubated for 30 minutes at room temperature. After three 5-minute PBS washes, three drops of ready-to-use Streptavidin conjugated horseradish peroxidase (HRP) (Vector labs, PK-7100) was added to each sample and incubated for 30 minutes at room temperature. After a further three 5-minute washes with PBS, 3,3'-Diaminobenzidine (DAB) solution was made using a DAB substrate kit (Abcam, ab64238) by adding 1 drop of DAB chromogen to 1.5ml of hydrogen peroxide containing DAB substrate buffer. 120ul of this solution

was added to each slide for a maximum for 10 minutes (depending on staining intensity). Slides were then rinsed in PBS, removed from sequenza racks and transferred into a PBS containing glass dish. Counterstaining was performed with a 10 second incubation in Harris Haematoxylin, followed by washing in running water. Bluing of haematoxylin was performed with a 3-5 second incubation in saturated lithium carbonate solution. Samples were then dehydrated with 1-minute incubations in graded ethanol solutions of increasing concentration (30%, 50%, 80%, 100%) then cleared in 2 x 1 minute xylene incubations. Samples were then mounted using a xylene based mountant (DPX, CellPath, SEA-1304-00A) and a glass coverslip, then left to dry for a minimum of 1 hour.

**Table 2.3:** Antibodies used in mouse liver IHC

| REAGENT or RESOURCE | SOURCE | IDENTIFIER | DILUTION |
|---|---|---|---|
| **Mouse anti-p21** | BD biosciences | Cat #556431 | 1:200 |
| **Rabbit anti-IL-1 $\beta$** | Santa Cruz | sc-7884 | 1:50 |
| **Mouse anti-Nras** | Santa Cruz | sc-31 | 1:500 |
| **Rabbit anti-TLR2** | Invitrogen | PA5-20020 | 1:1000 |
| **Rat anti-F4/80** | Abcam | Ab6640 | 1:400 |
| **Rabbit anti-CD3** | Abcam | Ab5690 | 1:500 |
| **Biotinylated goat anti-mouse IgG** | Vector labs | Cat #BA9200 | 1:500 |
| **Biotinylated goat anti-rabbit IgG** | Vector labs | Cat #BA1000 | 1:500 |
| **Biotinylated goat anti-rat IgG** | Vector labs | Cat #BA9400 | 1:500 |

### 2.2.5 Immunofluorescence

3μm sections were prepared, dewaxed and rehydrated as described in 1.2.4. Antigen retrieval was performed using proteinase K (20ug/ml in TE buffer (500mM Tris-HCl (pH 7.5), 1mM EDTA (pH 8.0), 5mM $CaCl_2$, 0.5% Triton X-100 pH 7.5)). Slides were washed in PBS and permeabilisation was performed with a 0.1% Triton X-100 solution in PBS prior to incubation with primary antibodies (see table 2.4 for primary antibody details). Samples were then washed followed by incubation with appropriate fluorophore conjugated secondary antibodies (see table 2.4 for secondary antibody details). Samples

were then washed, stained with DAPI and mounted with Vectashield®. Samples were imaged using a confocal microscope using NIS-Elements software (Nikon).

**Table 2.4:** Antibodies used in mouse liver immunofluorescence

| REAGENT or RESOURCE | SOURCE | IDENTIFIER | DILUTION |
|---|---|---|---|
| **Mouse anti-Nras** | Santa Cruz | sc-31 | 1:500 |
| **Rat anti-F4/80** | Abcam | Ab6640 | 1:400 |
| **Goat anti-mouse AF488** | ThermoFisher | A11029 | 1:500 |
| **Goat anti-rat AF594** | ThermoFisher | A11007 | 1:500 |

### 2.2.6 Sudan black staining

Sudan black staining was performed using a biotinylated Sudan Black B chemical reagent (SenTraGor (GL13), Pan Biotech, AR8850020). FFPE tissue section were cut, dewaxed, rehydrated and blocked as described in chapter 2.2.4. Following blocking steps, slides were washed in 50% ethanol for 5 minutes, then 70% ethanol for a further 5 minutes. After this, one drop of filtered SenTraGor reagent was placed onto a cover slip then the microscope slide containing the sample was placed on top with the sample facing down and incubated for 8 minutes at room temperature. The glass coverslip was removed, and excess reagent was removed with tissue paper soaked in 70% ethanol. Samples were then incubated in 50% ethanol for 5 minutes. This was repeated for a total of 4 times, followed by 2 washes in PBS (1 x 30 seconds, 1 x 5 minutes) followed by a 5-minute wash in PBS

supplemented with 0.5% Triton X-100. Sample were finally washed in PBS for a further 5 minutes prior to incubation with an anti-biotin primary antibody (Abcam, ab201341) diluted in antibody diluent 1:200 overnight at 4$^{o}$C. Samples were then washed three times with PBS for 5 minutes, then incubated with HRP-conjugated secondary antibody (Vector, PI-2000) diluted in antibody diluent 1:500, for 1 hour at room temperature. Samples were then washed, and signal was revealed with DAB, counterstained and mounted as described in chapter 2.2.4.

### 2.2.7 Immunohistochemistry image analysis

Immunohistochemistry (IHC) slides were imaged using the Hamamatsu Nanozoomer XR microscope with NDP scan v3.1 software. IHC quantification (positive cell detection) was performed using QuPath software v0.2.3 using predefined RGB parameters for haematoxylin and DAB detection.

### 2.2.8 RNA extraction from tissue

Snap frozen liver tissue was used to isolate RNA. Using a scalpel, small fragments of frozen tissue were cut and placed into a 2ml microcentrifuge tube. A small metal ball bearing was placed into each tube with 1ml of Trizol reagent (Thermo Fisher, 15596026). The tubes containing tissue, ball bearing and trizole were then placed into a bead mill tissue homogeniser (TissueLyser LT , Qiagen, 85600) for 3 minutes. Samples were removed from the homogeniser, inverted then put back into the homogeniser

for a further 3 minutes. 200μl of chloroform was added (Sigma, 67-66-3) and the resulting mixture was centrifuged at 12,000rpm for 15 minutes. The RNA layer (clear top layer) was then aspirated carefully with a pipette and placed in a new 1.5ml microcentrifuge tube. Sample volume of 100% isopropanolol was added to the sample then the resulting mixture was added to a Qiagen RNeasy spin column. The column was centrifuged at 10,000rpm for 15 seconds and the flowthrough discarded. Following this, sequential washing with RW1 and RPE buffer, elution, RNA quantification, cDNA conversion and RT-qPCR was performed as detailed in chapter 2.1.3.

### 2.2.9 Plasmid cloning

In order to perform longitudinal *in vivo* imaging, we cloned a luciferase construct in place of GFP into the pT3-NRas$^{G12V}$-IRES-GFP transposon plasmid. Cloning design was performed with Dr Andrea Quintanilla. The MSCV-IRES-Luciferase plasmid was received from the Scott Lowe lab via addgene (plasmid #18760). Compatible unique restriction sites were identified – AvrII within the IRES sequence and AgeI after the GFP stop codon. DNA samples (transposon plasmid and luciferase plasmid) were mixed with 10X Cutsmart buffer (NEB, B7204S), AvrII (NEB, R0174) and AgeI – high fidelity (NEB, R3552) restriction enzymes and made up to 50ul with nuclease free $H_2O$. This mixture was incubated at 37$^oC$ for 15 minutes. Vector and insert DNA purification was performed by electrophoresis on an agarose gel. A 3% agarose gel, supplemented with SYBR safe DNA dye (Thermo Fisher, S33102), was placed into an electrophoresis chamber (Bio-

Rad PowerPac) and immersed in 1X Tris-acetate-EDTA buffer (TAE buffer: 40mM Tris, 20mM acetic acid, 1mM EDTA). DNA samples were mixed with 10X orange G dye and loaded into separate wells with 1KB and 100bp DNA ladders alongside them. The electrophoresis cell was run at 100V for approximately 20 minutes, until clear and separate bands of appropriate size were visible under a blue light transilluminator. Bands were cut with a scalpel and put into a clean 1.5ml microcentrifuge tube. DNA gel extraction was performed using a QIAquick Gel extraction kit (Qiagen, 28704). 3 x sample volume of solubilisation and binding buffer (QG buffer: 5.5M guanidine thiocyanate, 20mM Tris HCl pH7.5) was added to the tube and incubated at 50$^{o}$C for 10 minutes (or until all the gel had dissolved). 1 x sample volume of isopropanolol was added and the resulting mixture was added to the affinity column and centrifuged at 10,000rpm for 30 seconds. The flowthrough was discarded and the sample washed with 750ul of wash buffer (PE buffer: 10mM Tris-HCl pH7.5, 80% ethanol) twice. 36ul of elution buffer (QF buffer: 1.25M NaCl, 50mM MOPS pH7.0, 15% isopropanol) was added directly onto the filter membrane and incubated at room temperature for 3 minutes. This was then centrifuged at 10,000rpm for 30 seconds in a clean microcentrifuge tube to collect the eluate. DNA was then quantified using a nanodrop. Ligation was performed using T4 ligase by mixing 10X T4 DNA ligase buffer (NEB, B0202S), T4 DNA ligase (NEB, M0202S), DNA (at a ratio of 1:3 vector:insert) made up to 20ul with nuclease free $H_2O$. The mixture was mixed by gently flicking the tube and incubated at room temperature for 2 hours. Transformation was performed by adding 10ul of ligation mixture with

a thawed tube of Stable E.coli (NEB, C3040H), on ice for 30 minutes. Heat shock was performed by incubating the mixture at 42$^{o}$C for 30 seconds, then placing it back on ice for a further 5 minutes. 950μl of super optimal broth (SOC) media (thermo fisher, 15544034) was added to the mixture and incubated at 30$^{o}$C for 1 hour in a shaking incubator. During this incubation an lysogeny broth (LB) plate was warmed at 30$^{o}$C. After 1 hour, 100μl of the mixture was plated onto the pre-warmed LB plate and incubated at 30$^{o}$C overnight. Colonies were picked using a sterile pipette tip, streaked onto a predefined section of a new LB plate and placed directly into separate vials of a colony PCR plate filled with 1ml per vial of LB broth supplemented with ampicillin (1:1000). The new LB plate was incubated at 30$^{o}$C for a further 24 hours to be used to isolate positive colonies. The colony PCR plate was sealed and submitted for plasmid mini-prep and sequencing using the following primers:

F/W primer: acgagcattcctaggggtctttcc
R/V primer: aagatcgccgtgtaattctaaccggtag

Sequencing data was analysed using serial cloner software (v2.6.1) and positive colonies were identified and picked from the new LB plate. Positive colonies were grown, and plasmid was purified as described in chapter 2.2.1.

### 2.2.10 *In vivo* bioluminescence imaging

HTVI was performed as described in chapter 2.2.2 with the Luciferase tagged oncogenic *Nras* transposon (pT3-NRas$^{G12V}$-IRES-Luc). D-luciferin (PerkinElmer #122799) was dissolved in Dulbecco's PBS without calcium or magnesium (Thermo Fisher, 14190144) to achieve a concentration of 15mg/ml and filtered using a 0.2um syringe filter. D-luciferin solution was administered subcutaneously at a dose of 150mg/kg, resulting in an injection volume of 0.1ml/10g of body weight. Mice were then anaesthetised with isofluorane and oxygen at 200-300ml/min with 2-3% isofluorane in an induction chamber. Once mice were anaesthetised, they were placed on a tray with nose apertures to allow continuous administration of inhaled anaesthetic. To improve signal acquisition mouse abdomens were shaved prior to imaging. They were then placed inside an IVIS Lumina S5 *in vivo* imaging system (IVIS®) to image the bioluminescence signal. Optimal time to imaging was determined using a kinetic curve. Regions of interest (ROI) were set automatically, and count data was converted to radiance (photon flux) to allow quantitation and accurate comparison of images taken on different days. Following signal acquisition, mice were removed from the IVIS and allowed to recover in a heat box set to 30$^{o}$C. Photon flux for each ROI was recorded and signal was measured weekly to monitor clearance of *Nras$^{G12V}$* expressing hepatocytes.

## 2.3 Lung cancer model

### 2.3.1 Intranasal administration technique

Mice heterozygous for the conditional oncogenic *Kras* allele (*Kras*$^{LSL\text{-}G12D/+}$) +/- a homozygous floxed *Trp53* allele (*Kras*$^{LSL\text{-}G12D/+}$;*Trp53*$^{fl/fl}$) were used in this thesis. A STOP codon flanked by loxP sites is upstream of the oncogenic *Kras*$^{G12D}$ allele and loxP sites flank the *Trp53* allele, therefore following intranasal administration of Cre-recombinase expressing adenovirus (Ad5-CMV-Cre, University of Iowa, Viral Vector Core Facility) lung epithelial specific activation of *Kras*$^{G12D}$ +/- *Trp53* deletion occurs, and tumour formation is initiated (see Figure 1.10). Male or female mice of 8-12 weeks of age were included in this study. Mice were anaesthetised with an intraperitoneal injection of medetomidine/ketamine (6μl/g of body weight of a solution containing 20mg/ml ketamine (Zoetis, 40018605) and 0.05mg/ml metdetomidine (Orion Pharma, 134811-4) suspended in sterile 0.9% NaCl). Once mice were suitably anaesthetised they were intranasally inoculated with 40μl of virus solution (1.5x10^7 plaque forming units (PFU) of Ad5-CMV-Cre, suspended in minimum essential media (MEM) supplemented with 6mM $CaCl_2$). Following full inhalation, mice were given a 0.5ml subcutaneous injection of warmed 0.9% NaCl and their eyes were coated in lacrilube. They were then placed in a heat chamber set at 30$^{o}$C for 1 hour prior to reversal with Atipamezole (5μl/g of body weight of a solution containing 0.2mg/ml of Atipamezole (Orion Pharma, 134787-4) suspended in sterile 0.9% NaCl). Mice were then kept in the heated chamber until fully recovered.

### 2.3.2 Delivery of drug via nebulisation

To delivery drug via nebulisation, up to eight mice were placed inside a nebulisation chamber connected to a nebuliser (Philips Respironics, 4446A). 100μg of Pam2CSK4 was suspended in 3mls of 0.9% NaCl and placed into the nebuliser. The nebuliser was then driven by oxygen from a concentrator at a flow rate of 6L per minute allowing aerosolization of drug and entry into the nebuliser chamber (see figure 2.3). The nebulisation chamber was kept in a ventilated sterile tissue culture hood throughout. Different nebulisers were used to deliver control (0.9% NaCl only) and drug, to avoid cross contamination. Mice were closely monitored during and for at least 1 hour after the procedure to monitor for adverse effects. This was repeated weekly up to 10 weeks.

**Figure 2.3: Nebulised drug delivery.** Mice were placed in a chamber externally connected to a nebuliser, into which drug (Pam2CSK4) or placebo (0.9% NaCl) was placed and driven by oxygen from and $O_2$ concentrator.

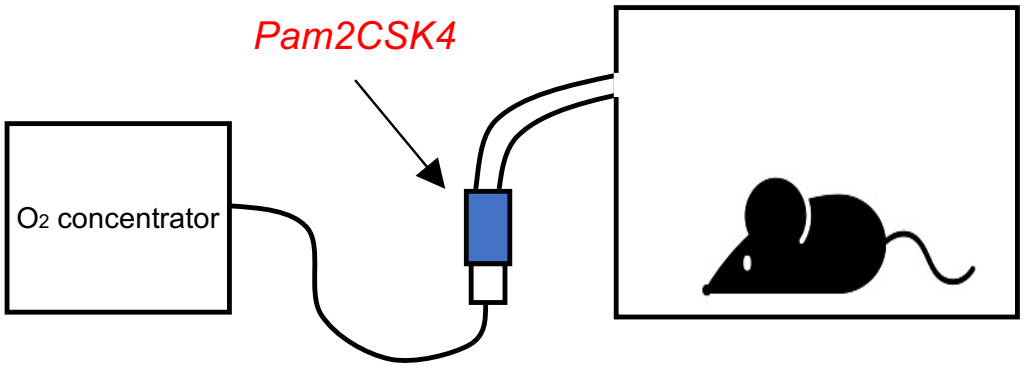

### 2.3.3 Delivery of drug via intranasal inoculation

Mice were anaesthetised as described in chapter 2.3.1 prior to intranasal inoculation of 100ng of recombinant IL1α/IL1β diluted in sterile PBS. Following inoculation mice were recovered as described in chapter 2.3.1 and monitored closely for adverse effects for up to 4 hours after dosing.

### 2.3.4 Dissection and tissue processing

At specified time points, mice were culled humanely by cervical dislocation and exsanguination. The trachea was identified and sutured at the proximal end and the lungs were inflated with 0.5ml of NBF. The lungs were then dissected, and the trachea cut distal to the suture, and the lungs were placed in NBF overnight at room temperature. The following day NBF was replaced with 70% ethanol solution and samples were submitted to the histology department for processing, paraffin embedding and haematoxylin and eosin (H&E) staining.

### 2.3.5 Immunohistochemistry

IHC protocols for lung tissue were as described in chapter 2.2.4 with the exception that for some assays (CD8 staining) biotinylated secondary antibodies were not required (see table 2.5 for antibodies used in mouse lung IHC). In these instances, avidin/biotin block was not required and HRP conjugated anti-rabbit polymer (Dako, K4003) was used prior to application of DAB.

**Table 2.5:** Antibodies used in mouse lung IHC

| REAGENT or RESOURCE | SOURCE | IDENTIFIER | DILUTION |
|---|---|---|---|
| **Rabbit monoclonal anti-Ki67** | Abcam | Ab16667 | 1:100 |
| **Mouse anti-p21** | BD biosciences | Cat #556431 | 1:200 |
| **Rat anti-p19/arf** | Abcam | Ab174939 | 1:200 |
| **Goat anti-IL-1 $\alpha$** | R&D systems | AF-400 | 1:100 |
| **Rabbit anti-IL-1 $\beta$** | Santa Cruz | sc-7884 | 1:100 |
| **Rabbit anti-SAA1** | Biorbyt | orb228668 | 1:100 |
| **Rabbit anti-CD3** | Abcam | Ab5690 | 1:500 |
| **Rabbit anti-CD4** | Abcam | Ab183685 | 1:1000 |
| **Rabbit anti-CD8** | Abcam | Ab217344 | 1:2000 |
| **Rabbit anti-CD68** | Abcam | Ab125212 | 1:1000 |
| **Biotinylated goat anti-mouse IgG** | Vector labs | Cat #BA9200 | 1:500 |
| **Biotinylated goat anti-rabbit IgG** | Vector labs | Cat #BA1000 | 1:500 |
| **Biotinylated rabbit anti-goat IgG** | Vector labs | Cat #BA5000 | 1:500 |
| **Anti-rabbit HRP polymer** | Dako | K4003 | N/A |

### 2.3.6 Image analysis (NDP and QuPath)

H&E and IHC stained slides were imaged using the Hamamatsu Nanozoomer XR microscope with NDP scan v3.1 software. Tumour burden was calculated in a blinded fashion by measuring the area of tumour tissue and dividing it by total lung area using NDP viewer v2 software. Tumour

grading was performed in a blinded fashion by two independent reviewers (Dr Fraser Millar and Dr John Connelly) using predefined criteria as outlined by DuPage et al (DuPage et al., 2009). Inter-rater agreement was calculated using Cohen's kappa coefficient. IHC quantification (positive cell detection and H-score analysis) was performed using QuPath software v0.2.3 using predefined RGB parameters for haematoxylin and DAB detection. For tumour intrinsic factors such as Ki67, p21 expression and Arf expression total number of positive cells divided by total number of cells was used to quantify expression, whereas for tumour infiltrating immune cells positive cells were normalised to tumour area to account for tumour size. For cytoplasmic/membrane staining H-score analysis was used to take into account both number of positive cells and staining intensity. The H-score was calculated by QuPath software using the following formula:

H-score = (3 x % of cells scoring 3)+(2 x % of cells scoring 2)+(1 x % of cells scoring 1)

H-score was calculated automatically by QuPath after setting predefined DAB intensity levels for each threshold (0-3) to markedly improve reproducibility of analysis.

### 2.3.7 pSECC lentivirus production and titre

To achieve epithelial specific knockout of *Tlr2* in lung tumours the pSECC lentivirus system was used to perform *in vivo* somatic genome

editing. This lentiviral system allows concurrent epithelial expression of Cre-recombinase (to activate oncogenic *Kras*$^{G12D}$) and CRISPR/Cas9 machinery to knockout *Tlr2* at the lung epithelium only. All plasmids required for pSECC lentivirus generation were prepared with Qiagen maxi preps as detailed in chapter 2.2.1. gTlr2 and control (gTomato) expressing pSECC plasmids were cloned by Dr Andrea Quintanilla prior to me joining the lab (see table 2.6 for gRNA sequences). 293T cells were passaged as detailed in chapter 2.1.1 and plated at a ratio of 1:4 of original density. The following day a 75μl/ml solution of polyethylenimine (PEI) in null DMEM was prepared, vortexed and incubated at room temperature for 5 minutes. Lentiviral plasmid solutions were prepared by adding 7.5μg of PAX2 plasmid, 2.5μg of VSVG plasmid and 10μg of pSECC gRNA (both Tlr2 gRNA and non-targeted control gRNA) plasmid and adding these to null DMEM up to 500μl. A GFP expressing plasmid (pUltra-GFP) was used as a transfection control. An equal volume of PEI solution was then added to each plasmid solution, vortexed and incubated at room temperature for 10 minutes. Following this, each solution was added to a 10cm plate of 293T cells dropwise and cells were placed back in a 37$^{o}$C incubator at 5% $CO_2$ and incubated overnight. The next day media was changed to remove PEI solution and warmed fresh media was applied for a further 24 hours. The GFP transfection control plate was visualised with a fluorescent microscope to ensure adequate transfection efficiency. Lentivirus containing media was then aspirated from each plate and syringe filtered through a 0.45um filter into a sterile 50ml falcon. Lenti-X concentrator solution (Takara, 631232) was added at a volume of one third of

the volume of viral supernatant and mixed by gentle inversion. This was incubated at 4$^{o}$C for 4 hours prior to centrifugation at 1500 *x g* for 45 minutes at 4$^{o}$C. Supernatant was discarded and the remaining viral pellet was resuspended in OptiMEM (Thermo Fisher, 31985070) and immediately aliquoted and frozen at -80$^{o}$C. Some lentiviral solution was kept for titration. 3TZ cells (a mouse fibroblast cell line that expresses the loxP-STOP-loxP betaGal cassette (Psarras et al., 2004)) were passaged in the same media as 293T cells (as detailed in chapter 2.1.1) and seeded into a 6 well-plate at a density of 10,000 cells per well in 1ml of media and incubated overnight. The following day media was removed and replaced with 1ml of pSECC lentivirus containing media containing lentivirus of the following volumes (0μl, 10μl, 20μl, 40μl, 80μl, 160μl). These cells were then placed back into the incubator for 2 days. Following this, media was removed and cells were washed carefully with PBS and fixed with fixative solution (0.1% glutaraldehyde, 2% formaldehyde in PBS) for 2 minutes at room temperature in a fume hood. Cells were then washed three times with PBS supplemented with 1mM $MgCl_2$ (pH6) and then incubated in X-Gal staining solution (X-gal 20mg/ul, $MgCl_2$ 0.05M, $K_3FE\ (CN)_6$ 100mM, $K_4Fe\ (CN)_6$ *$3H_2O$ 100mM) and incubated overnight at 37$^{o}$C wrapped in foil. The next day staining solution was removed, and cells were washed with PBS twice prior to counting of BetaGal positive cells using a brightfield microscope. The following calculation was used to determine the transduction units (TU)/ml of the pSECC lentivirus solutions:

TU/ml = (# of cells at transduction) x [MOI/(ml of lentiviral stock used)]

The multiplicity of Infection (MOI) was determined by calculating the percentage of cell infected and consulting the MOI table from the Cellecta user manual (https://manuals.cellecta.com/lentiviral-construct-packaging-and-transduction/v10a/en/topic/lentiviral-titer-calculation). The titre was used to resuspend equal titres of control and *Tlr2* gRNA viral stock solutions in 40ul OptiMEM prior to intranasal inoculation as described in 2.3.1.

**Table 2.6:** Tlr2 and Tomato gRNA sequences used for pSECC plasmids

| sgRNA ID | Forward/Reverse | Target sequence |
|---|---|---|
| gTom | Forward | CACCGGGCCACGAGTTCGAGATCGA |
| | Reverse | AAACTCGATCTCGAACTCGTGGCCC |
| gTlr2 | Forward | CACCGCCTGGAGGTTCGCACACGCT |
| | Reverse | AAACAGCGTGTGCGAACCTCCAGGC |

### 2.3.8 Fluorescence activated cell sorting (FACS) analysis

Mice were culled humanely by cervical dislocation and exsanguination at predefined timepoints. The thoracic cavity was opened, and the lungs were perfused with up to 20ml ice cold PBS via the right ventricle to clear the lungs of all blood. The lung tissue was then dissected and weighed, then placed in a 50ml falcon with 5ml of ice cold RPMI 1640 (Lonza, BE12-702F). Lung tissue was then roughly diced in a petri dish using a scalpel and incubated in an enzyme solution (0.8mg/ml collagenase V, 0.625mg/ml collagenase D, 1mg/ml dispase, 30μg/ml DNase) in a shaking incubator at

37°C at 240rpm for 25 minutes. The tissue enzyme mix was intermittently shaken by hand during this incubation to ensure all tissue was immersed in enzyme solution. After the incubation the solution was poured through a 100μm cell strainer into a fresh 50ml falcon. Residual tissue fragments were gently mashed with the plunger of a 2.5ml sterile syringe and washed through with RPMI. The filtered tissue was topped up to 50ml RPMI then centrifuged at 300 *x g* for 5 minutes at 4°C. The supernatant was discarded, and the pellet was resuspended in a further 30ml RPMI and centrifuged at 300 *x g* for 5 minutes at 4°C. The supernatant was discarded then the remaining pellet was resuspended in 3mls of red blood cell lysis buffer (Sigma, R7757) and incubated on ice for 3 minutes. The samples were then centrifuged as previous, supernatant discarded and washed in 3ml FACS buffer (PBS + 0.05% BSA + 2mM EDTA). The samples were again centrifuged and resuspended in 4ml FACS buffer and passed through a 35μm cell strainer directly in FACS tubes prior to counting using the Muse cell analyser (Merck Millipore). 2 million cells per sample were added to fresh FACS tubes and pelleted with centrifugation at 300 *x g* for 5 minutes at 4°C. The supernatant was discarded, and the pellet resuspended by gently flicking the FACS tube. 10μl of mouse serum (Sigma, M5905) and 1μl of Fc block (anti-mouse CD16/32, Biolegend, 101302) was added to the remaining solution and incubated on ice for 10 minutes. Following this 1μl of each fluorophore conjugated primary antibody (see table 2.7 for primary antibody details) was added to each sample and incubated on ice for 20 minutes. Samples were then topped up with 500μl of FACS buffer and centrifuged at

300 *x g* for 5 minutes at 4°C. Supernatant was discarded and the cell pellet was resuspended in 500μl of FACS buffer and taken to the FACS facility. For intracellular staining, after counting cells were incubated with a cell stimulation/protein transport inhibitor cocktail (Thermo Fisher, 00-4975-93) for 4 hours at 37°C. Samples were then washed in FACS buffer and incubated with Zombie UV fixable viability dye (Biolegend, 77474) suspended in PBS at a ratio of 1:100, for 30 minutes at room temperature. Samples were again washed with FACS buffer and cell surface staining was performed as detailed above. After washing with FACS buffer, samples were then fixed using the FoxP3/Transcription factor staining buffer set (Thermo Fisher, 00-5523-00). 1ml of fixation/permeabilization working solution (1 part concentrate to 3 parts diluent) was added to each sample and incubated at 4°C overnight in the dark. The following day 2ml of permeabilization buffer (1 part 10X concentrate to 9 parts $dH_2O$) was added to samples and they were then centrifuged at 500 *x g* for 5 minutes at room temperature. The supernatant was discarded, and samples were washed once more in permeabilization buffer prior to serum block at room temperature for 10 minutes. 1μl of fluorophore conjugated primary antibodies for intracellular proteins were added and samples were incubated in the dark for 30 minutes at room temperature. Samples were then washed one final time with permeabilization buffer, centrifuged at 500 *x g* for 5 minutes, then resuspended in 500μl FACS buffer and taken to the FACS facility. Samples were analysed on a BD LSR Fortessa X-20 analyser using BD FACSDiva v8.0.1 software. Data were analysed using FloJo software v10.2. Gating was

designed using fluorescence minus one (FMO) samples. Compensation was performed manually using single antibody stained OneComp eBeads (Thermo Fisher, 01-1111-41). Total cell number was determined by multiplying the percentage of live fluorophore positive cells by the total number of cells isolated per sample and this was normalised to tissue weight.

**Table 2.7:** Antibodies used in FACS analysis

| REAGENT or RESOURCE | SOURCE | IDENTIFIER | DILUTION |
|---|---|---|---|
| **Anti-mouse CD45 (Brilliant Violet 421)** | Biolegend | 103133 | 1:100 |
| **Anti-mouse CD3 (PE/Cyanine7)** | Biolegend | 100219 | 1:100 |
| **Anti-mouse CD4 (PE)** | Biolegend | 100407 | 1:100 |
| **Anti-mouse CD8 (Super bright 600)** | Invitrogen | 63-0081-80 | 1:100 |
| **Anti-mouse TCR $\gamma\delta$ (Alexa Fluor® 488)** | Biolegend | 118127 | 1:100 |
| **Anti-mouse/human CD11b (APC)** | Biolegend | 101211 | 1:100 |
| **Anti-mouse CD11c (APC/Cyanine7)** | Biolegend | 117323 | 1:100 |
| **Anti-mouse Siglec-F (PE)** | Biolegend | 155505 | 1:100 |
| **Anti-mouse Ly6C (FITC)** | Biolegend | 128005 | 1:100 |
| **Anti-mouse Ly6G (Alexa Fluor® 700)** | Biolegend | 127621 | 1:100 |

| | | | |
|---|---|---|---|
| **Anti-mouse CD19 (PE/Cyanine7)** | Biolegend | 115519 | 1:100 |
| **Anti-mouse CD335 (PE/Cyanine7)** | Biolegend | 137617 | 1:100 |
| **7AAD viability staining solution** | Biolegend | 420403 | 5ul per sample |
| **Zombie UV Fixable viability dye** | Biolegend | 77474 | 1:100 |
| **Anti-mouse FoxP3 (Alexa Fluor® 700** | Biolegend | 126421 | 1:100 |
| **Anti-mouse ROR$\gamma$T (APC)** | eBiosciences | 17-6988-80 | 1:100 |
| **Anti-mouse TCR $\gamma\delta$ (PerCP/Cy5.5)** | Biolegend | 118117 | 1:100 |
| **Anti-mouse IL-17A (FITC)** | eBiosciences | 11-7177-81 | 1:100 |

## 2.4 Human lung cancer analysis

### 2.4.1 Tissue acquisition

Formal request for sections from FFPE Human lung adenocarcinoma resection specimens was requested from the Lothian NRS Bioresource and Tissue Governance Unit (request no. SR1382) with approved ethical status (Bioresource ethical approval 15/ES/0094). This was done in collaboration with Professor William Wallace (Consultant Cardiothoracic Pathologist, NHS Lothian/University of Edinburgh). Sections from FFPE Human squamous carcinoma-in-situ lesions were received from collaborators from University College London (Professor Sam Janes/Dr Vitor Teixeira). These samples

were acquired from patients enrolled in the University College London Hospital (UCLH) surveillance study, and formal approval/ethical status was obtained from the UCLH Pathology department by our collaborators.

### 2.4.2 Immunohistochemistry and image analysis

IHC protocols for human lung cancer samples were as described in chapter 2.2.4 (see table 2.8 for antibodies used in human samples analysis). Validation of antibodies for human tissue was performed on formalin fixed paraffin embedded pellets of IMR-90 cells transduced with either an ER-STOP cassette (negative control) or ER-RAS cassette (positive control). H&E and IHC stained slides were imaged using the Hamamatsu Nanozoomer XR microscope with NDP scan v3.1 software. To compare expression between/within samples IHC quantification (H-score analysis) was performed using QuPath software v0.2.3 as described in chapter 2.3.6 on areas of normal epithelium (if present) and tumour epithelium. Areas of pre-invasive lung adenocarcinoma (lepidic adenocarcinoma) and invasive adenocarcinoma were identified by Professor William Wallace, and H-score analysis was performed to compare expression levels between these two areas. To compare expression levels in preinvasive squamous samples, areas of lesion epithelium were identified on H&E slides and H-score was performed using QuPath. For correlation analysis, tumour epithelium was identified on H&E images and labelled on QuPath. These areas of epithelium were then identified on consecutive sections stained for TLR2 and IL-1$\beta$ and IHC quantification (H-score analysis) was performed. Paired H-scores for

TLR2 and IL-1$\beta$ were recorded in an excel file and imported into R (v4.0.3) for Pearson correlation analysis.

**Table 2.8:** Antibodies used in human lung IHC

| REAGENT or RESOURCE | SOURCE | IDENTIFIER | DILUTION |
|---|---|---|---|
| **Rabbit anti-Human TLR2** | Novus Bio | NBP2-24861 | 1:250 |
| **Mouse anti-Human IL1B** | Santa Crus | sc-32294 | 1:100 |
| **Biotinylated goat anti-rabbit IgG** | Vector labs | Cat #BA1000 | 1:500 |
| **Biotinylated goat anti-mouse IgG** | Vector labs | Cat #BA9200 | 1:500 |

### 2.4.3 RNA sequencing data download

All RNA sequencing data download and handling was done under the direct supervision of Dr Alison Meynert from the University of Edinburgh Bioinformatic Analysis Core (BAC). Access to the RNA-sequencing dataset (EGAD00001005479) was formally requested from the contact person as listed on the European Genome-Phenome Archive (EGA). Following approval, I was granted a username and password allowing access to this dataset from the EGA website. Prior to downloading the BAM files, an appropriate data management plan was written and submitted to dmponline.dcc.ac.uk. The data download was performed using the Edinburgh Compute and Data Facility (ECDF) Linux Compute Cluster (Eddie). To perform the data download from the EGA, a conda environment was created. An environment directory was created in our designated group

space on Eddie and a conda environment was created within this directory. Following this, the python-based download client pyega3 was installed into the conda environment from the bioconda channel. Using a wild west node (node2c15) on Eddie, the conda environment was activated within a screen session. An EGA credentials file containing my EGA username and password was created in my fileset on Eddie in JavaScript Object Notation (JSON) format. The download was then commenced using pyega3 and the EGA credentials file. Following completion of the dataset download, BAM files were checked by running a samtools app using a shell script to check for errors with the BAM file download. BAM files were converted to FASTQ files using a Nextflow pipeline premade by Dr Alison Meynert. Nextflow (v20.12.0) was downloaded into my software folder on Eddie using a command from the nextflow website (https://www.nextflow.io/). To run the nextflow pipeline a conda environment was activated as described above and the 'bam2fastq' command was executed. Output data (FASTQ files) were saved on Eddie.

### 2.4.4 RNA sequencing data analysis

All RNA sequencing data analysis was done under the direct supervision of Dr Philippe Gautier from the University of Edinburgh Bioinformatic Analysis Core (BAC). Nextflow (v20.12.0) was downloaded and the Nextflow nf-core RNA-seq pipeline v3.0 was run on Eddie (see figure 2.4 for full pipeline configuration). RNA sequencing reads were aligned to the human genome (GRCh38) using STAR (v2.6.1) (Dobin et al., 2013) and read counts were quantified using Salmon (v1.4.0). Reads counts (.rds format)

were then downloaded from Eddie and imported into R (v4.0.3). Metadata detailing individual lesion histology was downloaded from the source publication (Chen et al., 2019) and read count data was aligned to histology (preinvasive vs invasive lung adenocarcinoma). Differential gene expression analysis was performed using the DESeq2 package (Love et al., 2014) in R (v4.0.3). Histograms of individual gene counts were plotted to determine data distribution. Gene count data were subsequently plotted and analysed using the ggplot2 and ggsignif packages in R.

**Figure 2.4:** Nextflow nf-core RNA-seq pipeline 3.0 configuration

```
Pipeline Configuration:
-----------------------
 - revision: master
 - runName: silly_chandrasekhar
 - containerEngine: singularity
 - launchDir: /gpfs/igmmfs01/eddie/FM-Preinvasive-LUAD/analysis/
nextflow_rnaseq
 - workDir: /gpfs/igmmfs01/eddie/FM-Preinvasive-LUAD/analysis/
nextflow_rnaseq/work
 - projectDir: /exports/igmm/eddie/FM-Preinvasive-LUAD/analysis/
nextflow_rnaseq/.nextflow/assets/nf-core/rnaseq
 - userName: fmillar
 - profile: singularity
 - configFiles: /exports/igmm/eddie/FM-Preinvasive-LUAD/analysis/
nextflow_rnaseq/.nextflow/assets/nf-core/rnaseq/nextflow.config, /
gpfs/igmmfs01/edd
ie/FM-Preinvasive-LUAD/analysis/nextflow_rnaseq/test.config
 - input: nextflow_samples.csv
 - email: fraser.millar@ed.ac.uk
 - genome: GRCh38
 - fasta: s3://ngi-igenomes/igenomes//Homo_sapiens/NCBI/GRCh38/
Sequence/WholeGenomeFasta/genome.fa
 - gtf: s3://ngi-igenomes/igenomes//Homo_sapiens/NCBI/GRCh38/
Annotation/Genes/genes.gtf
 - gene_bed: s3://ngi-igenomes/igenomes//Homo_sapiens/NCBI/GRCh38/
Annotation/Genes/genes.bed
 - star_index: s3://ngi-igenomes/igenomes//Homo_sapiens/NCBI/GRCh38/
Sequence/STARIndex/
 - igenomes_base: /exports/igmm/eddie/NextGenResources/igenomes/
 - skip_trimming: true
 - skip_markduplicates: true
 - skip_qualimap: true
 - max_memory: 256 GB
 - max_time: 10d
 - Date Started: 2021-03-18T08:06:20.593Z
 - Date Completed: 2021-03-18T10:32:10.659Z
 - Pipeline script file path: /exports/igmm/eddie/FM-Preinvasive-
LUAD/analysis/nextflow_rnaseq/.nextflow/assets/nf-core/rnaseq/
main.nf
 - Pipeline script hash ID: 4b892cc54e3b768dca93d19da30a907a
 - Pipeline repository Git URL: https://github.com/nf-core/rnaseq
 - Pipeline repository Git Commit:
3643a94411b65f42bce5357c5015603099556ad9
 - Pipeline Git branch/tag: master
 - Nextflow Version: 20.12.0-edge
 - Nextflow Build: 5459
 - Nextflow Compile Timestamp: 12-12-2020 09:14 UTC

--
nf-core/rnaseq
https://github.com/nf-core/rnaseq
```

# 3 : Results chapter 1

# Identification of a regulatory role for *Tlr2* in OIS/SASP *in vivo*

## 3.1 Chapter aims

As described in 1.4.2, *Tlr2* regulates OIS and expression of the SASP (Hari et al., 2019). Whether this is also the case *in vivo* is yet to be established, and the functional consequences of this regulation also remain to be investigated. The first aim of this thesis was to set up a well characterised *in vivo* model of OIS in our lab and investigate the role *Tlr2* has in the regulation of OIS and the SASP *in vivo*. The hydrodynamic tail vein injection (HTVI) model (as described in 2.2), allowing overexpression of oncogenes in murine hepatocytes was used and the functional consequences of *Tlr2* loss was investigated. In this chapter, the results from the HTVI model experiments are described.

## 3.2 Inducing OIS and SASP *in vivo* using HTVI

### 3.2.1 Overexpressing oncogenes *in vivo*

*Nras* encoding transposons and transposase expressing plasmids were received from the Scott Lowe lab. In collaboration with Dr Luke Boulter

(Human Genetics Unit, University of Edinburgh) hydrodynamic delivery of DNA plasmids diluted in 0.9% NaCl was performed (as described in 2.2). Immunohistochemistry (IHC) staining on FFPE liver samples harvested six days after HTVI demonstrated widespread expression of Nras following delivery of both the oncogenic (*Nras*$^{G12V}$) and effector loop mutant negative control (*Nras*$^{G12V/D38A}$) expressing transposon constructs (Figure 3.1).

**Figure 3.1: Nras expression following transposon delivery.**

IHC staining for Nras on FFPE liver sections harvested from mice six days after hydrodynamic delivery of Nras encoding transposon constructs. Representative staining from n=4-5 mice per group.

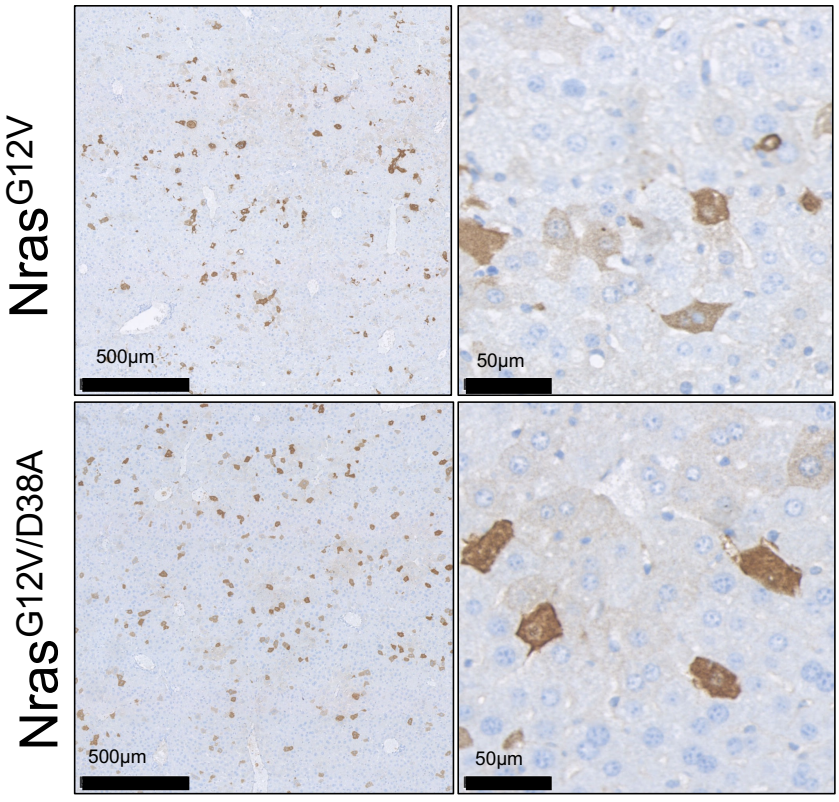

### 3.2.2 Oncogene expression induces OIS *in vivo*

To determine whether oncogenic *Nras* (hereafter $Nras^{G12V}$) overexpression induces OIS both IHC and RT-qPCR analysis was performed to measure levels of various senescence markers. Firstly, despite similar Nras levels, expression of p21 and lipofuscin (stained by Sudan Black B – SBB) was abundant in $Nras^{G12V}$ expressing hepatocytes when compared with negative controls ($Nras^{G12V/D38A}$) (Figure 3.2). Due to poor staining quality automated IHC quantification was not possible, therefore these data are qualitative representations only.

**Figure 3.2: *Nras*$^{G12V}$ induces the expression of OIS markers at the protein level.** IHC staining for Nras, p21 and Sudan Black B (Biotin-SBB) on FFPE liver sections harvested from mice six days after hydrodynamic delivery of *Nras* encoding transposon constructs. Representative staining from n=4-5 mice per group.

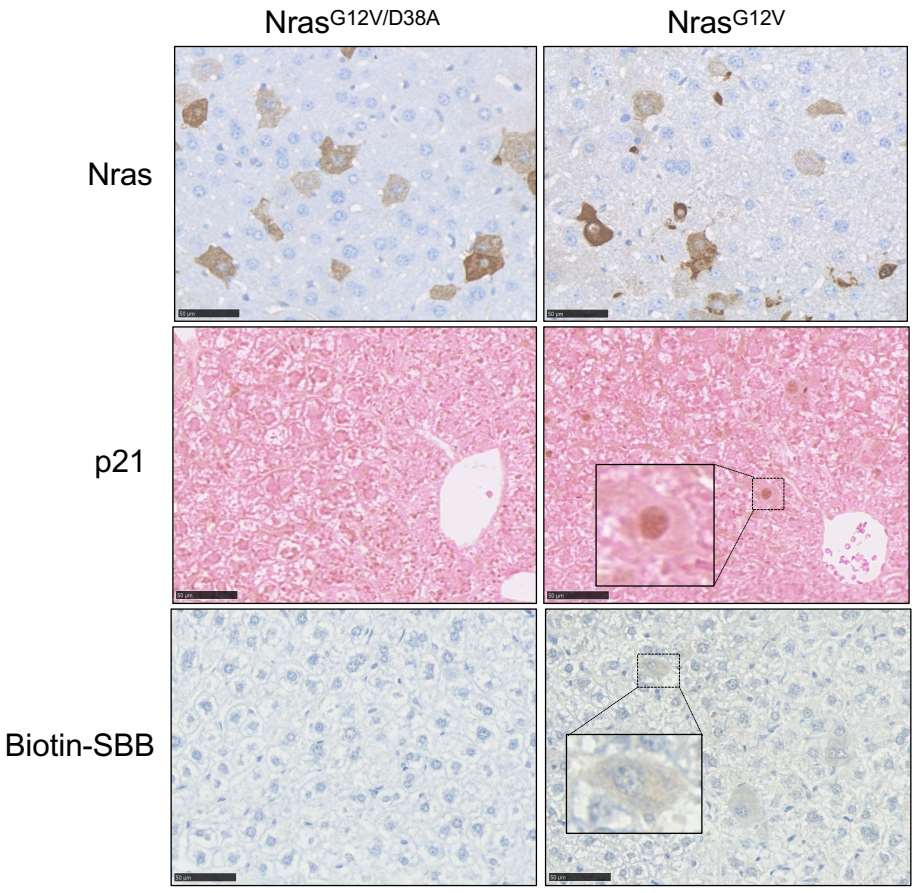


Gene expression of OIS markers using RT-qPCR was then performed on RNA isolated from snap frozen liver samples. This demonstrated that expression of Decoy receptor 2 (*Dcr2*) and p19-Arf (*Arf*, **a**lternate **r**eading **f**rame of *Cdkn2a* locus) were increased in *Nras*$^{G12V}$ expressing samples (Figure 3.3), however there was no significant increase in expression of *Cdkn1a* (p21). These results suggest that expression of *Nras*$^{G12V}$ induces senescence *in vivo*.

**Figure 3.3: *Nras*$^{G12V}$ induces the expression of OIS markers at the RNA level.** mRNA expression analysis of *Cdkn1a* (p21), *Dcr2* and *Arf* in snap frozen liver samples six days following hydrodynamic delivery of Nras transposons. n=4-5 mice per group. Statistical analysis was performed using the students *t*-test. **p<0.01, ****p<0.0001.

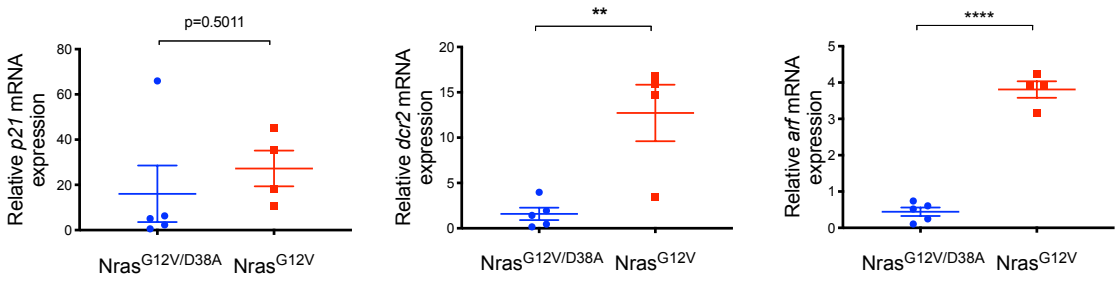


### 3.2.3 Oncogene expression induces SASP expression *in vivo*

To assess whether oncogene expression also induces expression of the SASP, IHC staining for the key SASP factor IL-1β was performed, revealing that IL-1β was expressed in *Nras*$^{G12V}$ expressing hepatocytes, but was absent in negative control samples (Figure 3.4). Unfortunately, staining for other SASP factors including IL-1α and A-SAA was unsuccessful in these samples. As detailed previously, due to poor staining quality automated IHC quantification was not possible therefore these data are qualitative representations only.

**Figure 3.4: *Nras*$^{G12V}$ induces IL-1β protein expression.** IHC staining for Nras and IL-1β on FFPE liver sections harvested from mice six days after hydrodynamic delivery of Nras encoding transposon constructs. Representative staining from n=4-5 mice per group.

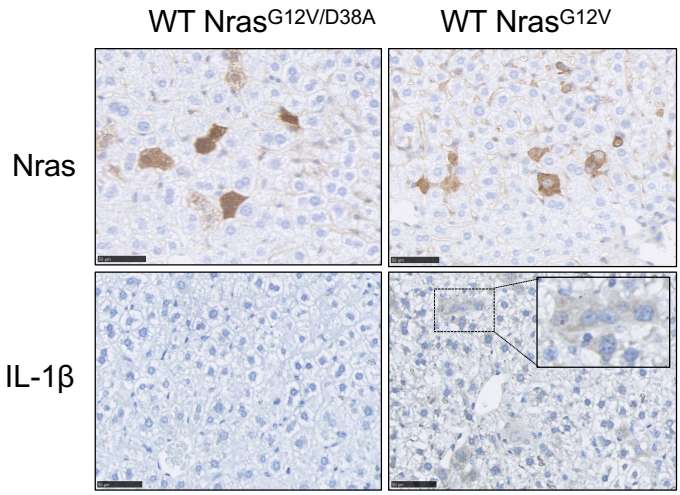


RT-qPCR analysis was then performed and revealed significant upregulation of the key SASP factors *Il-1α* and *Il-1β* in *Nras*$^{G12V}$ expressing samples (Figure 3.5), suggesting that SASP expression is induced following expression of oncogenes *in vivo*.

**Figure 3.5: *Nras*$^{G12V}$ induces the expression of SASP markers at the RNA level.** mRNA expression analysis of the SASP factors *Il-1*$\alpha$ and *Il-1*$\beta$ in snap frozen liver samples six days following hydrodynamic delivery of Nras transposons. n=4-5 mice per group. Statistical analysis was performed using the Student's *t*-test. **p<0.01.

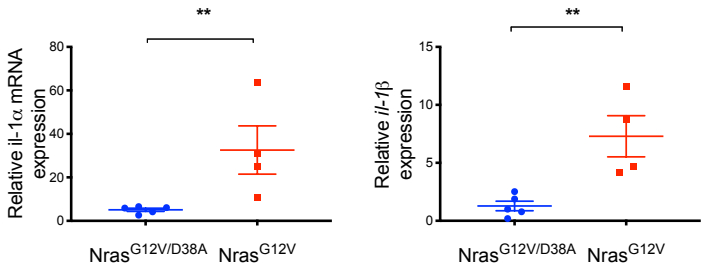


## 3.3 The role of Tlr2 in the regulation of OIS and SASP expression

### 3.3.1 *Tlr2* expression increases following oncogene activation

To assess whether OIS and expression of the SASP coincides with increased *Tlr2* expression *in vivo* RT-qPCR and IHC analysis was performed. *Tlr2* expression was indeed significantly increased in *Nras*$^{G12V}$ expressing samples compared to controls (Figure 3.6).

**Figure 3.6: *Nras*$^{G12V}$ induces the expression of *Tlr2*.** mRNA expression analysis of *Tlr2* in snap frozen liver samples six days following hydrodynamic delivery of *Nras* transposons. n=4-5 mice per group. Statistical analysis was performed using the Student's *t*-test. **p<0.01.

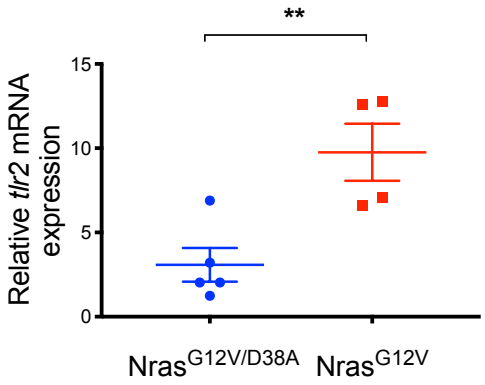


IHC analysis also demonstrated that Tlr2 protein expression was increased in *Nras*$^{G12V}$ expressing hepatocytes (Figure 3.7). Furthermore, IHC for Tlr2 and Nras was performed on serial sections suggesting that increased Tlr2 expression occurs in *Nras*$^{G12V}$ overexpressing cells (figure 3.7). It must be noted however that again automated quantification was not performed due to poor staining quality.

**Figure 3.7: Tlr2 expression is increased in *Nras$^{G12V}$* expressing cells.** IHC staining for Nras and Tlr2 on serial FFPE liver sections harvested from mice six days after hydrodynamic delivery of *Nras* encoding transposon constructs. Representative staining from n=4-5 mice per group.

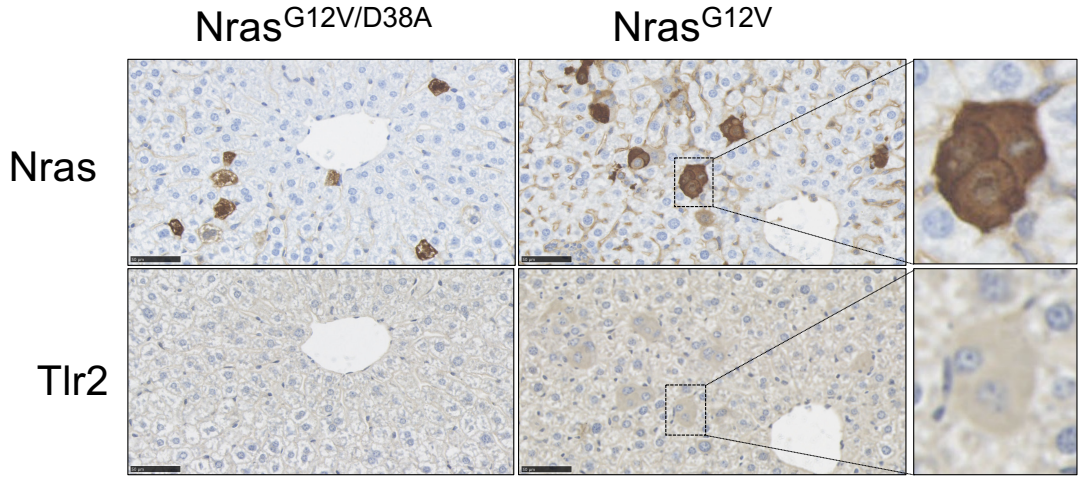


### 3.3.2 Tlr2 expression regulates OIS

To investigate whether Tlr2 regulates the OIS response, as had previously been shown *in vitro* (Hari et al., 2019), HTVI was performed on *Tlr2* knockout mice (*Tlr2$^{-/-}$*) and wild-type (WT) controls. Similar to data described in 3.2.2 and 3.2.3, IHC analysis revealed activation of OIS following HTVI delivery of *Nras$^{G12V}$* encoding transposons in WT mice. However, following HTVI delivery of *Nras$^{G12V}$* transposons in *Tlr2$^{-/-}$* mice, this activation was impaired (Figure 3.8), suggesting *Tlr2* is required for the induction of OIS. As discussed previously, automated quantification of these IHC results was not performed due to poor staining quality.

**Figure 3.8: OIS is dependent on Tlr2 activity.** IHC analysis for Nras, p21, Sudan Black B (SBB), and Tlr2 in wild-type (WT) or Tlr2 null (*Tlr2*$^{-/-}$) mice six days following hydrodynamic delivery of *Nras* encoding transposons. Representative staining from n=3 mice per group.

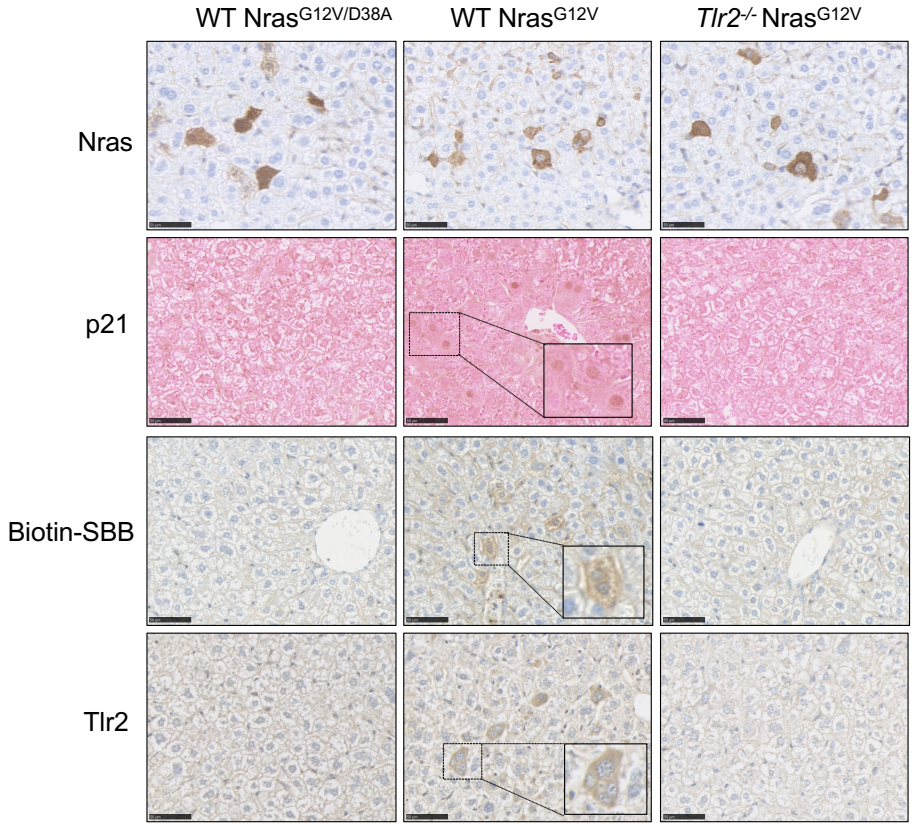


The expression of key OIS marker genes (*p21*, *Dcr2* and *Arf*) was performed using RT-qPCR. This revealed a slight increase in expression of these genes following *Nras*$^{G12V}$ expression in WT hepatocytes, however this result was not statistically significant. In *Tlr2*$^{-/-}$ mice there was no observed increase (Figure 3.9). Reliable conclusions cannot be drawn from these data as no statistically significant differences were observed.

**Figure 3.9: Expression of OIS markers in wild-type and *Tlr2*$^{-/-}$ liver samples.** mRNA expression analysis for the OIS marker genes *Cdkn1a* (*p21)*, *Dcr2* and *Arf* in snap frozen liver samples from wild-type (WT) and *Tlr2* null (*Tlr2*$^{-/-}$) mice six days after hydrodynamic delivery of *Nras* encoding transposons. Statistical analysis was performed using a one-way ANOVA with a post-hoc Tukey test for multiple comparisons.

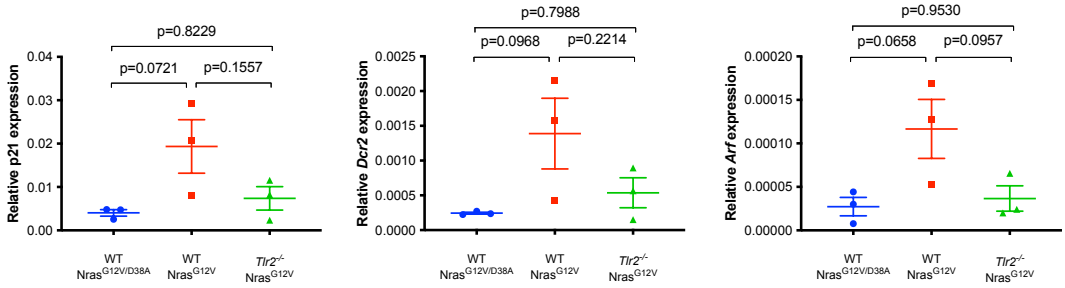


### 3.3.3 The effect of Tlr2 on the expression of the SASP *in vivo*

To assess whether *Tlr2* regulates expression of the SASP *in vivo*, RT-qPCR analysis was performed to assess the expression of key SASP factors (*Il-1*$\alpha$, *Il-1*$\beta$ and *Il-6*) in WT and *Tlr2*$^{-/-}$ mice following HTVI delivery of *Nras* encoding transposons. Significantly increased expression of *Il-1*$\beta$ and *Il-6* was observed following overexpression of *Nras*$^{G12V}$ in wild-type (WT) hepatocytes when compared with effector loop mutant negative controls (*Nras*$^{G12V/D38A}$), however the increase observed in *Il-1*$\alpha$ was not statistically significant (Figure 3.10). When this was repeated in *Tlr2*$^{-/-}$ samples, there was no significant increase in expression of any of the measured SASP factors. Indeed, there was a significant reduction in the expression of *Il-1*$\alpha$ and *Il-1*$\beta$ when comparing *Nras*$^{G12V}$ expressing WT and *Tlr2*$^{-/-}$ samples, however there was no significant reduction in *Il-6* expression (Figure 3.10).

Taken together, these data suggest that active Tlr2 is required to induce expression of the SASP during OIS, and that loss of Tlr2 impairs the induction of SASP expression.

**Figure 3.10: Expression of *Il-1β* and *Il-6* is dependent on Tlr2 activity.** mRNA expression analysis for key SASP factors (*Il-1α*, *Il-1β* and *Il-6*) in snap frozen wild-type (WT) and *Tlr2* null (*Tlr2*$^{-/-}$) liver samples six days following hydrodynamic delivery of *Nras* encoding transposons. n=3 mice per group. Statistical analysis was performed using a one-way ANOVA with a post-hoc Tukey test for multiple comparisons. *p<0.05, **p<0.01.

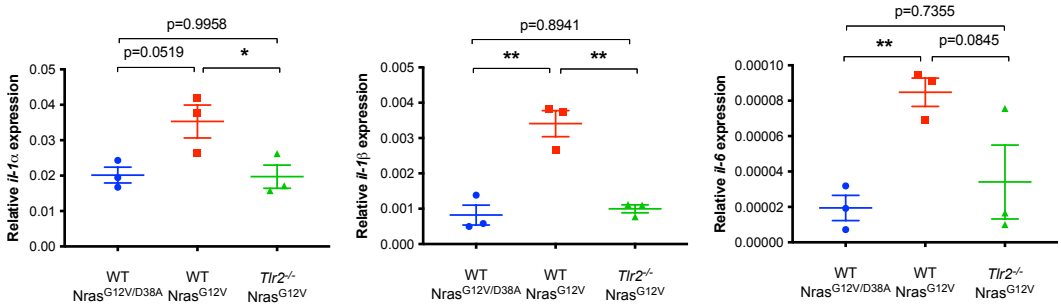


This was investigated further using IHC staining for IL-1β, which suggested that SASP expression was from hepatocytes rather than infiltrating immune cells (figure 3.11).

**Figure 3.11: IL-1β protein expression is dependent on Tlr2 activity.** IHC staining for Nras and IL-1β in wild-type (WT) and *Tlr2* null (*Tlr2*$^{-/-}$) FFPE liver sections six days following hydrodynamic delivery of *Nras* encoding transposons. Representative images from n=3 mice per group.

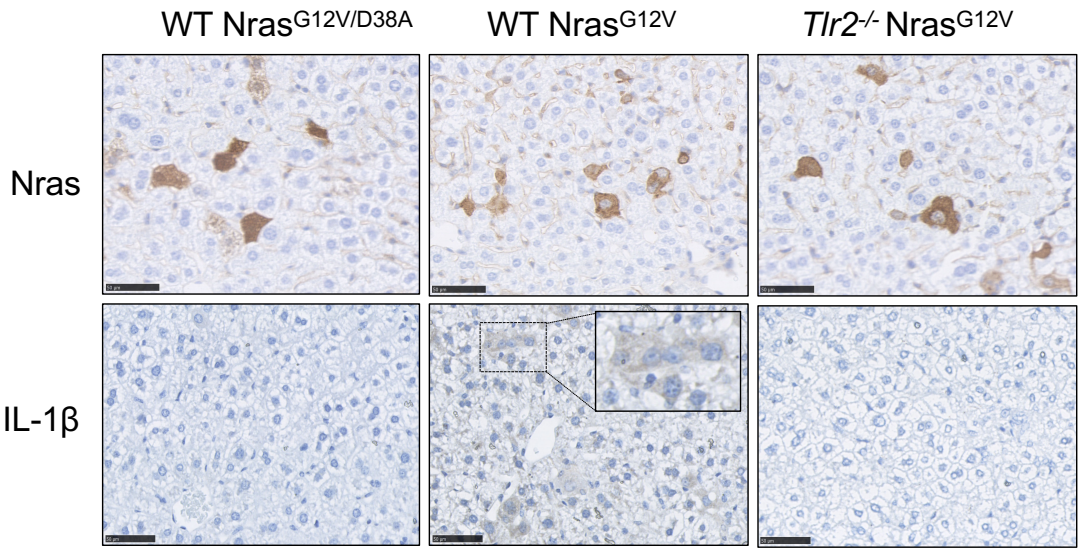


## 3.4 Senescence surveillance and Tlr2

### 3.4.1 Immune cell recruitment to senescent cells is impaired following Tlr2 loss

As discussed in 1.3.2, immune mediated clearance of senescent cells (so called 'senescence surveillance') is regulated by the SASP (Kang et al., 2011; Xue et al., 2007). Data described in 3.3 suggests that *Tlr2* is required for optimal induction of OIS and the SASP, therefore the effect of *Tlr2* loss on senescence surveillance was investigated. The HTVI model has been used to elegantly characterise senescence surveillance (Kang et al., 2011) therefore this model was used to investigate the role *Tlr2* has in this process.

Firstly, IHC staining for key immune cell markers including macrophages (F4/80), T-cells (CD3) and neutrophils (MPO) was performed in WT and *Tlr2*$^{-/-}$ samples six days after HTVI delivery of *Nras* encoding transposons. Interestingly, significantly increased recruitment of macrophages was observed in WT samples overexpressing *Nras*$^{G12V}$ and a clear biological trend towards increased T-cells and neutrophils was also observed, although the latter did not reach statistical significance (Figure 3.12-13). Macrophage recruitment was markedly impaired in *Tlr2*$^{-/-}$ mice (Figure 3.12-13), suggesting that Tlr2 regulates the recruitment of immune cells during OIS.

**Figure 3.12: Immune cell recruitment is dependent on Tlr2 activity**.

IHC staining for the immune cell markers F4/80 (macrophages), CD3 (T-cells) and MPO (neutrophils) in wild-type (WT) or *Tlr2* null (*Tlr2*$^{-/-}$) FFPE liver sections six days after hydrodynamic delivery of *Nras* encoding transposons. Representative images from n=3 mice per group.

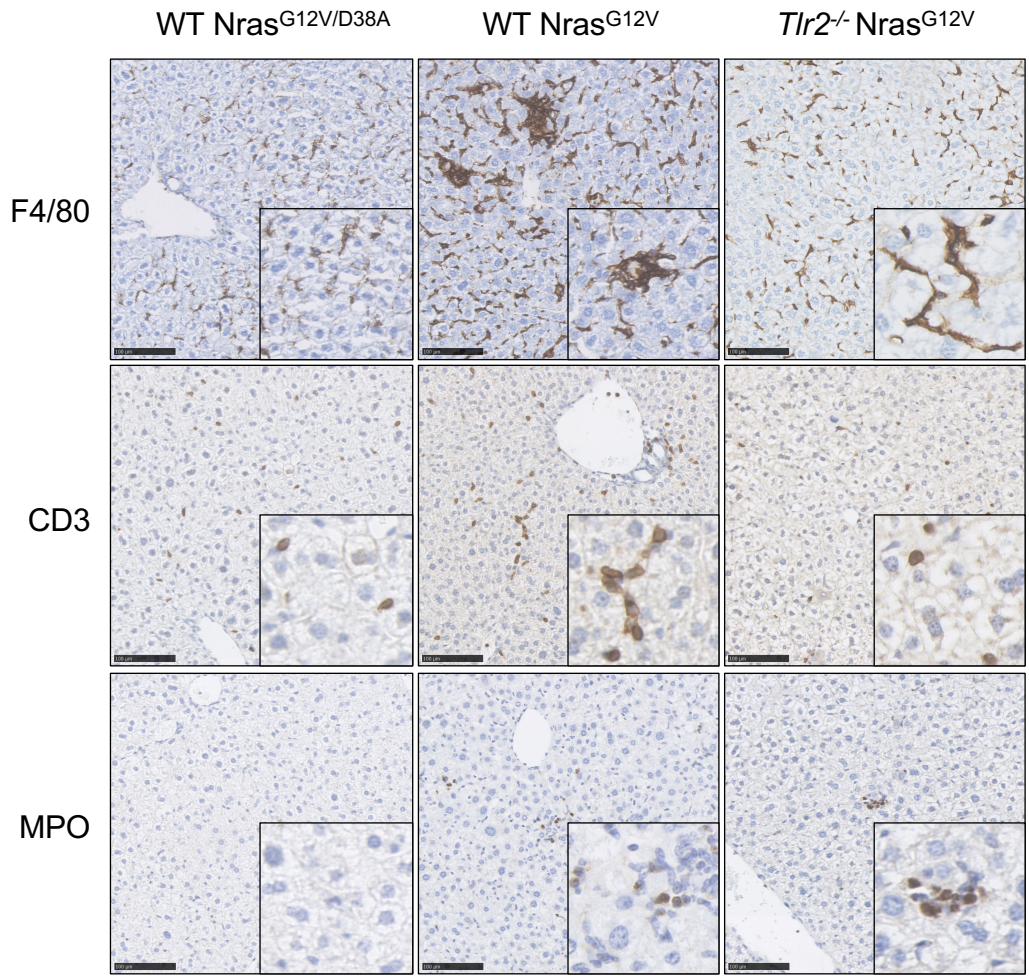

**Figure 3.13:** Quantification of immune cell populations from samples described in figure 3.12. n=3 mice per group. Statistical analysis was performed using a one-way ANOVA with a post-hoc Tukey test for multiple comparisons. *p<0.05.

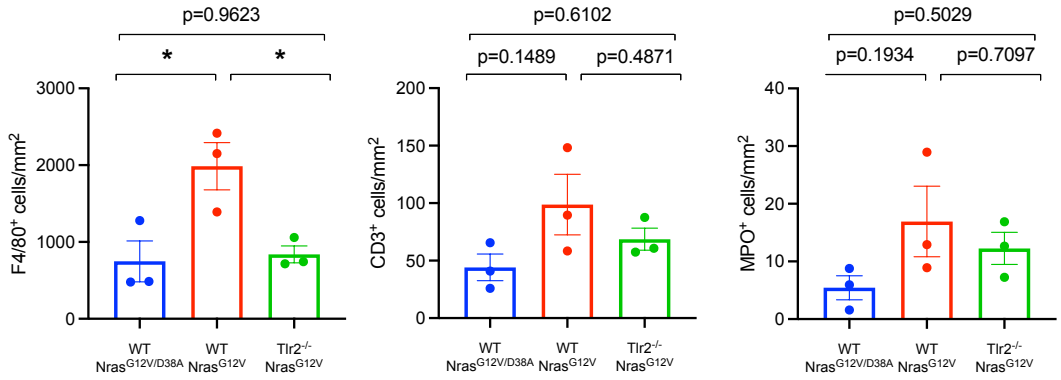


Senescence surveillance is a CD4$^+$ T-cell mediated response, however recruited monocytes act as the effector cells, clearing *Nras*$^{G12V}$ expressing cells (Kang et al., 2011). To assess whether the F4/80$^+$ cells observed are recruited to *Nras*$^{G12V}$ expressing cells co-immunofluorescence was performed to stain for Nras and F4/80. This revealed clear recruitment of F4/80$^+$ macrophages surrounding Nras expressing hepatocytes (Figure 3.14). This phenotype was not observed in negative controls (Nras$^{G12V/D38A}$) and was impaired in *Tlr2*$^{-/-}$ hepatocytes expressing Nras$^{G12V}$ (Figure 3.14) suggesting that *Tlr2* mediates the recruitment of immune cells to senescent cells.

**Figure 3.14: Tlr2 loss impairs macrophage recruitment to *Nras*$^{G12V}$ expressing cells.** Co-immunofluorescence staining for Nras (green), F4/80 (red) and DAPI (blue) six days following hydrodynamic delivery of *Nras* encoding transposons in wild-type (WT) and Tlr2 null (*Tlr2*$^{-/-}$) FFPE liver sections. Representative images from n=3 mice per group.

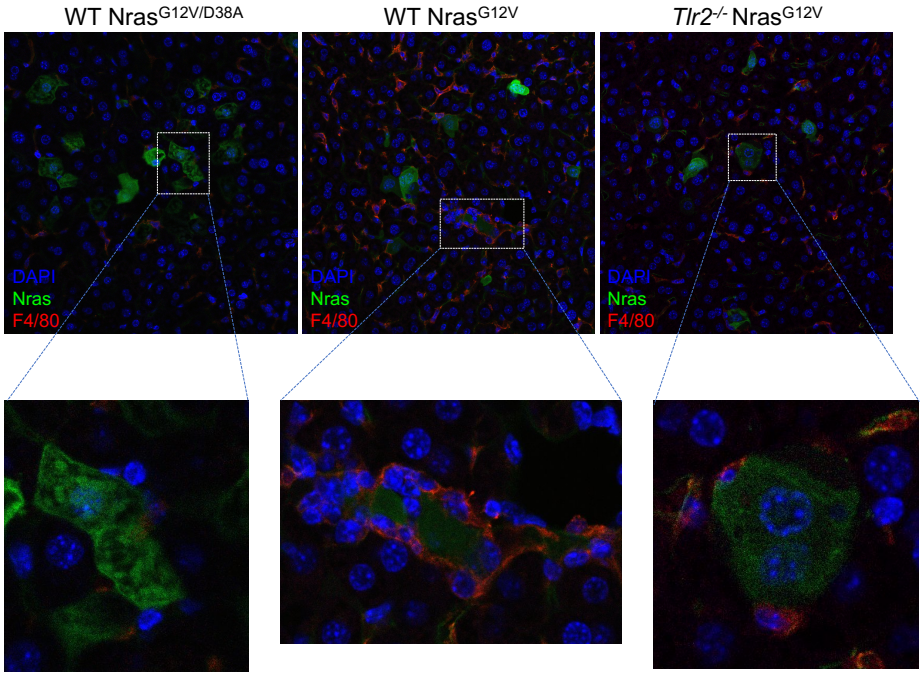


### 3.4.2 Senescence surveillance following *Tlr2* loss

Using the HTVI model, it has been shown that by day 12 following HTVI significant clearance of *Nras*$^{G12V}$ expressing hepatocytes occurs (Kang et al., 2011) and this model has been used extensively to determine regulators of senescence surveillance (Eggert et al., 2016; Goncalves et al., 2021; Wiggins et al., 2019). To assess whether impaired recruitment of immune cells translates to impaired clearance of senescent cells HTVI using *Nras*$^{G12V}$ encoding transposons was again performed on WT and *Tlr2*$^{-/-}$ mice. These mice were culled at 6 and 12 days after HTVI and Nras positive cells

were quantified manually. There was a reduction in Nras positive cells at day 12 compared to day 6 in WT mice, however this did not reach statistical significance. Furthermore, *Tlr2*$^{-/-}$ *Nras*$^{G12V}$ expressing hepatocytes were also unchanged at day 12 when compared with WT controls (Figure 3.15).

**Figure 3.15: Senescence surveillance and Tlr2 loss. (a)** IHC staining for Nras at day 6 and day 12 after hydrodynamic delivery of *Nras*$^{G12V}$ encoding transposons in wild-type (WT) and *Tlr2* null (*Tlr2*$^{-/-}$) FFPE liver sections. **(b)** Corresponding quantification for samples described in (a). n=3-7 mice per group. Statistical analysis was performed using a one-way ANOVA with a post-hoc Tukey test for multiple comparisons.

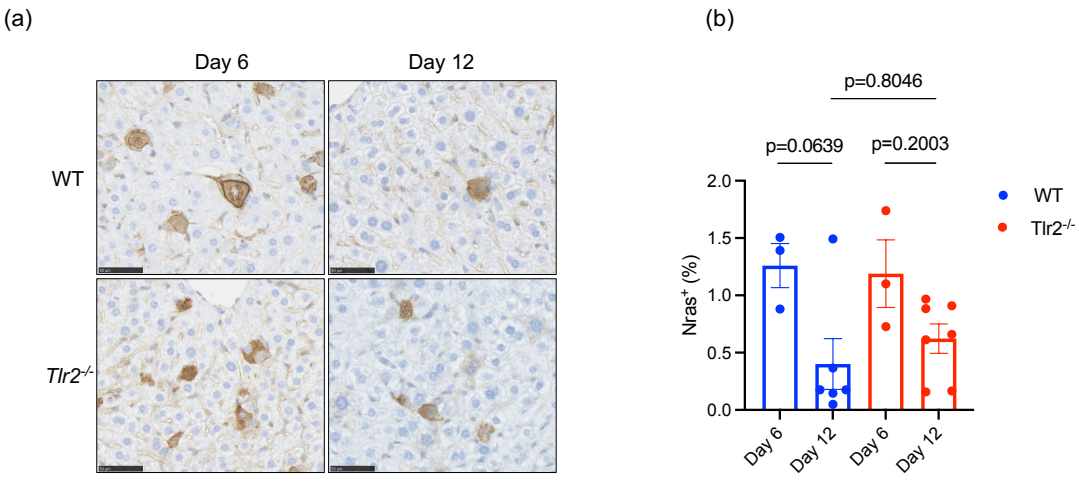


The *Nras*$^{G12V}$ expressing transposon co-expresses GFP (pT3-NRas$^{G12V}$-IRES-GFP), which serves as an independent marker of transposon integration. To investigate immune mediated clearance further, a luciferase cassette was cloned into the *Nras*$^{G12V}$ encoding transposon in place of GFP. Therefore, every *Nras*$^{G12V}$ expressing hepatocyte would co-express the enzyme luciferase. Mice were subcutaneously injected with luciferin-D.

Luciferase catalyses the oxidation of luciferin resulting in the formation of oxyluciferin in an electronically excited state. Oxyluciferin then releases a photon of light as it reverts to ground state, and these photons can be detected by bioluminescence imaging platforms. Therefore, co-expression of *Nras*$^{G12V}$ and luciferase allows longitudinal *in vivo* imaging using bioluminescence, which acts as a marker of *Nras*$^{G12V}$ expression. The Nras$^{G12V}$-Luciferase transposon was delivered to WT and *Tlr2*$^{-/-}$ mice using the HTVI method (Figure 3.16).

**Figure 3.16: Transposon plasmid for bioluminescent imaging.** The Nras$^{G12V}$-Luciferase expressing transposon is co-delivered with the transposase (SB13) expressing plasmid using the HTVI technique. Transposon cloning was performed under the supervision of Dr Andrea Quintanilla, University of Edinburgh.

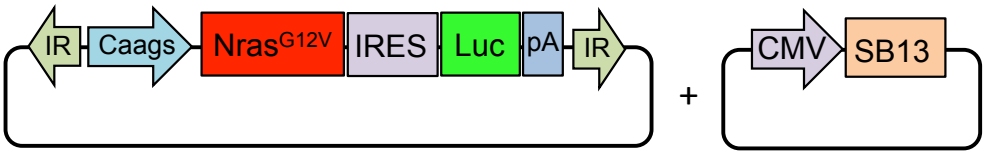


These mice were then imaged every 7 days for 3 weeks. There was no significant difference in bioluminescence signal observed in WT and *Tlr2*$^{-/-}$ mice after 7 days. This signal was markedly reduced at day 14, however only reached statistical significance in the *Tlr2*$^{-/-}$ context, suggesting that *Tlr2*$^{-/-}$ hepatocytes are cleared more readily that WT controls (Figure 3.17). However, these data do not account for transient expression of the transposon plasmid which likely occurs at earlier timepoints. Nonetheless, comparisons between WT and *Tlr2*$^{-/-}$ mice between 7 and 14 days suggests

that Tlr2 loss does not impair senescence surveillance. There was a significant reduction in signal between day 14 and day 21 in WT control mice, however this signal was maintained in *Tlr2*$^{-/-}$ mice, perhaps suggesting that late clearance is impaired in *Tlr2*$^{-/-}$ mice.

**Figure 3.17: Longitudinal bioluminescent imaging to assess senescence surveillance with Tlr2 loss. (a)** Representative bioluminescence imaging of wild-type (WT) and Tlr2 null (*Tlr2*$^{-/-}$) mice 7, 14 and 21 days after hydrodynamic delivery of Nras$^{G12V}$-Luciferase co-expressing transposons. **(b)** Quantification (Total photon flux) of samples described in (a). n=3-4 mice per group. *p<0.05, ***p<0.001

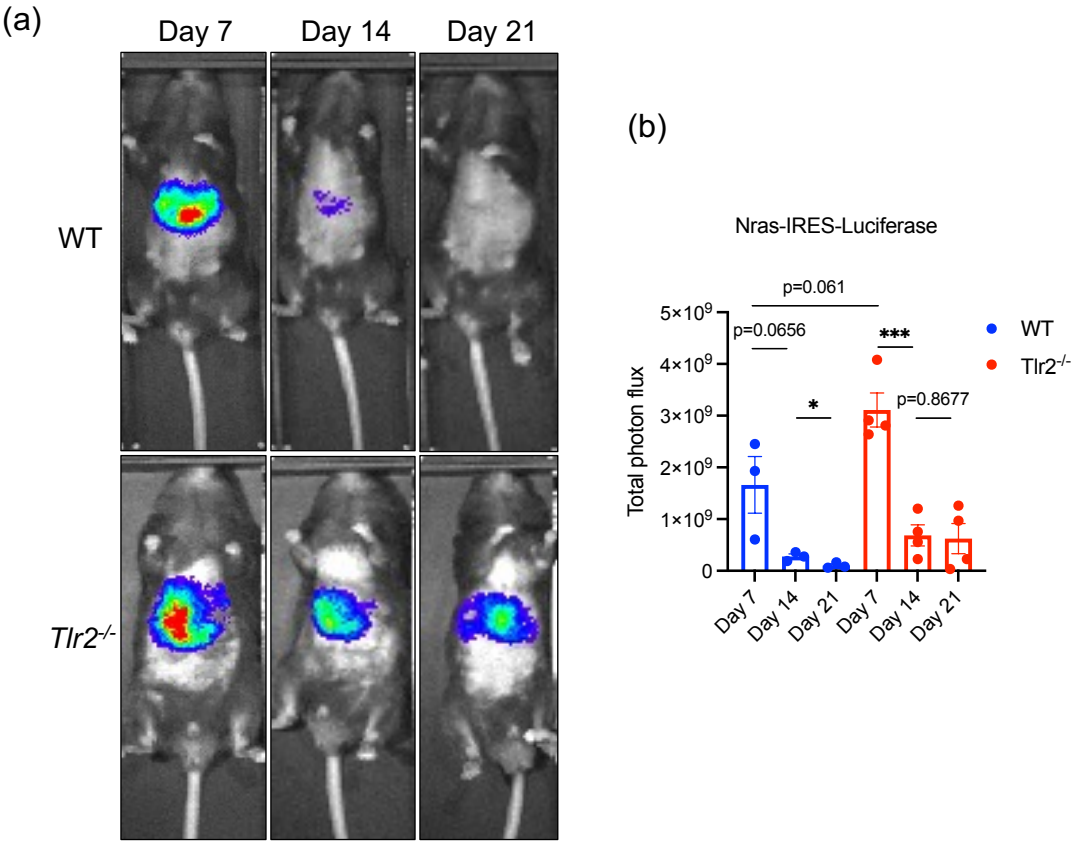

## 3.5 Apoptosis following *Tlr2* loss

Despite impaired OIS, SASP expression and immune cell recruitment in *Tlr2*$^{-/-}$ mice, *Nras*$^{G12V}$ expressing hepatocyte clearance was not significantly impaired (as shown in 3.4.2). Significant loss of *Nras*$^{G12V}$ expressing *Tlr2*$^{-/-}$ hepatocytes does occur (Figure 3.15 and 3.17) and the likelihood is that other non-Tlr2 dependent factors controlling senescence surveillance are still at play. Another possibility is that *Tlr2*$^{-/-}$ *Nras*$^{G12V}$ expressing cells are cleared by an alternate mechanism. A key feature of senescent cells is a robust resistance to apoptotic stimuli due to activation of the Bcl-2 protein family (principally Bcl-W and Bcl-xl) (Yosef et al., 2016). Impairing a cell's ability to undergo senescence (by *Tlr2* loss, for example) would theoretically pave the way for a more robust response to apoptotic stimuli. To investigate this, IHC staining for activated (cleaved) caspase 3, a central protein involved in the execution phase of apoptosis, was performed. Interestingly, at both day 6 and 12 after HTVI delivery of *Nras*$^{G12V}$ transposons, increased cleaved caspase 3 expression was observed in *Tlr2*$^{-/-}$ samples, in comparison to WT controls (Figure 3.18), suggesting that an increased apoptotic response may mediate the significant clearance of *Nras*$^{G12V}$ expressing hepatocytes observed in *Tlr2*$^{-/-}$ mice.

**Figure 3.18: Apoptosis is increased following Tlr2 loss. (a)** IHC staining for cleaved caspase 3 in wild-type (WT) and Tlr2 null (*Tlr2*$^{-/-}$) FFPE liver sections 6 and 12 days after hydrodynamic delivery of *Nras*$^{G12V}$ encoding transposons. **(b)** Corresponding quantification from samples described in (b). n=3-8 mice per group. Statistical analysis was performed using a one-way ANOVA with a post-hoc Tukey test for multiple comparisons. *p<0.05.

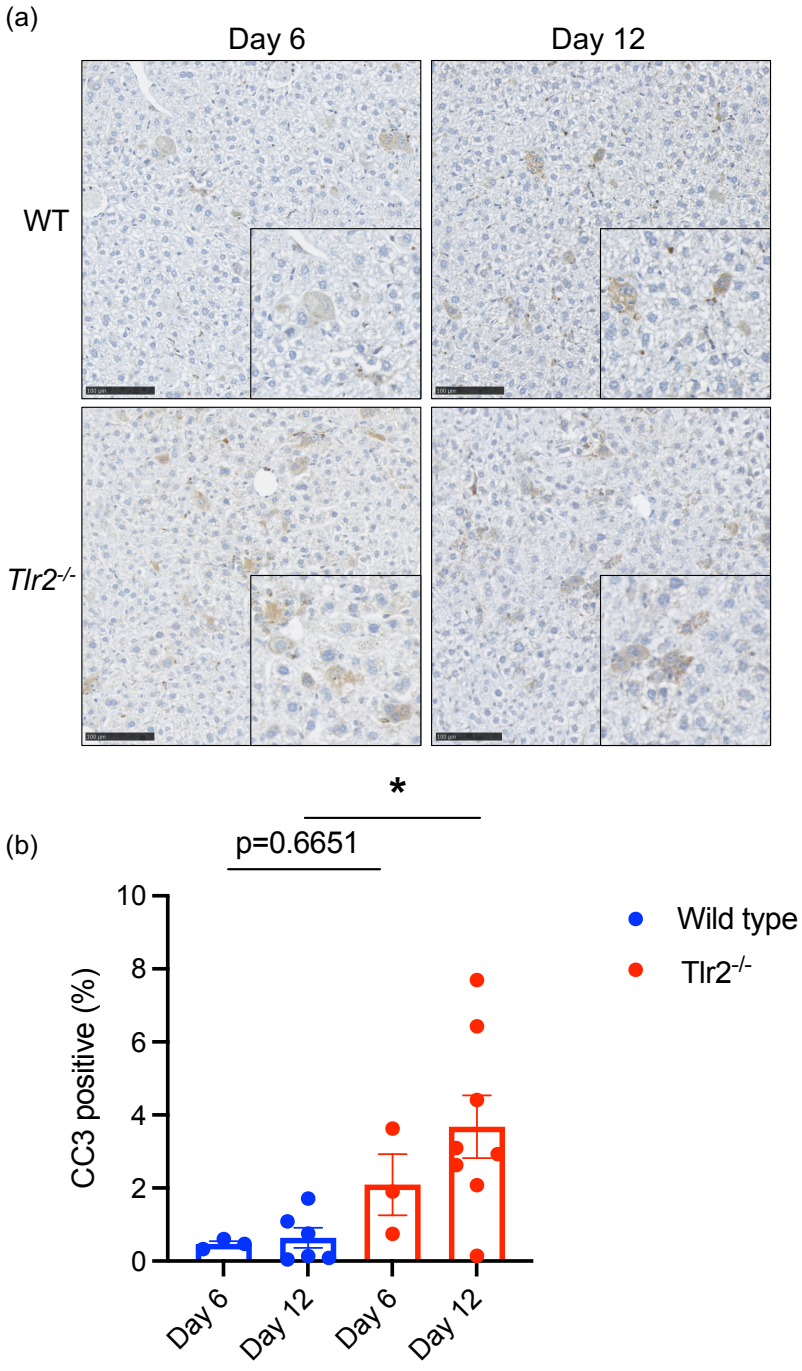

## 3.6 Chapter summary

In this chapter, the aim was to establish a well-characterised *in vivo* model of OIS in our lab and use this model to investigate the role Tlr2 has during this process. The HTVI model was successfully established, and it was used to demonstrate robust activation of OIS and the SASP *in vivo*. Following loss of *Tlr2* this response was markedly impaired, however this did not translate into impaired senescence surveillance. Continued clearance of *Tlr2*$^{-/-}$ cells may be explained by increased apoptosis. From these data, it can be concluded that *Tlr2* does regulate OIS and the SASP *in vivo* but does not clearly regulate senescence surveillance.

# 4 : Results chapter 2

# Characterising the role of TLR2 in human non-small cell lung cancer

## 4.1 Chapter aims

Chapter three describes data confirming that *Tlr2* regulates OIS and the SASP *in vivo*. These processes are key tumour suppressor mechanisms. OIS is widespread in preinvasive lung tumours whereby it likely acts as a barrier to malignant progression (Collado et al., 2005). Furthermore, *Tlr2* is widely expressed in the lung (McCoy et al., 2021). It was therefore hypothesised that *Tlr2* has a tumour suppressor function in non-small cell lung cancer (NSCLC). The aim of this chapter is to determine whether TLR2 signalling is active in human NSCLC and investigate whether this signalling mediates a tumour suppressor function. Gene expression data (RNA sequencing and microarray) from the two main subtypes of NSCLC (lung adenocarcinoma - LUAD and lung squamous carcinoma - LUSC) were analysed along with FFPE samples of invasive and preinvasive disease. In this chapter, the results of analysis of human lung cancer samples are described.

## 4.2 *TLR2* expression correlates with improved prognosis in human lung adenocarcinoma

In collaboration with Dr Andy Sims (CRUK Edinburgh Centre, University of Edinburgh) *TLR2* gene expression in LUAD samples from the Cancer Genome Atlas (TCGA) (Cancer Genome Atlas Research, 2014) were analysed. High *TLR2* expression significantly correlated with improved overall survival (Figure 4.1), suggesting that *TLR2* may have a tumour suppressor function in NSCLC.

**Figure 4.1: *TLR2* expression correlates with survival in lung adenocarcinoma.** Kaplan-Meier survival analysis of lung adenocarcinoma patients stratified as TLR2-high vs TLR2-low expressing tumours from the cancer genome atlas. Statistical analysis was performed using the log-rank (Mantel-Cox) test. Data courtesy of Dr Andy Sims.

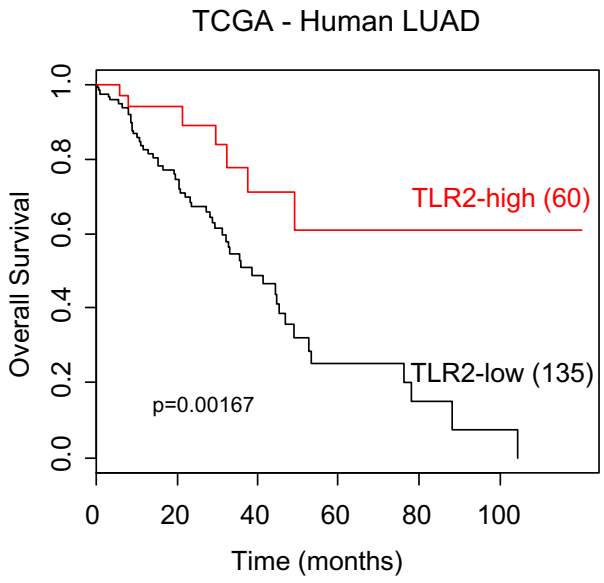

Importantly, the majority of LUAD samples in the TCGA are stage 1 (652/1046). When survival analysis was performed on stage 1 TCGA samples only, the survival benefit of high TLR2 expression remained (Figure 4.2), suggesting that the result outlined in figure 4.1 was not due to lower stage lesions exhibiting higher TLR2 expression than late-stage lesions with inherently poorer survival.

**Figure 4.2: *TLR2* expression correlates with survival in stage 1 lung adenocarcinoma.** Kaplan-Meier survival analysis of lung adenocarcinoma patients stratified as TLR2-high vs TLR2-low expressing tumours from the cancer genome atlas. Statistical analysis was performed using the log-rank (Mantel-Cox) test. Data analysed using kmplot.com.

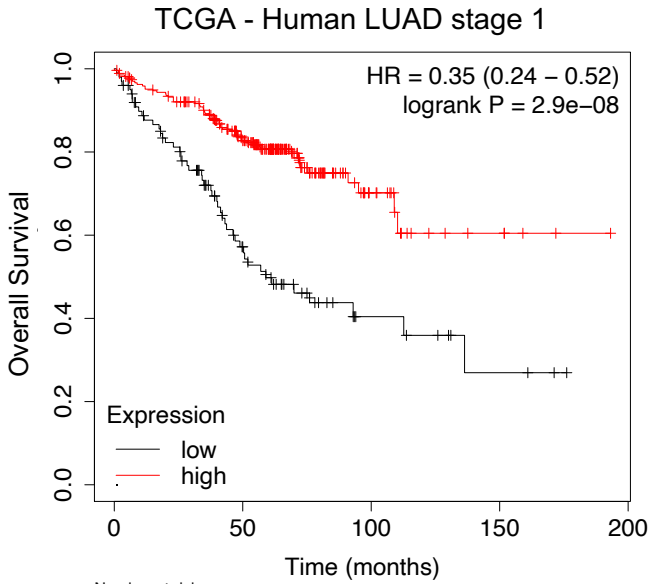


Following this result, a possible tumour suppressor function for *TLR2* was investigated using collaborations with clinicians from the University of Edinburgh (Professor William Wallace) and University College London

(Professor Sam Janes). Furthermore, we reanalysed a published RNA sequencing dataset of surgically resected preinvasive and invasive LUAD lesions (Chen et al., 2019).

## 4.3 *TLR2* and SASP expression in human LUAD

### 4.3.1 *TLR2* and the SASP is expressed in LUAD tumour epithelium

Firstly, in order to establish whether *TLR2* and the SASP is expressed in tumour epithelium, IHC staining was performed on FFPE surgical resection specimens of early stage (stage 1 and 2) human LUAD acquired from the Lothian Bioresource (in collaboration with Professor Wallace). Staining for TLR2 and IL-1β revealed extensive TLR2 and IL-1β expression in tumour epithelium, which was significantly increased compared to paired normal lung epithelium (Figure 4.3).

**Figure 4.3: TLR2 and IL-1β expression is increased in early-stage lung adenocarcinoma. (a)** IHC staining for TLR2 and IL-1β in paired normal lung epithelium (normal) and lung adenocarcinoma (LUAD). **(b)** H-score quantification for samples described in (a). Each dot represents one sample. n=10. Statistical analysis was performed using a paired *t*-test. ****p<0.0001.

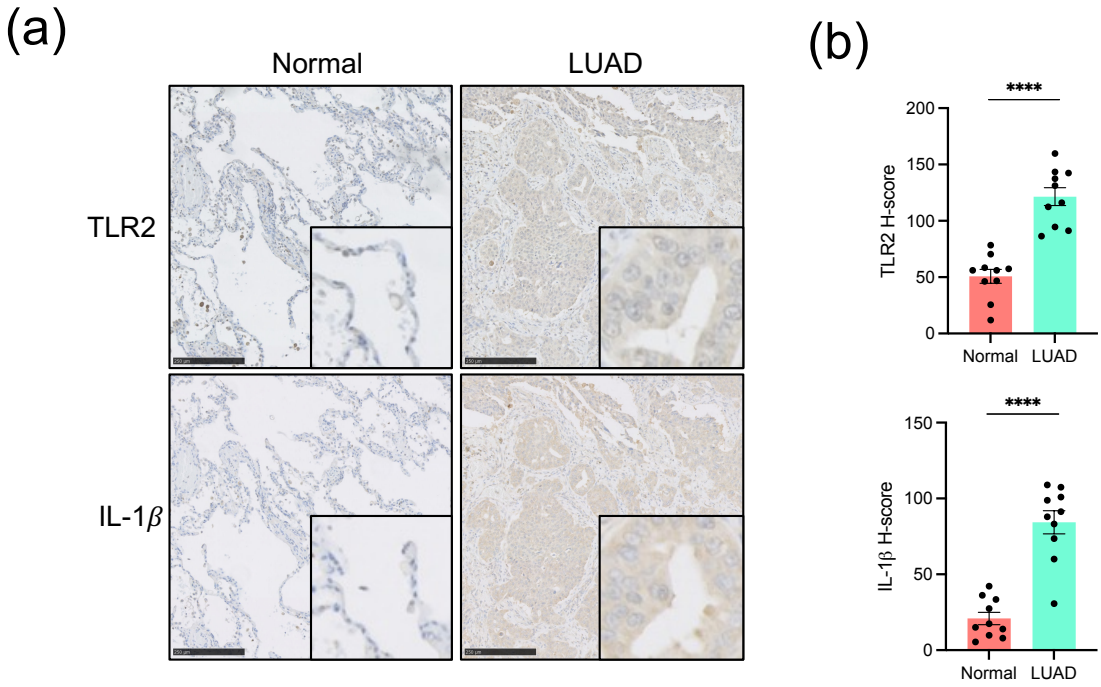


Furthermore, IHC staining for TLR2 and IL-1β was performed on consecutive sections, which revealed an overlap between TLR2 and IL-1β signal at the tumour epithelium (Figure 4.3). To confirm the correlation of TLR2 and IL-1β expression, automated H-score analysis on predefined tumour regions was performed using the software tool QuPath (Bankhead et al., 2017). Correlation between TLR2 and IL-1β H-score data was then assessed using Pearson correlation analysis, revealing a significantly positive correlation (Figure 4.4) in LUAD epithelium.

**Figure 4.4: TLR2 and IL-1β expression is positively correlated.** Scatter plot of TLR2 and IL-1β H-score analysis on serial IHC sections from predefined tumour regions. Each dot represents one tumour area from 12 samples in total. Analysis is performed using Pearson correlation analysis between TLR2 and IL-1β H-scores.

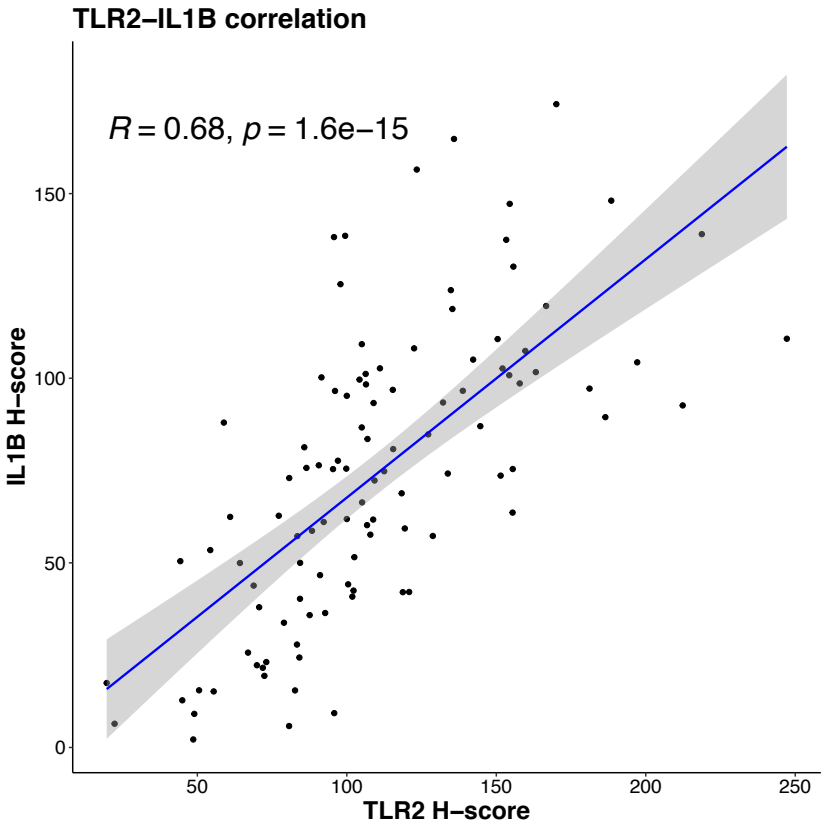


In collaboration with Professor William Wallace, lepidic (preinvasive) areas of adenocarcinoma were identified within the early-stage invasive LUAD resection specimens and TLR2 and IL-1β expression was measured using QuPath. This revealed that both TLR2 and IL-1β were also significantly increased in preinvasive epithelium compared to normal epithelium (Figure 4.5).

**Figure 4.5: TLR2 and IL-1β expression is increased in lepidic (preinvasive) lung adenocarcinoma. (a)** IHC staining for TLR2 and IL-1β in paired normal lung epithelium (normal) and lepidic (preinvasive) lung adenocarcinoma. **(b)** H-score quantification for samples described in (a). Each dot represents one sample. n=9. Statistical analysis was performed using a paired *t*-test. ***p<0.001.

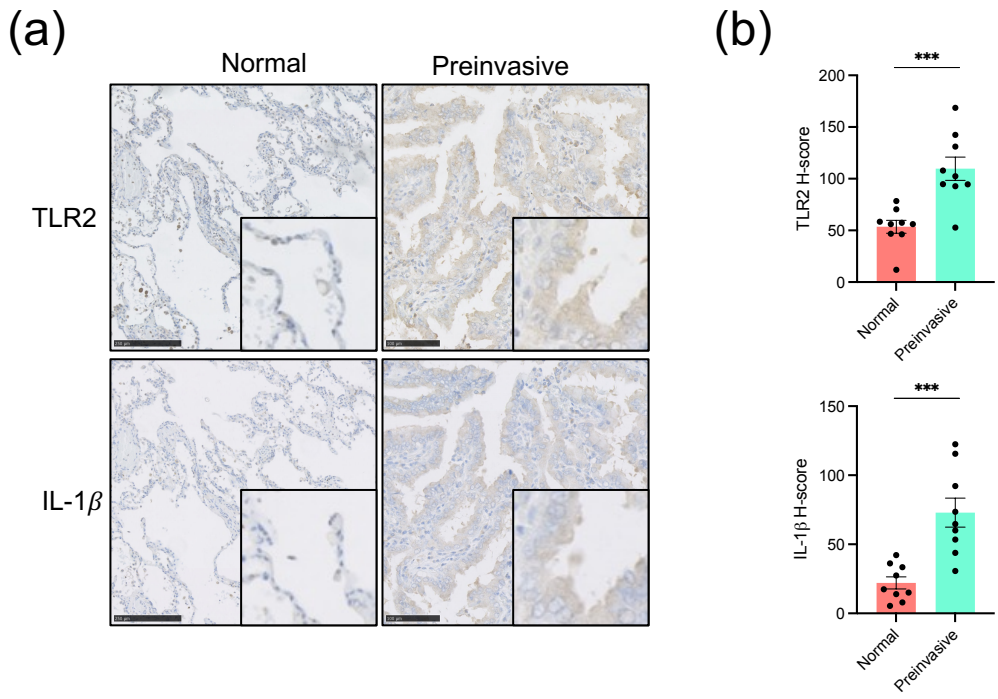


These data show that TLR2 and IL-1β are highly expressed in both preinvasive and invasive LUAD epithelium, and expression is strongly correlated.

### 4.3.2 *TLR2* expression is increased in preinvasive LUAD

Given that TLR2 and the SASP factor IL-1β are highly expressed in preinvasive and invasive LUAD epithelium (within the same tumour), the expression levels in individual preinvasive vs invasive lesions were investigated. Differential gene expression analysis was performed on a

published RNA sequencing dataset of preinvasive adenocarcinoma (AIS – adenocarcinoma in situ, MIA - minimally invasive adenocarcinoma) and invasive adenocarcinoma (LUAD) samples (Chen et al., 2019). Principal component analysis (PCA) demonstrated significant overlap of gene expression profiles of AIS and MIA lesions (Figure 4.6), therefore these preinvasive lesions were grouped together for further analysis.

**Figure 4.6: Gene expression profiles of lung adenocarcinoma precursor lesions.** Principal component analysis (PCA) of adenocarcinoma in situ (AIS), minimally invasive adenocarcinoma (MIA) and invasive lung adenocarcinoma (LUAD) lesions. Data analysed with the support of Dr Philippe Gautier.

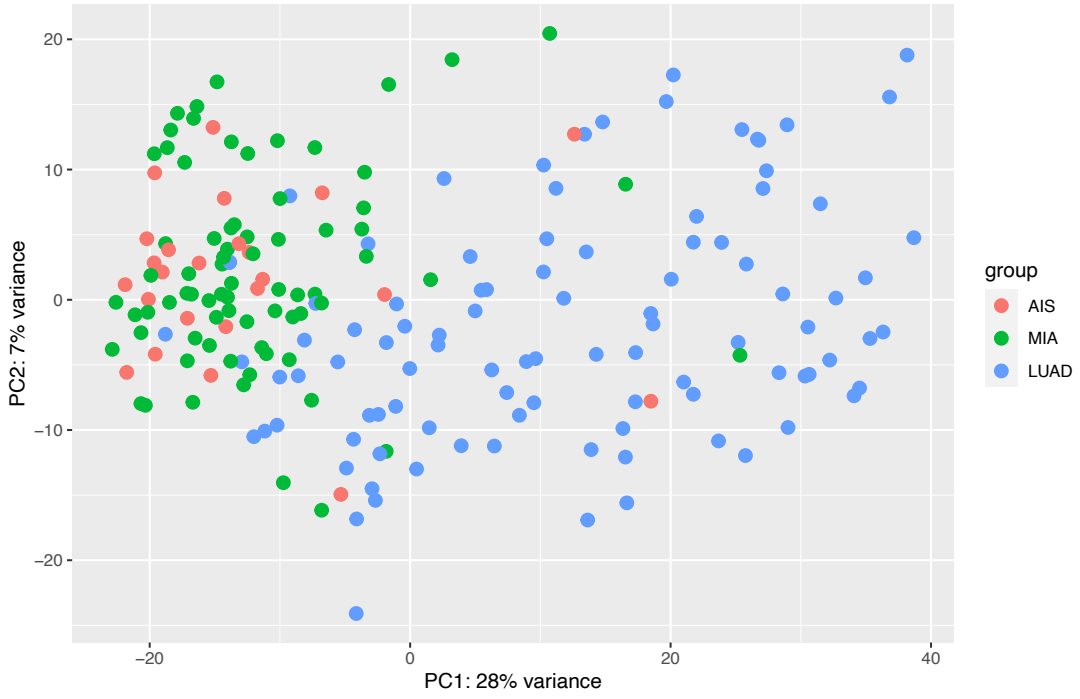

*TLR2* expression was compared between preinvasive (AIS/MIA) and invasive (LUAD) samples and it was demonstrated that *TLR2* expression is significantly increased in preinvasive lesions (Figure 4.7).

**Figure 4.7: *TLR2* expression is increased in preinvasive lung adenocarcinoma lesions.** Normalised *TLR2* read counts from preinvasive (AIS/MIA) and invasive (LUAD) samples. Each dot represents one sample. Statistical analysis was performed using the Mann-Whitney test.

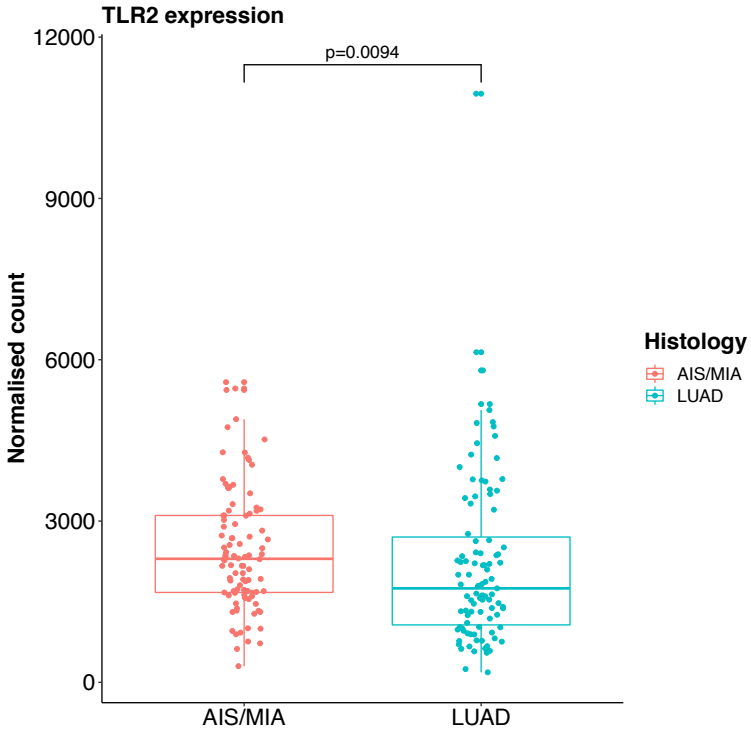


### 4.3.3 SASP expression is increased in preinvasive LUAD

Data from our HTVI murine model demonstrated that *Tlr2* regulates expression of the SASP (chapter 3). Therefore, the expression of several SASP factors was compared in preinvasive and invasive LUAD lesions by

analysing published RNA sequencing data (Chen et al., 2019). The analysis showed the SASP factors *IL1A* and *IL6* exhibit increased expression in preinvasive lesions, however there was no significant difference in *IL1B* expression (Figure 4.8).

**Figure 4.8: SASP expression is increased in preinvasive lung adenocarcinoma lesions.** Normalised read counts for the SASP factors *IL1A*, *IL1B* and *IL6* from preinvasive (AIS/MIA) and invasive (LUAD) samples. Each dot represents one sample. Statistical analysis was performed using the Mann-Whitney test.

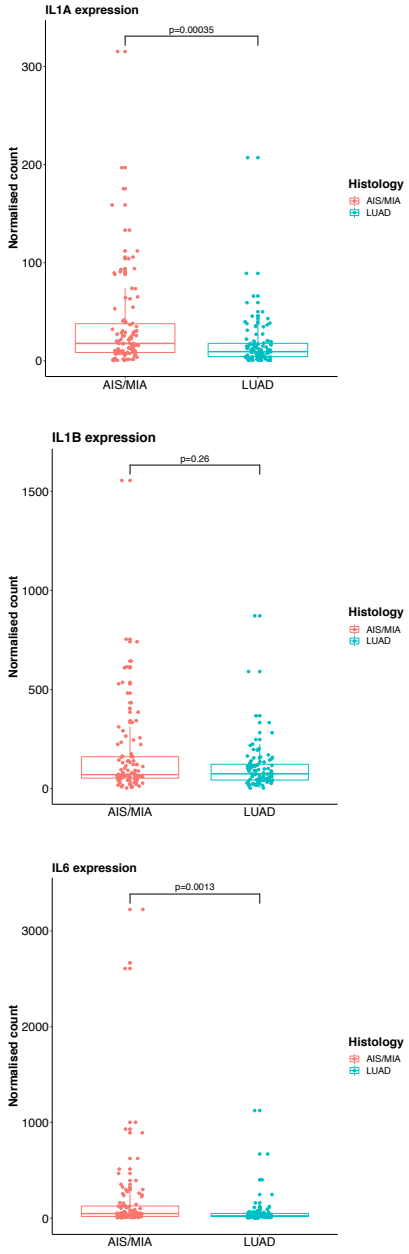

*TLR2* and SASP factor read counts were then analysed for correlation by plotting read counts on a scatter plot and performing Pearson correlation analysis. However, there was no significant positive correlation demonstrated between *TLR2* and any SASP factor (TLR2-ILB correlation shown in Figure 4.9).

**Figure 4.9: *TLR2* and *IL1B* RNA expression does not positively correlate.** Scatter plot of *TLR2* and *IL1B* read counts. Each dot represents one sample. Analysis is performed using Pearson correlation analysis.

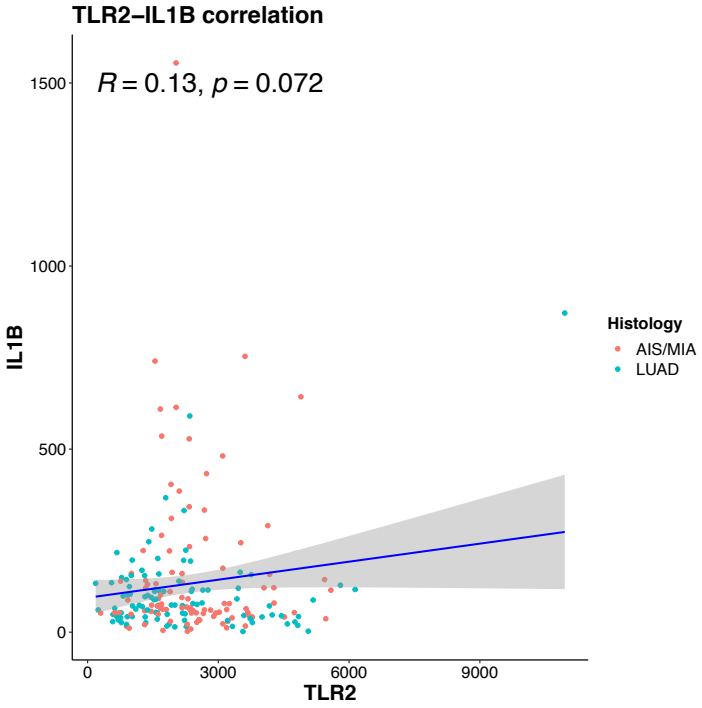


*TLR2* and SASP gene expression is high in immune cells, and correlation between the expression of these genes in immune cells is not expected. Therefore, this may explain the lack of positive correlation seen in

these bulk RNA sequencing samples, unlike the positive correlation observed at the protein level (Figure 4.4, chapter 4.3.1).

## 4.4 *TLR2* and SASP expression in preinvasive LUSC

### 4.4.1 *TLR2* expression correlates with clinical regression in preinvasive LUSC

Professor Sam Janes (University College London) is in possession of a unique biobank of clinically and molecularly phenotyped preinvasive LUSC lesions that have undergone longitudinal follow up using autofluorescence bronchoscopy, allowing the repeated identification and biopsy sampling of individual lesions over time (Figure 4.10).

**Figure 4.10**: **Autofluorescence bronchoscopy allows the identification of preinvasive large airway lesions.** Endobronchial view (via a bronchoscope) with normal white light (left) and autofluorescence bronchoscopy (AFB - right) allowing identification of preinvasive lesions and biopsy sampling. Image adjusted from olympusmedical.com.

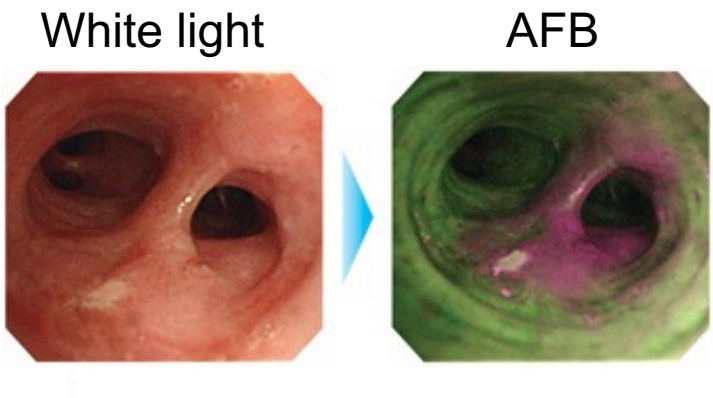

Upon longitudinal follow up it has been shown that not all high grade preinvasive LUSC lesions (high grade dysplasia/carcinoma in situ) progress to invasive malignancy. In fact, around 30% regress back to normal epithelium (Jeremy George et al., 2007) (Figure 4.11).

**Figure 4.11: Not all preinvasive squamous lung lesions progress to cancer.** Longitudinal follow up and serial endobronchial biopsy (performed using autofluorescence bronchoscopy) demonstrated that only 50% of high grade preinvasive LUSC lesions progress to invasive malignancy, with up to 30% regressing back to normal epithelium. H&E images courtesy of Dr Vitor Teixeira/Professor Sam Janes.

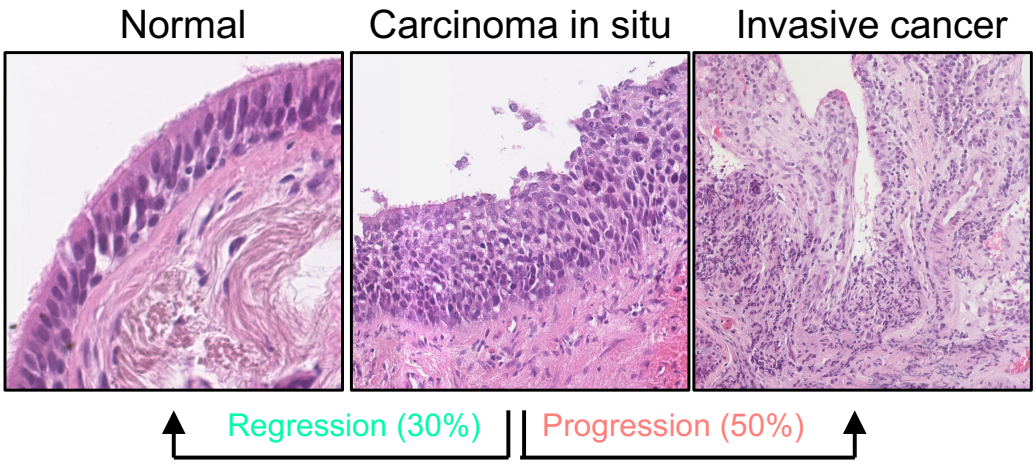


Using gene expression microarray platforms, Professor Janes' team have analysed the gene expression profiles of lesions that have subsequently gone on to either progress to invasive malignancy or regress to normal epithelium (Teixeira et al., 2019). Importantly, gene expression was measured in lesion epithelium only, as stroma was removed using laser capture microdissection prior to RNA extraction. Data analysed by Dr Adam

Pennycuick (UCL), revealed that *TLR2* expression is significantly increased in regressive lesions (Figure 4.12).

**Figure 4.12: *TLR2* expression is associated with clinical regression.** *TLR2* gene expression was measured, and expression levels were compared between lesions of equal grade that subsequently either progressed to invasive cancer (Prog.) or regressed to normal epithelium (Reg.). Each dot represents one sample. Statistical analysed was performed using a linear mixed effect model. Data courtesy of Dr Adam Pennycuick (UCL).

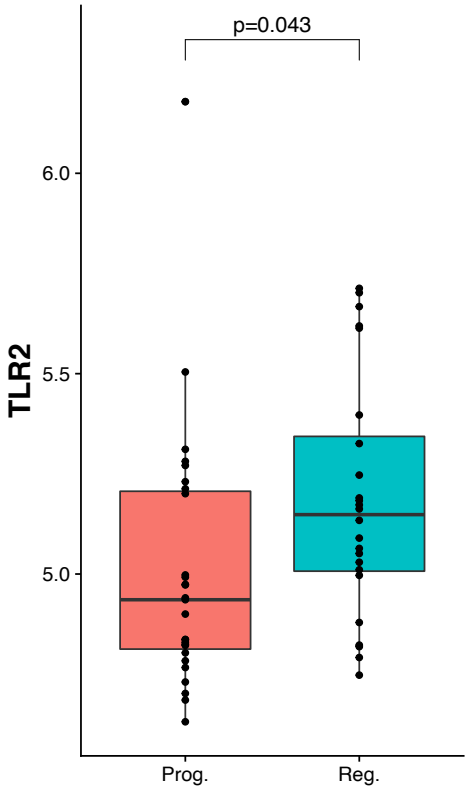


FFPE samples of progressive and regressive lesions from UCL were obtained in order to determine whether this differential expression occurs at the protein level. IHC staining for TLR2 was performed and again

demonstrated that TLR2 expression is increased in regressive lesions (Figure 4.13).

**Figure 4.13: TLR2 protein expression is associated with clinical regression. (a)** IHC staining for TLR2 was performed and compared between lesions of equal grade that subsequently either progressed to invasive cancer (Progressive) or regressed to normal epithelium (Regressive). **(b)** H-score quantification was performed using QuPath. Each dot represents one sample. n=3-4. Statistical analysis was performed using the Students *t*-test.

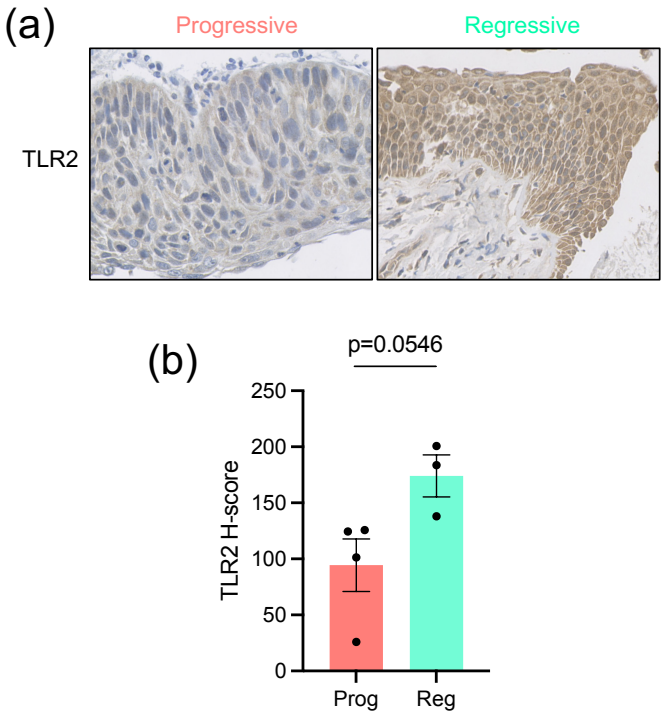


Whole genome sequencing of preinvasive LUSC lesions was performed by Professor Janes' team. There were no observed inactivating point mutations in *TLR2* in either progressive or regressive samples, however there were several samples exhibiting shallow deletions (loss of one

copy of the TLR2 gene). The likelihood of shallow deletions being present in progressive vs regressive lesions was analysed using Fisher's exact test and revealed that *TLR2* shallow deletions were more likely in progressive samples (p=0.07), suggesting that these shallow deletions may underpin the reduced *TLR2* expression observed in progressive lesions. Furthermore, shallow deletions in either *TLR2* or *TLR10* (the TLR2 binding partner shown to regulate OIS and the SASP (Hari et al., 2019)) was significantly more likely in progressive lesions (p=0.0086). This effect was specific for *TLR2* and its binding partners, as non-TLR2 associated plasma membrane TLRs (TLR4/5) showed no association with lesion progression (Table 4.1).

**Table 4.1:** The likelihood of shallow deletions of specific TLR genes being associated with lesion progression was assessed using Fisher's exact test. Data courtesy of Dr Adam Pennycuick (UCL).

| Gene | P-value |
|---|---|
| ***TLR2*** | 0.07113 |
| ***TLR2* or *TLR10*** | 0.008564 |
| ***TLR4*** | 0.6927 |
| ***TLR5*** | 1 |

### 4.4.2 SASP expression correlates with clinical regression in preinvasive LUSC

To investigate whether expression of the *TLR2* controlled SASP correlates with clinical regression, gene expression of SASP components that were regulated by TLR2 (as identified in (Hari et al., 2019)) were

measured in progressive and regressive samples. The geometric mean of gene expression values for all *TLR2* regulated SASP components was calculated for each sample and progressive vs regressive samples were compared, revealing that regressive samples had significantly increased expression of *TLR2* regulated SASP components compared to progressive samples (Figure 4.14).

**Figure 4.14: SASP expression is associated with clinical regression. (a)** TLR2 regulated SASP gene expression was measured and compared between lesions of equal grade that subsequently either progressed to invasive cancer (Prog.) or regressed to normal epithelium (Reg.). Each dot represents one lesion. Statistical analysed was performed using a linear mixed effect model. **(b)** Heat map showing differential expression of each TLR2 regulated SASP component in progressive vs regressive lesions. Data courtesy of Dr Adam Pennycuick (UCL).

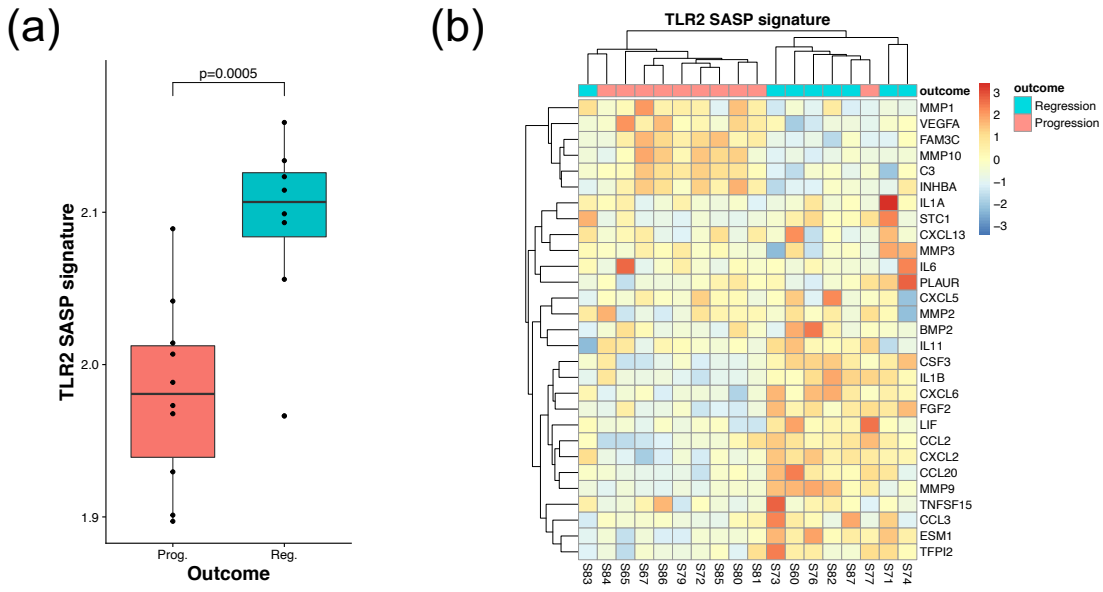

IHC staining for the key SASP factor IL-1β was then performed on FFPE samples of progressive and regressive lesions, and again confirmed that differential expression also occurs at the protein level (Figure 4.15).

**Figure 4.15: IL-1β protein expression is associated with clinical regression. (a)** IHC staining for IL-1β was performed and compared between lesions of equal grade that subsequently either progressed to invasive cancer (Progressive) or regressed to normal epithelium (Regressive). **(b)** H-score quantification was performed using QuPath. Each dot represents one sample. n=3-5. Statistical analysis was performed using the student *t*-test. *p<0.05.

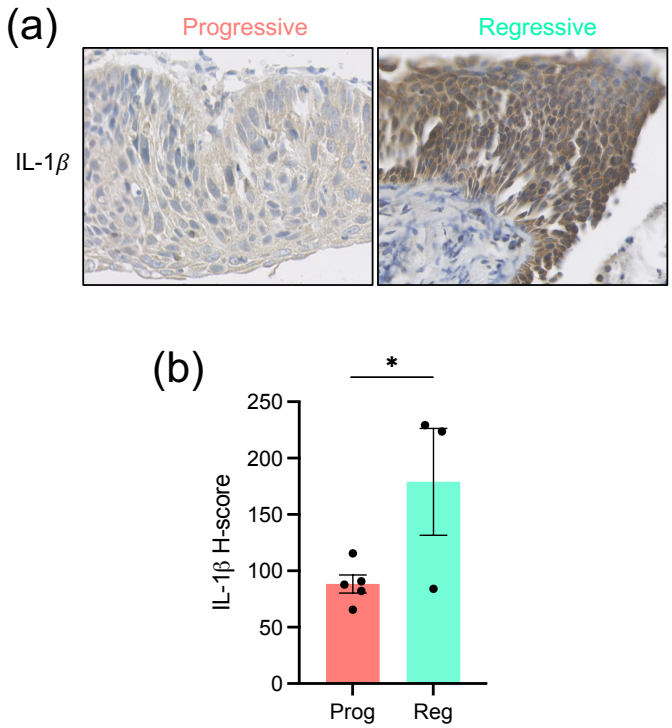


### 4.4.3 *TLR2* expression correlates with the expression of the SASP in preinvasive LUSC

To investigate whether expression of *TLR2* and the SASP is positively correlated the expression values were plotted on a scatter plot and subjected

to Pearson correlation analysis by Dr Adam Pennycuick (UCL). *TLR2* gene expression showed significant positive correlation with SASP gene expression in preinvasive LUSC epithelium (Figure 4.16) .

**Figure 4.16: *TLR2* and SASP expression are positively correlated in preinvasive squamous lung lesions.** Scatter plot of *TLR2* gene expression (TLR2) and the geometric mean of SASP gene expression (TLR2 SASP signature) in lesions of equal grade that subsequently either progressed to invasive cancer (Prog.) or regressed to normal epithelium (Reg.). Data was analysed using Pearson correlation analysis. Each dot represents one sample. Data courtesy of Dr Adam Pennycuick (UCL).

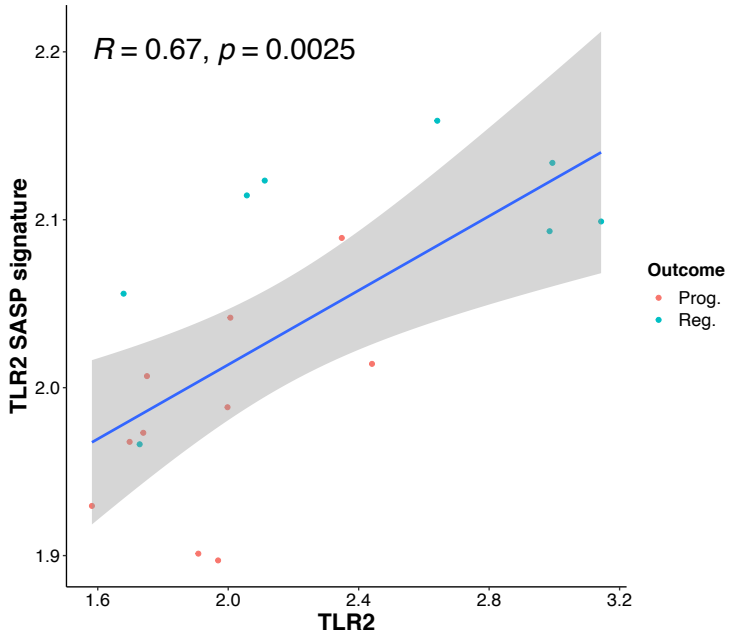


A similar analysis was performed using IHC H-score analysis on serial section stained for TLR2 and IL-1β, and again revealed significantly positive correlation between TLR2 and IL-1β expression (Figure 4.17), further

suggesting that TLR2 regulates SASP expression in preinvasive lesion epithelium.

**Figure 4.17: TLR2 and IL-1β expression are positively correlated in preinvasive squamous lung lesions.** Scatter plot of TLR2 and IL-1β H-score analysis in lesions of equal grade that subsequently either progressed to invasive cancer (Prog.) or regressed to normal epithelium (Reg.). Each dot represents one sample. Data was analysed using Pearson correlation analysis.

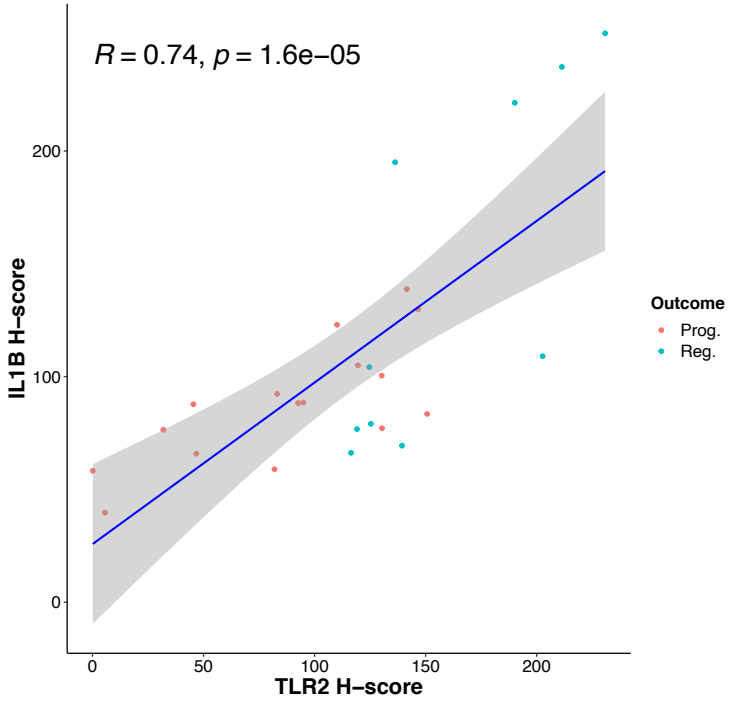


### 4.4.4 *TLR2* expression correlates with the expression of the acute phase response in preinvasive LUSC

Work from previous lab members (Dr Priya Hari) demonstrated that TLR2 regulates several components of the acute phase response (APR). The most strongly of which is acute phase serum amyloid A proteins 1 and 2

(A-SAAs) (Hari et al., 2019). Therefore, the gene expression levels of acute phase response proteins, including A-SAAs, were analysed as per SASP proteins (described in chapters 4.4.2 and 4.4.3) by Dr Adam Pennycuick. Interestingly, APR expression was significantly increased in regressive lesions (Figure 4.18).

**Figure 4.18: Expression of the acute phase response is associated with clinical regression. (a)** Acute phase response gene expression was measured and compared between lesions of equal grade that subsequently either progressed to invasive cancer (Prog.) or regressed to normal epithelium (Reg.). Each dot represents one sample. Statistical analysed was performed using a linear mixed effect model. **(b)** Heat map showing differential expression of each acute phase response component in progressive vs regressive lesions. Data courtesy of Dr Adam Pennycuick (UCL).

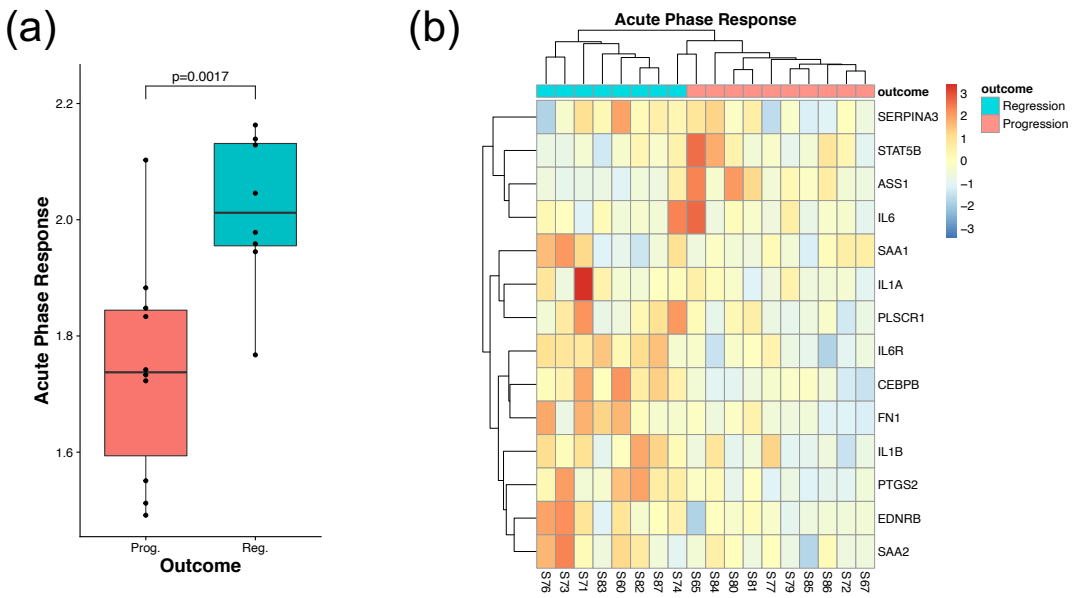

Furthermore, *TLR2* expression showed significant moderate positive correlation with APR expression (Figure 4.19). While this correlation is not as striking as the correlation between TLR2 and the TLR2-SASP signature, it nonetheless suggests that TLR2 also regulates the APR in this context.

**Figure 4.19: *TLR2* and the acute phase response are positively correlated in preinvasive squamous lung lesions.** Scatter plot of TLR2 and the geometric mean of acute phase response gene expression. Data was analysed using Pearson correlation analysis. Data courtesy of Dr Adam Pennycuick (UCL).

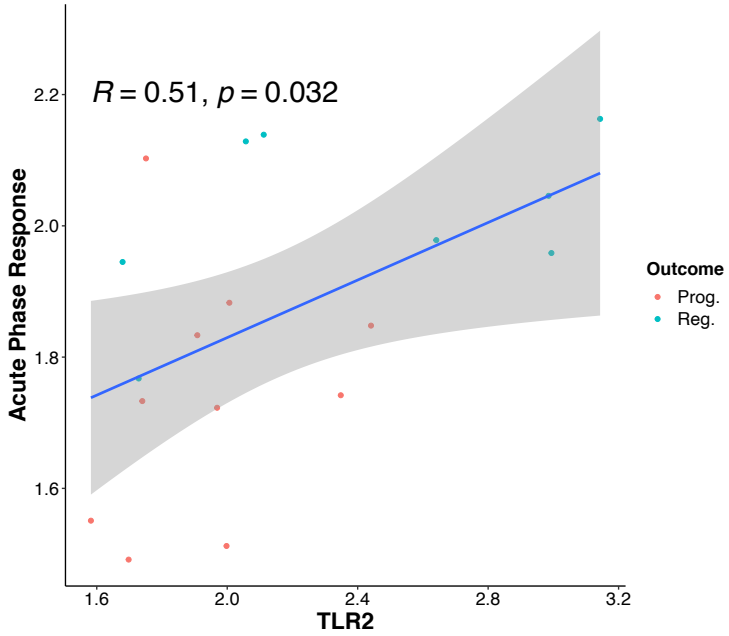

## 4.5 Chapter summary

In this chapter, the aim was to determine whether TLR2 signalling is active in human NSCLC and investigate whether this signalling plays a tumour suppressor function. Gene expression and IHC data from clinical samples of preinvasive and invasive LUAD and preinvasive LUSC were described and demonstrated that TLR2 and SASP signalling is highly active in human lung tumour epithelium. Furthermore, *TLR2* expression was increased in preinvasive LUAD and significantly correlated with clinical regression in preinvasive LUSC. From these data, it can be concluded that TLR2-SASP signalling is active in early-stage lung cancer, where it likely has a tumour suppressor function, preventing tumour progression to invasive malignancy.

# 5 : Results chapter 3

# Characterising the tumour suppressor role of *Tlr2* in non-small cell lung cancer

## 5.1 Chapter aims

Chapter four describes data demonstrating that *TLR2* and the SASP are highly expressed in human preinvasive NSCLC epithelium where they correlate with clinical regression and improved survival. These data suggest a tumour suppressor function for *TLR2* and the SASP in NSCLC. The aim of this thesis chapter is to test the hypothesis that *Tlr2* has a tumour suppressor role in lung tumours and investigate the mechanism of *Tlr2* mediated lung tumour suppression using a genetically engineered mouse model (GEMM) of NSCLC. The well-described loxP-STOP-loxP $Kras^{G12D}$ (hereafter $Kras^{LSL\text{-}G12D/+}$) mouse model was used, allowing tissue specific activation of oncogenic *Kras* signalling (Jackson et al., 2001). Using this model, the effect of *Tlr2* loss was investigated and functional studies were performed to characterise the mechanism of *Tlr2* mediated tumour suppression. In this chapter, the results from the NSCLC murine model experiments are described.

## 5.2 The effect of *Tlr2* loss on NSLC progression

### 5.2.1 *Tlr2* loss increases tumour number and size

*Kras*$^{LSL\text{-}G12D/+}$ mice on either a wild type (WT) or *Tlr2* null (*Tlr2*$^{-/-}$) background were intranasally inoculated with Adenovirus that expresses Cre-recombinase under the control of the CMV promoter (AdenoCre). Following transient local expression of Cre-recombinase, the STOP codon is removed upstream of the oncogenic *Kras*$^{G12D}$ allele, prompting activation of oncogenic *Kras* signalling at the lung epithelium (see Figure 1.9, chapter 1.6.7). Mice were humanely culled between 8-15 weeks later and lung tissue was harvested for histological analysis. *Tlr2*$^{-/-}$ mice exhibited more tumours and an increased tumour burden (tumour area/total lung area) indicating increased tumour formation and growth following *Tlr2* loss (Figure 5.1).

**Figure 5.1: Tlr2 loss enhances lung tumour initiation and growth. (a)** H&E images of lung tumours 12 weeks after AdenoCre inoculation in wild type (WT) or *Tlr2* null (*Tlr2*$^{-/-}$) *Kras*$^{LSL\text{-}G12D/+}$ mice with corresponding quantification for mice culled at 8-, 12- and 15-weeks post inoculation (p.i) in **(b)**. Each dot represents one mouse. n=3-4 (8 weeks), 5-6 (12 weeks) and 2-4 (15 weeks). Statistical analysis was performed using the Student's *t*-test. *p<0.05, **p<0.01.

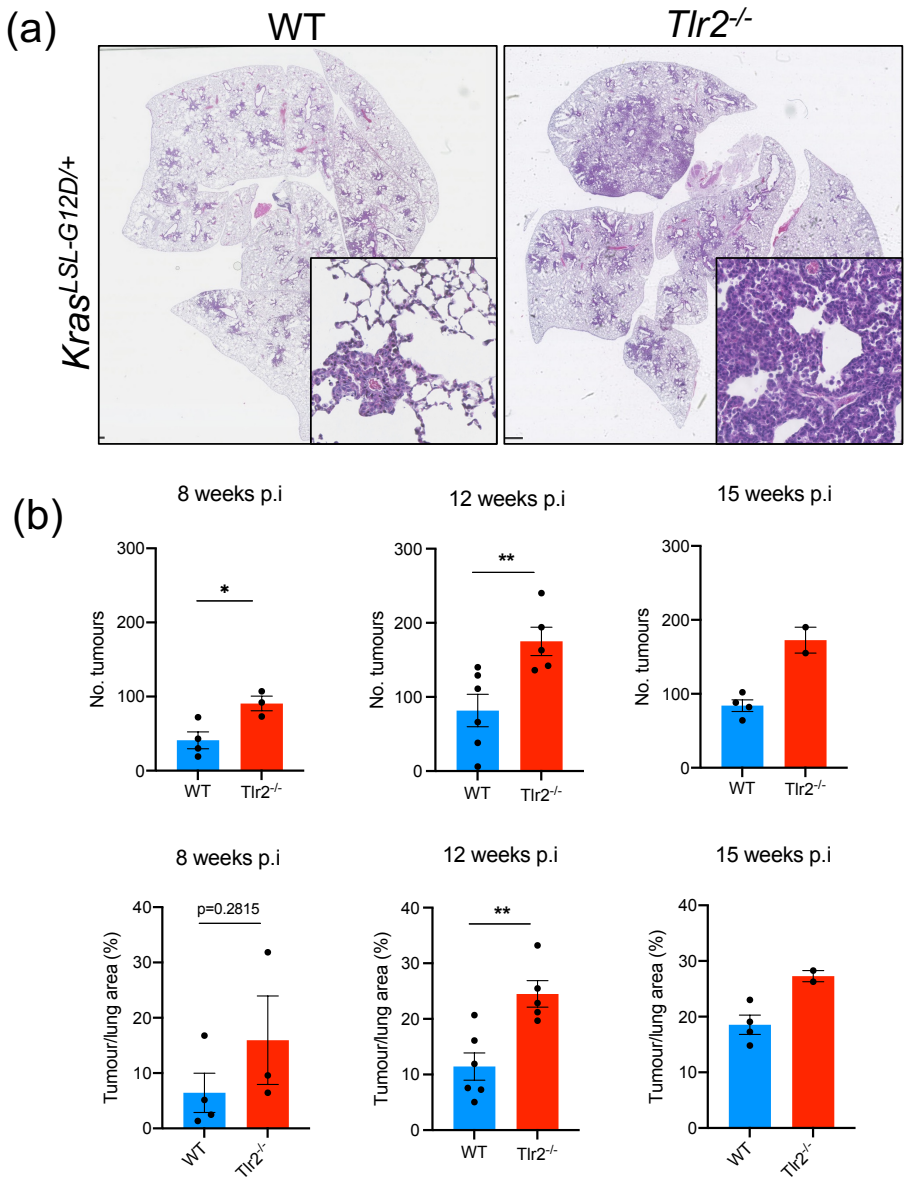

Lung tumour grading was then performed by two independent reviewers (Dr Fraser Millar and Dr John Connelly (Pathology SpR), University of Edinburgh) using predefined criteria (DuPage et al., 2009) as summarised in table 5.1.

**Table 5.1:** Lung tumour grading criteria, as described in (DuPage et al., 2009)

| Grade | Histology | Features |
|---|---|---|
| 1 | Atypical adenomatous hyperplasia | Hyperplastic, uniform nuclei, nucleoli absent |
| 2 | Adenoma | Large nuclei, prominent nucleoli |
| 3 | Adenocarcinoma | Cellular pleomorphism, nuclear atypia |
| 4 | Invasive adenocarcinoma | Irregular mitoses, invasive stroma (desmoplasia), invasion into lymphatic/blood vessels and pleura |

Inter-rater agreement was assessed using Cohens Kappa coefficient which revealed very good agreement (weighted Kappa 0.854, unweighted Kappa 0.789 (95% CI 0.698-0.880)). While there was no statistically significant difference in tumour grades, there was a trend towards reduced grade 1 lesions and increased grade 2 lesions in *Tlr2*$^{-/-}$ mice (Figure 5.2). Taken together, these data suggest that *Tlr2* loss promotes lung tumour progression.

**Figure 5.2: Tlr2 loss does not significantly affect histological tumour grade.** Tumour grading (as outlined in table 5.1) of lung tumours from wild type (WT) or *Tlr2* null (*Tlr2*$^{-/-}$) *Kras*$^{LSL\text{-}G12D/+}$ mice 12 weeks after AdenoCre inoculation. Each dot represents one mouse. n=5-6 mice. Statistical analysis was performed using the Student's *t*-test. ns – non-significant.

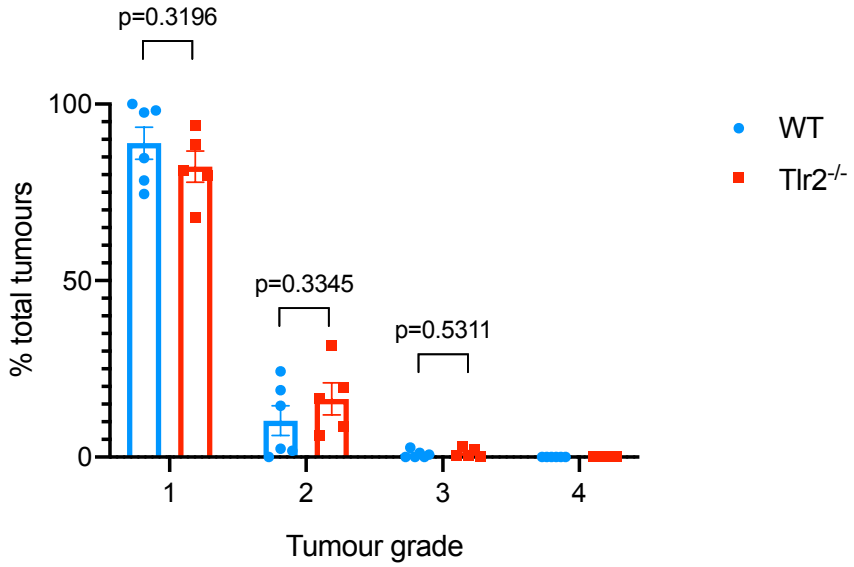


### 5.2.2 *Tlr2* loss worsens survival in murine NSCLC

To further determine the effect *Tlr2* loss has on lung tumour growth and survival, *Kras*$^{LSL\text{-}G12D/+}$ mice with either a WT or *Tlr2*$^{-/-}$ background were inoculated with AdenoCre then aged to morbidity. Mice were monitored daily with weekly weights recorded. Symptoms of moderate-severe breathless and weight loss precipitated immediate humane culling. Survival analysis was performed using a Kaplan-Meier curve (Figure 5.3). This demonstrated a significant survival disadvantage in *Tlr2*$^{-/-}$ mice. The mechanism of this tumour suppressor effect was then investigated, focusing on the role of *Tlr2*

in OIS and the SASP as previously outlined in (Hari et al., 2019) and chapter 3.

**Figure 5.3: Tlr2 loss impairs survival in lung tumour bearing mice.** Kaplan-Meier plot of survival of *Kras*$^{LSL\text{-}G12D/+}$ mice with either a WT (blue) or *Tlr2*$^{-/-}$ (red) background after inoculation with AdenoCre. Mice were aged to morbidity and were humanely culled once approaching the project license severity limit (moderate-severe breathless and weight loss >10%). n=13-15 mice. Statistical analysis was performed using the Mantel cox log-rank test.

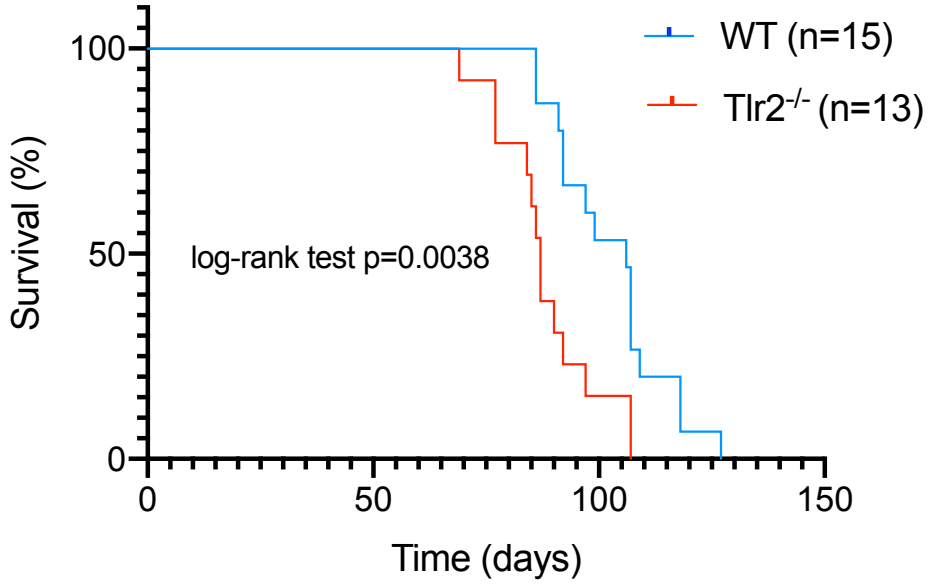

## 5.3 *Tlr2* loss and OIS in NSCLC

### 5.3.1 *Tlr2* loss impairs OIS in lung tumours primarily via p53-p21 signalling

To determine whether *Tlr2* loss impairs OIS in lung tumours, IHC analysis was performed. Staining for the proliferation marker Ki67, and markers of the two main tumour suppressor pathways activated in senescence (p53-p21 and p16-Rb) was performed. IHC staining for the cell cycle inhibitor p21 was used as a marker of p53-p21 pathways activation and Arf (alternate reading frame of the *Cdkn2a* locus) was used as a surrogate marker of p16-Rb pathway activation. Tumours enriched in senescent cells should demonstrate a low proliferative index (low Ki67 index) and high p21 and Arf expression, therefore these stains were used as markers of OIS. *Tlr2*$^{-/-}$ tumours exhibited significantly increased Ki67 expression, significantly reduced p21 expression and a trend towards reduced Arf expression (Figure 5.4), suggesting that *Tlr2*$^{-/-}$ tumours have an impaired ability to undergo OIS and that Tlr2 functions mainly via p53-p21 signalling to mediate this effect.

**Figure 5.4: Tlr2 loss impairs cell cycle arrest pathway activation. (a)** IHC staining for Ki67, p21 and Arf in lung tumours from *Kras*$^{LSL\text{-}G12D/+}$ mice with either a WT or *Tlr2*$^{-/-}$ background 12 weeks after inoculation with AdenoCre, with corresponding quantification in **(b)**. Five tumours chosen at random in a blinded fashion were analysed per mouse (each dot represents one tumour). n=5-6 mice per group. Statistical analysis was performed using the Student's *t*-test. ns – non-significant, *p<0.05, ***p<0.001.

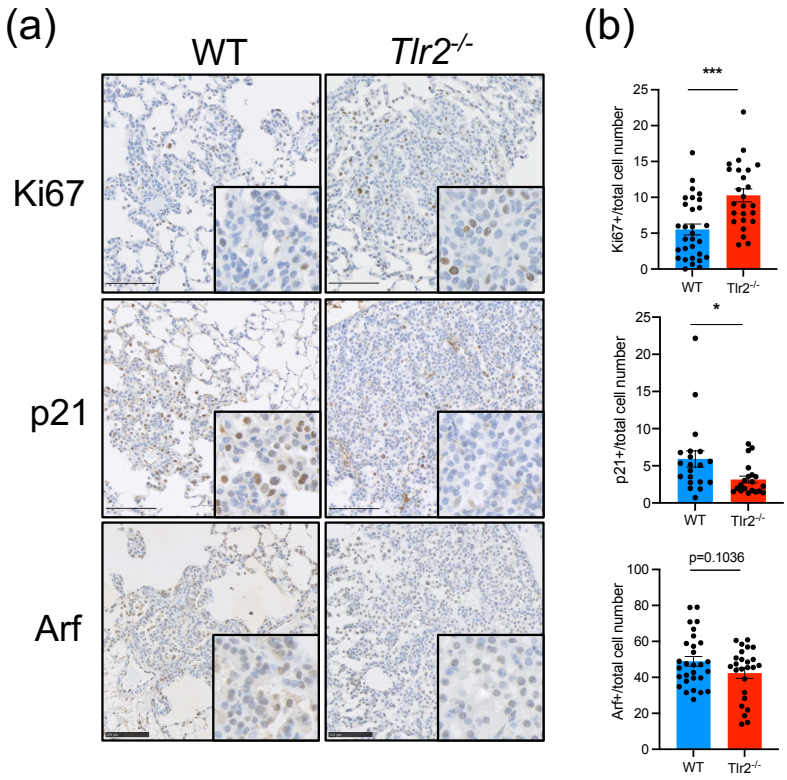


## 5.4 The tumour suppressor effect of *Tlr2* is not solely dependent on p53-p21 signalling

*Trp53* (the murine gene encoding p53) is a key regulator of OIS and data from chapter 5.3 indicates that *Tlr2* functions via p53-p21 signalling. To determine whether the tumour suppressor effect of *Tlr2* in murine NSCLC is

entirely dependent on p53-p21 signalling, a murine model allowing concurrent activation of *Kras*$^{G12D}$ and deletion of *Trp53* was used. So called 'KP' mice are heterozygous for the *Kras*$^{LSL\text{-}G12D}$ allele and homozygous for the 'floxed' *Trp53* allele. Therefore, local expression of Cre-recombinase concurrently activates *Kras*$^{LSL\text{-}G12D}$ and deletes *Trp53* (see Figure 1.10, chapter 1.6.7).

### 5.4.1 *Tlr2* loss increases tumour number and growth in KP mice

KP mice on either a WT or *Tlr2*$^{-/-}$ background were intranasally inoculated with AdenoCre and were humanely culled 12 weeks later. Lung tumour burden was increased in *Tlr2*$^{-/-}$ KP mice (Figure 5.5), suggesting that the tumour suppressor function of *Tlr2* is not entirely dependent on *Trp53*.

**Figure 5.5: Tlr2 loss enhances lung tumour growth in KP mice. (a)** H&E images of lung tumours 12 weeks after AdenoCre inoculation in wild type (WT) or *Tlr2* null (*Tlr2*$^{-/-}$) KP mice with corresponding quantification in **(b)**. Five tumours analysed per mouse (each dot represents one tumour). n=7-10 mice per group. Statistical analysis was performed using the Student's *t*-test. ns – non-significant, *p<0.05.

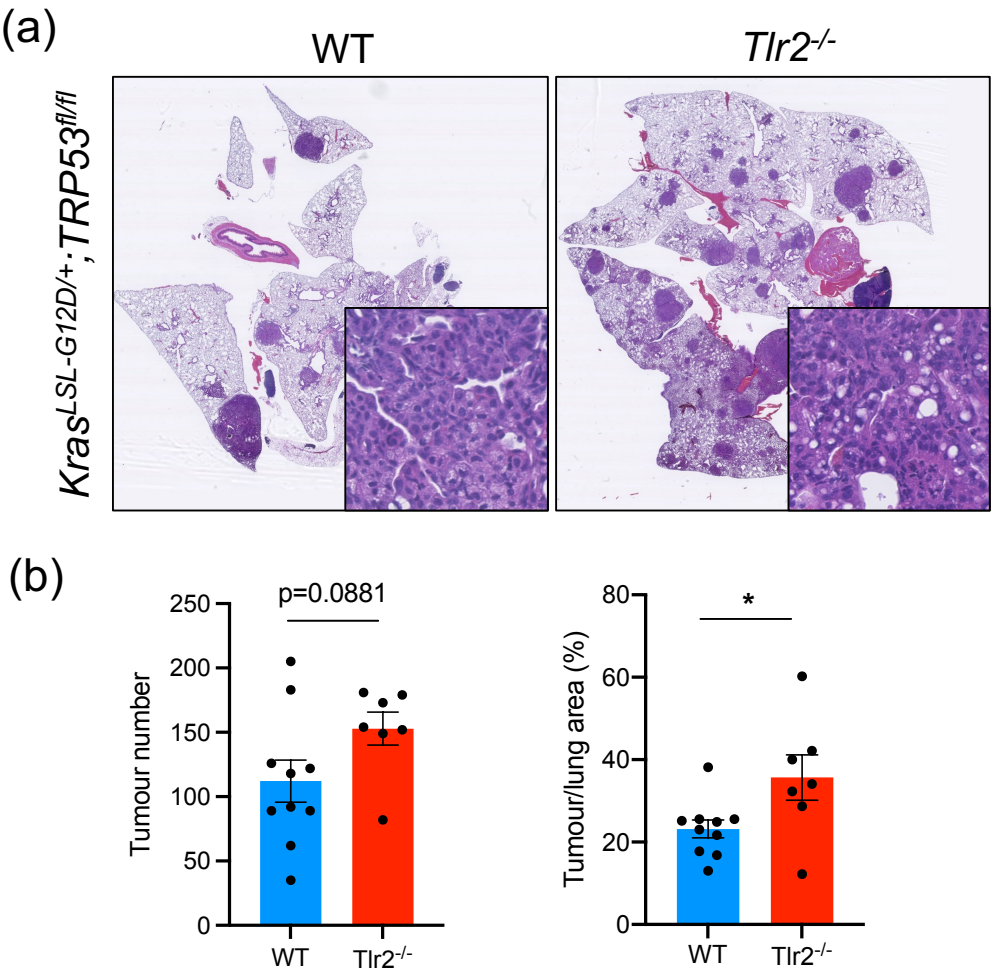


Tumour grading was then performed (as described table 5.1) and revealed a significant increase in high grade tumours (grade 2 and 3) and a significant reduction in low grade tumours (grade 1) in *Tlr2*$^{-/-}$ mice (Figure 5.6).

**Figure 5.6: Tlr2 loss leads to advanced histological grade in KP lung tumours.** Tumour grading (as outlined in table 14) of lung tumour from wild type (WT) or *Tlr2* null (*Tlr2*$^{-/-}$) KP mice 12 weeks after AdenoCre inoculation. Each dot represents one mouse. n=7-10 mice per group. Statistical analysis was performed using the Student's *t*-test. ns – non-significant, *p<0.05, **p<0.01, ***p<0.001.

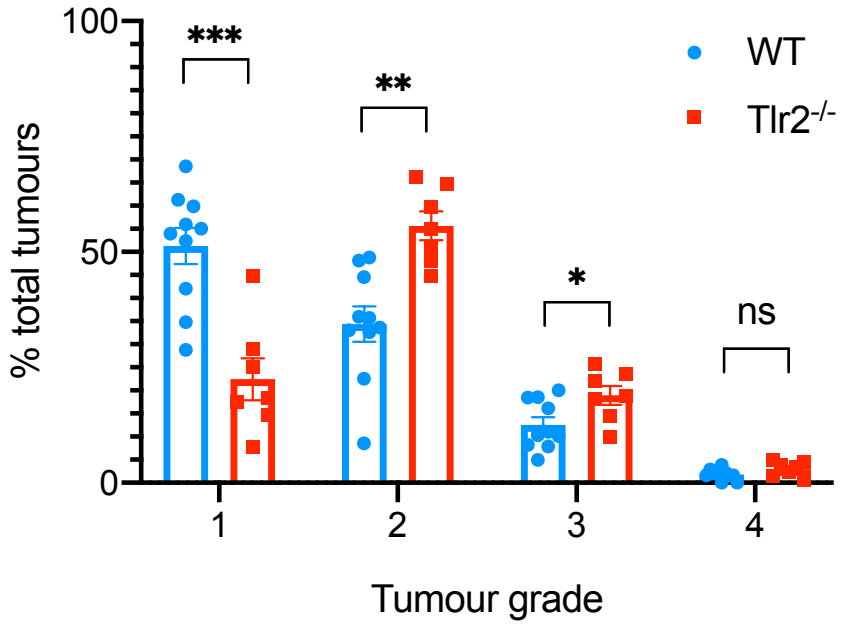


Tumour proliferation was also measured using Ki67 IHC staining and revealed that *Tlr2*$^{-/-}$ tumours from KP mice had a significantly increased proliferative index in comparison to control (Figure 5.7) further suggesting that the tumour suppressor role of *Tlr2* is not fully dependent on *Trp53* signalling.

**Figure 5.7: Tlr2 loss enhances proliferation in KP lung tumours. (a)** Ki67 IHC staining on lung tumours 12 weeks after AdenoCre inoculation in wild type (WT) or *Tlr2* null (*Tlr2*$^{-/-}$) KP mice with corresponding quantification in **(b)**. Five of the highest-grade tumours were analysed per mouse in a blinded fashion (each dot represents one tumour). n=7-10 mice per group. Statistical analysis was performed using the Student's *t*-test. *p<0.05.

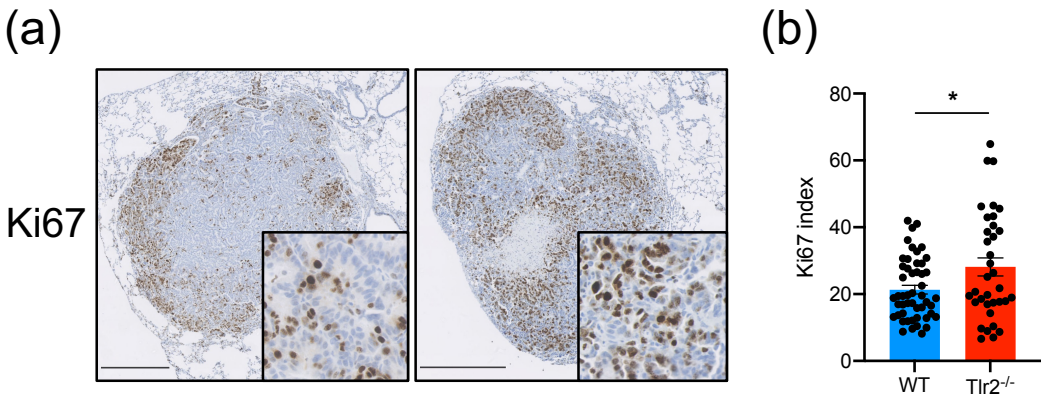


## 5.5 *Tlr2* loss impairs expression of the SASP in lung tumours

The SASP can function as a key non-cell autonomous tumour suppressor mechanism. Induction of the SASP is not reliant on tumour suppressor pathways and therefore experiments were performed to assess whether altered SASP expression was responsible for the *Trp53* independent tumour suppressor effects of *Tlr2*.

### 5.5.1 SASP expression is impaired in *Kras*$^{LSL\text{-}G12D/+}$ lung tumours following *Tlr2* loss

To determine whether *Tlr2* loss impairs expression of the SASP, IHC staining for the SASP factors interleukin-1α (IL-1α), interleukin-1β (IL-1β) and acute phase serum amyloid A (A-SAA) was performed on lung tumour sections from WT and *Tlr2*$^{-/-}$ *Kras*$^{LSL\text{-}G12D/+}$ mice (with intact *Trp53*). This revealed that *Tlr2*$^{-/-}$ lung tumours in *Kras*$^{LSL\text{-}G12D/+}$ mice express significantly lower levels of all three SASP factors (Figure 5.8). These data suggest that *Tlr2* is integral to the expression of the SASP in lung tumours, as is the case *in vitro* and in the HTVI model ((Hari et al., 2019) and chapter 3).

**Figure 5.8: Tlr2 impairs SASP expression in lung tumours. (a)** IHC staining for IL-1α, IL-1β and A-SAA in lung tumours from *Kras*$^{LSL\text{-}G12D/+}$ mice with either a WT or *Tlr2*$^{-/-}$ background with corresponding quantification in **(b)**. Five tumours analysed per mouse (each dot represents one tumour). n=5-6 mice per group. Statistical analysis was performed using the Student's *t*-test. ***p<0.001, ****p<0.0001.

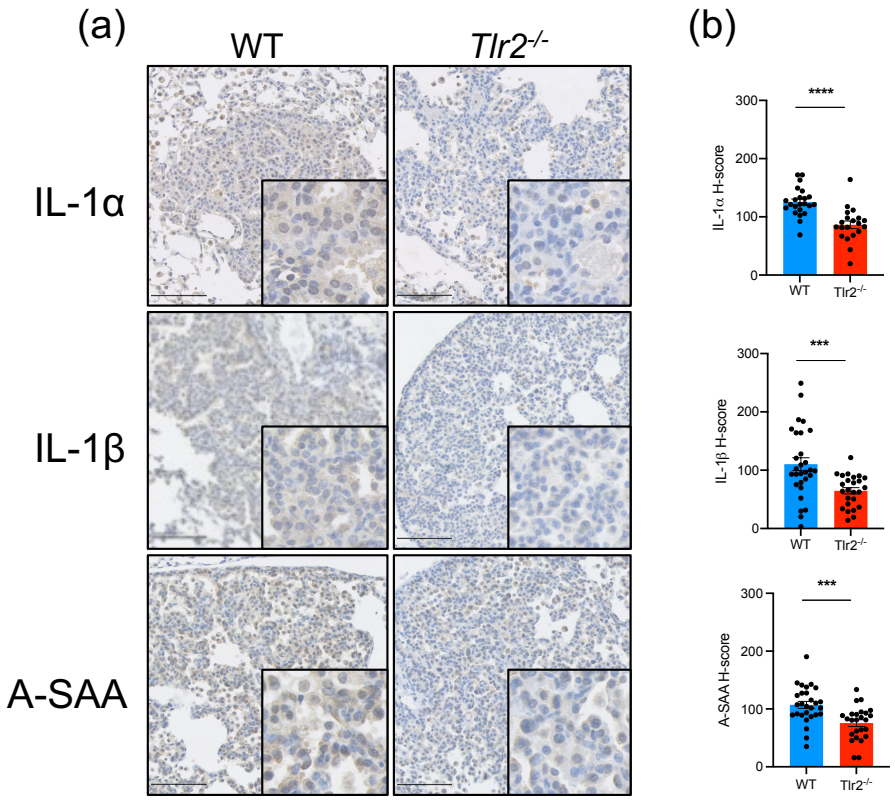


### 5.5.2 SASP expression is impaired in KP lung tumours following *Tlr2* loss

To determine whether SASP expression is dependent on *Trp53* signalling, IHC staining for the SASP factors IL-1α, IL-1β and A-SAA was performed on KP lung tumours with either a WT or *Tlr2*$^{-/-}$ background. This staining revealed that *Tlr2*$^{-/-}$ tumours from KP mice express significantly lower levels of all three SASP factors (Figure 5.9), confirming that *Tlr2* regulates

expression of these pro-inflammatory SASP factors in murine lung tumours independently of *Trp53*. This may explain the persisting lung tumour promoting effect of *Tlr2* loss in the absence of *Trp53*.

**Figure 5.9: Tlr2 impairs SASP expression in KP lung tumours. (a)** IHC staining for IL-1α, IL-1β and A-SAA in lung tumours from KP mice with either a WT or *Tlr2*$^{-/-}$ background with corresponding quantification in **(b)**. Five tumours analysed per mouse (each dot represents one tumour). n=7-10 mice per group. Statistical analysis was performed using the Student's *t*-test. ***p<0.001, ****p<0.0001.

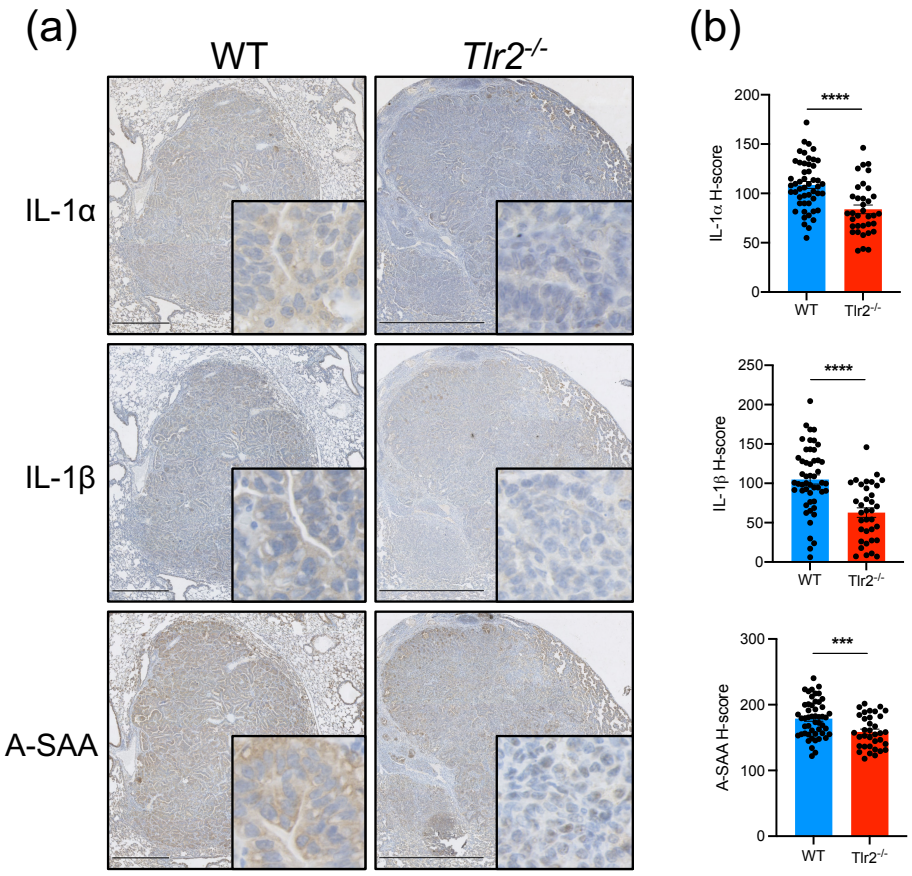

## 5.6 *Tlr2* loss impairs immune cell recruitment to lung tumours

### 5.6.1 Immune cell analysis in lung tumours

The SASP is integral in the regulation of senescence surveillance (Kang et al., 2011; Xue et al., 2007). Therefore, immune cell recruitment to lung tumours in WT and *Tlr2*$^{-/-}$ mice was investigated. Multicolour flow cytometry was performed on lung single cell suspensions from tumour bearing mice, and IHC staining for immune cell markers was performed on FFPE samples from tumour bearing mice. A flow cytometry panel was designed to analyse both lymphoid and myeloid population and is outlined in Figure 5.10.

**Figure 5.10: Immune cell population analysis using flow cytometry.** Flow cytometry gating strategy used to analyse lymphoid and myeloid populations in lung single cell suspensions. Gating protocol from (Busch et al., 2016).

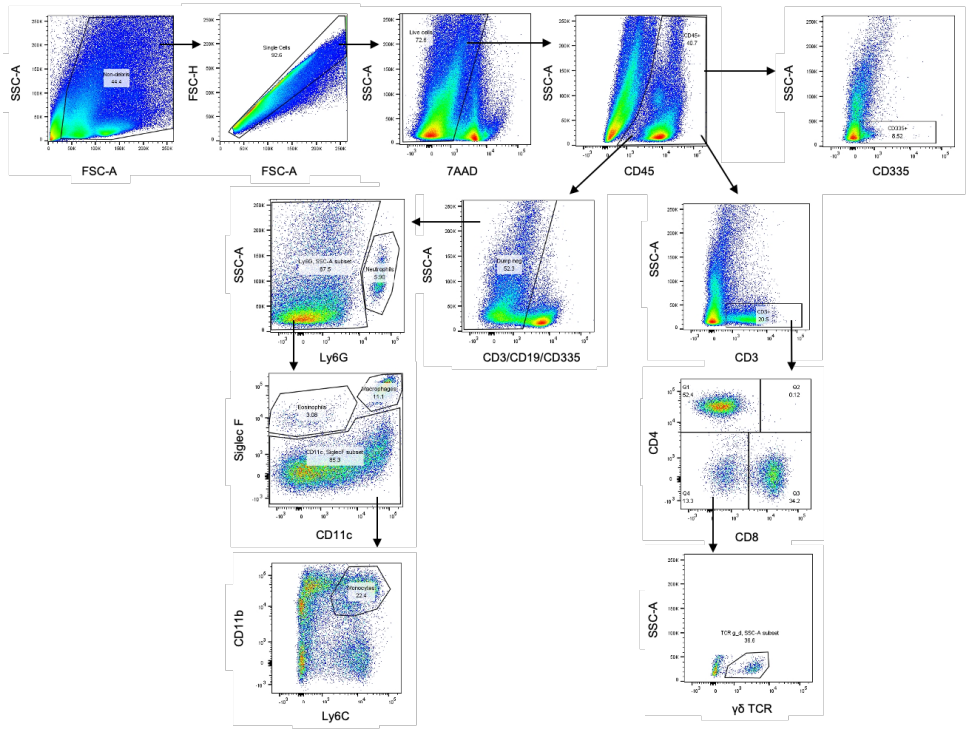


A significant reduction in total immune cells ($CD45^+$ cells) was observed in tumour bearing lungs from *Tlr2*$^{-/-}$ mice (Figure 5.11), suggesting that tumour immune cell recruitment is impaired following *Tlr2* loss. This result prompted further analysis into different immune cell populations to determine what population is affected by *Tlr2* loss.

**Figure 5.11: Tlr2 loss impairs total immune cell recruitment to lung tumours.** Total CD45$^{+}$ cells per gram of tissue were quantified using flow cytometry on lung single cell suspensions isolated from tumour bearing lungs from WT (blue) or *Tlr2*$^{-/-}$ (red) *Kras*$^{LSL\text{-}G12D/+}$ mice. Each dot represents one mouse. n=12 mice per group. Statistical analysis was performed using the Student's *t*-test. *p<0.05.

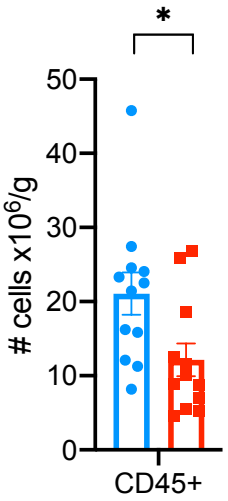


### 5.6.2 Macrophage/monocyte recruitment is impaired following *Tlr2* loss

Myeloid populations were analysed as described in Figure 5.10. There was a significant reduction in macrophages and a non-significant trend towards a reduction in monocytes in *Tlr2*$^{-/-}$ tumour bearing lungs (Figure 5.12).

**Figure 5.12: Myeloid derived population analysis using flow cytometry. (a)** Representative flow cytometry analysis of myeloid cells in lung single cell suspensions from tumour bearing wild-type (WT) and *Tlr2* null (*Tlr2*$^{-/-}$) mice. % denotes the percentage of parent population. Corresponding quantification in **(b)**. Each dot represents one mouse. Mono – monocytes, Eos – Eosinophils, Mac – Macrophages, Neut – Neutrophils. n=12 mice per group. Statistical analysis was performed using the Student's *t*-test. *p<0.05.

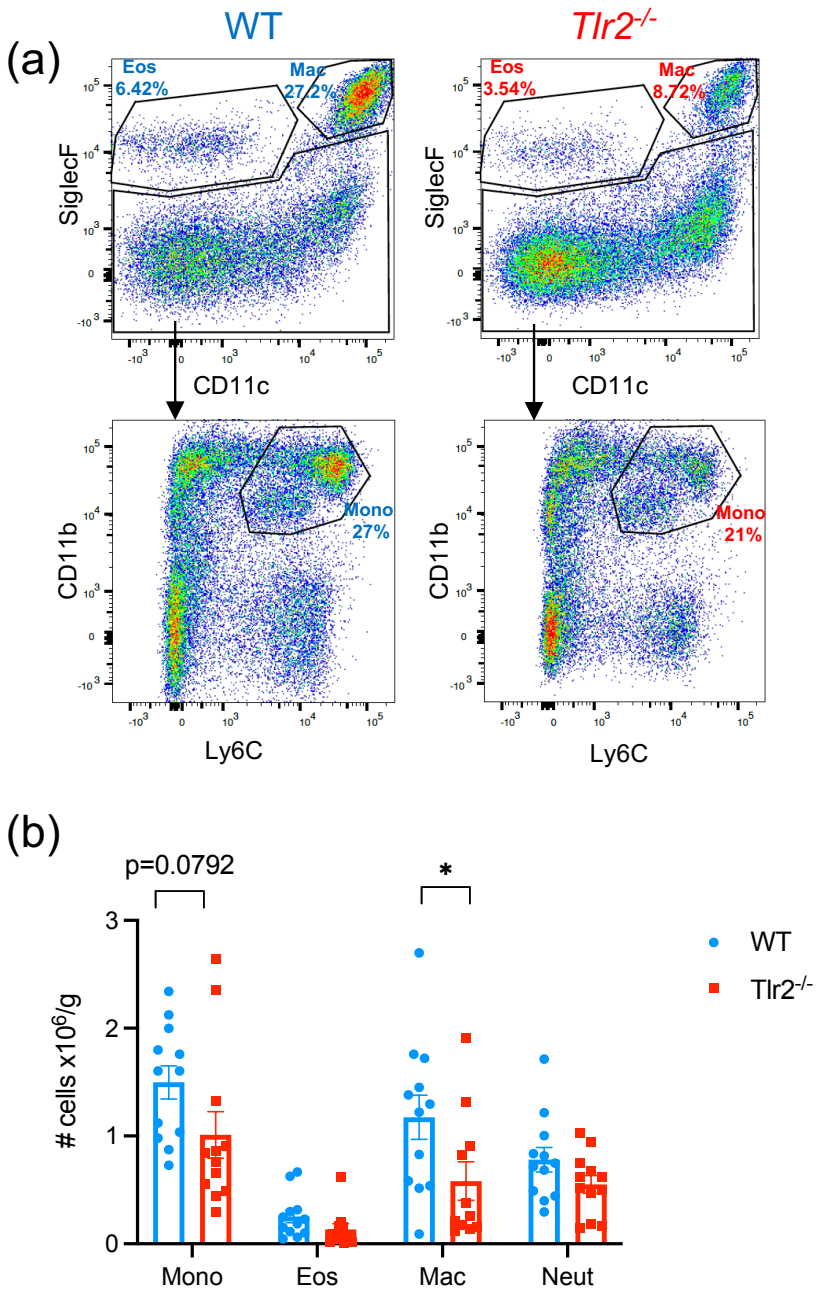

A limitation of the flow cytometry experiments is that the whole lung is sampled, not just tumours. To further assess the recruitment of immune cells to lung tumours specifically, IHC staining for the pan monocyte/macrophage marker CD68 was performed. Quantification of CD68+ cells within lung tumours was performed and revealed significantly reduced infiltration of $CD68^{+}$ cells in *Tlr2*$^{-/-}$ lung tumours (Figure 5.13), suggesting that recruitment/proliferation of monocyte/macrophages to lung tumours is impaired in *Tlr2*$^{-/-}$ mice.

**Figure 5.13: Monocyte/macrophage recruitment is impaired in *Tlr2*$^{-/-}$ lung tumours. (a)** CD68 IHC staining on lung tumours 12 weeks after AdenoCre inoculation in wild type (WT) or *Tlr2* null (*Tlr2*$^{-/-}$) *Kras*$^{LSL\text{-}G12D/+}$ mice with corresponding quantification in **(b)**. Five tumours analysed per mouse (each dot represents one tumour). n=5-6 mice per group. Statistical analysis was performed using the Student's *t*-test. **p<0.01.

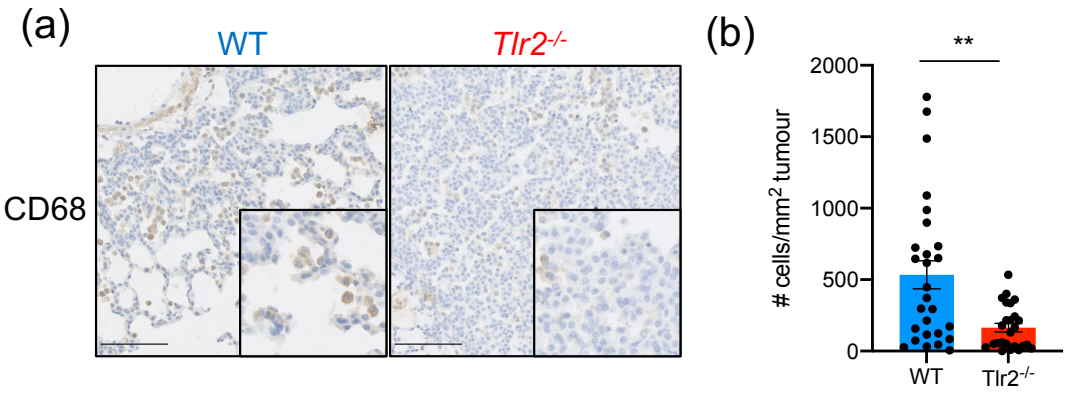

### 5.6.3 Lymphoid cell recruitment is maintained following Tlr2 loss

Lymphoid populations were analysed as described in Figure 5.10. While there was a trend towards a reduction in $CD3^+$ cells, this was not statistically significant. Furthermore, there was no significant difference in T-cell subsets ($CD4^+$, $CD8^+$ and NK cells) (Figure 5.14).

**Figure 5.14: Lymphoid derived population analysis using flow cytometry. (a)** Representative flow cytometry analysis of lymphoid cells in lung single cell suspensions from tumour bearing wild-type (WT) and *Tlr2* null (*Tlr2*$^{-/-}$) mice. % denotes the percentage of parent population. Corresponding quantification in **(b)**. CD3+ – total T-cells, CD4+ – CD4$^{+}$ T-cells, CD8+ – CD8$^{+}$ T-cells, NK – Natural killer cells. Each dot represents one mouse. n=12 mice per group. Statistical analysis was performed using the Student's *t*-test. ns – non-significant.

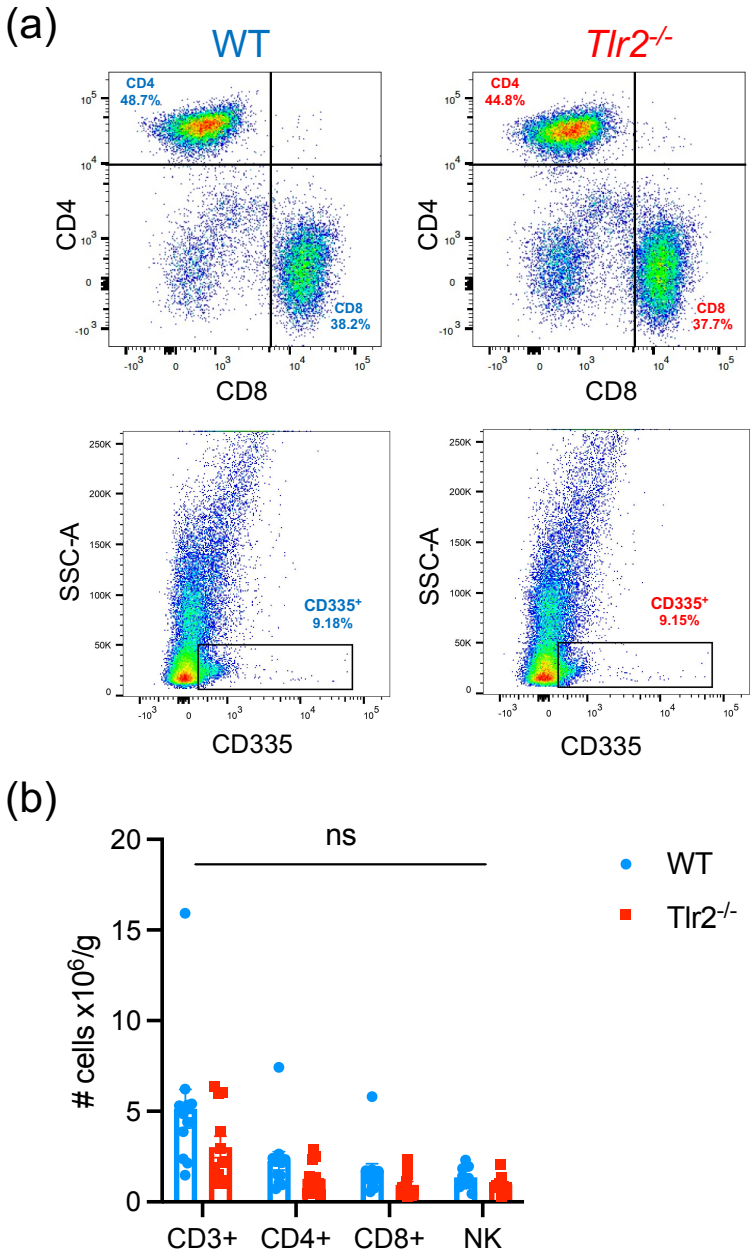

To investigate this further and to assess lymphoid cell recruitment to lung tumours specifically, IHC staining for the pan T-cell marker CD3 and specific T-cell markers CD4 and CD8 was performed. This also revealed no significant difference between WT and *Tlr2*$^{-/-}$ samples (Figure 5.15), suggesting that tumour associated lymphoid populations are unchanged following *Tlr2* loss.

**Figure 5.15: T-cell recruitment is unchanged in *Tlr2*$^{-/-}$ lung tumours. (a)** IHC staining for CD3, CD4 and CD8 on lung tumours 12 weeks after AdenoCre inoculation in wild type (WT) or *Tlr2* null (*Tlr2*$^{-/-}$) *Kras*$^{LSL\text{-}G12D/+}$ mice with corresponding quantification in **(b)**. Five tumours analysed per mouse (each dot represents one tumour). n=5-6 mice per group. Statistical analysis was performed using the Student's *t*-test.

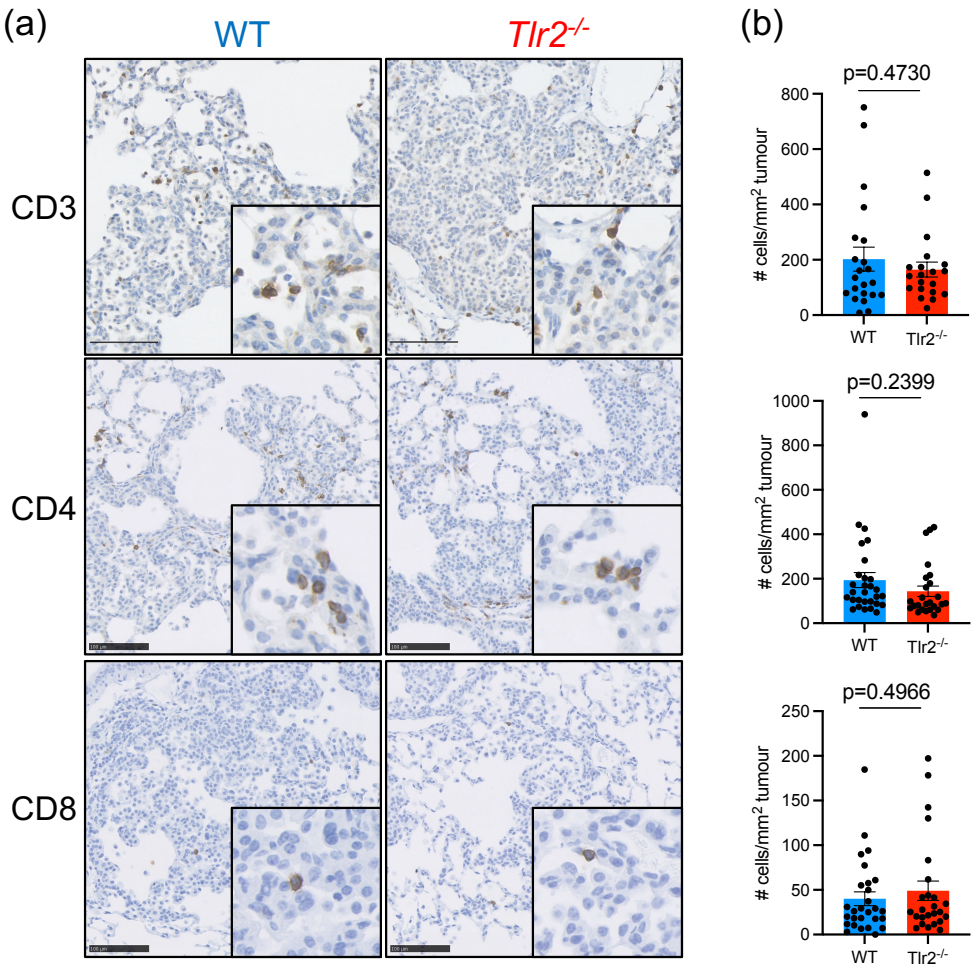


### 5.6.4 Gamma-delta T-cells and *Tlr2*

Gamma-delta ($\gamma\delta$) T-cells are tissue resident innate lymphoid cells that have been shown to enhance tumour progression following expansion of the commensal lung microbiota (Jin et al., 2019a). Conceivably, given the

integral role TLRs play in innate immune responses, *Tlr2* loss may permit expansion of the lung microbiota and thus promote tumour growth. To investigate this, γδ T-cells were analysed using flow cytometry as described in Figure 5.10. There was no significant expansion of γδ T-cells in *Tlr2*$^{-/-}$ lungs (in fact a trend towards a reduction was observed) (Figure 5.16), suggesting that dysbiosis mediated γδ T-cell expansion is unlikely to be the underlying cause of enhanced tumour progression following *Tlr2* loss.

**Figure 5.16: Gamma-delta T-cell population analysis using flow cytometry. (a)** Representative flow cytometry analysis of γδ T-cells in lung single cell suspensions from tumour bearing wild-type (WT) and *Tlr2* null (*Tlr2*$^{-/-}$) mice. % denotes the percentage of parent population. Corresponding quantification in **(b)**. Each dot represents one mouse. γδ TCR – γδ T-cells. n=12 mice per group. Statistical analysis was performed using the Student's *t*-test. ns – non-significant.

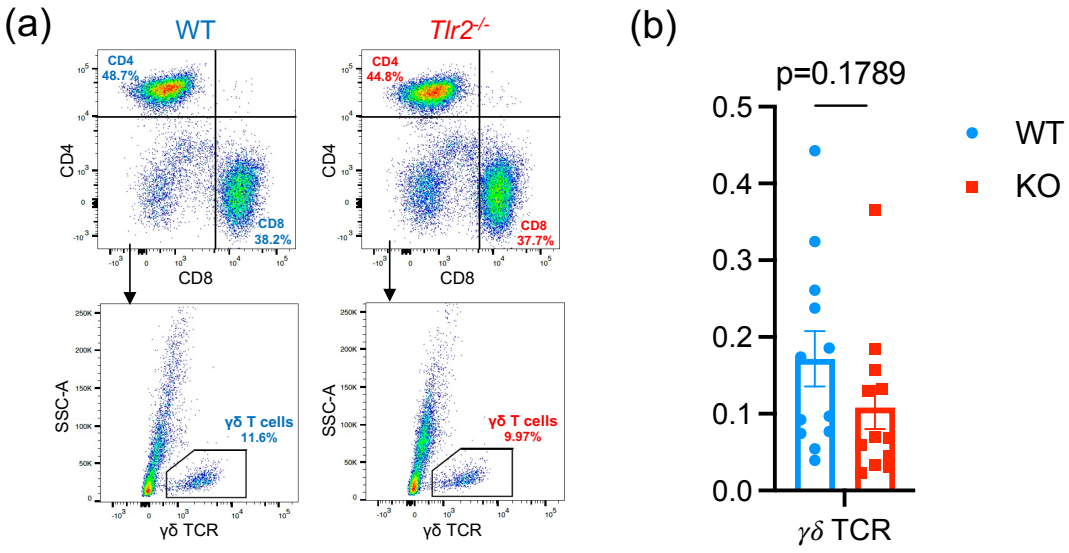

### 5.6.5 Th17 cell differentiation is impaired possibly due to reduced A-SAA expression

Th17 cells are T-cells that protect the gut barrier from pathogenic microbes (Honda and Littman, 2016) but have also been shown to be integral in several pro-inflammatory diseases (McGeachy et al., 2019). Following microbial stimulation, naïve $CD4^+$ T-cells differentiate into IL17A producing Th17 cells to exhibit homeostatic functions at the gut epithelial barrier. In this context, the cytokine production of Th17 cells is regulated by serum amyloid A (A-SAA) proteins, which are secreted by neighbouring gut epithelial cells (Ivanov et al., 2009; Sano et al., 2015). This SAA-Th17 signalling axis has been shown to be hijacked in pathogenic settings such as autoimmune disease (Lee et al., 2020) however the role this signalling axis plays in malignant disease has not yet been investigated. Given the key role *Tlr2* plays in the regulation of A-SAA protein expression in lung tumours, preliminary experiments analysing IL17A producing Th17 cells in lung single cell suspensions from tumour bearing mice were performed. A separate flow cytometry panel was designed for use on stimulated fixed cells (required for intracellular cytokine staining) as shown in Figure 5.17.

**Figure 5.17: Th17 cell population analysis using flow cytometry.** Flow cytometry panel used to analyse the proportion of CD4+ cells that co-express Th17 cell markers (RORγT$^{+}$FoxP3$^{-}$IL17A$^{+}$).

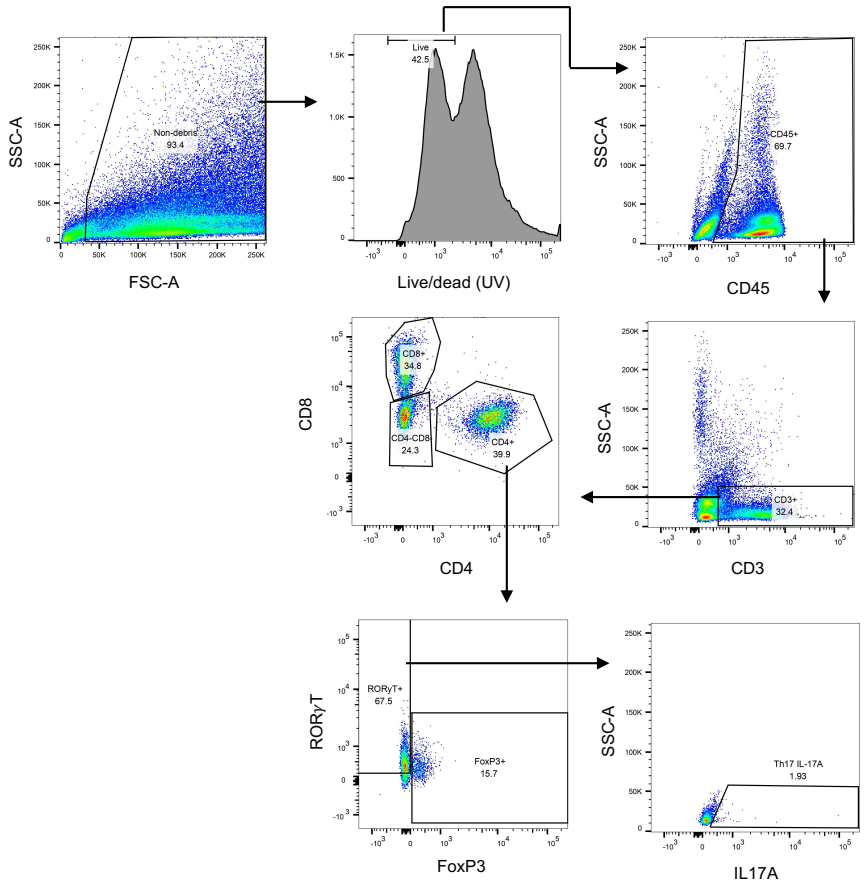


The number of Th17 cells (CD4$^{+}$RORγT$^{+}$FoxP3$^{-}$IL17A$^{+}$) identified was small, suggesting that this population of cells is not abundant in the lung. While the experiment did not show any significant difference between groups, there was a non-significant reduction of Th17 cells in *Tlr2*$^{-/-}$ samples from both *Kras*$^{LSL\text{-}G12D/+}$ and KP mice (Figure 5.18), suggesting that reduced A-SAA expression following *Tlr2* loss could impair the differentiation of Th17 cells. The precise role this has in enhancing lung tumour progression is yet to be investigated, but one possibility is that reduced Th17 cell differentiation

impairs lung epithelial barrier function which promotes tumour growth, as has been shown in other forms of cancer (Brennan et al., 2010; Soler et al., 1999). Nonetheless, these data are preliminary at best, and this line of investigation warrants further research.

**Figure 5.18: Th17 cell differentiation is reduced following Tlr2 loss. (a)** Representative flow cytometry analysis of IL17A$^+$ Th17 cells (CD4$^+$FoxP3$^-$ ROR$\gamma$T$^+$IL17A$^+$) in lung single cell suspensions from tumour bearing wild-type (WT) and *Tlr2* null (*Tlr2*$^{-/-}$) mice. % denotes the percentage of parent population. Corresponding quantification in *Kras*$^{LSL\text{-}G12D/+}$ mice in **(b)** and KP mice in **(c)**. Each dot represents one mouse. n=3-5 mice per group. Statistical analysis was performed using the Student's *t*-test. ns – non-significant.

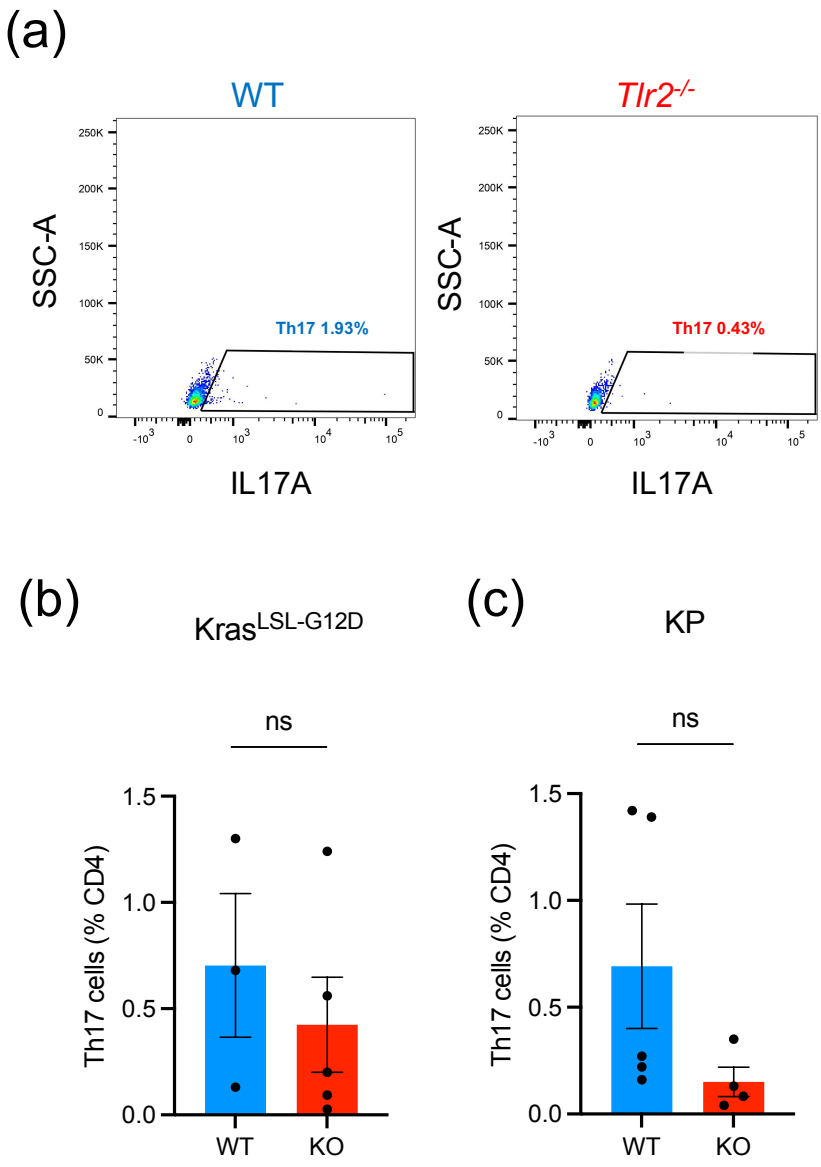

## 5.7 Cell intrinsic *Tlr2* loss regulates expression of the SASP and immune cell recruitment

### 5.7.1 *In vivo* somatic genome editing in the *Kras*$^{LSL\text{-}G12D/+}$ model

To determine whether the tumour promoting effect of *Tlr2* loss is due to epithelial, or global *Tlr2* loss (in particular immune cell *Tlr2* loss) *in vivo* somatic genome editing was performed using the pSECC lentivirus system (Sanchez-Rivera et al., 2014). These lentiviral constructs concurrently express Cre-recombinase and Cas9/CRISPR gRNAs therefore allow gene editing primarily in *Kras*$^{G12D}$ activated epithelial cells (Figure 5.19). Gene editing in lung resident immune cells cannot be excluded, however.

**Figure 5.19: pSECC lentiviral construct.** Schematic representative of the pSECC lentivirus plasmid. The gRNA construct is driven by the U6 promoter, whereas the Cas9 and Cre recombinase (linked by the self-cleaving peptide 2A) are driven by the EFS promoter.

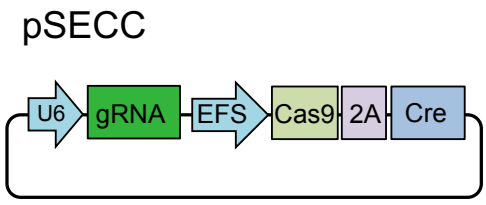


pSECC plasmids expressing *Tlr2* gRNA and non-target controls (Tomato gRNA) were cloned by Dr Andrea Quintanilla prior to me joining the lab. Plasmids were expanded and generated as described in chapter 2.2.1, and pSECC lentivirus was generated using PEI mediated transfection in 293T cells as described in chapter 2.3.7. To confirm that these plasmids are

able to edit the mouse *Tlr2* locus, mouse embryonic fibroblasts were infected with either empty vector (EV), non-target (gTomato) or three separate *Tlr2* gRNA expressing pSECC lentiviruses and RNA and protein was extracted three days later. Of note, the pSECC plasmid does not contain a selection cassette, therefore residual expression was expected from cells that were not infected with the pSECC lentivirus. RT-qPCR analysis revealed a reduction in *Tlr2* transcript expression with one of the gRNAs (No.1) but an increase with the other two (No.2 and No.3) (Figure 5.20).

**Figure 5.20: pSECC lentiviral validation (RNA).** *Tlr2* mRNA expression analysis from mouse embryonic fibroblasts (MEFs) three days after infection with empty vector (EV), non-target control (gTomato) and 3 x *Tlr2* gRNA (gRNA 1-3) expressing pSECC lentiviruses. RQ – Relative quantification.

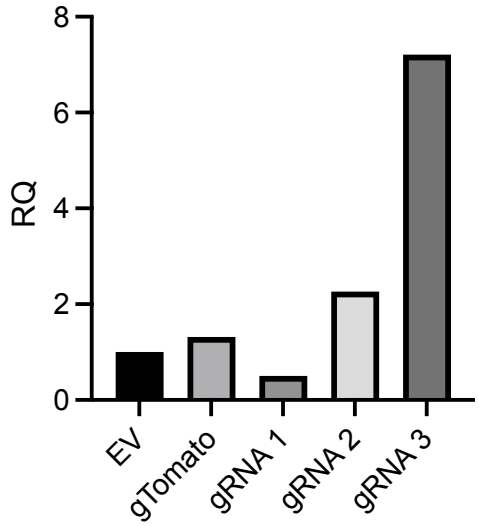


The *Tlr2* RT-qPCR primer sequences were in fact upstream of the gRNA target sites, therefore RT-qPCR with these primer sequences was not suitable to confirm effective knockout as transcript upstream to indels would

still be detected. Western blotting was therefore performed from protein extracted from the same cells and revealed efficient knockout in all three gRNA expressing samples (Figure 5.21).

**Figure 5.21: pSECC lentiviral validation (protein).** Representative Western blot analysis of Tlr2 protein expression in lysates isolated from mouse embryonic fibroblasts (MEFs) 3 days after infection with empty vector (EV), non-target control (gTomato) and 3 x *Tlr2* gRNA (gRNA 1-3) expressing pSECC lentiviruses. n=3.

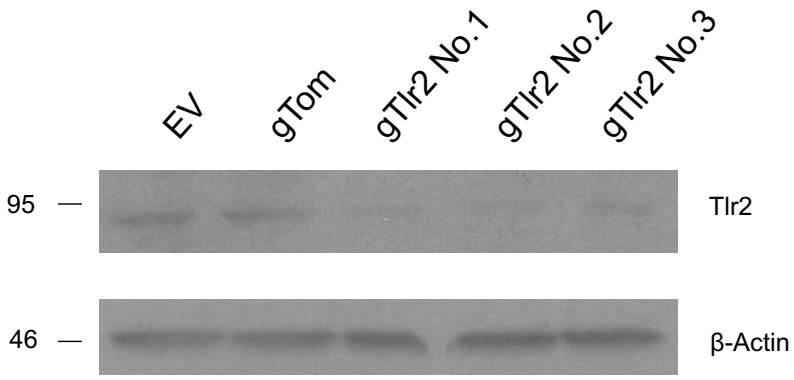


It was then decided to use gTomato and 2 x *Tlr2* gRNA expressing viruses (No.1 and No.2). These viruses were generated on a larger scale, concentrated and titrated as described in chapter 2.3.7. Titration was performed with between 10-80ul of concentrated virus solution in a 6 well plate with 10,000 cells and revealed a low titre, with only gTomato and gTlr2 No.1 viruses inducing high enough beta-gal expression to calculate MOI reliably (see table 5.2).

**Table 5.2:** Results from the pSECC titration using 3TZ cells. MOI (multiplicity of infection), TU (transfection units).

| Plasmid | MOI | Titre (TU/ml) | Dilution |
|---|---|---|---|
| gTomato | 0.15 | 18,750 | 24ul virus, 16ul MEM |
| gTlr2 No.1 | 0.09 | 11,250 | 40ul virus |
| gTlr2 No.2 | N/A | N/A | N/A |

The transfection efficiency (assessed using a GFP expressing plasmid (pUltra) as a transfection control) was very high (90-100%). Furthermore, when infection of 3TZ cells was performed with pUltra expressing virus, infection efficiency was almost 100%, confirming viral envelope and packaging vectors (VSVG and PAX2) were intact and viable lentivirus had been generated. Lastly, 3TZ cells were infected with AdenoCre, which induced significantly higher beta-gal expression (45.5% → MOI 0.6), confirming that recombination in 3TZ cells does occur with adequate Cre-recombinase expression. Therefore, the calculated dilutions based on the initial titration were used for gTomato and gTlr2 No.1 lentiviruses.

### 5.7.2 Epithelial *Tlr2* loss promotes tumour growth

*Kras*$^{LSL\text{-}G12D/+}$ mice were inoculated with either gTomato or gTlr2 No.1 lentiviruses. These mice were left for 35 weeks as minimal symptoms of lung tumour formation were exhibited (as expected given the low viral titre). Mice were then humanely culled, and lung tissue was harvested for histological analysis. Tumour burden analysis was performed and showed a very small

tumour burden in both cohorts, however this was increased in mice who received the gTlr2 lentivirus (Figure 5.22).

**Figure 5.22: *Tlr2* targeting pSECC lentivirus increases lung tumour burden.** Tumour burden analysis on lung sections from *Kras*$^{LSL\text{-}G12D/+}$ mice 35 weeks after inoculation with non-target control (gTomato) and *Tlr2* targeting (gTlr2) pSECC lentiviruses. Each dot represents one mouse. n=8 mice per group. Statistical analysis was performed using the Student's *t*-test. *p<0.05.

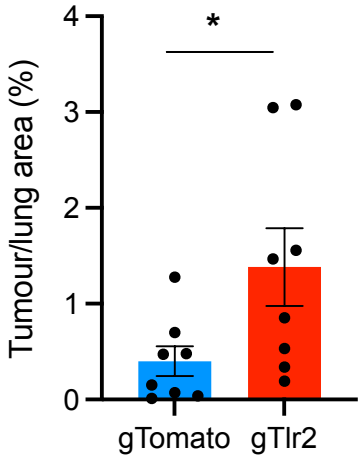


Given the issues with the low titration and low abundance of tumours, tumour burden analysis was deemed to be unreliable. However, individual tumours were able to be reliably analysed for proliferation, SASP expression and immune cell recruitment. To assess tumour proliferation Ki67 IHC was performed and revealed an increased proliferative index in gTlr2 targeted

tumours (Figure 5.23), suggesting that epithelial *Tlr2* loss promotes tumour growth.

**Figure 5.23: *Tlr2* targeting pSECC lentivirus increases lung tumour proliferation. (a)** Ki67 IHC staining in lung tumours from *Kras*$^{LSL\text{-}G12D/+}$ mice inoculated with non-target control (gTom) and *Tlr2* targeting (gTlr2) pSECC lentiviruses, with corresponding quantification in **(b)**. Each dot represents one tumour. n=8 mice per group. Statistical analysis was performed using the students *t*-test.

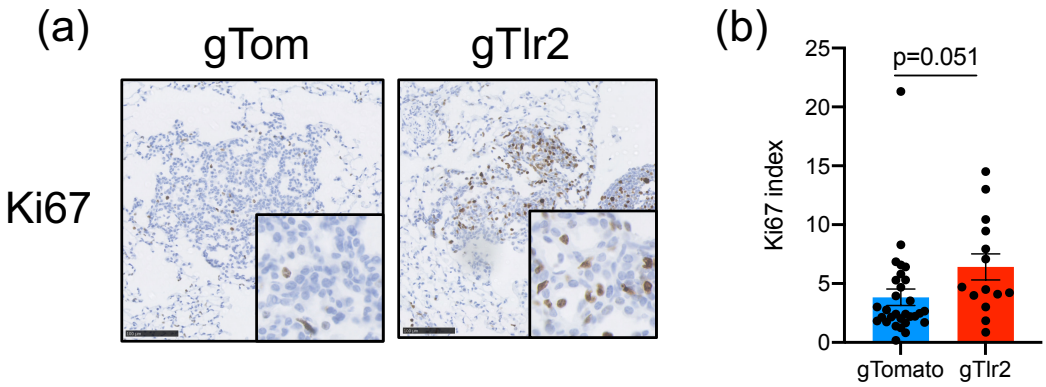


### 5.7.3 Epithelial *Tlr2* loss impairs expression of the SASP

To analyse the effect of epithelial *Tlr2* loss on SASP expression, IHC staining for the key SASP factors IL-1α, IL-1β and A-SAA was performed, revealing a significant reduction in the expression of all three SASP factors in gTlr2 targeted tumours (Figure 5.24). Overall, these data suggest that epithelial *Tlr2* regulates expression of the SASP.

**Figure 5.24: *Tlr2* targeting pSECC lentivirus impairs SASP expression. (a)** IHC staining for IL-1α, IL-1β and A-SAA on lung tumours from *Kras*$^{LSL-G12D/+}$ mice 35 weeks after inoculation with non-target control (gTom) and *Tlr2* targeting (gTlr2) pSECC lentiviruses, with corresponding quantification in **(b)**. Each dot represents one tumour. n=8 mice per group. Statistical analysis was performed using the student t-test. ***p<0.001.

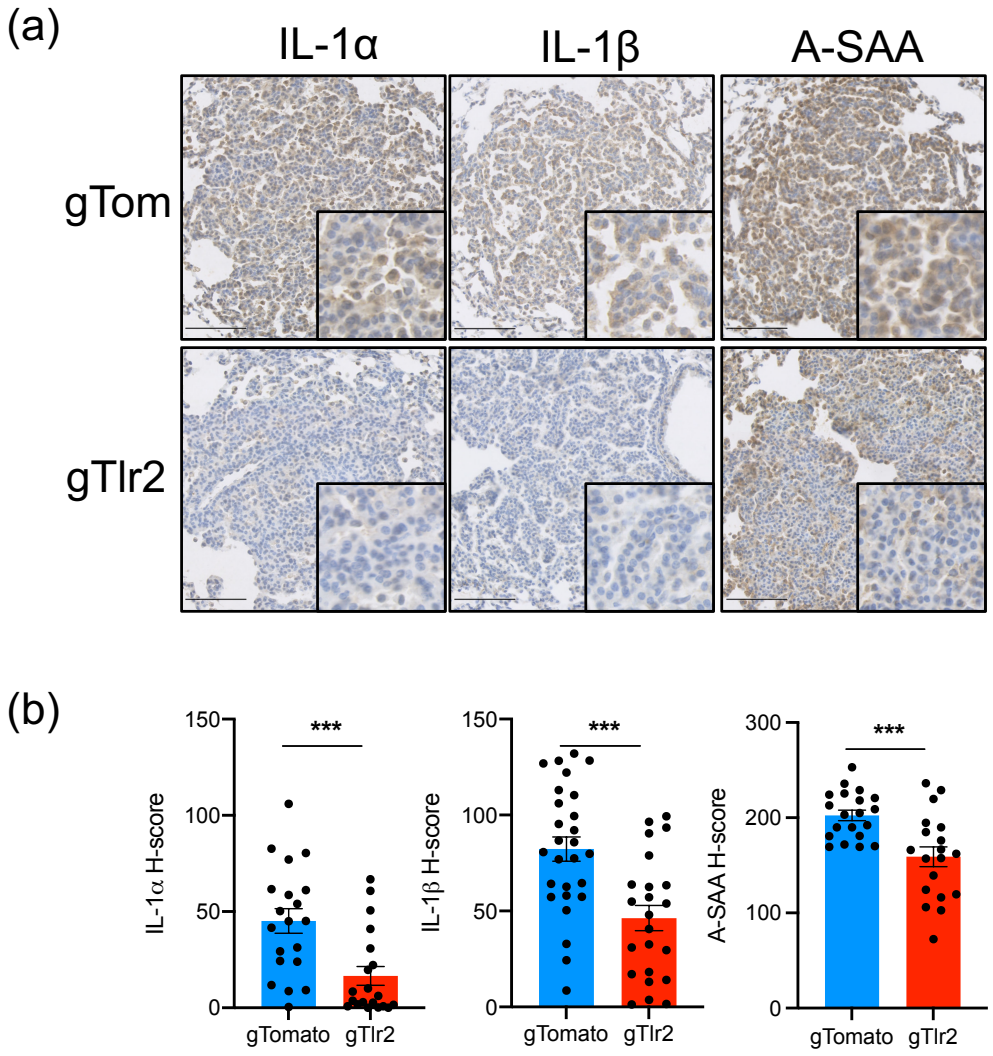

### 5.7.4 Epithelial *Tlr2* loss impairs monocyte/macrophage recruitment to lung tumours

To determine whether impaired SASP expression results in impaired monocyte/macrophage recruitment to lung tumours (as seen in our global KO mice) IHC staining for the pan monocyte/macrophage marker CD68 was performed in the pSECC targeted tumours. This revealed significantly reduced recruitment of $CD68^{+}$ cells to tumours induced by gTlr2 expressing lentivirus (Figure 5.25), suggesting that epithelial *Tlr2* loss impairs recruitment of monocyte/macrophages via impaired SASP expression.

**Figure 5.25: *Tlr2* targeting pSECC lentivirus impairs monocyte/macrophage recruitment. (a)** CD68 IHC staining in lung tumours from $Kras^{LSL\text{-}G12D/+}$ mice inoculated with non-target control (gTom) and *Tlr2* targeting (gTlr2) pSECC lentiviruses, with corresponding quantification in **(b)**. Each dot represents one tumour. n=8 mice per group. Statistical analysis was performed using the students *t*-test. **p<0.01.

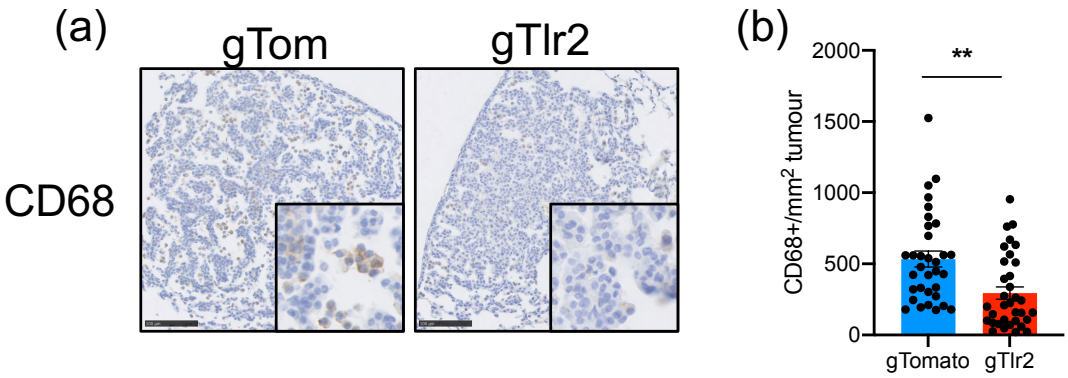

### 5.7.5 *Tlr2*$^{-/-}$ monocyte/macrophages can respond to local SASP factors

To further investigate whether epithelial *Tlr2* loss and impaired SASP expression mediates the reduced recruitment of monocyte/macrophages to lung tumours, recombinant SASP factors (rIL-1α and rIL-1β) or PBS control were delivered intranasally to *Tlr2*$^{-/-}$ mice. The local recruitment of CD68$^{+}$ cells was then assessed using IHC staining. This revealed a significant increase in lung CD68$^{+}$ cells following rIL-1α/rIL-1β inoculation in comparison to PBS inoculated controls (Figure 5.26), confirming that *Tlr2*$^{-/-}$ monocytes/macrophages can respond to local SASP factors. This further suggests that immune cell loss of *Tlr2* does not underlie the impaired recruitment of monocyte/macrophages to lung tumours that is seen in *Kras*$^{LSL\text{-}G12D/+}$;*Tlr2*$^{-/-}$ mice.

**Figure 5.26: *Tlr2*$^{-/-}$ monocytes/macrophages are able to respond to local SASP factors. (a)** CD68 IHC staining in *Tlr2* null (*Tlr2*$^{-/-}$) mice after intranasal delivery of PBS (control) or recombinant SASP factors (rIL-1α/rIL-1β) with corresponding quantification in **(b)**. Each dot represents one mouse. n=4-5 mice per group. Statistical analysis was performed using the student *t*-test. *p<0.05.

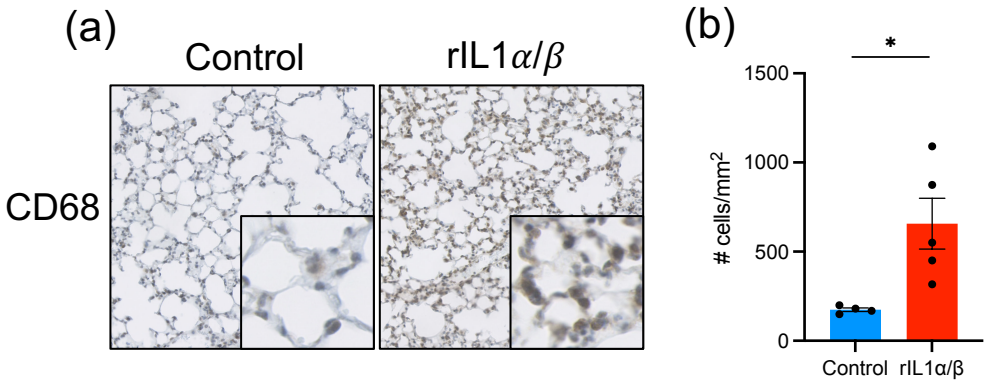

This experiment was then repeated in *Tlr2* wild-type (*Tlr2*$^{+/+}$) mice, to ensure that what we saw in *Tlr2*$^{-/-}$ mice was not an impaired response. Wild-type monocyte/macrophages were also able to responds to local recombinant SASP factor delivery to a similar extend to *Tlr2*$^{-/-}$ cells (Figure 5.27). Taken together, these experiments confirm that *Tlr2*$^{-/-}$ monocyte/macrophages can respond to local SASP factors and this response is not impaired compared to wild-type controls.

**Figure 5.27: *Tlr2*$^{+/+}$ monocytes/macrophages can respond to local SASP factors. (a)** CD68 IHC staining in *Tlr2* wild-type (*Tlr2*$^{+/+}$) mice after intranasal delivery of PBS (control) or recombinant SASP factors (rIL-1$\alpha$/rIL-1$\beta$) with corresponding quantification in **(b)**. Each dot represents one mouse. n=7 mice per group. Statistical analysis was performed using the student *t*-test. *p<0.05.

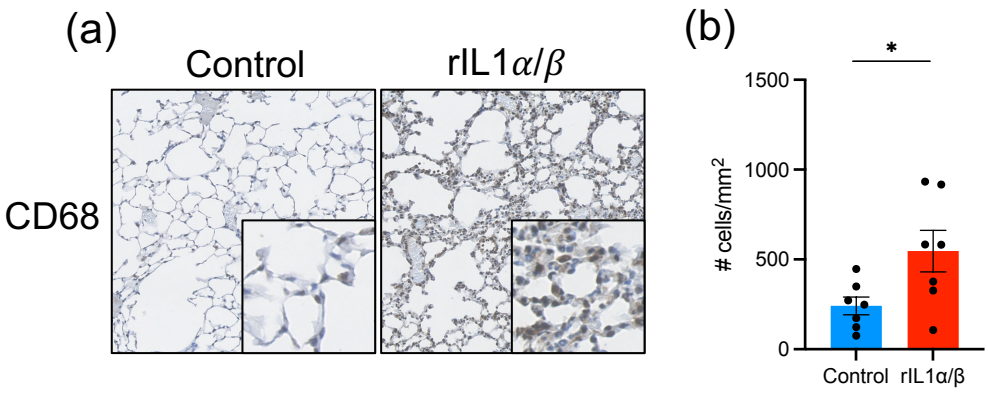


## 5.8 Tlr2 agonists inhibit lung tumour growth

### 5.8.1 Local delivery of Tlr2 agonist *in vivo*

To determine whether exogenous activation of Tlr2 signalling can inhibit lung tumour growth, a method to repeatedly deliver a synthetic agonist

of Tlr2 was developed. Pam2CSK4 (a synthetic lipopeptide agonist of Tlr2) was used as it had been shown to robustly activate TLR2 signalling and the SASP *in vitro* (Hari et al., 2019). Nebulised delivery was chosen as the most suitable method as it allowed repeated local delivery of drug without the need for a general anaesthetic. Collaborators at the Centre for Inflammation Research (Professor Sarah Walmsley and Tyler Morrison, Centre for Inflammation Research, University of Edinburgh) regularly use nebulised lipopolysaccharide (LPS) as a method to induce acute lung injury in mouse models. The dose of LPS used in this instance is high (3mg/ml) and induces a florid inflammatory infiltrate hours after delivery. To the best of our knowledge, Pam2CSK4 had never been delivered via nebulisation. Therefore, a considerably lower dose of Pam2CSK4 was chosen. Initial pilot experiments were performed delivering 50ug Pam2CSK4 delivered in 3ml 0.9% NaCl every 2 weeks. Mice developed no adverse effects using this protocol therefore dosing was increased to 100ug weekly, again with no adverse effects. This dose and dosing schedule (Figure 5.28) was used for all subsequent experiments. *Kras*$^{LSL\text{-}G12D/+}$ mice were inoculated with AdenoCre and 2 weeks later subjected to a weekly treatment with nebulised Pam2CSK4 (Figure 5.28).

**Figure 5.28: Nebulised delivery of Pam2CSK4. (a)** Schematic showing the method of nebulised delivery of Pam2CSK4. Mice were kept in a box attached to the nebuliser. The nebuliser was driven by 6L/min oxygen from an oxygen concentrator. **(b)** Dosing schedule of AdenoCre inoculated mice. Mice were inoculated with AdenoCre as described previously prior to commencing weekly dosing with Pam2CSK4 2 weeks later.

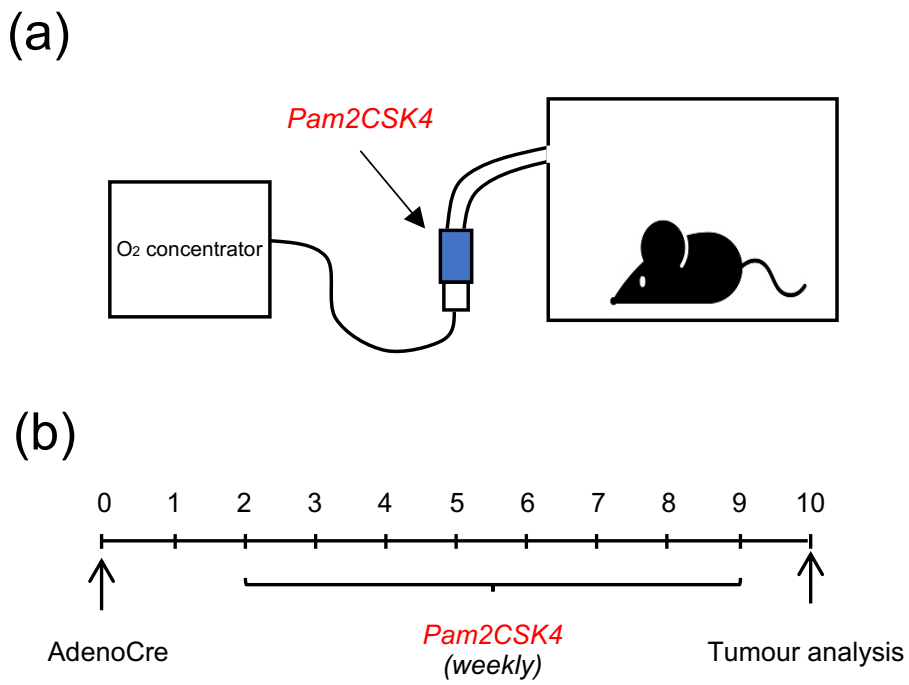


### 5.8.2 Pam2CSK4 activates OIS and inhibits tumour growth

To determine the effect of Pam2CSK4 delivery on OIS and tumour growth, *Kras*$^{LSL\text{-}G12D/+}$ mice were subjected to Pam2CSK4 treatment as outlined in 5.8.1. After completion of the treatment protocol, mice were humanely culled, and lung tissue was harvested for histological analysis. IHC staining was performed to determine Ki67 and p21 expression in control and Pam2CSK4 treated tumours. While Ki67 expression was unchanged

(perhaps reflecting the already low expression level in these *Tlr2*$^{+/+}$ tumours), p21 expression was significantly increased following Pam2CSK4 treatment (Figure 5.29).

**Figure 5.29: Pam2CSK4 treatment induces OIS. (a)** IHC staining for Ki67 and p21 in lung tumours from control and Pam2CSK4 treated *Kras*$^{LSL\text{-}G12D/+}$ mice with corresponding quantification in **(b)**. Five tumours analysed at random in a blinded fashion per mouse (each dot represents one tumour). n=8 mice per group. Statistical analysis was performed using the Student's *t*-test. *p<0.05.

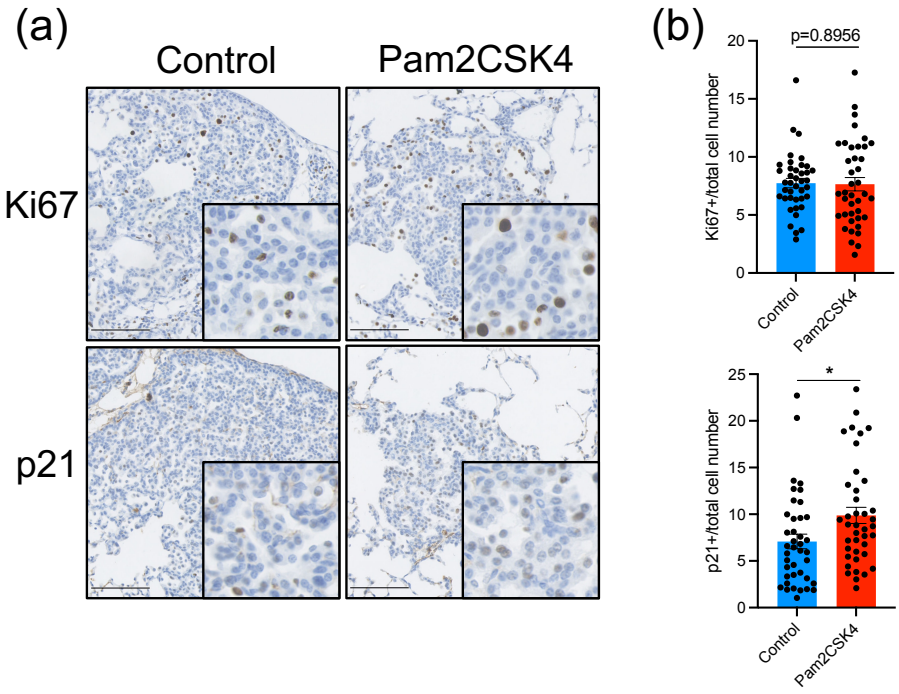


These changes were also associated with a significant reduction in tumour burden (Figure 5.30). Tumour number was unchanged, however. This is likely explained by the fact that tumours were initiated 2 weeks prior to commencing Pam2CSK4 treatment. These data suggest that activating Tlr2

signalling with a Tlr2 agonist impairs lung tumour growth consistent with activation of OIS.

**Figure 5.30: Pam2CSK4 treatment impairs lung tumour growth.**

**(a)** H&E staining of lung tumours from control and Pam2CSK4 treated *Kras*$^{LSL\text{-}G12D/+}$ mice. **(b)** Tumour number and tumour burden quantification from mice described in (a). Each dot represents one mouse. n=8 mice per group. Statistical analysis was performed using the Student's *t*-test. *p<0.05.

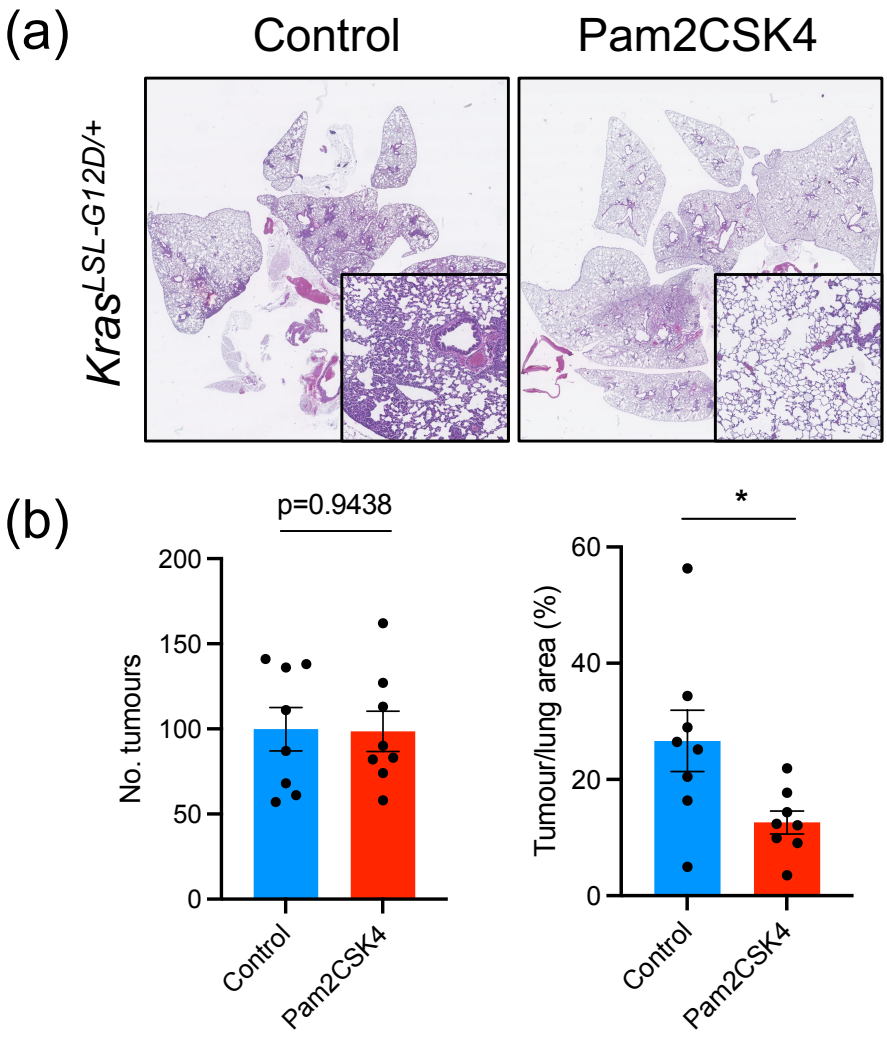

### 5.8.3 Pam2CSK4 activates expression of the SASP in lung tumours

To determine whether Pam2CSK4 induces expression of the SASP, IHC staining for the key SASP factors IL-1$\alpha$, IL-1$\beta$ and A-SAA was performed. This showed significantly increased expression of IL-1$\alpha$ and A-SAA but no significant change in IL-1$\beta$ expression in Pam2CSK4 treated tumours when compared with controls (Figure 5.31). These data suggest that Pam2CSK4 treatment also induces expression of the SASP.

**Figure 5.31: Pam2CSK4 treatment increases SASP expression. (a)** IHC staining for the key SASP factors IL-1α, IL-1β and A-SAA in lung tumours from control and Pam2CSK4 treated *Kras*$^{LSL\text{-}G12D/+}$ mice with corresponding quantification in **(b)**. Five tumours chosen at random in a blinded fashion were analysed per mouse (each dot represents one tumour). n=8 mice per group. Statistical analysis was performed using the Student's t-test. *p<0.05.

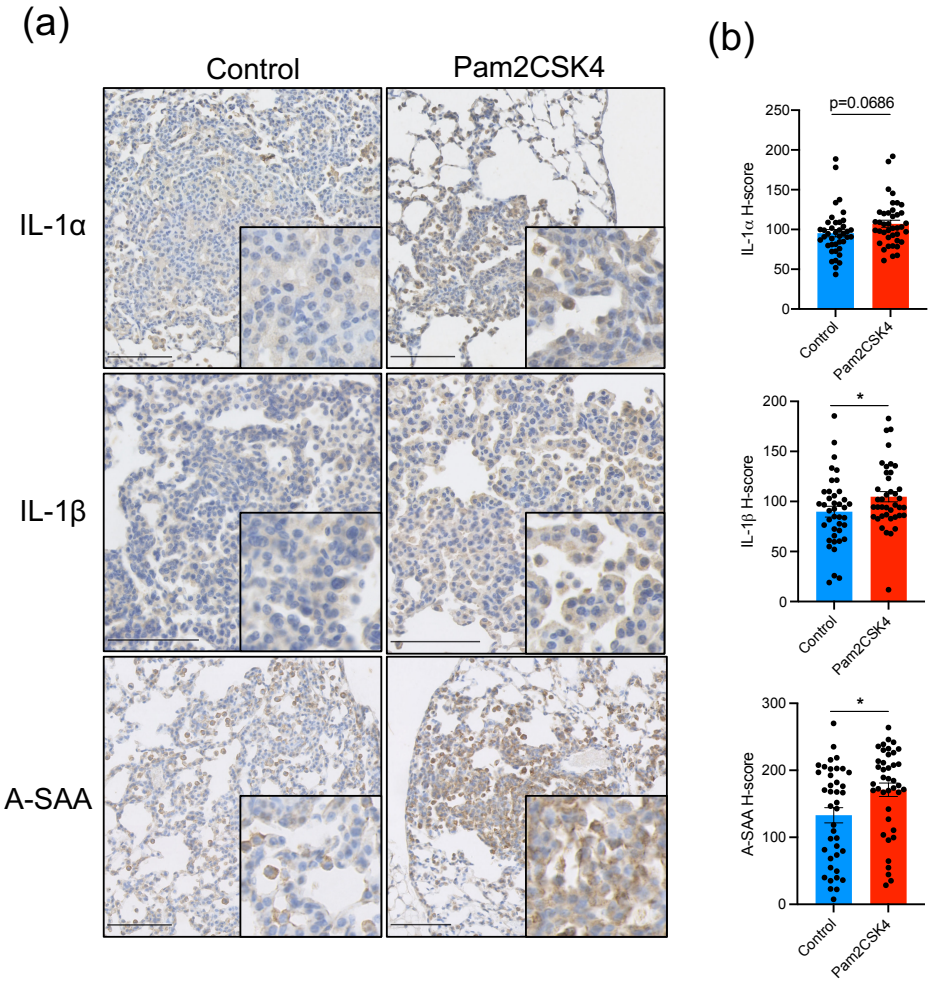


### 5.8.4 Pam2CSK4 impairs immune cell recruitment likely via TLR tolerance

The effect of Pam2CSK4 treatment on immune cell recruitment to tumours was then determined. IHC staining for the pan T-cell marker CD3

and monocyte/macrophage marker CD68 was performed. There was no difference in T-cell infiltration following Pam2CSK4 treatment, however a significant reduction in monocyte/macrophage recruitment was observed in Pam2CSK4 treated tumours (Figure 5.32).

**Figure 5.32: Pam2CSK4 treatment and immune cell recruitment. (a)** IHC staining for T-cells (CD3) and monocyte/macrophages (CD68) in lung tumours from control and Pam2CSK4 treated *Kras*$^{LSL\text{-}G12D/+}$ mice with corresponding quantification in **(b)**. Five tumours chosen at random in a blinded fashion were analysed per mouse. Each dot represents one tumour. n=8 mice per group. Statistical analysis was performed using the students t-test. ns – non-significant, **p<0.01.

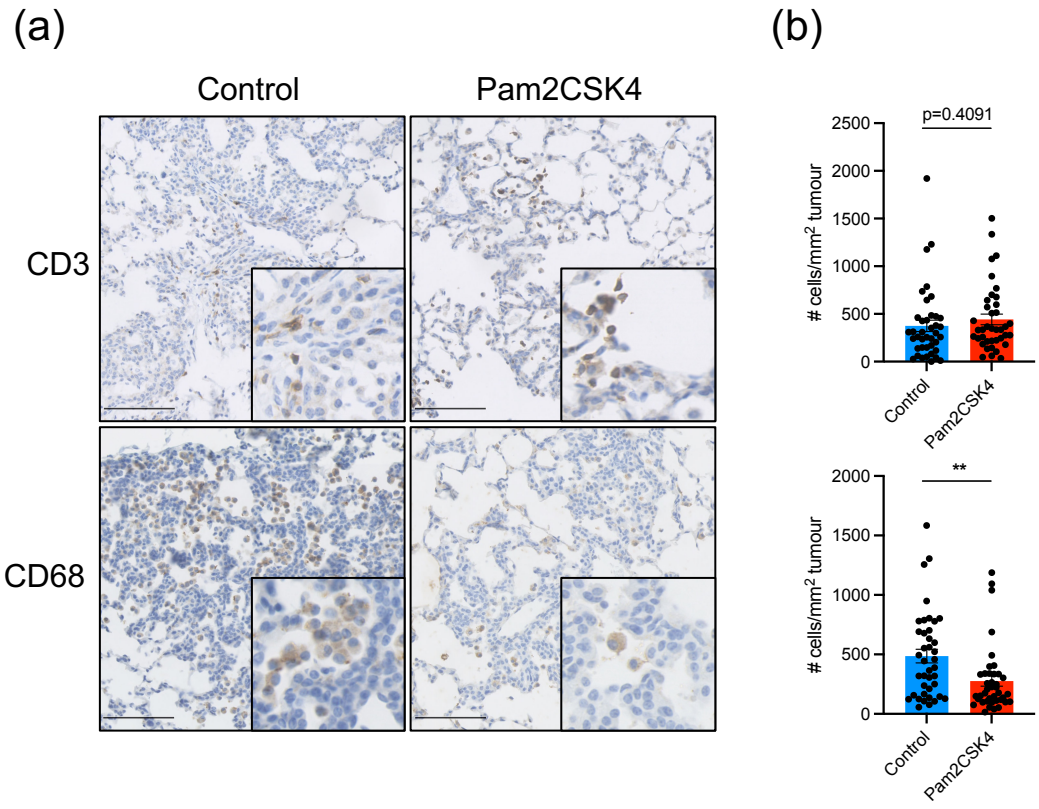

This unexpected finding can likely be explained by TLR tolerance which is a well-recognised phenomenon in monocyte derived populations via repression of NF-κB signalling (Butcher et al., 2018). The role of immune surveillance is likely to be most important at the earliest timepoints, therefore it is plausible that initial treatment with Pam2CSK4 encourages immune surveillance but repeated stimulation (as performed in our experiments) leads to eventual TLR tolerance and depletion of monocytes/macrophages. Further experiments to determine whether initial Pam2CSK4 treatment induces the recruitment of immune cells at early timepoints are warranted.

### 5.8.5 Pam2CSK relies on Tlr2 signalling to mediate these effects

To confirm that the effect of Pam2CSK4 treatment is indeed mediated via activation of Tlr2 signalling, Pam2CSK4 treatment was performed on *Tlr2*$^{-/-}$ *Kras*$^{LSL\text{-}G12D/+}$ mice. No significant difference in tumour burden, Ki67 expression or SASP (IL-1β) expression was observed between control and Pam2CSK4 treated *Tlr2*$^{-/-}$ mice (Figure 5.33). These data confirm that intact Tlr2 signalling is required to mediate the tumour inhibiting effects of Pam2CSK4.

**Figure 5.33: Pam2CSK4 activity is dependent on functional Tlr2. (a)** H&E and IHC staining for Ki67 and the SASP factor IL-1β in lung tumours from control and Pam2CSK4 treated *Tlr2*$^{-/-}$ Kras$^{LSL\text{-}G12D/+}$ mice with corresponding quantification in **(b)**. For tumour burden analysis: each dot represents one mouse. For IHC analysis: five tumours chosen at random in a blinded fashion were analysed per mouse. Each dot represents one tumour. n=4 mice per group. Statistical analysis was performed using the Student's t-test.

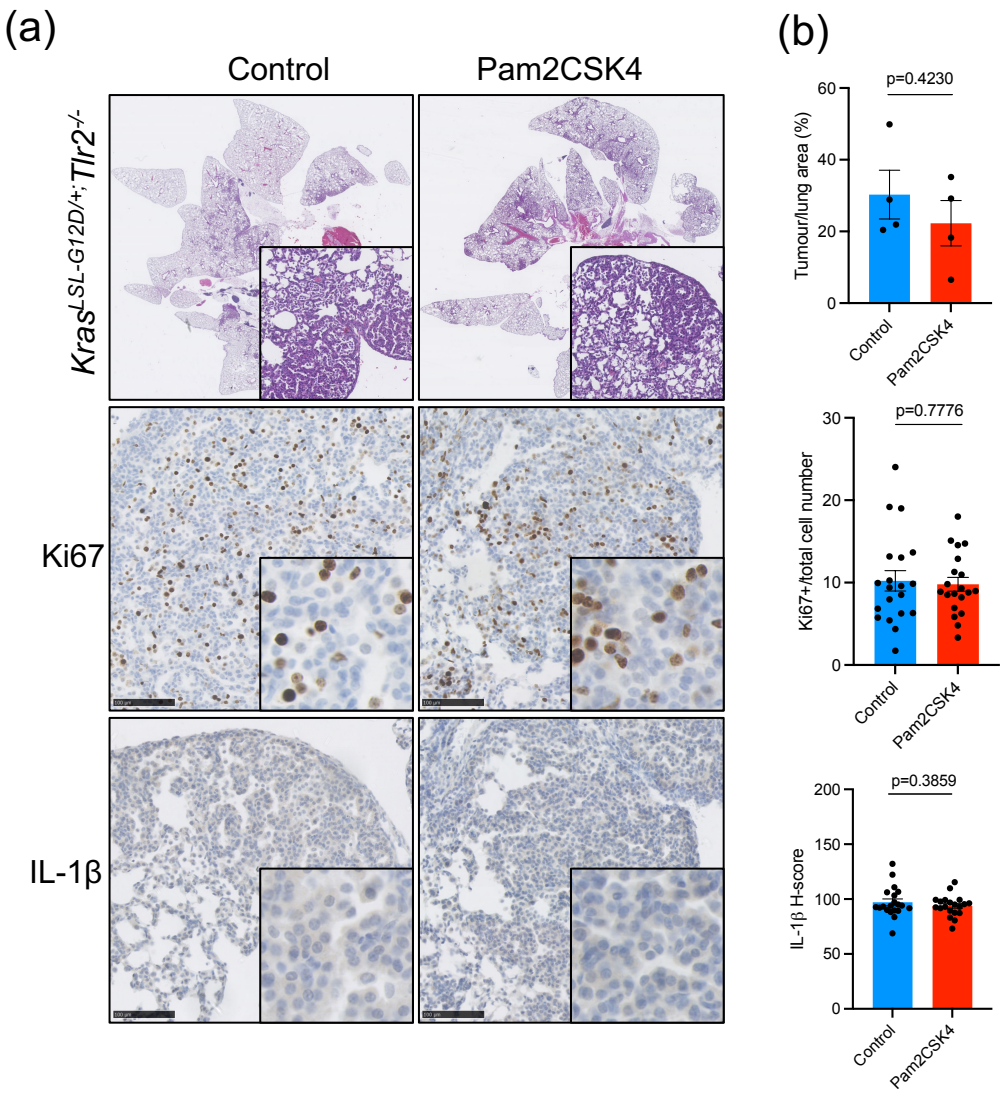

## 5.9 Chapter summary

In this chapter, the aim was to investigate whether *Tlr2* loss promotes tumour progression in a murine model of NSCLC and to investigate the mechanism of any tumour suppressor effect. Using the *Kras*$^{LSL\text{-}G12D/+}$ mouse model it was shown that loss of *Tlr2* significantly promotes tumour growth and shortens survival. This tumour suppressor effect is mediated by both cell autonomous regulation of p53-p21 signalling and *Trp53* independent regulation of SASP expression. The impaired expression of the SASP results in reduced recruitment of myeloid derived immune cells to lung tumours however we did not show evidence of impaired lung tumour immune surveillance. Furthermore, activating Tlr2 signalling using a synthetic agonist significantly reduced tumour growth, an effect that required the presence of intact Tlr2. From these data, it can be concluded that *Tlr2* has a tumour suppressor function in murine NSCLC via activation of senescence-associated tumour suppressor responses and SASP mediated immune surveillance.

# 6 : Discussion

## 6.1 Summary of results

Oncogene induced senescence (OIS) is a key tumour suppressor mechanism *in vivo* (Collado et al., 2005; Collado and Serrano, 2010). A previous student in our lab (Dr Priya Hari) identified *TLR2* as a key regulator of OIS and expression of the senescence-associated secretory phenotype (SASP) using a well described *in vitro* model of OIS (Hari et al., 2019). The main focus of this thesis was to determine whether *Tlr2* regulates OIS and the SASP *in vivo*, and whether this translates into a tumour suppressor function in non-small cell lung cancer (NSCLC).

### 6.1.1 Chapter 3

To determine the role of *Tlr2* in OIS and the SASP *in vivo* a mouse model of OIS was used, whereby hydrodynamic delivery of oncogenic *Nras* ($Nras^{G12V}$) encoding transposons with transposase expressing plasmids results in uptake and expression of the desired constructs in murine hepatocytes. Using a combination of immunohistochemistry (IHC) and quantitative PCR (RT-qPCR) it was shown that $Nras^{G12V}$ expressing hepatocytes express several markers of OIS and the SASP. Following *Tlr2* loss, the expression of these markers is impaired, confirming that intact Tlr2 is required for the OIS/SASP response *in vivo*. The impact this impaired

response has on senescence surveillance (whereby immune cells are recruited to and subsequently clear premalignant senescent cells) was then investigated using two separate approaches. Despite an impairment of macrophage recruitment in *Tlr2*$^{-/-}$ mice, the data presented did not demonstrate a significant impairment of clearance of senescent cells in *Tlr2*$^{-/-}$ mice. Preliminary evidence suggests that *Tlr2*$^{-/-}$ oncogene expressing hepatocytes are cleared by alternate mechanism (apoptosis). It was therefore concluded that *Tlr2* is a key regulator of OIS and the SASP *in vivo,* however does not clearly regulate the immune mediated clearance of senescent cells.

### 6.1.2 Chapter 4

OIS is widespread in preinvasive lung tumours (Collado et al., 2005) and *Tlr2* is highly expressed in the murine lung (McCoy et al., 2021). The aim of chapter 4 was to investigate whether *TLR2* signalling is active in human NSCLC and to determine whether this signalling has a tumour suppressor function in early disease. TCGA data showed that high *TLR2* expression significantly correlates with improved survival in human lung adenocarcinoma (LUAD)(Figure 4.1). IHC performed on human LUAD samples revealed significantly increased epithelial expression of TLR2 and SASP factors when compared with paired normal epithelium. Furthermore, this expression was significantly positively correlated, suggesting a potential regulatory role for TLR2 in the expression of the SASP in LUAD tumour epithelium. Re-analysis of a published RNA sequencing dataset of preinvasive and invasive LUAD

lesions (Chen et al., 2019) revealed increased expression of *TLR2* and several SASP factors in preinvasive disease, suggesting a tumour suppressor role in this context. Longitudinal follow up of LUAD precursor lesions is not possible as these lesions are treated definitively by surgical resection. However, preinvasive lung squamous cell carcinoma (LUSC) lesions are amenable to repeated sampling via autofluorescence bronchoscopy, allowing longitudinal follow up and repeated molecular characterisation of lesions that either subsequently progress to malignancy or regress to normal epithelium (Teixeira et al., 2019). In collaboration with Professor Sam Janes and Dr Adam Pennycuick (University College London) it was shown that regressive preinvasive LUSC lesions express significantly higher levels of *TLR2* and SASP factors when compared to lesions that progress to invasive malignancy. *TLR2* expression was again significantly correlated with SASP expression, further suggesting a regulatory role for TLR2 in this context. It was therefore concluded that TLR2-SASP signalling is active in human NSCLC tumour epithelium and significantly correlates with clinical regression, suggesting that TLR2-SASP signalling is a tumour suppressor mechanism in NSCLC.

### 6.1.3 Chapter 5

The aim of chapter 5 was to confirm that *Tlr2* has a tumour suppressor role and characterise the mechanism of *Tlr2* mediated lung tumour suppression in a genetically engineered mouse model of NSCLC. A model whereby lung epithelium specific activation of oncogenic *Kras* (*Kras*$^{G12D}$) is

achieved upon inhalation of Cre-recombinase expressing adenovirus was used to investigate the tumour suppressor function of *Tlr2*. *Tlr2* null (*Tlr2*$^{-/-}$) mice developed a significantly increased number of lung tumours and a significantly increased lung tumour burden, in comparison to controls. This translated into a significant survival disadvantage for *Tlr2*$^{-/-}$ mice. The mechanism of this effect was investigated and using IHC staining it was revealed that *Tlr2*$^{-/-}$ tumours express significantly less markers of key cell intrinsic senescence associated tumour suppressor pathways (principally p53-p21). Interestingly, the effect of *Tlr2* loss was not fully dependent on intact p53-p21 signalling, as *Tlr2* loss in the absence of *Trp53* still promoted tumour growth. *Tlr2* loss impaired the expression of the SASP independently of *Trp53* status, suggesting that regulation of the SASP also contributed to the tumour suppressor effect of Tlr2 signalling. A key non-cell autonomous tumour suppressor function of the SASP is in the recruitment of immune cells that clear premalignant cells (Kang et al., 2011; Xue et al., 2007). Using multicolour flow cytometry analysis and IHC staining it was revealed that *Tlr2*$^{-/-}$ tumours have impaired recruitment of immune cells, principally monocyte/macrophages, suggesting that this may at least in part underly the tumour promoting effect of *Tlr2* loss. Importantly, it was shown that epithelial *Tlr2* was responsible for this phenotype, as *in vivo* somatic genome editing performed using a lentiviral vector (Sanchez-Rivera et al., 2014) to delete *Tlr2* in the lung epithelium only revealed a similar outcome when compared to global knockout mice. These data, coupled with data from chapter 3 revealing impaired senescence surveillance in the HTVI model following *Tlr2*

loss, suggests that *Tlr2* loss may impair senescence surveillance in early lung tumour formation. Lastly, to determine whether tumour growth could be inhibited by activating Tlr2 signalling, inhalational delivery of a synthetic Tlr2 agonist (Pam2CSK4) was used. Lung tumours in mice treated with Pam2CSK4 were significantly smaller and expressed higher levels of OIS and SASP markers. It was therefore concluded that *Tlr2* has a tumour suppressor function in murine NSCLC, via regulation of OIS and the SASP. Data from this chapter also highlighted the potential to harness the TLR2 signalling pathway as a novel therapeutic target for early-stage NSCLC.

## 6.2 Mouse models

### 6.2.1 Hydrodynamic tail vein injection model of OIS

The hydrodynamic tail vein injection (HTVI) method of transposon delivery is a well described *in vivo* model of OIS and has been used to elegantly characterise the mechanism of senescence surveillance (Kang et al., 2011). The HTVI technique allows the delivery of transposon constructs expressing a combination of oncogenes, genetic tags (for example GFP), and even shRNA or CRIPSR/Cas9 constructs, making it an easily manipulatable model to study a variety of disease processes. Indeed, as described in this thesis, cloning in a luciferase construct in place of the GFP tag in the pT3-NRas$^{G12V}$-IRES-GFP transposon allowed the longitudinal monitoring of senescent cell clearance by bioluminescent imaging. The HTVI model is especially useful when studying the early genetic and molecular

changes during malignant transformation. Forced *Nras*$^{G12V}$ expression results in a robust OIS response after just 6 days, in concert with expression of the SASP and subsequent senescence surveillance (Kang et al., 2011). Therefore, unlike other disease models, phenotypic assessment of OIS is fast and does not require the formation of overt tumours. However, the HTVI technique is technically challenging, and ensuring equal transposon expression is difficult. Furthermore, widespread multifocal expression of the same oncogene does not accurately recapitulate human disease. While multifocal lesions can be present in human disease, these are often genetically distinct tumours or metastases that have divergent genetic evolution. Therefore, the HTVI model allows the examination of the acute response to multifocal oncogene activation, whereas in human multifocal disease we can only examine persisting and often genetically divergent clones. Nonetheless, HTVI is an excellent model to help answer specific biological questions and to study the molecular mechanisms of OIS *in vivo*.

### 6.2.2 *Kras*$^{LSL\text{-}G12D/+}$ model of lung cancer

The *Kras*$^{LSL\text{-}G12D/+}$ mouse model, first designed and described by the lab of Professor Tyler Jacks (Jackson et al., 2001), allows tissue specific activation of oncogenic *Kras*$^{G12D}$ following intranasal/intratracheal inoculation with Cre-recombinase expressing adenovirus (DuPage et al., 2009). *Kras* is the most frequently mutated oncogene in human LUAD (Cancer Genome Atlas Research, 2014) (the most common subtype of NSCLC) therefore while the histology does not accurately recapitulate human LUAD, this model can

accurately recapitulate the early genetic events in human disease. Dosing is easy and reproducible, and the technique is established in our lab making it an ideal model to study the role of *Tlr2* in early lung tumorigenesis. However, as described for the HTVI model in chapter 6.2.1, the *Kras*$^{LSL\text{-}G12D/+}$ mouse model also results in genetically similar multifocal lesions, perhaps not accurately recapitulating human disease. Interestingly, clonally related multifocal lesions have been described in human squamous lung cancer, mediated via migration of mutated premalignant cells across histologically healthy epithelium (Pipinikas et al., 2014). This, coupled with likely divergent genetic evolution of individual tumour lesions perhaps overcomes this perceived drawback. Furthermore, with the *Kras*$^{LSL\text{-}G12D/+}$ mouse model, adenoviral dosing can be titrated down to markedly reduce tumour number and allow the development of advanced lesions which permits the study of both early and late-stage malignancy (Jackson et al., 2001). While this and similar models have been used to investigate the differing immune profile of early lung tumours induced by different genetic drivers (Busch et al., 2016), tumours from the *Kras*$^{LSL\text{-}G12D/+}$ mouse model have few protein-altering mutations and are therefore unlikely to express significant numbers of neoantigens (McFadden et al., 2016). Heightened $CD8^+$ T-cell responses can be achieved by forced expression of T-cell antigens, however this is not sustained and is characterised by a poorly functioning exhausted T-cell response (DuPage et al., 2011). Therefore, due to the limitations of the *Kras*$^{LSL\text{-}G12D/+}$ mouse model we cannot comment on whether heightened T-cell mediated immunity via the *Tlr2* regulated SASP contributes to lesion

regression, as seen in human NSCLC precursors (Pennycuick et al., 2020). However, given we observe a tumour suppressor response in the absence of neo-antigens, this suggests that a canonical T-cell mediated response is not required for *Tlr2* mediated tumour suppression.

The flow cytometry panel used in this thesis to study lung immune populations does not allow determination of the activation state of immune cells nor evidence of potential exhaustion. NK (Schmidt et al., 2019) and T-cell (DuPage et al., 2011) exhaustion has been shown to be a feature in late-stage lung tumours in this model, therefore further studies to analyse the activation state of immune cells following *Tlr2* loss are warranted.

The majority of murine experiments in this thesis (including experiments with the $Kras^{LSL\text{-}G12D/+}$ mouse) used global *Tlr2* KO mice. Therefore, the underlying effect of immune cell *Tlr2* loss was a potential confounder in our results. While use of pSECC lentiviral constructs allowing *in vivo* somatic genome editing (Sanchez-Rivera et al., 2014) demonstrated that epithelial loss does likely underlie the observed phenotype, a contribution of immune cell loss cannot be fully excluded. The use of the $Tlr2^{fl/fl}$ mouse (which has recently become available), would permit lung epithelial cell specific knockout using high titre adenovirus and would help determine the precise role played by epithelial and immune cell *Tlr2* when compared with the results from our global KO experiments.

In summary, despite some drawbacks relating to the utility of this model to study immune responses, the $Kras^{LSL\text{-}G12D/+}$ mouse model is a well-placed model to study potential tumour suppressors in NSCLC. While with the

dosing regimen used in this thesis permitted the study of early-stage malignancy only (as was required), this can be easily down titrated to permit the organic development of late-stage disease.

## 6.3 Regulation of the SASP by *Tlr2*

The tumour suppressor role of cellular senescence was initially thought to be a cell intrinsic phenomenon relating solely to the cell cycle arrest (Lowe et al., 2004). However, the SASP has since been shown to have wide and context dependent effects on tumorigenesis including both pro- and anti-tumorigenic functions (Faget et al., 2019) (as discussed in chapter 1.3). The immune surveillance of senescent cells occurs in embryonic development whereby senescent ectodermal and mesodermal cells recruit macrophages leading to the subsequent clearance of senescent cells (Munoz-Espin et al., 2013; Storer et al., 2013). This phenomenon appears to have been hijacked in the context of malignancy, hence immune mediated clearance of senescent premalignant cells is a key tumour suppressor function of the SASP (Kang et al., 2011; Xue et al., 2007). So called 'senescence surveillance' is a response dependent on $CD4^+$ T-cells however recruited monocyte/macrophages act as the effector cells mediating clearance of senescent cells. In concert with this, studies in this thesis revealed a significant impairment of SASP expression by *Tlr2* deficient $Nras^{G12V}$ expressing hepatocytes, which resulted in a significant impairment of $F4/80^+$ macrophage recruitment to $Nras^{G12V}$ expressing hepatocytes. This however did not translate into a significant impairment of clearance of $Nras^{G12V}$

expressing hepatocytes. Impaired expression of the SASP was also observed in *Tlr2*$^{-/-}$ lung tumours which again resulted in a significant reduction in the recruitment of immune cells (predominantly monocytes/macrophages). Recently it has been shown than endothelial Tlr2 signalling supports the recruitment of immune cells to tumours via expression of proinflammatory cell adhesion molecules (McCoy et al., 2021), therefore it is possible that endothelial *Tlr2* loss is a contributing factor to the reduced immune infiltration we see in our global *Tlr2*$^{-/-}$ mice. However, the same study demonstrated extensive epithelial expression of *Tlr2* in the murine lung using the TLR2-IRES-EGFP reporter mouse, suggesting that epithelial *Tlr2* could also be vital in regulating this process and explain why we see such a specific tumour suppressor effect for *Tlr2* in lung cancer. Furthermore, it was confirmed that lung epithelial *Tlr2* loss underpins the observed phenotype in this thesis following *in vivo* CRIPSR/Cas9 mediated deletion of *Tlr2* in lung epithelial cells in concert with *Kras*$^{G12D}$ activation. While a trend towards reduced T-cell recruitment/infiltration was observed in *Tlr2*$^{-/-}$ lung tumours, these changes were not significant. This phenotype is mirrored in studies of *Kras*$^{G12D}$ driven pancreatic premalignancies, whereby T-cell infiltration is unchanged following genetic loss of the key SASP factor IL-1$\alpha$, however F4/80$^{+}$ macrophage infiltration is significantly impaired (Lau et al., 2019). However, as discussed above (chapter 6.2.2) the lack of T-cell activating neoantigens may render this model suboptimal to study tumour T-cell responses (McFadden et al., 2016).

Overall, this thesis describes convincing evidence that *Tlr2* loss impairs expression of the SASP *in vivo* in two separate disease models (covering two separate organ systems). However, a reduction of *Tlr2*$^{-/-}$ senescent hepatocytes did still occur after initial oncogene activation, suggesting that residual clearance mechanisms are still functional (either senescence surveillance or heightened apoptosis). While data demonstrating that *Tlr2* loss impairs senescence surveillance in the context of lung cancer has not been shown, the impaired recruitment of immune cells to lung tumours strongly suggests that impaired immune clearance is a plausible mechanism of tumour progression following *Tlr2* loss. Further studies involving depletion of specific immune cell subsets (for example clodronate mediated depletion of monocytes/macrophages) will help determine the role of immune clearance in lung tumour progression.

## 6.4 Regulation of OIS and the SASP independent of *Trp53*

*TP53* is major cell cycle regulator and limits tumorigenesis by inducing cell cycle arrest, apoptosis and cellular senescence (Vousden and Lane, 2007). It has also been shown to suppress expression of the SASP and pro-inflammatory signalling (Coppe et al., 2008b; Freund et al., 2011; Komarova et al., 2005), therefore loss of functional p53 can promote tumour progression via cell autonomous and non-cell autonomous processes (Lujambio et al., 2013). To determine whether *Tlr2* acts via *Trp53* (the murine homolog of *TP53*), a mouse model allowing simultaneous *Kras*$^{G12D}$ activation and *Trp53* deletion following Cre-recombinase expression (so called ‘KP’

mice) was utilised. Interestingly, *Tlr2*$^{-/-}$ deficient KP mice developed a significantly increased lung tumour burden in comparison with wild-type controls, and this was associated with significantly advanced tumour grade. Furthermore, the expression of key SASP factors was also impaired in lung tumours from *Tlr2*$^{-/-}$ KP mice, suggesting that Tlr2-SASP signalling is not solely dependent on p53-p21 signalling. The senescence associated cell cycle arrest in OIS is mediated via activation of both p53-p21 and p16-Rb tumour suppressor pathways (Collado and Serrano, 2010) and previous work from the Acosta lab demonstrated that TLR2 acts via both of these pathways to reinforce the growth arrest following oncogene activation *in vitro* (Hari et al., 2019). The precise delineation between the *Trp53* dependent and independent tumour suppressor function of TLR2-SASP signalling in this context is as yet unclear. The data presented in this thesis suggests that the TLR2-SASP reinforces the cell cycle arrest (primarily via p53-p21 tumour suppressor pathways) and mediates recruitment of immune cells that perturb tumour growth via senescence surveillance. Indeed, activation of p53-p21 signalling in lung tumours is supported by the increased p21 expression observed in lung tumours from *Tlr2* wild-type Kras$^{LSL\text{-}G12D/+}$ mice and enhanced expression following treatment with a TLR2 agonist. Interestingly, suppression of p16 has recently been shown to perturb expression of the SASP following oncogene activation (Buj et al., 2021) suggesting that intact p16-Rb signalling in our *Trp53* null tumours may maintain SASP expression. Recently it has been shown that mutant TRP53 interferes with cGAS-STING-TBK1 signalling, subsequently impairing the innate immune response and

promoting cancer progression (Ghosh et al., 2021). This effect is not observed in *Trp53* null cells, suggesting that mutant Trp53 exerts gain of function activities to inactivate tumour immune surveillance. cGAS-STING activation is a key event in OIS and expression of the SASP mediated via cytoplasmic chromatin sensing (Dou et al., 2017; Gluck et al., 2017) and previous lab members demonstrated that TLR2 functions downstream of this activation (Hari et al., 2019). Therefore, it remains to be determined whether intact cGAS-STING activation may also explain the persistent effect of *Tlr2* loss we observed in *Trp53* null tumours.

## 6.5 *TLR2* and the SASP in human lung cancer

The analysis of *TLR2* expression in human LUAD samples from the cancer genome atlas (Cancer Genome Atlas Research, 2014) revealed that high expression significantly correlates with improved survival. Importantly, immunostaining revealed that expression of TLR2 and the key SASP factor IL-1β is high in tumour epithelium. Reduced expression of *TLR2* and key SASP factors was observed in human LUAD lesions in comparison to LUAD precursor lesions (adenocarcinoma in situ - AIS/minimally invasive adenocarcinoma - MIA), suggesting a tumour suppressor role for TLR2-SASP signalling in this context. Further analysis of the expression profile of even earlier LUAD precursor lesions (atypical adenomatous hyperplasia – AAH), either using RNA sequencing datasets or IHC would help further determine the role of TLR2 and SASP signalling in LUAD progression. Unfortunately, the prognostic significance of the observed expression profiles in AIS/MIA and LUAD lesions was not able to be determined as these data

were from surgical resection specimens, preventing longitudinal follow up of lesion outcome. To assess prognostic significance in another context, gene expression microarray data was analysed by collaborators (Dr Adam Pennycuick, UCL) from human preinvasive lung squamous carcinoma (LUSC) lesions that had undergone longitudinal follow-up, detailing either subsequent progression to invasive malignancy or histological regression (Teixeira et al., 2019). Strikingly, the expression of *TLR2* and the *TLR2* regulated SASP was significantly associated with clinical regression, further supporting the hypothesis that *TLR2* and the SASP have a tumour suppressor function in human lung cancer.

*Kras* mutations are infrequent in human LUSC (as opposed to being the most frequently mutated oncogene in LUAD). It could therefore be argued that correlation between LUAD/$Kras^{G12D}$ driven lung cancer models and preinvasive LUSC is not valid. However, the upregulation of *TLR2* and the SASP is not confined to oncogenic *RAS* induced senescence alone. Indeed, previous work from the Acosta lab identified similar upregulation in multiple forms of senescence associated with genotoxic stress (including therapy-induced senescence, mutant *BRAF* induced senescence in melanoma, DNA damage induced senescence and replicative senescence) (Hari et al., 2019). Furthermore, similar epithelial specific toll-like receptor inflammatory signalling has been identified in murine prostate intraepithelial neoplasia (PIN) caused by *Pten* deletion (Dart et al., 2017) and has been shown to mediate senescence in tubular epithelial cells in the murine kidney after injury (Jin et al., 2019b). Therefore, the role of *TLR2* and the SASP extends

beyond *RAS* induced senescence alone. Despite LUAD and LUSC being distinct disease entities with different genetic drivers, a common role for TLR2 mediated SASP signalling is possible given the common role of these pathways across multiple forms of senescence (both oncogene-induced and otherwise).

While this thesis did not investigate whether TLR2-SASP signalling was associated with immune infiltration in human lung cancer, published work by colleagues using the same LUSC dataset revealed that immune surveillance is heavily implicated in lesion regression (Pennycuick et al., 2020). Furthermore, gene expression profiling of preinvasive LUSC lesions has revealed an abundance of immune sensing during the early stages of LUSC tumorigenesis with activated T-cells and myeloid cells (including macrophages) peaking immediately prior to invasion (Mascaux et al., 2019). Furthermore, multispectral imaging and deconvolution analysis of RNA sequencing data revealed increased macrophages and other myeloid cells in high grade dysplastic lesions, with subsequent activation of genes involved in immunosuppression promoting immune evasion and progression to invasive cancer (Mascaux et al., 2019). This was associated with a reduction in $CD3^+$ T-cells and $CD68^+$ macrophages in both the epithelium and stroma of invasive cancer lesions, further supporting a role of immune surveillance in limiting lung tumour progression. While this thesis has not shown definitively that TLR2-SASP signalling mediates immune surveillance in human lung premalignancy, the striking correlation between *TLR2* and the *TLR2* regulated SASP with clinical regression suggests that this mechanism is

plausible. Indeed, re-analysis of data from Mascaux et al (Mascaux et al., 2019) by collaborators (Dr Adam Pennycuick, UCL) revealed that *TLR2* and *TLR2* regulated SASP expression peaks in high grade lesions in concert with immune activation, further suggesting that TLR2-SASP signalling is involved in immune surveillance (data not shown). Macrophages make up the majority of the tumour immune infiltrate in human lung cancer (Conway et al., 2016) and this was mirrored in the *Kras*$^{LSL\text{-}G12D/+}$ lung cancer mouse model used in this thesis. Previously, studies examining total macrophage density in human tumours have shown that macrophages have been correlated with a poorer prognosis in most cancers (Bingle et al., 2002). In lung cancer, 'high' macrophage counts in tumour resection specimens has been associated with shorter survival (Chen et al., 2003) and higher risk of disease recurrence (Arenberg et al., 2000). However, other studies did not observe any relationship between total macrophage density and survival (Toomey et al., 2003) and subsequent analyses taking into account the microanatomical location of tumour associated macrophages (TAMs) revealed that increased macrophage density within tumour islets was associated with significantly improved survival (Dai et al., 2010; Kim et al., 2008; Welsh et al., 2005), whereas stromal macrophages were associated with worse survival (Dai et al., 2010; Kawai et al., 2008; Welsh et al., 2005). Furthermore, studies examining the polarisation of TAMs revealed that high levels of 'M1' macrophages were associated with improved survival (Ma et al., 2010; Ohri et al., 2009). However, the validity of the M1 vs M2 paradigm of macrophage activation *in vivo* is at best an oversimplification, with several markers of

each phenotype discovered *in vitro* with limited applicability *in vivo* (Martinez and Gordon, 2014; Nahrendorf and Swirski, 2016). Indeed, the studies discussed above (Ma et al., 2010; Ohri et al., 2009) used HLA-DR as a marker of M1 polarisation, and this has since been shown to be a general macrophage marker, therefore at best these HLA-DR$^+$ macrophages can be designated as non-M2 rather than definite M1 macrophages (Conway et al., 2016).

Taken together, data described in this thesis show that TLR2-SASP signalling is active in human lung tumour epithelium, and that this is correlated with improved survival and clinical regression of preinvasive lesions. While definitive proof of a regulatory role for TLR2-SASP signalling in lung tumour immune surveillance is lacking, substantial correlative data suggests that this could indeed be the case.

## 6.6 *TLR2* as a tumour suppressor gene?

The classical 'two-hit' definition of a tumour suppressor gene, whereby biallelic loss of gene function (via either inherited or somatic mutation) is required to initiate neoplastic growth, was first established following studies into retinoblastoma in children (Knudson, 1971). Analysis of hereditary cases of retinoblastoma revealed that patients inherited one inactivating mutation in the gene now known as *RB1* before undergoing a 'second hit' with a somatic mutation (normally via somatic mitotic recombination) in the remaining functional allele (Friend et al., 1986; Lee et al., 1987). The 'two-hit' model is sufficient to initiate many inherited paediatric cancers, however in reality the

majority of non-hereditary cancers require multiple mutational events and manifest in an iterative manner via somatic mutations and repeated rounds of clonal expansion (Vogelstein and Kinzler, 1993). Therefore the 'two-hit' definition refers to the loss of an individual tumour suppressor gene function (due to the loss of both alleles), rather than to the mutational events required to initiate tumourigenesis. *TLR2* certainly does not fit into this definition, as biallelic loss of *TLR2* is not a recognised feature in any human tumour type (to the best of my knowledge). The 'two-hit' hypothesis, while clearly relevant in most hereditary malignancies, does not necessarily comply with the biology of sporadic cancers and many recurring regions of monoallelic chromosomal deletions have been identified in several cancer types (Berger et al., 2011). The most commonly mutated tumour suppressor gene in human cancer, *TP53*, does not always fit into the two-hit definition. For example, $Trp53^{+/-}$ mice exhibit intermediate sensitivity to cancer formation somewhere between $Trp53^{+/+}$ and $Trp53^{-/-}$ littermates (Venkatachalam et al., 1998). This suggests that the level of expression of a tumour suppressor gene is important, and the remaining functional allele is not always sufficient to compensate for monoallelic loss (so called haploinsufficiency). Furthermore, tumours formed due to hereditary human cancer syndromes caused by dominant negative point mutations in *TP53* often do not harbour mutations in the remaining functional *TP53* allele (Varley et al., 1997) demonstrating that haploinsufficiency also occurs in human tumours. In some instances, haploinsufficiency of a tumour suppressor gene can be more tumourigenic that biallelic loss. Homozygous deletion of *Pten* in the prostate

results in activation of cellular senescence and enhanced tumour suppressive functions (with intact *Trp53*), whereas heterozygous loss of *Pten* enhances proliferation without activating senescence (Berger et al., 2011). While biallelic loss of *TLR2* is not described, shallow deletions of *TLR2* are observed in preinvasive LUSC samples, with more shallow deletions in samples that subsequently progressed to invasive malignancy (p=0.07). Shallow deletion in either *TLR2* or *TLR10* (the TLR2 partner shown to regulate OIS and the SASP (Hari et al., 2019)) was also increased in progressive samples (p=0.0086). This effect was specific for *TLR2* and its binding partners, as there was no observed association between shallow deletions in non-TLR2 associated plasma membrane TLRs (TLR4/5) and lesion progression. Furthermore, the majority of invasive LUSC samples from the TCGA exhibit both *TLR2* and *TLR10* shallow deletions. While *TLR2* does not fit the classic 'two-hit' definition of a tumour suppressor gene, lower expression of *TLR2* may well be caused at least in part by shallow deletions, suggesting *TLR2* haploinsufficiency does occur. Further experiments with the $Kras^{LSL\text{-}G12D/+}$ model on a $Tlr2^{+/-}$ background will help determine whether *Tlr2* haploinsufficiency does occurs in this context.

## 6.7 Potential clinical applications

### 6.7.1 TLR2 as a therapeutic target

Data presented in chapter 5 demonstrated that activation of Tlr2 with a synthetic agonist (Pam2CSK4) inhibits lung tumour growth. This is

encouraging and highlights the potential for TLR2 activation to be a novel therapeutic target in early-stage lung cancer. Lung epithelial cells are able to up-regulate TLR expression, subsequently enhancing antimicrobial responses (Chaudhuri et al., 2005), and inactivating TLR polymorphisms (including TLR2) can increase susceptibility to pulmonary infections (Velez et al., 2010). Therefore, modulation of TLR expression has been discussed as a potential treatment for chronic lung diseases. The utility of TLR2 activating vaccines has been explored and these have been found to induce immune cell maturation and improve the response to tumour-associated glycopeptide antigens (Ingale et al., 2009; Ingale et al., 2007), therefore targeting TLR2 activity has potential as an anticancer strategy. *TLR2* is not known to undergo biallelic deletion in NSCLC but may undergo monoallelic loss (shallow deletion - as discussed above in chapter 6.6). This can be considered a further vulnerability for targeting as functional plasma membrane TLR2 would still be available for therapeutic modulation.

While mice in this study showed no obvious adverse effects, it is likely that long-term modulation of a key innate immune pathway would come with significant side effects. Indeed, the reduction in lung monocyte/macrophage populations after repeated Pam2CSK4 dosing, likely due to Toll-like receptor tolerance (Butcher et al., 2018), points to the sensitivity of immune cells to pharmacological modulation of this pathway. Studies examining the long-term side effects of Pam2CSK4 administration were not performed as part of this thesis. Over and above potential toxicity, in order to employ TLR2 activation as a therapeutic strategy the reliable identification of patients with

preinvasive disease would be required. Early-stage lung cancer is classically asymptomatic and computed tomography (CT) scans cannot yet reliably identify preinvasive disease (with the exception of peripheral ground glass opacities representing AIS/MIA lesions (Lee et al., 2013; Ma et al., 2019)). Nonetheless, with the advent of low-dose CT (LDCT) screening and the renewed interest in non-invasive biomarker research (Calvayrac et al., 2017; Guibert et al., 2020), the reliable identification of patents with preinvasive disease may be on the horizon. While surgical resection should always be the mainstay of treatment for solitary early lung cancer lesions, conceivably modulation of TLR2-SASP signalling could be an appropriate strategy for patients with multifocal disease or those not fit for surgery/radiotherapy.

### 6.7.2 The SASP as a biomarker of lung pre-malignancy

LDCT screening for the detection of early-stage lung cancer has been shown to significantly improve lung cancer mortality (de Koning et al., 2020; National Lung Screening Trial Research et al., 2011). This has not yet been adopted in the United Kingdom but will likely be standard practice over the coming years. This approach is not without its drawbacks; LDCT screening can be associated with a high false positive rate, resulting in significant anxiety and potentially dangerous investigations in healthy patients. Furthermore, risk prediction tools used to assess an individual's suitability for screening can underestimate risk in certain patient demographics (Lebrett et al., 2020) and it has been reported that only one third of new lung cancer patients would have met eligibility criteria for LDCT screening (Wu et al.,

2016). Non-invasive biomarkers of early-stage disease could simultaneously improve screening population selection and improve diagnostic accuracy of LDCT screening (for example with indeterminate pulmonary nodules) (Oudkerk et al., 2021). Data in this thesis demonstrates that *TLR2* and the SASP are widely expressed in lung tumour epithelium, including in the preinvasive setting. SASP factors are readily secreted into the bloodstream, therefore are likely to represent candidate biomarkers of preinvasive disease. SASP factors are widely expressed in other contexts (such as infection and inflammation) therefore specificity could be improved by analysing a panel of known tumour associated SASP factors. Senescent cells (and tumour cells in general) are known to secrete extracellular vesicles (EVs) into the peripheral circulation that contain proteins, lipids and genomic material (O'Driscoll, 2015; Thakur et al., 2014). EVs mediate intercellular communication in physiological settings (Maas et al., 2017) but also become components of the SASP following the induction of cellular senescence (Misawa et al., 2020). Therefore, EVs are excellent candidate biomarkers for the early detection of cancer. Indeed, proteomic profiling of isolated EVs can not only identify cancer early but can determine cancer type (Hoshino et al., 2020). Therefore conceivably, TLR2-SASP components (or other lung cancer specific SASP components) could be measured in lung specific EVs as a marker of lung preinvasive disease burden. Patients with a high preinvasive disease burden could be targeted for LDCT screening to allow the timely identification of overt lung tumour formation and curative treatment with surgical resection. Furthermore, indeterminate pulmonary nodules identified via LDCT screening

could be further stratified as high vs low risk, based on TLR2-SASP levels identified in circulating EVs.

## 6.8 Future work

This thesis did not directly show that TLR2 mediated recruitment of monocytes/macrophages leads to clearance of premalignant cells in the lung. Therefore, future work in the short-medium term will seek to answer this question. As touched on previously (chapter 6.3) monocyte/macrophage depletion can be achieved by a combination of local and systemic delivery of clodronate liposomes, and this approach has been used previously to deplete macrophages in chemically induced lung cancer mouse models (Fritz et al., 2014). This experiment will help delineate the cell autonomous vs non-cell autonomous functions of TLR2 mediated tumour suppression in NSCLC. Furthermore, the utility of the TLR2 regulated SASP as a biomarker of early-stage lung cancer could be investigated with a proof of principle *in vivo* study using the *Kras*$^{LSL\text{-}G12D/+}$ mouse model. Repeated blood sampling and high throughput SASP measurements can be performed using a forward phase antibody microarray (in collaboration with the HTPU microarray service, University of Edinburgh). Tumour progression can be monitored longitudinally using micro computed tomography (microCT) imaging and correlated with SASP measurement as discussed above.

This thesis has only begun to describe the interplay between the SASP and the immune system in the context of lung tumourigenesis. In order to further characterise this highly complex process, better models recapitulating

the complex genetics of human lung cancer are required, as are methods to analyse in more detail the response of the immune system to lung tumour formation. In the long term (likely involving subsequent fellowship applications), immune single cell RNA sequencing approaches could be employed in neoantigen rich lung cancer models with or without functioning SASP expression to allow identification of SASP-immune mediated tumour suppressor processes. Subsequent validation and functional studies would help identify processes that are amenable to pharmacological modulation. With the impending roll out of lung cancer screening the availability of early-stage clinical samples is only going to improve and this will hopefully support the translation of any druggable tumour suppressor processes into the clinic.

## 6.9 Final conclusions

OIS is a complex tumour suppressor process, the precise regulation of which is yet to be fully understood. *TLR2* is clearly integral to not only the activation of OIS but in the expression of the SASP. This thesis has described data suggesting that the important *in vitro* observations that *TLR2* regulates OIS and the SASP indeed hold true in the *in vivo* setting (Hari et al., 2019), and *Tlr2* has a tumour suppressor function in murine models of NSCLC via regulation of the SASP. Strikingly, TLR2-SASP signalling is highly active in human NSCLC, where it correlates with improved survival and clinical regression of preinvasive lesions, suggesting that *TLR2* also has a tumour suppressor function in human disease. While questions remain about the precise cell autonomous vs non-cell autonomous mechanisms of TLR2 mediated tumour suppression, the prospect of utilising this pathway for therapeutic gain is real, as is harnessing the highly active TLR2 mediated SASP for the early detection of lung cancer.

# References

Ablasser, A., Goldeck, M., Cavlar, T., Deimling, T., Witte, G., Rohl, I., Hopfner, K.P., Ludwig, J., and Hornung, V. (2013). cGAS produces a 2'-5'-linked cyclic dinucleotide second messenger that activates STING. Nature *498*, 380-384.

Acosta, J.C., Banito, A., Wuestefeld, T., Georgilis, A., Janich, P., Morton, J.P., Athineos, D., Kang, T.W., Lasitschka, F., Andrulis, M.*, et al.* (2013). A complex secretory program orchestrated by the inflammasome controls paracrine senescence. Nat Cell Biol *15*, 978-990.

Acosta, J.C., O'Loghlen, A., Banito, A., Guijarro, M.V., Augert, A., Raguz, S., Fumagalli, M., Da Costa, M., Brown, C., Popov, N.*, et al.* (2008). Chemokine signaling via the CXCR2 receptor reinforces senescence. Cell *133*, 1006-1018.

Adams, P.D. (2007). Remodeling chromatin for senescence. Aging Cell *6*, 425-427.

Aifuwa, I., Giri, A., Longe, N., Lee, S.H., An, S.S., and Wirtz, D. (2015). Senescent stromal cells induce cancer cell migration via inhibition of RhoA/ROCK/myosin-based cell contractility. Oncotarget *6*, 30516-30531.

Akira, S., Uematsu, S., and Takeuchi, O. (2006). Pathogen recognition and innate immunity. Cell *124*, 783-801.

Alberg, A.J., Brock, M.V., Ford, J.G., Samet, J.M., and Spivack, S.D. (2013). Epidemiology of lung cancer: Diagnosis and management of lung cancer, 3rd ed: American College of Chest Physicians evidence-based clinical practice guidelines. Chest *143*, e1S-e29S.

Angelini, P.D., Zacarias Fluck, M.F., Pedersen, K., Parra-Palau, J.L., Guiu, M., Bernado Morales, C., Vicario, R., Luque-Garcia, A., Navalpotro, N.P.,

Giralt, J.*, et al.* (2013). Constitutive HER2 signaling promotes breast cancer metastasis through cellular senescence. Cancer Res *73*, 450-458.

Aoshiba, K., Tsuji, T., Kameyama, S., Itoh, M., Semba, S., Yamaguchi, K., and Nakamura, H. (2013). Senescence-associated secretory phenotype in a mouse model of bleomycin-induced lung injury. Exp Toxicol Pathol *65*, 1053-1062.

Aoshiba, K., Tsuji, T., and Nagai, A. (2003). Bleomycin induces cellular senescence in alveolar epithelial cells. Eur Respir J *22*, 436-443.

Arenberg, D.A., Keane, M.P., DiGiovine, B., Kunkel, S.L., Strom, S.R., Burdick, M.D., Iannettoni, M.D., and Strieter, R.M. (2000). Macrophage infiltration in human non-small-cell lung cancer: the role of CC chemokines. Cancer Immunol Immunother *49*, 63-70.

Aznar, E., Oroval, M., Pascual, L., Murguia, J.R., Martinez-Manez, R., and Sancenon, F. (2016). Gated Materials for On-Command Release of Guest Molecules. Chem Rev *116*, 561-718.

Baker, D.J., Childs, B.G., Durik, M., Wijers, M.E., Sieben, C.J., Zhong, J., Saltness, R.A., Jeganathan, K.B., Verzosa, G.C., Pezeshki, A.*, et al.* (2016). Naturally occurring p16(Ink4a)-positive cells shorten healthy lifespan. Nature *530*, 184-189.

Baker, D.J., Perez-Terzic, C., Jin, F., Pitel, K.S., Niederlander, N.J., Jeganathan, K., Yamada, S., Reyes, S., Rowe, L., Hiddinga, H.J.*, et al.* (2008). Opposing roles for p16Ink4a and p19Arf in senescence and ageing caused by BubR1 insufficiency. Nat Cell Biol *10*, 825-836.

Baker, D.J., Wijshake, T., Tchkonia, T., LeBrasseur, N.K., Childs, B.G., van de Sluis, B., Kirkland, J.L., and van Deursen, J.M. (2011). Clearance of p16Ink4a-positive senescent cells delays ageing-associated disorders. Nature *479*, 232-236.

Ballester, B., Milara, J., and Cortijo, J. (2019). Idiopathic Pulmonary Fibrosis and Lung Cancer: Mechanisms and Molecular Targets. Int J Mol Sci *20*.

Bankhead, P., Loughrey, M.B., Fernandez, J.A., Dombrowski, Y., McArt, D.G., Dunne, P.D., McQuaid, S., Gray, R.T., Murray, L.J., Coleman, H.G.*, et al.* (2017). QuPath: Open source software for digital pathology image analysis. Sci Rep *7*, 16878.

Barradas, M., Anderton, E., Acosta, J.C., Li, S., Banito, A., Rodriguez-Niedenfuhr, M., Maertens, G., Banck, M., Zhou, M.M., Walsh, M.J.*, et al.* (2009). Histone demethylase JMJD3 contributes to epigenetic control of INK4a/ARF by oncogenic RAS. Genes Dev *23*, 1177-1182.

Bartkova, J., Rezaei, N., Liontos, M., Karakaidos, P., Kletsas, D., Issaeva, N., Vassiliou, L.V., Kolettas, E., Niforou, K., Zoumpourlis, V.C.*, et al.* (2006). Oncogene-induced senescence is part of the tumorigenesis barrier imposed by DNA damage checkpoints. Nature *444*, 633-637.

Basisty, N., Kale, A., Jeon, O.H., Kuehnemann, C., Payne, T., Rao, C., Holtz, A., Shah, S., Sharma, V., Ferrucci, L.*, et al.* (2020). A proteomic atlas of senescence-associated secretomes for aging biomarker development. PLoS Biol *18*, e3000599.

Bauer, A.K., Dixon, D., DeGraff, L.M., Cho, H.Y., Walker, C.R., Malkinson, A.M., and Kleeberger, S.R. (2005). Toll-like receptor 4 in butylated hydroxytoluene-induced mouse pulmonary inflammation and tumorigenesis. J Natl Cancer Inst *97*, 1778-1781.

Bauer, A.K., Upham, B.L., Rondini, E.A., Tennis, M.A., Velmuragan, K., and Wiese, D. (2017). Toll-like receptor expression in human non-small cell lung carcinoma: potential prognostic indicators of disease. Oncotarget *8*, 91860-91875.

Bavik, C., Coleman, I., Dean, J.P., Knudsen, B., Plymate, S., and Nelson, P.S. (2006). The gene expression program of prostate fibroblast senescence

modulates neoplastic epithelial cell proliferation through paracrine mechanisms. Cancer Res *66*, 794-802.

Beausejour, C.M., Krtolica, A., Galimi, F., Narita, M., Lowe, S.W., Yaswen, P., and Campisi, J. (2003). Reversal of human cellular senescence: roles of the p53 and p16 pathways. EMBO J *22*, 4212-4222.

Beck, J., Horikawa, I., and Harris, C. (2020). Cellular Senescence: Mechanisms, Morphology, and Mouse Models. Vet Pathol *57*, 747-757.

Benson, E.K., Zhao, B., Sassoon, D.A., Lee, S.W., and Aaronson, S.A. (2009). Effects of p21 deletion in mouse models of premature aging. Cell Cycle *8*, 2002-2004.

Berger, A.H., Knudson, A.G., and Pandolfi, P.P. (2011). A continuum model for tumour suppression. Nature *476*, 163-169.

Besancenot, R., Chaligne, R., Tonetti, C., Pasquier, F., Marty, C., Lecluse, Y., Vainchenker, W., Constantinescu, S.N., and Giraudier, S. (2010). A senescence-like cell-cycle arrest occurs during megakaryocytic maturation: implications for physiological and pathological megakaryocytic proliferation. PLoS Biol *8*.

Bhat, R., Crowe, E.P., Bitto, A., Moh, M., Katsetos, C.D., Garcia, F.U., Johnson, F.B., Trojanowski, J.Q., Sell, C., and Torres, C. (2012). Astrocyte senescence as a component of Alzheimer's disease. PLoS One *7*, e45069.

Bingle, L., Brown, N.J., and Lewis, C.E. (2002). The role of tumour-associated macrophages in tumour progression: implications for new anticancer therapies. J Pathol *196*, 254-265.

Bock, F.J., and Tait, S.W.G. (2020). Mitochondria as multifaceted regulators of cell death. Nat Rev Mol Cell Biol *21*, 85-100.

Bracken, A.P., Kleine-Kohlbrecher, D., Dietrich, N., Pasini, D., Gargiulo, G., Beekman, C., Theilgaard-Monch, K., Minucci, S., Porse, B.T., Marine, J.C.,

*et al.* (2007). The Polycomb group proteins bind throughout the INK4A-ARF locus and are disassociated in senescent cells. Genes Dev *21*, 525-530.

Braig, M., Lee, S., Loddenkemper, C., Rudolph, C., Peters, A.H., Schlegelberger, B., Stein, H., Dorken, B., Jenuwein, T., and Schmitt, C.A. (2005). Oncogene-induced senescence as an initial barrier in lymphoma development. Nature *436*, 660-665.

Brennan, K., Offiah, G., McSherry, E.A., and Hopkins, A.M. (2010). Tight junctions: a barrier to the initiation and progression of breast cancer? J Biomed Biotechnol *2010*, 460607.

Brugarolas, J., Bronson, R.T., and Jacks, T. (1998). p21 is a critical CDK2 regulator essential for proliferation control in Rb-deficient cells. J Cell Biol *141*, 503-514.

Bubna, A.K. (2015). Imiquimod - Its role in the treatment of cutaneous malignancies. Indian J Pharmacol *47*, 354-359.

Buj, R., Leon, K.E., Anguelov, M.A., and Aird, K.M. (2021). Suppression of p16 alleviates the senescence-associated secretory phenotype. Aging (Albany NY) *13*, 3290-3312.

Burd, C.E., Sorrentino, J.A., Clark, K.S., Darr, D.B., Krishnamurthy, J., Deal, A.M., Bardeesy, N., Castrillon, D.H., Beach, D.H., and Sharpless, N.E. (2013). Monitoring tumorigenesis and senescence in vivo with a p16(INK4a)-luciferase model. Cell *152*, 340-351.

Busch, S.E., Hanke, M.L., Kargl, J., Metz, H.E., MacPherson, D., and Houghton, A.M. (2016). Lung Cancer Subtypes Generate Unique Immune Responses. J Immunol *197*, 4493-4503.

Butcher, S.K., O'Carroll, C.E., Wells, C.A., and Carmody, R.J. (2018). Toll-Like Receptors Drive Specific Patterns of Tolerance and Training on Restimulation of Macrophages. Front Immunol *9*, 933.

Callister, M.E., Baldwin, D.R., Akram, A.R., Barnard, S., Cane, P., Draffan, J., Franks, K., Gleeson, F., Graham, R., Malhotra, P.*, et al.* (2015). British Thoracic Society guidelines for the investigation and management of pulmonary nodules. Thorax *70 Suppl 2*, ii1-ii54.

Calvayrac, O., Pradines, A., Pons, E., Mazières, J., and Guibert, N. (2017). Molecular biomarkers for lung adenocarcinoma. European Respiratory Journal *49*, 1601734.

Camidge, D.R., Bang, Y.J., Kwak, E.L., Iafrate, A.J., Varella-Garcia, M., Fox, S.B., Riely, G.J., Solomon, B., Ou, S.H., Kim, D.W.*, et al.* (2012). Activity and safety of crizotinib in patients with ALK-positive non-small-cell lung cancer: updated results from a phase 1 study. Lancet Oncol *13*, 1011-1019.

Camolotto, S.A., Pattabiraman, S., Mosbruger, T.L., Jones, A., Belova, V.K., Orstad, G., Streiff, M., Salmond, L., Stubben, C., Kaestner, K.H.*, et al.* (2018). FoxA1 and FoxA2 drive gastric differentiation and suppress squamous identity in NKX2-1-negative lung cancer. Elife *7*.

Campaner, S., Doni, M., Hydbring, P., Verrecchia, A., Bianchi, L., Sardella, D., Schleker, T., Perna, D., Tronnersjo, S., Murga, M.*, et al.* (2010). Cdk2 suppresses cellular senescence induced by the c-myc oncogene. Nat Cell Biol *12*, 54-59; sup pp 51-14.

Campisi, J. (1997a). Aging and cancer: the double-edged sword of replicative senescence. J Am Geriatr Soc *45*, 482-488.

Campisi, J. (1997b). The biology of replicative senescence. Eur J Cancer *33*, 703-709.

Campisi, J. (2005). Senescent cells, tumor suppression, and organismal aging: good citizens, bad neighbors. Cell *120*, 513-522.

Cancer Genome Atlas Research, N. (2012). Comprehensive genomic characterization of squamous cell lung cancers. Nature *489*, 519-525.

Cancer Genome Atlas Research, N. (2014). Comprehensive molecular profiling of lung adenocarcinoma. Nature *511*, 543-550.

Canudas, A.M., Gutierrez-Cuesta, J., Rodriguez, M.I., Acuna-Castroviejo, D., Sureda, F.X., Camins, A., and Pallas, M. (2005). Hyperphosphorylation of microtubule-associated protein tau in senescence-accelerated mouse (SAM). Mech Ageing Dev *126*, 1300-1304.

Capell, B.C., Drake, A.M., Zhu, J., Shah, P.P., Dou, Z., Dorsey, J., Simola, D.F., Donahue, G., Sammons, M., Rai, T.S.*, et al.* (2016). MLL1 is essential for the senescence-associated secretory phenotype. Genes Dev *30*, 321-336.

Carlson, C.M., Frandsen, J.L., Kirchhof, N., McIvor, R.S., and Largaespada, D.A. (2005). Somatic integration of an oncogene-harboring Sleeping Beauty transposon models liver tumor development in the mouse. Proc Natl Acad Sci U S A *102*, 17059-17064.

Chang, J., Wang, Y., Shao, L., Laberge, R.M., Demaria, M., Campisi, J., Janakiraman, K., Sharpless, N.E., Ding, S., Feng, W.*, et al.* (2016). Clearance of senescent cells by ABT263 rejuvenates aged hematopoietic stem cells in mice. Nat Med *22*, 78-83.

Chaudhuri, N., Dower, S.K., Whyte, M.K., and Sabroe, I. (2005). Toll-like receptors and chronic lung disease. Clin Sci (Lond) *109*, 125-133.

Chen, D., Dai, C., Kadeer, X., Mao, R., Chen, Y., and Chen, C. (2018). New horizons in surgical treatment of ground-glass nodules of the lung: experience and controversies. Ther Clin Risk Manag *14*, 203-211.

Chen, H., Carrot-Zhang, J., Zhao, Y., Hu, H., Freeman, S.S., Yu, S., Ha, G., Taylor, A.M., Berger, A.C., Westlake, L.*, et al.* (2019). Genomic and immune profiling of pre-invasive lung adenocarcinoma. Nat Commun *10*, 5472.

Chen, J.J., Yao, P.L., Yuan, A., Hong, T.M., Shun, C.T., Kuo, M.L., Lee, Y.C., and Yang, P.C. (2003). Up-regulation of tumor interleukin-8 expression

by infiltrating macrophages: its correlation with tumor angiogenesis and patient survival in non-small cell lung cancer. Clin Cancer Res *9*, 729-737.

Chen, Q., and Ames, B.N. (1994). Senescence-like growth arrest induced by hydrogen peroxide in human diploid fibroblast F65 cells. Proc Natl Acad Sci U S A *91*, 4130-4134.

Chen, Q., Fischer, A., Reagan, J.D., Yan, L.J., and Ames, B.N. (1995). Oxidative DNA damage and senescence of human diploid fibroblast cells. Proc Natl Acad Sci U S A *92*, 4337-4341.

Chen, Q.M., Liu, J., and Merrett, J.B. (2000a). Apoptosis or senescence-like growth arrest: influence of cell-cycle position, p53, p21 and bax in H2O2 response of normal human fibroblasts. Biochem J *347*, 543-551.

Chen, Q.M., Prowse, K.R., Tu, V.C., Purdom, S., and Linskens, M.H. (2001). Uncoupling the senescent phenotype from telomere shortening in hydrogen peroxide-treated fibroblasts. Exp Cell Res *265*, 294-303.

Chen, Q.M., Tu, V.C., Catania, J., Burton, M., Toussaint, O., and Dilley, T. (2000b). Involvement of Rb family proteins, focal adhesion proteins and protein synthesis in senescent morphogenesis induced by hydrogen peroxide. J Cell Sci *113 ( Pt 22)*, 4087-4097.

Chen, Z., Trotman, L.C., Shaffer, D., Lin, H.K., Dotan, Z.A., Niki, M., Koutcher, J.A., Scher, H.I., Ludwig, T., Gerald, W.*, et al.* (2005). Crucial role of p53-dependent cellular senescence in suppression of Pten-deficient tumorigenesis. Nature *436*, 725-730.

Chesnokova, V., Wong, C., Zonis, S., Gruszka, A., Wawrowsky, K., Ren, S.G., Benshlomo, A., and Yu, R. (2009). Diminished pancreatic beta-cell mass in securin-null mice is caused by beta-cell apoptosis and senescence. Endocrinology *150*, 2603-2610.

Chicas, A., Wang, X., Zhang, C., McCurrach, M., Zhao, Z., Mert, O., Dickins, R.A., Narita, M., Zhang, M., and Lowe, S.W. (2010). Dissecting the unique

role of the retinoblastoma tumor suppressor during cellular senescence. Cancer Cell *17*, 376-387.

Childs, B.G., Baker, D.J., Kirkland, J.L., Campisi, J., and van Deursen, J.M. (2014). Senescence and apoptosis: dueling or complementary cell fates? EMBO Rep *15*, 1139-1153.

Chinta, S.J., Lieu, C.A., Demaria, M., Laberge, R.M., Campisi, J., and Andersen, J.K. (2013). Environmental stress, ageing and glial cell senescence: a novel mechanistic link to Parkinson's disease? J Intern Med *273*, 429-436.

Chuprin, A., Gal, H., Biron-Shental, T., Biran, A., Amiel, A., Rozenblatt, S., and Krizhanovsky, V. (2013). Cell fusion induced by ERVWE1 or measles virus causes cellular senescence. Genes Dev *27*, 2356-2366.

Collado, M., Gil, J., Efeyan, A., Guerra, C., Schuhmacher, A.J., Barradas, M., Benguria, A., Zaballos, A., Flores, J.M., Barbacid, M.*, et al.* (2005). Tumour biology: senescence in premalignant tumours. Nature *436*, 642.

Collado, M., and Serrano, M. (2010). Senescence in tumours: evidence from mice and humans. Nat Rev Cancer *10*, 51-57.

Collins, K., and Mitchell, J.R. (2002). Telomerase in the human organism. Oncogene *21*, 564-579.

Conway, E.M., Pikor, L.A., Kung, S.H., Hamilton, M.J., Lam, S., Lam, W.L., and Bennewith, K.L. (2016). Macrophages, Inflammation, and Lung Cancer. Am J Respir Crit Care Med *193*, 116-130.

Coppe, J.P., Boysen, M., Sun, C.H., Wong, B.J., Kang, M.K., Park, N.H., Desprez, P.Y., Campisi, J., and Krtolica, A. (2008a). A role for fibroblasts in mediating the effects of tobacco-induced epithelial cell growth and invasion. Mol Cancer Res *6*, 1085-1098.

Coppe, J.P., Desprez, P.Y., Krtolica, A., and Campisi, J. (2010). The senescence-associated secretory phenotype: the dark side of tumor suppression. Annu Rev Pathol *5*, 99-118.

Coppe, J.P., Kauser, K., Campisi, J., and Beausejour, C.M. (2006). Secretion of vascular endothelial growth factor by primary human fibroblasts at senescence. J Biol Chem *281*, 29568-29574.

Coppe, J.P., Patil, C.K., Rodier, F., Sun, Y., Munoz, D.P., Goldstein, J., Nelson, P.S., Desprez, P.Y., and Campisi, J. (2008b). Senescence-associated secretory phenotypes reveal cell-nonautonomous functions of oncogenic RAS and the p53 tumor suppressor. PLoS Biol *6*, 2853-2868.

Courtois-Cox, S., Genther Williams, S.M., Reczek, E.E., Johnson, B.W., McGillicuddy, L.T., Johannessen, C.M., Hollstein, P.E., MacCollin, M., and Cichowski, K. (2006). A negative feedback signaling network underlies oncogene-induced senescence. Cancer Cell *10*, 459-472.

Crosbie, P.A., Balata, H., Evison, M., Atack, M., Bayliss-Brideaux, V., Colligan, D., Duerden, R., Eaglesfield, J., Edwards, T., Elton, P.*, et al.* (2019). Implementing lung cancer screening: baseline results from a community-based 'Lung Health Check' pilot in deprived areas of Manchester. Thorax *74*, 405-409.

Crosbie, P.A., Gabe, R., Simmonds, I., Kennedy, M., Rogerson, S., Ahmed, N., Baldwin, D.R., Booton, R., Cochrane, A., Darby, M.*, et al.* (2020). Yorkshire Lung Screening Trial (YLST): protocol for a randomised controlled trial to evaluate invitation to community-based low-dose CT screening for lung cancer versus usual care in a targeted population at risk. BMJ Open *10*, e037075.

Crow, Y.J., and Manel, N. (2015). Aicardi-Goutieres syndrome and the type I interferonopathies. Nat Rev Immunol *15*, 429-440.

Curtin, J.F., Liu, N., Candolfi, M., Xiong, W., Assi, H., Yagiz, K., Edwards, M.R., Michelsen, K.S., Kroeger, K.M., Liu, C.*, et al.* (2009). HMGB1 mediates endogenous TLR2 activation and brain tumor regression. PLoS Med *6*, e10.

d'Adda di Fagagna, F. (2008). Living on a break: cellular senescence as a DNA-damage response. Nat Rev Cancer *8*, 512-522.

d'Adda di Fagagna, F., Reaper, P.M., Clay-Farrace, L., Fiegler, H., Carr, P., Von Zglinicki, T., Saretzki, G., Carter, N.P., and Jackson, S.P. (2003). A DNA damage checkpoint response in telomere-initiated senescence. Nature *426*, 194-198.

d'Adda di Fagagna, F., Teo, S.H., and Jackson, S.P. (2004). Functional links between telomeres and proteins of the DNA-damage response. Genes Dev *18*, 1781-1799.

Dai, F., Liu, L., Che, G., Yu, N., Pu, Q., Zhang, S., Ma, J., Ma, L., and You, Z. (2010). The number and microlocalization of tumor-associated immune cells are associated with patient's survival time in non-small cell lung cancer. BMC Cancer *10*, 220.

Dankort, D., Filenova, E., Collado, M., Serrano, M., Jones, K., and McMahon, M. (2007). A new mouse model to explore the initiation, progression, and therapy of BRAFV600E-induced lung tumors. Genes Dev *21*, 379-384.

Dart, D.A., Uysal-Onganer, P., and Jiang, W.G. (2017). Prostate-specific PTen deletion in mice activates inflammatory microRNA expression pathways in the epithelium early in hyperplasia development. Oncogenesis *6*, 400.

Das, A.T., Tenenbaum, L., and Berkhout, B. (2016). Tet-On Systems For Doxycycline-inducible Gene Expression. Curr Gene Ther *16*, 156-167.

Davalos, A.R., Kawahara, M., Malhotra, G.K., Schaum, N., Huang, J., Ved, U., Beausejour, C.M., Coppe, J.P., Rodier, F., and Campisi, J. (2013). p53-

dependent release of Alarmin HMGB1 is a central mediator of senescent phenotypes. J Cell Biol *201*, 613-629.

De Cecco, M., Ito, T., Petrashen, A.P., Elias, A.E., Skvir, N.J., Criscione, S.W., Caligiana, A., Brocculi, G., Adney, E.M., Boeke, J.D.*, et al.* (2019). L1 drives IFN in senescent cells and promotes age-associated inflammation. Nature *566*, 73-78.

de Koning, H.J., van der Aalst, C.M., de Jong, P.A., Scholten, E.T., Nackaerts, K., Heuvelmans, M.A., Lammers, J.J., Weenink, C., Yousaf-Khan, U., Horeweg, N.*, et al.* (2020). Reduced Lung-Cancer Mortality with Volume CT Screening in a Randomized Trial. N Engl J Med *382*, 503-513.

Debacq-Chainiaux, F., Borlon, C., Pascal, T., Royer, V., Eliaers, F., Ninane, N., Carrard, G., Friguet, B., de Longueville, F., Boffe, S.*, et al.* (2005). Repeated exposure of human skin fibroblasts to UVB at subcytotoxic level triggers premature senescence through the TGF-beta1 signaling pathway. J Cell Sci *118*, 743-758.

Debacq-Chainiaux, F., Erusalimsky, J.D., Campisi, J., and Toussaint, O. (2009). Protocols to detect senescence-associated beta-galactosidase (SA-betagal) activity, a biomarker of senescent cells in culture and in vivo. Nat Protoc *4*, 1798-1806.

Demaria, M., Ohtani, N., Youssef, S.A., Rodier, F., Toussaint, W., Mitchell, J.R., Laberge, R.M., Vijg, J., Van Steeg, H., Dolle, M.E.*, et al.* (2014). An essential role for senescent cells in optimal wound healing through secretion of PDGF-AA. Dev Cell *31*, 722-733.

Denoyelle, C., Abou-Rjaily, G., Bezrookove, V., Verhaegen, M., Johnson, T.M., Fullen, D.R., Pointer, J.N., Gruber, S.B., Su, L.D., Nikiforov, M.A.*, et al.* (2006). Anti-oncogenic role of the endoplasmic reticulum differentially activated by mutations in the MAPK pathway. Nat Cell Biol *8*, 1053-1063.

Desdin-Mico, G., Soto-Heredero, G., Aranda, J.F., Oller, J., Carrasco, E., Gabande-Rodriguez, E., Blanco, E.M., Alfranca, A., Cusso, L., Desco, M.*, et al.* (2020). T cells with dysfunctional mitochondria induce multimorbidity and premature senescence. Science *368*, 1371-1376.

Dhomen, N., Reis-Filho, J.S., da Rocha Dias, S., Hayward, R., Savage, K., Delmas, V., Larue, L., Pritchard, C., and Marais, R. (2009). Oncogenic Braf induces melanocyte senescence and melanoma in mice. Cancer Cell *15*, 294-303.

Di, G.H., Liu, Y., Lu, Y., Liu, J., Wu, C., and Duan, H.F. (2014). IL-6 secreted from senescent mesenchymal stem cells promotes proliferation and migration of breast cancer cells. PLoS One *9*, e113572.

Di Leonardo, A., Linke, S.P., Clarkin, K., and Wahl, G.M. (1994). DNA damage triggers a prolonged p53-dependent G1 arrest and long-term induction of Cip1 in normal human fibroblasts. Genes Dev *8*, 2540-2551.

Di Micco, R., Fumagalli, M., Cicalese, A., Piccinin, S., Gasparini, P., Luise, C., Schurra, C., Garre, M., Nuciforo, P.G., Bensimon, A.*, et al.* (2006). Oncogene-induced senescence is a DNA damage response triggered by DNA hyper-replication. Nature *444*, 638-642.

Di Mitri, D., Mirenda, M., Vasilevska, J., Calcinotto, A., Delaleu, N., Revandkar, A., Gil, V., Boysen, G., Losa, M., Mosole, S.*, et al.* (2019). Re-education of Tumor-Associated Macrophages by CXCR2 Blockade Drives Senescence and Tumor Inhibition in Advanced Prostate Cancer. Cell Rep *28*, 2156-2168 e2155.

Di Mitri, D., Toso, A., Chen, J.J., Sarti, M., Pinton, S., Jost, T.R., D'Antuono, R., Montani, E., Garcia-Escudero, R., Guccini, I.*, et al.* (2014). Tumour-infiltrating Gr-1+ myeloid cells antagonize senescence in cancer. Nature *515*, 134-137.

Dickey, J.S., Redon, C.E., Nakamura, A.J., Baird, B.J., Sedelnikova, O.A., and Bonner, W.M. (2009). H2AX: functional roles and potential applications. Chromosoma *118*, 683-692.

Diez-Juan, A., and Andres, V. (2001). The growth suppressor p27(Kip1) protects against diet-induced atherosclerosis. FASEB J *15*, 1989-1995.

Dimri, G.P., Lee, X., Basile, G., Acosta, M., Scott, G., Roskelley, C., Medrano, E.E., Linskens, M., Rubelj, I., Pereira-Smith, O.*, et al.* (1995). A biomarker that identifies senescent human cells in culture and in aging skin in vivo. Proc Natl Acad Sci U S A *92*, 9363-9367.

Ding, L., Getz, G., Wheeler, D.A., Mardis, E.R., McLellan, M.D., Cibulskis, K., Sougnez, C., Greulich, H., Muzny, D.M., Morgan, M.B.*, et al.* (2008). Somatic mutations affect key pathways in lung adenocarcinoma. Nature *455*, 1069-1075.

Dirac, A.M., and Bernards, R. (2003). Reversal of senescence in mouse fibroblasts through lentiviral suppression of p53. J Biol Chem *278*, 11731-11734.

Dobin, A., Davis, C.A., Schlesinger, F., Drenkow, J., Zaleski, C., Jha, S., Batut, P., Chaisson, M., and Gingeras, T.R. (2013). STAR: ultrafast universal RNA-seq aligner. Bioinformatics *29*, 15-21.

Donington, J., Ferguson, M., Mazzone, P., Handy, J., Jr., Schuchert, M., Fernando, H., Loo, B., Jr., Lanuti, M., de Hoyos, A., Detterbeck, F.*, et al.* (2012). American College of Chest Physicians and Society of Thoracic Surgeons consensus statement for evaluation and management for high-risk patients with stage I non-small cell lung cancer. Chest *142*, 1620-1635.

Doria, A., Patti, M.E., and Kahn, C.R. (2008). The emerging genetic architecture of type 2 diabetes. Cell Metab *8*, 186-200.

Dou, Z., Ghosh, K., Vizioli, M.G., Zhu, J., Sen, P., Wangensteen, K.J., Simithy, J., Lan, Y., Lin, Y., Zhou, Z.*, et al.* (2017). Cytoplasmic chromatin triggers inflammation in senescence and cancer. Nature *550*, 402-406.

Dou, Z., Xu, C., Donahue, G., Shimi, T., Pan, J.A., Zhu, J., Ivanov, A., Capell, B.C., Drake, A.M., Shah, P.P.*, et al.* (2015). Autophagy mediates degradation of nuclear lamina. Nature *527*, 105-109.

Duan, X., Ponomareva, L., Veeranki, S., Panchanathan, R., Dickerson, E., and Choubey, D. (2011). Differential roles for the interferon-inducible IFI16 and AIM2 innate immune sensors for cytosolic DNA in cellular senescence of human fibroblasts. Mol Cancer Res *9*, 589-602.

DuPage, M., Cheung, A.F., Mazumdar, C., Winslow, M.M., Bronson, R., Schmidt, L.M., Crowley, D., Chen, J., and Jacks, T. (2011). Endogenous T cell responses to antigens expressed in lung adenocarcinomas delay malignant tumor progression. Cancer Cell *19*, 72-85.

DuPage, M., Dooley, A.L., and Jacks, T. (2009). Conditional mouse lung cancer models using adenoviral or lentiviral delivery of Cre recombinase. Nat Protoc *4*, 1064-1072.

Eberhardt, R., Anantham, D., Herth, F., Feller-Kopman, D., and Ernst, A. (2007). Electromagnetic navigation diagnostic bronchoscopy in peripheral lung lesions. Chest *131*, 1800-1805.

Eggert, T., Wolter, K., Ji, J., Ma, C., Yevsa, T., Klotz, S., Medina-Echeverz, J., Longerich, T., Forgues, M., Reisinger, F.*, et al.* (2016). Distinct Functions of Senescence-Associated Immune Responses in Liver Tumor Surveillance and Tumor Progression. Cancer Cell *30*, 533-547.

Engelman, J.A., Chen, L., Tan, X., Crosby, K., Guimaraes, A.R., Upadhyay, R., Maira, M., McNamara, K., Perera, S.A., Song, Y.*, et al.* (2008). Effective use of PI3K and MEK inhibitors to treat mutant Kras G12D and PIK3CA H1047R murine lung cancers. Nat Med *14*, 1351-1356.

Engelman, J.A., Zejnullahu, K., Mitsudomi, T., Song, Y., Hyland, C., Park, J.O., Lindeman, N., Gale, C.M., Zhao, X., Christensen, J.*, et al.* (2007). MET amplification leads to gefitinib resistance in lung cancer by activating ERBB3 signaling. Science *316*, 1039-1043.

Erusalimsky, J.D., and Kurz, D.J. (2005). Cellular senescence in vivo: its relevance in ageing and cardiovascular disease. Exp Gerontol *40*, 634-642.

Ewald, J.A., Desotelle, J.A., Wilding, G., and Jarrard, D.F. (2010). Therapy-induced senescence in cancer. J Natl Cancer Inst *102*, 1536-1546.

Faget, D.V., Ren, Q., and Stewart, S.A. (2019). Unmasking senescence: context-dependent effects of SASP in cancer. Nat Rev Cancer *19*, 439-453.

Farsam, V., Basu, A., Gatzka, M., Treiber, N., Schneider, L.A., Mulaw, M.A., Lucas, T., Kochanek, S., Dummer, R., Levesque, M.P.*, et al.* (2016). Senescent fibroblast-derived Chemerin promotes squamous cell carcinoma migration. Oncotarget *7*, 83554-83569.

Feng, G., Zheng, K., Cao, T., Zhang, J., Lian, M., Huang, D., Wei, C., Gu, Z., and Feng, X. (2018). Repeated stimulation by LPS promotes the senescence of DPSCs via TLR4/MyD88-NF-kappaB-p53/p21 signaling. Cytotechnology *70*, 1023-1035.

Feng, L., Cao, L., Zhang, Y., and Wang, F. (2016). Detecting Abeta deposition and RPE cell senescence in the retinas of SAMP8 mice. Discov Med *21*, 149-158.

Fernandes, S., Williams, G., Williams, E., Ehrlich, K., Stone, J., Finlayson, N., Bradley, M., Thomson, R.R., Akram, A.R., and Dhaliwal, K. (2021). Solitary pulmonary nodule imaging approaches and the role of optical fibre-based technologies. Eur Respir J *57*.

Ferone, G., Lee, M.C., Sage, J., and Berns, A. (2020). Cells of origin of lung cancers: lessons from mouse studies. Genes Dev *34*, 1017-1032.

Ferone, G., Song, J.Y., Sutherland, K.D., Bhaskaran, R., Monkhorst, K., Lambooij, J.P., Proost, N., Gargiulo, G., and Berns, A. (2016). SOX2 Is the Determining Oncogenic Switch in Promoting Lung Squamous Cell Carcinoma from Different Cells of Origin. Cancer Cell *30*, 519-532.

Folch, E.E., Pritchett, M.A., Nead, M.A., Bowling, M.R., Murgu, S.D., Krimsky, W.S., Murillo, B.A., LeMense, G.P., Minnich, D.J., Bansal, S.*, et al.* (2019). Electromagnetic Navigation Bronchoscopy for Peripheral Pulmonary Lesions: One-Year Results of the Prospective, Multicenter NAVIGATE Study. J Thorac Oncol *14*, 445-458.

Franceschi, C., and Campisi, J. (2014). Chronic inflammation (inflammaging) and its potential contribution to age-associated diseases. J Gerontol A Biol Sci Med Sci *69 Suppl 1*, S4-9.

Freund, A., Patil, C.K., and Campisi, J. (2011). p38MAPK is a novel DNA damage response-independent regulator of the senescence-associated secretory phenotype. EMBO J *30*, 1536-1548.

Friend, S.H., Bernards, R., Rogelj, S., Weinberg, R.A., Rapaport, J.M., Albert, D.M., and Dryja, T.P. (1986). A human DNA segment with properties of the gene that predisposes to retinoblastoma and osteosarcoma. Nature *323*, 643-646.

Fritz, J.M., Tennis, M.A., Orlicky, D.J., Lin, H., Ju, C., Redente, E.F., Choo, K.S., Staab, T.A., Bouchard, R.J., Merrick, D.T.*, et al.* (2014). Depletion of tumor-associated macrophages slows the growth of chemically induced mouse lung adenocarcinomas. Front Immunol *5*, 587.

Fuge, O., Vasdev, N., Allchorne, P., and Green, J.S. (2015). Immunotherapy for bladder cancer. Res Rep Urol *7*, 65-79.

Fuhrmann-Stroissnigg, H., Ling, Y.Y., Zhao, J., McGowan, S.J., Zhu, Y., Brooks, R.W., Grassi, D., Gregg, S.Q., Stripay, J.L., Dorronsoro, A.*, et al.*

(2017). Identification of HSP90 inhibitors as a novel class of senolytics. Nat Commun *8*, 422.

Fukazawa, R., Ikegam, E., Watanabe, M., Hajikano, M., Kamisago, M., Katsube, Y., Yamauchi, H., Ochi, M., and Ogawa, S. (2007). Coronary artery aneurysm induced by Kawasaki disease in children show features typical senescence. Circ J *71*, 709-715.

Fumagalli, M., Rossiello, F., Clerici, M., Barozzi, S., Cittaro, D., Kaplunov, J.M., Bucci, G., Dobreva, M., Matti, V., Beausejour, C.M.*, et al.* (2012). Telomeric DNA damage is irreparable and causes persistent DNA-damage-response activation. Nat Cell Biol *14*, 355-365.

Gandhi, L., Rodriguez-Abreu, D., Gadgeel, S., Esteban, E., Felip, E., De Angelis, F., Domine, M., Clingan, P., Hochmair, M.J., Powell, S.F.*, et al.* (2018). Pembrolizumab plus Chemotherapy in Metastatic Non-Small-Cell Lung Cancer. N Engl J Med *378*, 2078-2092.

Gao, D., Li, T., Li, X.D., Chen, X., Li, Q.Z., Wight-Carter, M., and Chen, Z.J. (2015). Activation of cyclic GMP-AMP synthase by self-DNA causes autoimmune diseases. Proc Natl Acad Sci U S A *112*, E5699-5705.

Garon, E.B., Rizvi, N.A., Hui, R., Leighl, N., Balmanoukian, A.S., Eder, J.P., Patnaik, A., Aggarwal, C., Gubens, M., Horn, L.*, et al.* (2015). Pembrolizumab for the treatment of non-small-cell lung cancer. N Engl J Med *372*, 2018-2028.

Gazdar, A.F. (2014). EGFR mutations in lung cancer: different frequencies for different folks. J Thorac Oncol *9*, 139-140.

Georgakopoulou, E.A., Tsimaratou, K., Evangelou, K., Fernandez Marcos, P.J., Zoumpourlis, V., Trougakos, I.P., Kletsas, D., Bartek, J., Serrano, M., and Gorgoulis, V.G. (2013). Specific lipofuscin staining as a novel biomarker to detect replicative and stress-induced senescence. A method applicable in cryo-preserved and archival tissues. Aging (Albany NY) *5*, 37-50.

Georgilis, A., Klotz, S., Hanley, C.J., Herranz, N., Weirich, B., Morancho, B., Leote, A.C., D'Artista, L., Gallage, S., Seehawer, M.*, et al.* (2018). PTBP1-Mediated Alternative Splicing Regulates the Inflammatory Secretome and the Pro-tumorigenic Effects of Senescent Cells. Cancer Cell *34*, 85-102 e109.

Ghochikyan, A., Pichugin, A., Bagaev, A., Davtyan, A., Hovakimyan, A., Tukhvatulin, A., Davtyan, H., Shcheblyakov, D., Logunov, D., Chulkina, M.*, et al.* (2014). Targeting TLR-4 with a novel pharmaceutical grade plant derived agonist, Immunomax(R), as a therapeutic strategy for metastatic breast cancer. J Transl Med *12*, 322.

Ghosh, M., Saha, S., Bettke, J., Nagar, R., Parrales, A., Iwakuma, T., van der Velden, A.W.M., and Martinez, L.A. (2021). Mutant p53 suppresses innate immune signaling to promote tumorigenesis. Cancer Cell.

Gire, V., Roux, P., Wynford-Thomas, D., Brondello, J.M., and Dulic, V. (2004). DNA damage checkpoint kinase Chk2 triggers replicative senescence. EMBO J *23*, 2554-2563.

Gluck, S., Guey, B., Gulen, M.F., Wolter, K., Kang, T.W., Schmacke, N.A., Bridgeman, A., Rehwinkel, J., Zender, L., and Ablasser, A. (2017). Innate immune sensing of cytosolic chromatin fragments through cGAS promotes senescence. Nat Cell Biol *19*, 1061-1070.

Goldstraw, P., Chansky, K., Crowley, J., Rami-Porta, R., Asamura, H., Eberhardt, W.E., Nicholson, A.G., Groome, P., Mitchell, A., Bolejack, V.*, et al.* (2016). The IASLC Lung Cancer Staging Project: Proposals for Revision of the TNM Stage Groupings in the Forthcoming (Eighth) Edition of the TNM Classification for Lung Cancer. J Thorac Oncol *11*, 39-51.

Goncalves, S., Yin, K., Ito, Y., Chan, A., Olan, I., Gough, S., Cassidy, L., Serrao, E., Smith, S., Young, A.*, et al.* (2021). COX2 regulates senescence secretome composition and senescence surveillance through PGE2. Cell Rep *34*, 108860.

Gonzalez-Gualda, E., Baker, A.G., Fruk, L., and Munoz-Espin, D. (2021). A guide to assessing cellular senescence in vitro and in vivo. FEBS J *288*, 56-80.

Gonzalez-Meljem, J.M., Haston, S., Carreno, G., Apps, J.R., Pozzi, S., Stache, C., Kaushal, G., Virasami, A., Panousopoulos, L., Mousavy-Gharavy, S.N.*, et al.* (2017). Stem cell senescence drives age-attenuated induction of pituitary tumours in mouse models of paediatric craniopharyngioma. Nat Commun *8*, 1819.

Gonzalez-Navarro, H., Abu Nabah, Y.N., Vinue, A., Andres-Manzano, M.J., Collado, M., Serrano, M., and Andres, V. (2010). p19(ARF) deficiency reduces macrophage and vascular smooth muscle cell apoptosis and aggravates atherosclerosis. J Am Coll Cardiol *55*, 2258-2268.

Gray, E.E., Treuting, P.M., Woodward, J.J., and Stetson, D.B. (2015). Cutting Edge: cGAS Is Required for Lethal Autoimmune Disease in the Trex1-Deficient Mouse Model of Aicardi-Goutieres Syndrome. J Immunol *195*, 1939-1943.

Guerrero, A., Herranz, N., Sun, B., Wagner, V., Gallage, S., Guiho, R., Wolter, K., Pombo, J., Irvine, E.E., Innes, A.J.*, et al.* (2019). Cardiac glycosides are broad-spectrum senolytics. Nat Metab *1*, 1074-1088.

Guibert, N., Pradines, A., Favre, G., and Mazieres, J. (2020). Current and future applications of liquid biopsy in nonsmall cell lung cancer from early to advanced stages. European Respiratory Review *29*, 190052.

Guo, H., Callaway, J.B., and Ting, J.P. (2015). Inflammasomes: mechanism of action, role in disease, and therapeutics. Nat Med *21*, 677-687.

Hackshaw, A.K., Law, M.R., and Wald, N.J. (1997). The accumulated evidence on lung cancer and environmental tobacco smoke. BMJ *315*, 980-988.

Han, C., Godfrey, V., Liu, Z., Han, Y., Liu, L., Peng, H., Weichselbaum, R.R., Zaki, H., and Fu, Y.-X. (2021). The AIM2 and NLRP3 inflammasomes trigger IL-1–mediated antitumor effects during radiation. Science Immunology *6*, eabc6998.

Hanks, S., Coleman, K., Reid, S., Plaja, A., Firth, H., Fitzpatrick, D., Kidd, A., Mehes, K., Nash, R., Robin, N.*, et al.* (2004). Constitutional aneuploidy and cancer predisposition caused by biallelic mutations in BUB1B. Nat Genet *36*, 1159-1161.

Hari, P., Millar, F.R., Tarrats, N., Birch, J., Quintanilla, A., Rink, C.J., Fernandez-Duran, I., Muir, M., Finch, A.J., Brunton, V.G.*, et al.* (2019). The innate immune sensor Toll-like receptor 2 controls the senescence-associated secretory phenotype. Sci Adv *5*, eaaw0254.

Harley, C.B., Futcher, A.B., and Greider, C.W. (1990). Telomeres shorten during ageing of human fibroblasts. Nature *345*, 458-460.

Harris, S.L., and Levine, A.J. (2005). The p53 pathway: positive and negative feedback loops. Oncogene *24*, 2899-2908.

Hartman, Z.C., Poage, G.M., den Hollander, P., Tsimelzon, A., Hill, J., Panupinthu, N., Zhang, Y., Mazumdar, A., Hilsenbeck, S.G., Mills, G.B.*, et al.* (2013). Growth of triple-negative breast cancer cells relies upon coordinate autocrine expression of the proinflammatory cytokines IL-6 and IL-8. Cancer Res *73*, 3470-3480.

Hayflick, L., and Moorhead, P.S. (1961). The serial cultivation of human diploid cell strains. Exp Cell Res *25*, 585-621.

Hays, J.T., and Ebbert, J.O. (2008). Varenicline for tobacco dependence. N Engl J Med *359*, 2018-2024.

Hayward, R.L., Macpherson, J.S., Cummings, J., Monia, B.P., Smyth, J.F., and Jodrell, D.I. (2003). Antisense Bcl-xl down-regulation switches the response to topoisomerase I inhibition from senescence to apoptosis in

colorectal cancer cells, enhancing global cytotoxicity. Clin Cancer Res *9*, 2856-2865.

Hecker, L., Logsdon, N.J., Kurundkar, D., Kurundkar, A., Bernard, K., Hock, T., Meldrum, E., Sanders, Y.Y., and Thannickal, V.J. (2014). Reversal of persistent fibrosis in aging by targeting Nox4-Nrf2 redox imbalance. Sci Transl Med *6*, 231ra247.

Hemann, M.T., Strong, M.A., Hao, L.Y., and Greider, C.W. (2001). The shortest telomere, not average telomere length, is critical for cell viability and chromosome stability. Cell *107*, 67-77.

Herbig, U., Ferreira, M., Condel, L., Carey, D., and Sedivy, J.M. (2006). Cellular senescence in aging primates. Science *311*, 1257.

Herbig, U., Jobling, W.A., Chen, B.P., Chen, D.J., and Sedivy, J.M. (2004). Telomere shortening triggers senescence of human cells through a pathway involving ATM, p53, and p21(CIP1), but not p16(INK4a). Mol Cell *14*, 501-513.

Herbst, R.S., Morgensztern, D., and Boshoff, C. (2018). The biology and management of non-small cell lung cancer. Nature *553*, 446-454.

Herbst, R.S., Soria, J.C., Kowanetz, M., Fine, G.D., Hamid, O., Gordon, M.S., Sosman, J.A., McDermott, D.F., Powderly, J.D., Gettinger, S.N.*, et al.* (2014). Predictive correlates of response to the anti-PD-L1 antibody MPDL3280A in cancer patients. Nature *515*, 563-567.

Herranz, N., Gallage, S., Mellone, M., Wuestefeld, T., Klotz, S., Hanley, C.J., Raguz, S., Acosta, J.C., Innes, A.J., Banito, A.*, et al.* (2015). mTOR regulates MAPKAPK2 translation to control the senescence-associated secretory phenotype. Nat Cell Biol *17*, 1205-1217.

Herth, F.J., Eberhardt, R., Sterman, D., Silvestri, G.A., Hoffmann, H., and Shah, P.L. (2015). Bronchoscopic transparenchymal nodule access

(BTPNA): first in human trial of a novel procedure for sampling solitary pulmonary nodules. Thorax *70*, 326-332.

Hinshaw, J.L., Lubner, M.G., Ziemlewicz, T.J., Lee, F.T., Jr., and Brace, C.L. (2014). Percutaneous tumor ablation tools: microwave, radiofrequency, or cryoablation--what should you use and why? Radiographics *34*, 1344-1362.

Hiramatsu, M., Inagaki, T., Inagaki, T., Matsui, Y., Satoh, Y., Okumura, S., Ishikawa, Y., Miyaoka, E., and Nakagawa, K. (2008). Pulmonary ground-glass opacity (GGO) lesions-large size and a history of lung cancer are risk factors for growth. J Thorac Oncol *3*, 1245-1250.

Hoare, M., Ito, Y., Kang, T.W., Weekes, M.P., Matheson, N.J., Patten, D.A., Shetty, S., Parry, A.J., Menon, S., Salama, R.*, et al.* (2016). NOTCH1 mediates a switch between two distinct secretomes during senescence. Nat Cell Biol *18*, 979-992.

Honda, K., and Littman, D.R. (2016). The microbiota in adaptive immune homeostasis and disease. Nature *535*, 75-84.

Hoshino, A., Kim, H.S., Bojmar, L., Gyan, K.E., Cioffi, M., Hernandez, J., Zambirinis, C.P., Rodrigues, G., Molina, H., Heissel, S.*, et al.* (2020). Extracellular Vesicle and Particle Biomarkers Define Multiple Human Cancers. Cell.

Howard, A.D., Kostura, M.J., Thornberry, N., Ding, G.J., Limjuco, G., Weidner, J., Salley, J.P., Hogquist, K.A., Chaplin, D.D., Mumford, R.A.*, et al.* (1991). IL-1-converting enzyme requires aspartic acid residues for processing of the IL-1 beta precursor at two distinct sites and does not cleave 31-kDa IL-1 alpha. J Immunol *147*, 2964-2969.

Howington, J.A., Blum, M.G., Chang, A.C., Balekian, A.A., and Murthy, S.C. (2013). Treatment of stage I and II non-small cell lung cancer: Diagnosis and management of lung cancer, 3rd ed: American College of Chest Physicians evidence-based clinical practice guidelines. Chest *143*, e278S-e313S.

Hynds, R.E., and Janes, S.M. (2017). Airway Basal Cell Heterogeneity and Lung Squamous Cell Carcinoma. Cancer Prev Res (Phila) *10*, 491-493.

Ichim, G., Lopez, J., Ahmed, S.U., Muthalagu, N., Giampazolias, E., Delgado, M.E., Haller, M., Riley, J.S., Mason, S.M., Athineos, D.*, et al.* (2015). Limited mitochondrial permeabilization causes DNA damage and genomic instability in the absence of cell death. Mol Cell *57*, 860-872.

Ingale, S., Wolfert, M.A., Buskas, T., and Boons, G.J. (2009). Increasing the antigenicity of synthetic tumor-associated carbohydrate antigens by targeting Toll-like receptors. Chembiochem *10*, 455-463.

Ingale, S., Wolfert, M.A., Gaekwad, J., Buskas, T., and Boons, G.J. (2007). Robust immune responses elicited by a fully synthetic three-component vaccine. Nat Chem Biol *3*, 663-667.

Innes, A.J., and Gil, J. (2019). IMR90 ER:RAS: A Cell Model of Oncogene-Induced Senescence. Methods Mol Biol *1896*, 83-92.

Ishikawa, H., and Barber, G.N. (2008). STING is an endoplasmic reticulum adaptor that facilitates innate immune signalling. Nature *455*, 674-678.

Ivanov, II, Atarashi, K., Manel, N., Brodie, E.L., Shima, T., Karaoz, U., Wei, D., Goldfarb, K.C., Santee, C.A., Lynch, S.V.*, et al.* (2009). Induction of intestinal Th17 cells by segmented filamentous bacteria. Cell *139*, 485-498.

Ivanov, A., Pawlikowski, J., Manoharan, I., van Tuyn, J., Nelson, D.M., Rai, T.S., Shah, P.P., Hewitt, G., Korolchuk, V.I., Passos, J.F.*, et al.* (2013). Lysosome-mediated processing of chromatin in senescence. J Cell Biol *202*, 129-143.

Iwai, Y., Ishida, M., Tanaka, Y., Okazaki, T., Honjo, T., and Minato, N. (2002). Involvement of PD-L1 on tumor cells in the escape from host immune system and tumor immunotherapy by PD-L1 blockade. Proc Natl Acad Sci U S A *99*, 12293-12297.

Iwanaga, K., Yang, Y., Raso, M.G., Ma, L., Hanna, A.E., Thilaganathan, N., Moghaddam, S., Evans, C.M., Li, H., Cai, W.W., *et al.* (2008). Pten inactivation accelerates oncogenic K-ras-initiated tumorigenesis in a mouse model of lung cancer. Cancer Res *68*, 1119-1127.

Jackson, E.L., Willis, N., Mercer, K., Bronson, R.T., Crowley, D., Montoya, R., Jacks, T., and Tuveson, D.A. (2001). Analysis of lung tumor initiation and progression using conditional expression of oncogenic K-ras. Genes Dev *15*, 3243-3248.

Jacobs, J.J., and de Lange, T. (2004). Significant role for p16INK4a in p53-independent telomere-directed senescence. Curr Biol *14*, 2302-2308.

Jacobs, J.J., Kieboom, K., Marino, S., DePinho, R.A., and van Lohuizen, M. (1999). The oncogene and Polycomb-group gene bmi-1 regulates cell proliferation and senescence through the ink4a locus. Nature *397*, 164-168.

Jain, A.K., and Barton, M.C. (2018). p53: emerging roles in stem cells, development and beyond. Development *145*.

Jeck, W.R., Siebold, A.P., and Sharpless, N.E. (2012). Review: a meta-analysis of GWAS and age-associated diseases. Aging Cell *11*, 727-731.

Jeremy George, P., Banerjee, A.K., Read, C.A., O'Sullivan, C., Falzon, M., Pezzella, F., Nicholson, A.G., Shaw, P., Laurent, G., and Rabbitts, P.H. (2007). Surveillance for the detection of early lung cancer in patients with bronchial dysplasia. Thorax *62*, 43-50.

Jeyapalan, J.C., Ferreira, M., Sedivy, J.M., and Herbig, U. (2007). Accumulation of senescent cells in mitotic tissue of aging primates. Mech Ageing Dev *128*, 36-44.

Jezierska, A., Kolosova, I.A., and Verin, A.D. (2011). Toll Like Receptors Signaling Pathways as a Target for Therapeutic Interventions. Curr Signal Transduct Ther *6*, 428-440.

Ji, H., Li, D., Chen, L., Shimamura, T., Kobayashi, S., McNamara, K., Mahmood, U., Mitchell, A., Sun, Y., Al-Hashem, R.*, et al.* (2006). The impact of human EGFR kinase domain mutations on lung tumorigenesis and in vivo sensitivity to EGFR-targeted therapies. Cancer Cell *9*, 485-495.

Ji, H., Wang, Z., Perera, S.A., Li, D., Liang, M.C., Zaghlul, S., McNamara, K., Chen, L., Albert, M., Sun, Y.*, et al.* (2007). Mutations in BRAF and KRAS converge on activation of the mitogen-activated protein kinase pathway in lung cancer mouse models. Cancer Res *67*, 4933-4939.

Jin, C., Lagoudas, G.K., Zhao, C., Bullman, S., Bhutkar, A., Hu, B., Ameh, S., Sandel, D., Liang, X.S., Mazzilli, S.*, et al.* (2019a). Commensal Microbiota Promote Lung Cancer Development via gammadelta T Cells. Cell *176*, 998-1013 e1016.

Jin, H., Zhang, Y., Ding, Q., Wang, S.S., Rastogi, P., Dai, D.F., Lu, D., Purvis, M., Cao, C., Wang, A.*, et al.* (2019b). Epithelial innate immunity mediates tubular cell senescence after kidney injury. JCI Insight *4*.

Jin, H., Zhang, Y., Liu, D., Wang, S.S., Ding, Q., Rastogi, P., Purvis, M., Wang, A., Elhadi, S., Ren, C.*, et al.* (2020). Innate Immune Signaling Contributes to Tubular Cell Senescence in the Glis2 Knockout Mouse Model of Nephronophthisis. Am J Pathol *190*, 176-189.

Johnson, L., Mercer, K., Greenbaum, D., Bronson, R.T., Crowley, D., Tuveson, D.A., and Jacks, T. (2001). Somatic activation of the K-ras oncogene causes early onset lung cancer in mice. Nature *410*, 1111-1116.

Jouhi, L., Renkonen, S., Atula, T., Makitie, A., Haglund, C., and Hagstrom, J. (2014). Different Toll-Like Receptor Expression Patterns in Progression toward Cancer. Front Immunol *5*, 638.

Jun, J.I., and Lau, L.F. (2010a). Cellular senescence controls fibrosis in wound healing. Aging (Albany NY) *2*, 627-631.

Jun, J.I., and Lau, L.F. (2010b). The matricellular protein CCN1 induces fibroblast senescence and restricts fibrosis in cutaneous wound healing. Nat Cell Biol *12*, 676-685.

Jung, T., Bader, N., and Grune, T. (2007). Lipofuscin: formation, distribution, and metabolic consequences. Ann N Y Acad Sci *1119*, 97-111.

Kang, C., Xu, Q., Martin, T.D., Li, M.Z., Demaria, M., Aron, L., Lu, T., Yankner, B.A., Campisi, J., and Elledge, S.J. (2015). The DNA damage response induces inflammation and senescence by inhibiting autophagy of GATA4. Science *349*, aaa5612.

Kang, T.W., Yevsa, T., Woller, N., Hoenicke, L., Wuestefeld, T., Dauch, D., Hohmeyer, A., Gereke, M., Rudalska, R., Potapova, A.*, et al.* (2011). Senescence surveillance of pre-malignant hepatocytes limits liver cancer development. Nature *479*, 547-551.

Karasawa, N., Nagatsu, I., Sakai, K., Nagatsu, T., Watanabe, K., and Onozuka, M. (1997). Immunocytochemical study of catecholaminergic neurons in the senescence-accelerated mouse (SAM-P8) brain. J Neural Transm (Vienna) *104*, 1267-1275.

Karlsson, J., Vaughan, H.J., and Green, J.J. (2018). Biodegradable Polymeric Nanoparticles for Therapeutic Cancer Treatments. Annu Rev Chem Biomol Eng *9*, 105-127.

Karuppagounder, V., Arumugam, S., Babu, S.S., Palaniyandi, S.S., Watanabe, K., Cooke, J.P., and Thandavarayan, R.A. (2017). The senescence accelerated mouse prone 8 (SAMP8): A novel murine model for cardiac aging. Ageing Res Rev *35*, 291-296.

Kato, D., Miyazawa, K., Ruas, M., Starborg, M., Wada, I., Oka, T., Sakai, T., Peters, G., and Hara, E. (1998). Features of replicative senescence induced by direct addition of antennapedia-p16INK4A fusion protein to human diploid fibroblasts. FEBS Lett *427*, 203-208.

Kawai, O., Ishii, G., Kubota, K., Murata, Y., Naito, Y., Mizuno, T., Aokage, K., Saijo, N., Nishiwaki, Y., Gemma, A.*, et al.* (2008). Predominant infiltration of macrophages and CD8(+) T Cells in cancer nests is a significant predictor of survival in stage IV nonsmall cell lung cancer. Cancer *113*, 1387-1395.

Kawasaki, T., and Kawai, T. (2014). Toll-like receptor signaling pathways. Front Immunol *5*, 461.

Khanna, A.K. (2009). Enhanced susceptibility of cyclin kinase inhibitor p21 knockout mice to high fat diet induced atherosclerosis. J Biomed Sci *16*, 66.

Kim, D.W., Min, H.S., Lee, K.H., Kim, Y.J., Oh, D.Y., Jeon, Y.K., Lee, S.H., Im, S.A., Chung, D.H., Kim, Y.T.*, et al.* (2008). High tumour islet macrophage infiltration correlates with improved patient survival but not with EGFR mutations, gene copy number or protein expression in resected non-small cell lung cancer. Br J Cancer *98*, 1118-1124.

Kim, Y.H., Choi, Y.W., Lee, J., Soh, E.Y., Kim, J.H., and Park, T.J. (2017). Senescent tumor cells lead the collective invasion in thyroid cancer. Nat Commun *8*, 15208.

Kissil, J.L., Walmsley, M.J., Hanlon, L., Haigis, K.M., Bender Kim, C.F., Sweet-Cordero, A., Eckman, M.S., Tuveson, D.A., Capobianco, A.J., Tybulewicz, V.L.*, et al.* (2007). Requirement for Rac1 in a K-ras induced lung cancer in the mouse. Cancer Res *67*, 8089-8094.

Knudson, A.G., Jr. (1971). Mutation and cancer: statistical study of retinoblastoma. Proc Natl Acad Sci U S A *68*, 820-823.

Komarova, E.A., Krivokrysenko, V., Wang, K., Neznanov, N., Chernov, M.V., Komarov, P.G., Brennan, M.L., Golovkina, T.V., Rokhlin, O.W., Kuprash, D.V.*, et al.* (2005). p53 is a suppressor of inflammatory response in mice. FASEB J *19*, 1030-1032.

Krishnamurthy, J., Torrice, C., Ramsey, M.R., Kovalev, G.I., Al-Regaiey, K., Su, L., and Sharpless, N.E. (2004). Ink4a/Arf expression is a biomarker of aging. J Clin Invest *114*, 1299-1307.

Krizhanovsky, V., Yon, M., Dickins, R.A., Hearn, S., Simon, J., Miething, C., Yee, H., Zender, L., and Lowe, S.W. (2008). Senescence of activated stellate cells limits liver fibrosis. Cell *134*, 657-667.

Krtolica, A., Parrinello, S., Lockett, S., Desprez, P.Y., and Campisi, J. (2001). Senescent fibroblasts promote epithelial cell growth and tumorigenesis: a link between cancer and aging. Proc Natl Acad Sci U S A *98*, 12072-12077.

Kuilman, T., Michaloglou, C., Vredeveld, L.C., Douma, S., van Doorn, R., Desmet, C.J., Aarden, L.A., Mooi, W.J., and Peeper, D.S. (2008). Oncogene-induced senescence relayed by an interleukin-dependent inflammatory network. Cell *133*, 1019-1031.

Kurz, D.J., Decary, S., Hong, Y., and Erusalimsky, J.D. (2000). Senescence-associated (beta)-galactosidase reflects an increase in lysosomal mass during replicative ageing of human endothelial cells. J Cell Sci *113 ( Pt 20)*, 3613-3622.

Kustanovich, A., Schwartz, R., Peretz, T., and Grinshpun, A. (2019). Life and death of circulating cell-free DNA. Cancer Biol Ther *20*, 1057-1067.

Kwon, M.C., and Berns, A. (2013). Mouse models for lung cancer. Mol Oncol *7*, 165-177.

Laberge, R.M., Sun, Y., Orjalo, A.V., Patil, C.K., Freund, A., Zhou, L., Curran, S.C., Davalos, A.R., Wilson-Edell, K.A., Liu, S*., et al.* (2015). MTOR regulates the pro-tumorigenic senescence-associated secretory phenotype by promoting IL1A translation. Nat Cell Biol *17*, 1049-1061.

Lang, G.A., Iwakuma, T., Suh, Y.A., Liu, G., Rao, V.A., Parant, J.M., Valentin-Vega, Y.A., Terzian, T., Caldwell, L.C., Strong, L.C*., et al.* (2004).

Gain of function of a p53 hot spot mutation in a mouse model of Li-Fraumeni syndrome. Cell *119*, 861-872.

Lau, L., Porciuncula, A., Yu, A., Iwakura, Y., and David, G. (2019). Uncoupling the Senescence-Associated Secretory Phenotype from Cell Cycle Exit via Interleukin-1 Inactivation Unveils Its Protumorigenic Role. Mol Cell Biol *39*.

Lawrenson, K., Grun, B., Benjamin, E., Jacobs, I.J., Dafou, D., and Gayther, S.A. (2010). Senescent fibroblasts promote neoplastic transformation of partially transformed ovarian epithelial cells in a three-dimensional model of early stage ovarian cancer. Neoplasia *12*, 317-325.

Lazzerini Denchi, E., Attwooll, C., Pasini, D., and Helin, K. (2005). Deregulated E2F activity induces hyperplasia and senescence-like features in the mouse pituitary gland. Mol Cell Biol *25*, 2660-2672.

Lebrett, M.B., Balata, H., Evison, M., Colligan, D., Duerden, R., Elton, P., Greaves, M., Howells, J., Irion, K., Karunaratne, D.*, et al.* (2020). Analysis of lung cancer risk model (PLCOM2012 and LLPv2) performance in a community-based lung cancer screening programme. Thorax *75*, 661-668.

Lederle, W., Depner, S., Schnur, S., Obermueller, E., Catone, N., Just, A., Fusenig, N.E., and Mueller, M.M. (2011). IL-6 promotes malignant growth of skin SCCs by regulating a network of autocrine and paracrine cytokines. Int J Cancer *128*, 2803-2814.

Lee, A.C., Fenster, B.E., Ito, H., Takeda, K., Bae, N.S., Hirai, T., Yu, Z.X., Ferrans, V.J., Howard, B.H., and Finkel, T. (1999). Ras proteins induce senescence by altering the intracellular levels of reactive oxygen species. J Biol Chem *274*, 7936-7940.

Lee, B.Y., Han, J.A., Im, J.S., Morrone, A., Johung, K., Goodwin, E.C., Kleijer, W.J., DiMaio, D., and Hwang, E.S. (2006). Senescence-associated beta-galactosidase is lysosomal beta-galactosidase. Aging Cell *5*, 187-195.

Lee, D.H., Wolstein, J.M., Pudasaini, B., and Plotkin, M. (2012a). INK4a deletion results in improved kidney regeneration and decreased capillary rarefaction after ischemia-reperfusion injury. Am J Physiol Renal Physiol *302*, F183-191.

Lee, H.J., Lee, C.H., Jeong, Y.J., Chung, D.H., Goo, J.M., Park, C.M., and Austin, J.H. (2012b). IASLC/ATS/ERS International Multidisciplinary Classification of Lung Adenocarcinoma: novel concepts and radiologic implications. J Thorac Imaging *27*, 340-353.

Lee, J.Y., Hall, J.A., Kroehling, L., Wu, L., Najar, T., Nguyen, H.H., Lin, W.Y., Yeung, S.T., Silva, H.M., Li, D.*, et al.* (2020). Serum Amyloid A Proteins Induce Pathogenic Th17 Cells and Promote Inflammatory Disease. Cell *183*, 2036-2039.

Lee, W.H., Bookstein, R., Hong, F., Young, L.J., Shew, J.Y., and Lee, E.Y. (1987). Human retinoblastoma susceptibility gene: cloning, identification, and sequence. Science *235*, 1394-1399.

Lee, Y.-L., Cheng, W.-E., Chen, S.-C., Liao, W.-C., Shih, C.-M., and Chen, C.-Y. (2013). Dection of early lung cancer in patient with ground-glass opacity (GGO) lung lesion by HRCT in Taiwan. European Respiratory Journal *42*, 1822.

Lesina, M., Wormann, S.M., Morton, J., Diakopoulos, K.N., Korneeva, O., Wimmer, M., Einwachter, H., Sperveslage, J., Demir, I.E., Kehl, T.*, et al.* (2016). RelA regulates CXCL1/CXCR2-dependent oncogene-induced senescence in murine Kras-driven pancreatic carcinogenesis. J Clin Invest *126*, 2919-2932.

Li, G., Xue, M., Chen, W., and Yi, S. (2018). Efficacy and safety of radiofrequency ablation for lung cancers: A systematic review and meta-analysis. Eur J Radiol *100*, 92-98.

Li, T., Kon, N., Jiang, L., Tan, M., Ludwig, T., Zhao, Y., Baer, R., and Gu, W. (2012). Tumor suppression in the absence of p53-mediated cell-cycle arrest, apoptosis, and senescence. Cell *149*, 1269-1283.

Lian, J., Yue, Y., Yu, W., and Zhang, Y. (2020). Immunosenescence: a key player in cancer development. J Hematol Oncol *13*, 151.

Lin, C., Song, H., Huang, C., Yao, E., Gacayan, R., Xu, S.M., and Chuang, P.T. (2012). Alveolar type II cells possess the capability of initiating lung tumor development. PLoS One *7*, e53817.

Lin, H., Yan, J., Wang, Z., Hua, F., Yu, J., Sun, W., Li, K., Liu, H., Yang, H., Lv, Q.*, et al.* (2013). Loss of immunity-supported senescence enhances susceptibility to hepatocellular carcinogenesis and progression in Toll-like receptor 2-deficient mice. Hepatology *57*, 171-182.

Liton, P.B., Challa, P., Stinnett, S., Luna, C., Epstein, D.L., and Gonzalez, P. (2005). Cellular senescence in the glaucomatous outflow pathway. Exp Gerontol *40*, 745-748.

Liu, D., and Hornsby, P.J. (2007). Senescent human fibroblasts increase the early growth of xenograft tumors via matrix metalloproteinase secretion. Cancer Res *67*, 3117-3126.

Liu, F., Wu, S., Ren, H., and Gu, J. (2011). Klotho suppresses RIG-I-mediated senescence-associated inflammation. Nat Cell Biol *13*, 254-262.

Liu, Y., Sanoff, H.K., Cho, H., Burd, C.E., Torrice, C., Mohlke, K.L., Ibrahim, J.G., Thomas, N.E., and Sharpless, N.E. (2009). INK4/ARF transcript expression is associated with chromosome 9p21 variants linked to atherosclerosis. PLoS One *4*, e5027.

Loeser, R.F. (2009). Aging and osteoarthritis: the role of chondrocyte senescence and aging changes in the cartilage matrix. Osteoarthritis Cartilage *17*, 971-979.

Love, M.I., Huber, W., and Anders, S. (2014). Moderated estimation of fold change and dispersion for RNA-seq data with DESeq2. Genome Biol *15*, 550.

Lowe, E.L., Crother, T.R., Rabizadeh, S., Hu, B., Wang, H., Chen, S., Shimada, K., Wong, M.H., Michelsen, K.S., and Arditi, M. (2010). Toll-like receptor 2 signaling protects mice from tumor development in a mouse model of colitis-induced cancer. PLoS One *5*, e13027.

Lowe, S.W., Cepero, E., and Evan, G. (2004). Intrinsic tumour suppression. Nature *432*, 307-315.

Lozano-Torres, B., Galiana, I., Rovira, M., Garrido, E., Chaib, S., Bernardos, A., Munoz-Espin, D., Serrano, M., Martinez-Manez, R., and Sancenon, F. (2017). An OFF-ON Two-Photon Fluorescent Probe for Tracking Cell Senescence in Vivo. J Am Chem Soc *139*, 8808-8811.

Lujambio, A., Akkari, L., Simon, J., Grace, D., Tschaharganeh, D.F., Bolden, J.E., Zhao, Z., Thapar, V., Joyce, J.A., Krizhanovsky, V.*, et al.* (2013). Non-cell-autonomous tumor suppression by p53. Cell *153*, 449-460.

Luo, X., Fu, Y., Loza, A.J., Murali, B., Leahy, K.M., Ruhland, M.K., Gang, M., Su, X., Zamani, A., Shi, Y.*, et al.* (2016). Stromal-Initiated Changes in the Bone Promote Metastatic Niche Development. Cell Rep *14*, 82-92.

Ma, J., Liu, L., Che, G., Yu, N., Dai, F., and You, Z. (2010). The M1 form of tumor-associated macrophages in non-small cell lung cancer is positively associated with survival time. BMC Cancer *10*, 112.

Ma, T., Hu, Y., and Qu, D. (2019). CT-imaging and pathological analysis of preinvasive lesions and minimally invasive adenocarcinoma presented as pulmonary ground-glass opacity. European Respiratory Journal *54*, PA3029.

Maas, S.L.N., Breakefield, X.O., and Weaver, A.M. (2017). Extracellular Vesicles: Unique Intercellular Delivery Vehicles. Trends Cell Biol *27*, 172-188.

Macip, S., Igarashi, M., Fang, L., Chen, A., Pan, Z.Q., Lee, S.W., and Aaronson, S.A. (2002). Inhibition of p21-mediated ROS accumulation can rescue p21-induced senescence. EMBO J *21*, 2180-2188.

Mannarino, M., Cherif, H., Li, L., Sheng, K., Rabau, O., Jarzem, P., Weber, M.H., Ouellet, J.A., and Haglund, L. (2021). Toll-like receptor 2 induced senescence in intervertebral disc cells of patients with back pain can be attenuated by o-vanillin. Arthritis Res Ther *23*, 117.

Martens, U.M., Chavez, E.A., Poon, S.S., Schmoor, C., and Lansdorp, P.M. (2000). Accumulation of short telomeres in human fibroblasts prior to replicative senescence. Exp Cell Res *256*, 291-299.

Martinez, F.O., and Gordon, S. (2014). The M1 and M2 paradigm of macrophage activation: time for reassessment. F1000Prime Rep *6*, 13.

Martinon, F., Burns, K., and Tschopp, J. (2002). The inflammasome: a molecular platform triggering activation of inflammatory caspases and processing of proIL-beta. Mol Cell *10*, 417-426.

Mascaux, C., Angelova, M., Vasaturo, A., Beane, J., Hijazi, K., Anthoine, G., Buttard, B., Rothe, F., Willard-Gallo, K., Haller, A.*, et al.* (2019). Immune evasion before tumour invasion in early lung squamous carcinogenesis. Nature *571*, 570-575.

Masutomi, K., Yu, E.Y., Khurts, S., Ben-Porath, I., Currier, J.L., Metz, G.B., Brooks, M.W., Kaneko, S., Murakami, S., DeCaprio, J.A.*, et al.* (2003). Telomerase maintains telomere structure in normal human cells. Cell *114*, 241-253.

McCoy, M.G., Nascimento, D.W., Veleeparambil, M., Murtazina, R., Gao, D., Tkachenko, S., Podrez, E., and Byzova, T.V. (2021). Endothelial TLR2 promotes proangiogenic immune cell recruitment and tumor angiogenesis. Science Signaling *14*, eabc5371.

McFadden, D.G., Politi, K., Bhutkar, A., Chen, F.K., Song, X., Pirun, M., Santiago, P.M., Kim-Kiselak, C., Platt, J.T., Lee, E.*, et al.* (2016). Mutational landscape of EGFR-, MYC-, and Kras-driven genetically engineered mouse models of lung adenocarcinoma. Proc Natl Acad Sci U S A *113*, E6409-E6417.

McGeachy, M.J., Cua, D.J., and Gaffen, S.L. (2019). The IL-17 Family of Cytokines in Health and Disease. Immunity *50*, 892-906.

McGranahan, N., Furness, A.J., Rosenthal, R., Ramskov, S., Lyngaa, R., Saini, S.K., Jamal-Hanjani, M., Wilson, G.A., Birkbak, N.J., Hiley, C.T.*, et al.* (2016). Clonal neoantigens elicit T cell immunoreactivity and sensitivity to immune checkpoint blockade. Science *351*, 1463-1469.

McGranahan, N., Rosenthal, R., Hiley, C.T., Rowan, A.J., Watkins, T.B.K., Wilson, G.A., Birkbak, N.J., Veeriah, S., Van Loo, P., Herrero, J.*, et al.* (2017). Allele-Specific HLA Loss and Immune Escape in Lung Cancer Evolution. Cell *171*, 1259-1271 e1211.

McHugh, D., and Gil, J. (2018). Senescence and aging: Causes, consequences, and therapeutic avenues. J Cell Biol *217*, 65-77.

Mercer, J., Figg, N., Stoneman, V., Braganza, D., and Bennett, M.R. (2005). Endogenous p53 protects vascular smooth muscle cells from apoptosis and reduces atherosclerosis in ApoE knockout mice. Circ Res *96*, 667-674.

Michaloglou, C., Vredeveld, L.C., Soengas, M.S., Denoyelle, C., Kuilman, T., van der Horst, C.M., Majoor, D.M., Shay, J.W., Mooi, W.J., and Peeper, D.S. (2005). BRAFE600-associated senescence-like cell cycle arrest of human naevi. Nature *436*, 720-724.

Milanovic, M., Fan, D.N.Y., Belenki, D., Dabritz, J.H.M., Zhao, Z., Yu, Y., Dorr, J.R., Dimitrova, L., Lenze, D., Monteiro Barbosa, I.A.*, et al.* (2018). Senescence-associated reprogramming promotes cancer stemness. Nature *553*, 96-100.

Minagawa, S., Araya, J., Numata, T., Nojiri, S., Hara, H., Yumino, Y., Kawaishi, M., Odaka, M., Morikawa, T., Nishimura, S.L.*, et al.* (2011). Accelerated epithelial cell senescence in IPF and the inhibitory role of SIRT6 in TGF-beta-induced senescence of human bronchial epithelial cells. Am J Physiol Lung Cell Mol Physiol *300*, L391-401.

Minamino, T., Orimo, M., Shimizu, I., Kunieda, T., Yokoyama, M., Ito, T., Nojima, A., Nabetani, A., Oike, Y., Matsubara, H.*, et al.* (2009). A crucial role for adipose tissue p53 in the regulation of insulin resistance. Nat Med *15*, 1082-1087.

Misawa, T., Tanaka, Y., Okada, R., and Takahashi, A. (2020). Biology of extracellular vesicles secreted from senescent cells as senescence-associated secretory phenotype factors. Geriatr Gerontol Int *20*, 539-546.

Mizuno, S., Bogaard, H.J., Kraskauskas, D., Alhussaini, A., Gomez-Arroyo, J., Voelkel, N.F., and Ishizaki, T. (2011). p53 Gene deficiency promotes hypoxia-induced pulmonary hypertension and vascular remodeling in mice. Am J Physiol Lung Cell Mol Physiol *300*, L753-761.

Moiseeva, O., Mallette, F.A., Mukhopadhyay, U.K., Moores, A., and Ferbeyre, G. (2006). DNA damage signaling and p53-dependent senescence after prolonged beta-interferon stimulation. Mol Biol Cell *17*, 1583-1592.

Mok, T.S., Wu, Y.L., Thongprasert, S., Yang, C.H., Chu, D.T., Saijo, N., Sunpaweravong, P., Han, B., Margono, B., Ichinose, Y.*, et al.* (2009). Gefitinib or carboplatin-paclitaxel in pulmonary adenocarcinoma. N Engl J Med *361*, 947-957.

Molina, J.R., Yang, P., Cassivi, S.D., Schild, S.E., and Adjei, A.A. (2008). Non-small cell lung cancer: epidemiology, risk factors, treatment, and survivorship. Mayo Clin Proc *83*, 584-594.

Molofsky, A.V., Slutsky, S.G., Joseph, N.M., He, S., Pardal, R., Krishnamurthy, J., Sharpless, N.E., and Morrison, S.J. (2006). Increasing

p16INK4a expression decreases forebrain progenitors and neurogenesis during ageing. Nature *443*, 448-452.

Morales, A., Eidinger, D., and Bruce, A.W. (1976). Intracavitary Bacillus Calmette-Guerin in the treatment of superficial bladder tumors. J Urol *116*, 180-183.

Morley, J.E., Armbrecht, H.J., Farr, S.A., and Kumar, V.B. (2012). The senescence accelerated mouse (SAMP8) as a model for oxidative stress and Alzheimer's disease. Biochim Biophys Acta *1822*, 650-656.

Muller, E., Christopoulos, P.F., Halder, S., Lunde, A., Beraki, K., Speth, M., Oynebraten, I., and Corthay, A. (2017). Toll-Like Receptor Ligands and Interferon-gamma Synergize for Induction of Antitumor M1 Macrophages. Front Immunol *8*, 1383.

Müller, E., Speth, M., Christopoulos, P.F., Lunde, A., Avdagic, A., Øynebråten, I., and Corthay, A. (2018). Both Type I and Type II Interferons Can Activate Antitumor M1 Macrophages When Combined With TLR Stimulation. Front Immunol *9*, 2520.

Munoz-Espin, D., Canamero, M., Maraver, A., Gomez-Lopez, G., Contreras, J., Murillo-Cuesta, S., Rodriguez-Baeza, A., Varela-Nieto, I., Ruberte, J., Collado, M.*, et al.* (2013). Programmed cell senescence during mammalian embryonic development. Cell *155*, 1104-1118.

Munoz-Espin, D., and Serrano, M. (2014). Cellular senescence: from physiology to pathology. Nat Rev Mol Cell Biol *15*, 482-496.

Murray, N., and Turrisi, A.T., 3rd (2006). A review of first-line treatment for small-cell lung cancer. J Thorac Oncol *1*, 270-278.

Nagaraj, A.S., Lahtela, J., Hemmes, A., Pellinen, T., Blom, S., Devlin, J.R., Salmenkivi, K., Kallioniemi, O., Mayranpaa, M.I., Narhi, K.*, et al.* (2017). Cell of Origin Links Histotype Spectrum to Immune Microenvironment Diversity in

Non-small-Cell Lung Cancer Driven by Mutant Kras and Loss of Lkb1. Cell Rep *18*, 673-684.

Nahrendorf, M., and Swirski, F.K. (2016). Abandoning M1/M2 for a Network Model of Macrophage Function. Circ Res *119*, 414-417.

Narita, M., Nunez, S., Heard, E., Narita, M., Lin, A.W., Hearn, S.A., Spector, D.L., Hannon, G.J., and Lowe, S.W. (2003). Rb-mediated heterochromatin formation and silencing of E2F target genes during cellular senescence. Cell *113*, 703-716.

National Lung Screening Trial Research, T., Aberle, D.R., Adams, A.M., Berg, C.D., Black, W.C., Clapp, J.D., Fagerstrom, R.M., Gareen, I.F., Gatsonis, C., Marcus, P.M.*, et al.* (2011). Reduced lung-cancer mortality with low-dose computed tomographic screening. N Engl J Med *365*, 395-409.

Nettesheim, P., and Hammons, A.S. (1971). Induction of squamous cell carcinoma in the respiratory tract of mice. J Natl Cancer Inst *47*, 697-701.

Nicholson, A.G., Perry, L.J., Cury, P.M., Jackson, P., McCormick, C.M., Corrin, B., and Wells, A.U. (2001). Reproducibility of the WHO/IASLC grading system for pre-invasive squamous lesions of the bronchus: a study of inter-observer and intra-observer variation. Histopathology *38*, 202-208.

Noureddine, H., Gary-Bobo, G., Alifano, M., Marcos, E., Saker, M., Vienney, N., Amsellem, V., Maitre, B., Chaouat, A., Chouaid, C.*, et al.* (2011). Pulmonary artery smooth muscle cell senescence is a pathogenic mechanism for pulmonary hypertension in chronic lung disease. Circ Res *109*, 543-553.

O'Brien, W., Stenman, G., and Sager, R. (1986). Suppression of tumor growth by senescence in virally transformed human fibroblasts. Proc Natl Acad Sci U S A *83*, 8659-8663.

O'Driscoll, L. (2015). Expanding on exosomes and ectosomes in cancer. N Engl J Med *372*, 2359-2362.

Ohri, C.M., Shikotra, A., Green, R.H., Waller, D.A., and Bradding, P. (2009). Macrophages within NSCLC tumour islets are predominantly of a cytotoxic M1 phenotype associated with extended survival. Eur Respir J *33*, 118-126.

Olive, K.P., Tuveson, D.A., Ruhe, Z.C., Yin, B., Willis, N.A., Bronson, R.T., Crowley, D., and Jacks, T. (2004). Mutant p53 gain of function in two mouse models of Li-Fraumeni syndrome. Cell *119*, 847-860.

Oliveira-Nascimento, L., Massari, P., and Wetzler, L.M. (2012). The Role of TLR2 in Infection and Immunity. Front Immunol *3*, 79.

Olovnikov, A.M. (1971). [Principle of marginotomy in template synthesis of polynucleotides]. Dokl Akad Nauk SSSR *201*, 1496-1499.

Ou, H.L., Hoffmann, R., Gonzalez-Lopez, C., Doherty, G.J., Korkola, J.E., and Munoz-Espin, D. (2021). Cellular senescence in cancer: from mechanisms to detection. Mol Oncol *15*, 2634-2671.

Oudkerk, M., Liu, S., Heuvelmans, M.A., Walter, J.E., and Field, J.K. (2021). Lung cancer LDCT screening and mortality reduction - evidence, pitfalls and future perspectives. Nat Rev Clin Oncol *18*, 135-151.

Palussiere, J., Catena, V., and Buy, X. (2017). Percutaneous thermal ablation of lung tumors - Radiofrequency, microwave and cryotherapy: Where are we going? Diagn Interv Imaging *98*, 619-625.

Pao, W., Wang, T.Y., Riely, G.J., Miller, V.A., Pan, Q., Ladanyi, M., Zakowski, M.F., Heelan, R.T., Kris, M.G., and Varmus, H.E. (2005). KRAS mutations and primary resistance of lung adenocarcinomas to gefitinib or erlotinib. PLoS Med *2*, e17.

Parrinello, S., Coppe, J.P., Krtolica, A., and Campisi, J. (2005). Stromal-epithelial interactions in aging and cancer: senescent fibroblasts alter epithelial cell differentiation. J Cell Sci *118*, 485-496.

Pennycuick, A., Teixeira, V.H., AbdulJabbar, K., Raza, S.E.A., Lund, T., Akarca, A.U., Rosenthal, R., Kalinke, L., Chandrasekharan, D.P., Pipinikas, C.P.*, et al.* (2020). Immune Surveillance in Clinical Regression of Preinvasive Squamous Cell Lung Cancer. Cancer Discov *10*, 1489-1499.

Physicians, R.C.o. (2016). National Lung Cancer Audit annual report.

Pipinikas, C.P., Kiropoulos, T.S., Teixeira, V.H., Brown, J.M., Varanou, A., Falzon, M., Capitanio, A., Bottoms, S.E., Carroll, B., Navani, N.*, et al.* (2014). Cell migration leads to spatially distinct but clonally related airway cancer precursors. Thorax *69*, 548-557.

Politi, K., Zakowski, M.F., Fan, P.D., Schonfeld, E.A., Pao, W., and Varmus, H.E. (2006). Lung adenocarcinomas induced in mice by mutant EGF receptors found in human lung cancers respond to a tyrosine kinase inhibitor or to down-regulation of the receptors. Genes Dev *20*, 1496-1510.

Powell, H.A., Tata, L.J., Baldwin, D.R., Stanley, R.A., Khakwani, A., and Hubbard, R.B. (2013). Early mortality after surgical resection for lung cancer: an analysis of the English National Lung cancer audit. Thorax *68*, 826-834.

Pribluda, A., Elyada, E., Wiener, Z., Hamza, H., Goldstein, R.E., Biton, M., Burstain, I., Morgenstern, Y., Brachya, G., Billauer, H.*, et al.* (2013). A senescence-inflammatory switch from cancer-inhibitory to cancer-promoting mechanism. Cancer Cell *24*, 242-256.

Price, J.S., Waters, J.G., Darrah, C., Pennington, C., Edwards, D.R., Donell, S.T., and Clark, I.M. (2002). The role of chondrocyte senescence in osteoarthritis. Aging Cell *1*, 57-65.

Probin, V., Wang, Y., Bai, A., and Zhou, D. (2006). Busulfan selectively induces cellular senescence but not apoptosis in WI38 fibroblasts via a p53-independent but extracellular signal-regulated kinase-p38 mitogen-activated protein kinase-dependent mechanism. J Pharmacol Exp Ther *319*, 551-560.

Psarras, S., Karagianni, N., Kellendonk, C., Tronche, F., Cosset, F.L., Stocking, C., Schirrmacher, V., Boehmer Hv, H., and Khazaie, K. (2004). Gene transfer and genetic modification of embryonic stem cells by Cre- and Cre-PR-expressing MESV-based retroviral vectors. J Gene Med *6*, 32-42.

Raggi, C., and Berardi, A.C. (2012). Mesenchymal stem cells, aging and regenerative medicine. Muscles Ligaments Tendons J *2*, 239-242.

Rakoff-Nahoum, S., and Medzhitov, R. (2009). Toll-like receptors and cancer. Nat Rev Cancer *9*, 57-63.

Ramirez, R.D., Morales, C.P., Herbert, B.S., Rohde, J.M., Passons, C., Shay, J.W., and Wright, W.E. (2001). Putative telomere-independent mechanisms of replicative aging reflect inadequate growth conditions. Genes Dev *15*, 398-403.

Rebbaa, A., Zheng, X., Chou, P.M., and Mirkin, B.L. (2003). Caspase inhibition switches doxorubicin-induced apoptosis to senescence. Oncogene *22*, 2805-2811.

Reck, M., and Rabe, K.F. (2017). Precision Diagnosis and Treatment for Advanced Non-Small-Cell Lung Cancer. N Engl J Med *377*, 849-861.

Reck, M., Rodriguez-Abreu, D., Robinson, A.G., Hui, R., Csoszi, T., Fulop, A., Gottfried, M., Peled, N., Tafreshi, A., Cuffe, S.*, et al.* (2016). Pembrolizumab versus Chemotherapy for PD-L1-Positive Non-Small-Cell Lung Cancer. N Engl J Med *375*, 1823-1833.

Rehm, S., and Kelloff, G.J. (1991). Histologic characterization of mouse bronchiolar cell hyperplasia, metaplasia, and neoplasia induced intratracheally by 3-methylcholanthrene. Exp Lung Res *17*, 229-244.

Ricardi, U., Badellino, S., and Filippi, A.R. (2015). Stereotactic body radiotherapy for early stage lung cancer: History and updated role. Lung Cancer *90*, 388-396.

Riley, J.S., Quarato, G., Cloix, C., Lopez, J., O'Prey, J., Pearson, M., Chapman, J., Sesaki, H., Carlin, L.M., Passos, J.F.*, et al.* (2018). Mitochondrial inner membrane permeabilisation enables mtDNA release during apoptosis. EMBO J *37*.

Rodier, F., Coppe, J.P., Patil, C.K., Hoeijmakers, W.A., Munoz, D.P., Raza, S.R., Freund, A., Campeau, E., Davalos, A.R., and Campisi, J. (2009). Persistent DNA damage signalling triggers senescence-associated inflammatory cytokine secretion. Nat Cell Biol *11*, 973-979.

Rodier, F., Munoz, D.P., Teachenor, R., Chu, V., Le, O., Bhaumik, D., Coppe, J.P., Campeau, E., Beausejour, C.M., Kim, S.H.*, et al.* (2011). DNA-SCARS: distinct nuclear structures that sustain damage-induced senescence growth arrest and inflammatory cytokine secretion. J Cell Sci *124*, 68-81.

Rojas, A., Liu, G., Coleman, I., Nelson, P.S., Zhang, M., Dash, R., Fisher, P.B., Plymate, S.R., and Wu, J.D. (2011). IL-6 promotes prostate tumorigenesis and progression through autocrine cross-activation of IGF-IR. Oncogene *30*, 2345-2355.

Roninson, I.B. (2003). Tumor cell senescence in cancer treatment. Cancer Res *63*, 2705-2715.

Ruparel, M., Quaife, S.L., Dickson, J.L., Horst, C., Tisi, S., Hall, H., Taylor, M., Ahmed, A., Shaw, P., Burke, S.*, et al.* (2020). Lung Screen Uptake Trial: results from a single lung cancer screening round. Thorax *75*, 908-912.

Sanchez-Rivera, F.J., Papagiannakopoulos, T., Romero, R., Tammela, T., Bauer, M.R., Bhutkar, A., Joshi, N.S., Subbaraj, L., Bronson, R.T., Xue, W.*, et al.* (2014). Rapid modelling of cooperating genetic events in cancer through somatic genome editing. Nature *516*, 428-431.

Sano, T., Huang, W., Hall, J.A., Yang, Y., Chen, A., Gavzy, S.J., Lee, J.Y., Ziel, J.W., Miraldi, E.R., Domingos, A.I.*, et al.* (2015). An IL-23R/IL-22 Circuit

Regulates Epithelial Serum Amyloid A to Promote Local Effector Th17 Responses. Cell *163*, 381-393.

Sanz-Gonzalez, S.M., Barquin, L., Garcia-Cao, I., Roque, M., Gonzalez, J.M., Fuster, J.J., Castells, M.T., Flores, J.M., Serrano, M., and Andres, V. (2007). Increased p53 gene dosage reduces neointimal thickening induced by mechanical injury but has no effect on native atherosclerosis. Cardiovasc Res *75*, 803-812.

Sarkisian, C.J., Keister, B.A., Stairs, D.B., Boxer, R.B., Moody, S.E., and Chodosh, L.A. (2007). Dose-dependent oncogene-induced senescence in vivo and its evasion during mammary tumorigenesis. Nat Cell Biol *9*, 493-505.

Schafer, M.J., Zhang, X., Kumar, A., Atkinson, E.J., Zhu, Y., Jachim, S., Mazula, D.L., Brown, A.K., Berning, M., Aversa, Z.*, et al.* (2020). The senescence-associated secretome as an indicator of age and medical risk. JCI Insight *5*.

Schlereth, K., Charles, J.P., Bretz, A.C., and Stiewe, T. (2010). Life or death: p53-induced apoptosis requires DNA binding cooperativity. Cell Cycle *9*, 4068-4076.

Schmidt, L., Eskiocak, B., Kohn, R., Dang, C., Joshi, N.S., DuPage, M., Lee, D.Y., and Jacks, T. (2019). Enhanced adaptive immune responses in lung adenocarcinoma through natural killer cell stimulation. Proc Natl Acad Sci U S A *116*, 17460-17469.

Schmitt, C.A., Fridman, J.S., Yang, M., Lee, S., Baranov, E., Hoffman, R.M., and Lowe, S.W. (2002). A senescence program controlled by p53 and p16INK4a contributes to the outcome of cancer therapy. Cell *109*, 335-346.

Seidenfeld, J., Samson, D.J., Bonnell, C.J., Ziegler, K.M., and Aronson, N. (2006). Management of small cell lung cancer. Evid Rep Technol Assess (Full Rep), 1-154.

Serrano, M., Lin, A.W., McCurrach, M.E., Beach, D., and Lowe, S.W. (1997). Oncogenic ras provokes premature cell senescence associated with accumulation of p53 and p16INK4a. Cell *88*, 593-602.

Shahab, L., Goniewicz, M.L., Blount, B.C., Brown, J., McNeill, A., Alwis, K.U., Feng, J., Wang, L., and West, R. (2017). Nicotine, Carcinogen, and Toxin Exposure in Long-Term E-Cigarette and Nicotine Replacement Therapy Users: A Cross-sectional Study. Ann Intern Med *166*, 390-400.

Shivshankar, P., Brampton, C., Miyasato, S., Kasper, M., Thannickal, V.J., and Le Saux, C.J. (2012). Caveolin-1 deficiency protects from pulmonary fibrosis by modulating epithelial cell senescence in mice. Am J Respir Cell Mol Biol *47*, 28-36.

Siegel, R.L., Miller, K.D., and Jemal, A. (2020). Cancer statistics, 2020. CA Cancer J Clin *70*, 7-30.

Silva, M.J., Brodt, M.D., and Ettner, S.L. (2002). Long bones from the senescence accelerated mouse SAMP6 have increased size but reduced whole-bone strength and resistance to fracture. J Bone Miner Res *17*, 1597-1603.

Small, D.M., Bennett, N.C., Roy, S., Gabrielli, B.G., Johnson, D.W., and Gobe, G.C. (2012). Oxidative stress and cell senescence combine to cause maximal renal tubular epithelial cell dysfunction and loss in an in vitro model of kidney disease. Nephron Exp Nephrol *122*, 123-130.

Smith, D.A., Conkling, P., Richards, D.A., Nemunaitis, J.J., Boyd, T.E., Mita, A.C., de La Bourdonnaye, G., Wages, D., and Bexon, A.S. (2014). Antitumor activity and safety of combination therapy with the Toll-like receptor 9 agonist IMO-2055, erlotinib, and bevacizumab in advanced or metastatic non-small cell lung cancer patients who have progressed following chemotherapy. Cancer Immunol Immunother *63*, 787-796.

Socinski, M.A., and Bogart, J.A. (2007). Limited-stage small-cell lung cancer: the current status of combined-modality therapy. J Clin Oncol *25*, 4137-4145.

Soler, A.P., Miller, R.D., Laughlin, K.V., Carp, N.Z., Klurfeld, D.M., and Mullin, J.M. (1999). Increased tight junctional permeability is associated with the development of colon cancer. Carcinogenesis *20*, 1425-1431.

Sone, H., and Kagawa, Y. (2005). Pancreatic beta cell senescence contributes to the pathogenesis of type 2 diabetes in high-fat diet-induced diabetic mice. Diabetologia *48*, 58-67.

Song, L., Rawal, B., Nemeth, J.A., and Haura, E.B. (2011). JAK1 activates STAT3 activity in non-small-cell lung cancer cells and IL-6 neutralizing antibodies can suppress JAK1-STAT3 signaling. Mol Cancer Ther *10*, 481-494.

Song, Y.S., Lee, B.Y., and Hwang, E.S. (2005). Dinstinct ROS and biochemical profiles in cells undergoing DNA damage-induced senescence and apoptosis. Mech Ageing Dev *126*, 580-590.

Sousa-Victor, P., Gutarra, S., Garcia-Prat, L., Rodriguez-Ubreva, J., Ortet, L., Ruiz-Bonilla, V., Jardi, M., Ballestar, E., Gonzalez, S., Serrano, A.L.*, et al.* (2014). Geriatric muscle stem cells switch reversible quiescence into senescence. Nature *506*, 316-321.

Srinivasula, S.M., Poyet, J.L., Razmara, M., Datta, P., Zhang, Z., and Alnemri, E.S. (2002). The PYRIN-CARD protein ASC is an activating adaptor for caspase-1. J Biol Chem *277*, 21119-21122.

Stein, G.H., Drullinger, L.F., Soulard, A., and Dulic, V. (1999). Differential roles for cyclin-dependent kinase inhibitors p21 and p16 in the mechanisms of senescence and differentiation in human fibroblasts. Mol Cell Biol *19*, 2109-2117.

Steinfort, D.P., Bonney, A., See, K., and Irving, L.B. (2016). Sequential multimodality bronchoscopic investigation of peripheral pulmonary lesions. Eur Respir J *47*, 607-614.

Steinfort, D.P., and Herth, F.J.F. (2020). Bronchoscopic treatments for early-stage peripheral lung cancer: Are we ready for prime time? Respirology *25*, 944-952.

Stolze, B., Reinhart, S., Bulllinger, L., Frohling, S., and Scholl, C. (2015). Comparative analysis of KRAS codon 12, 13, 18, 61, and 117 mutations using human MCF10A isogenic cell lines. Sci Rep *5*, 8535.

Storer, M., Mas, A., Robert-Moreno, A., Pecoraro, M., Ortells, M.C., Di Giacomo, V., Yosef, R., Pilpel, N., Krizhanovsky, V., Sharpe, J.*, et al.* (2013). Senescence is a developmental mechanism that contributes to embryonic growth and patterning. Cell *155*, 1119-1130.

Sun, L., Wu, J., Du, F., Chen, X., and Chen, Z.J. (2013). Cyclic GMP-AMP synthase is a cytosolic DNA sensor that activates the type I interferon pathway. Science *339*, 786-791.

Sun, S., Schiller, J.H., and Gazdar, A.F. (2007). Lung cancer in never smokers--a different disease. Nat Rev Cancer *7*, 778-790.

Takacova, S., Slany, R., Bartkova, J., Stranecky, V., Dolezel, P., Luzna, P., Bartek, J., and Divoky, V. (2012). DNA damage response and inflammatory signaling limit the MLL-ENL-induced leukemogenesis in vivo. Cancer Cell *21*, 517-531.

Takahashi, A., Loo, T.M., Okada, R., Kamachi, F., Watanabe, Y., Wakita, M., Watanabe, S., Kawamoto, S., Miyata, K., Barber, G.N.*, et al.* (2018). Downregulation of cytoplasmic DNases is implicated in cytoplasmic DNA accumulation and SASP in senescent cells. Nat Commun *9*, 1249.

Takai, H., Smogorzewska, A., and de Lange, T. (2003). DNA damage foci at dysfunctional telomeres. Curr Biol *13*, 1549-1556.

Takeuchi, O., and Akira, S. (2010). Pattern recognition receptors and inflammation. Cell *140*, 805-820.

Tang, J.J., Shen, C., and Lu, Y.J. (2006). Requirement for pre-existing of p21 to prevent doxorubicin-induced apoptosis through inhibition of caspase-3 activation. Mol Cell Biochem *291*, 139-144.

Tavana, O., Benjamin, C.L., Puebla-Osorio, N., Sang, M., Ullrich, S.E., Ananthaswamy, H.N., and Zhu, C. (2010a). Absence of p53-dependent apoptosis leads to UV radiation hypersensitivity, enhanced immunosuppression and cellular senescence. Cell Cycle *9*, 3328-3336.

Tavana, O., Puebla-Osorio, N., Sang, M., and Zhu, C. (2010b). Absence of p53-dependent apoptosis combined with nonhomologous end-joining deficiency leads to a severe diabetic phenotype in mice. Diabetes *59*, 135-142.

Tchkonia, T., Morbeck, D.E., Von Zglinicki, T., Van Deursen, J., Lustgarten, J., Scrable, H., Khosla, S., Jensen, M.D., and Kirkland, J.L. (2010). Fat tissue, aging, and cellular senescence. Aging Cell *9*, 667-684.

Teixeira, V.H., Pipinikas, C.P., Pennycuick, A., Lee-Six, H., Chandrasekharan, D., Beane, J., Morris, T.J., Karpathakis, A., Feber, A., Breeze, C.E.*, et al.* (2019). Deciphering the genomic, epigenomic, and transcriptomic landscapes of pre-invasive lung cancer lesions. Nat Med *25*, 517-525.

Thakur, B.K., Zhang, H., Becker, A., Matei, I., Huang, Y., Costa-Silva, B., Zheng, Y., Hoshino, A., Brazier, H., Xiang, J.*, et al.* (2014). Double-stranded DNA in exosomes: a novel biomarker in cancer detection. Cell Res *24*, 766-769.

Tilstra, J.S., Robinson, A.R., Wang, J., Gregg, S.Q., Clauson, C.L., Reay, D.P., Nasto, L.A., St Croix, C.M., Usas, A., Vo, N.*, et al.* (2012). NF-kappaB

inhibition delays DNA damage-induced senescence and aging in mice. J Clin Invest *122*, 2601-2612.

Timofeev, O., Schlereth, K., Wanzel, M., Braun, A., Nieswandt, B., Pagenstecher, A., Rosenwald, A., Elsasser, H.P., and Stiewe, T. (2013). p53 DNA binding cooperativity is essential for apoptosis and tumor suppression in vivo. Cell Rep *3*, 1512-1525.

Toomey, D., Smyth, G., Condron, C., Kelly, J., Byrne, A.M., Kay, E., Conroy, R.M., Broe, P., and Bouchier-Hayes, D. (2003). Infiltrating immune cells, but not tumour cells, express FasL in non-small cell lung cancer: No association with prognosis identified in 3-year follow-up. Int J Cancer *103*, 408-412.

Topalian, S.L., Hodi, F.S., Brahmer, J.R., Gettinger, S.N., Smith, D.C., McDermott, D.F., Powderly, J.D., Carvajal, R.D., Sosman, J.A., Atkins, M.B.*, et al.* (2012). Safety, activity, and immune correlates of anti-PD-1 antibody in cancer. N Engl J Med *366*, 2443-2454.

Triana-Martinez, F., Picallos-Rabina, P., Da Silva-Alvarez, S., Pietrocola, F., Llanos, S., Rodilla, V., Soprano, E., Pedrosa, P., Ferreiros, A., Barradas, M.*, et al.* (2019). Identification and characterization of Cardiac Glycosides as senolytic compounds. Nat Commun *10*, 4731.

Tsuji, T., Aoshiba, K., and Nagai, A. (2004). Cigarette smoke induces senescence in alveolar epithelial cells. Am J Respir Cell Mol Biol *31*, 643-649.

Tsuji, T., Aoshiba, K., and Nagai, A. (2010). Alveolar cell senescence exacerbates pulmonary inflammation in patients with chronic obstructive pulmonary disease. Respiration *80*, 59-70.

Turke, A.B., Zejnullahu, K., Wu, Y.L., Song, Y., Dias-Santagata, D., Lifshits, E., Toschi, L., Rogers, A., Mok, T., Sequist, L.*, et al.* (2010). Preexistence and clonal selection of MET amplification in EGFR mutant NSCLC. Cancer Cell *17*, 77-88.

Turrisi, A.T., 3rd, Kim, K., Blum, R., Sause, W.T., Livingston, R.B., Komaki, R., Wagner, H., Aisner, S., and Johnson, D.H. (1999). Twice-daily compared with once-daily thoracic radiotherapy in limited small-cell lung cancer treated concurrently with cisplatin and etoposide. N Engl J Med *340*, 265-271.

Unterholzner, L., Keating, S.E., Baran, M., Horan, K.A., Jensen, S.B., Sharma, S., Sirois, C.M., Jin, T., Latz, E., Xiao, T.S.*, et al.* (2010). IFI16 is an innate immune sensor for intracellular DNA. Nat Immunol *11*, 997-1004.

Urban-Wojciuk, Z., Khan, M.M., Oyler, B.L., Fahraeus, R., Marek-Trzonkowska, N., Nita-Lazar, A., Hupp, T.R., and Goodlett, D.R. (2019). The Role of TLRs in Anti-cancer Immunity and Tumor Rejection. Front Immunol *10*, 2388.

Varela, I., Cadinanos, J., Pendas, A.M., Gutierrez-Fernandez, A., Folgueras, A.R., Sanchez, L.M., Zhou, Z., Rodriguez, F.J., Stewart, C.L., Vega, J.A.*, et al.* (2005). Accelerated ageing in mice deficient in Zmpste24 protease is linked to p53 signalling activation. Nature *437*, 564-568.

Varley, J.M., Thorncroft, M., McGown, G., Appleby, J., Kelsey, A.M., Tricker, K.J., Evans, D.G., and Birch, J.M. (1997). A detailed study of loss of heterozygosity on chromosome 17 in tumours from Li-Fraumeni patients carrying a mutation to the TP53 gene. Oncogene *14*, 865-871.

Velarde, M.C., Demaria, M., and Campisi, J. (2013). Senescent cells and their secretory phenotype as targets for cancer therapy. Interdiscip Top Gerontol *38*, 17-27.

Velez, D.R., Wejse, C., Stryjewski, M.E., Abbate, E., Hulme, W.F., Myers, J.L., Estevan, R., Patillo, S.G., Olesen, R., Tacconelli, A.*, et al.* (2010). Variants in toll-like receptors 2 and 9 influence susceptibility to pulmonary tuberculosis in Caucasians, African-Americans, and West Africans. Hum Genet *127*, 65-73.

Venkatachalam, S., Shi, Y.P., Jones, S.N., Vogel, H., Bradley, A., Pinkel, D., and Donehower, L.A. (1998). Retention of wild-type p53 in tumors from p53 heterozygous mice: reduction of p53 dosage can promote cancer formation. EMBO J *17*, 4657-4667.

Vijayachandra, K., Lee, J., and Glick, A.B. (2003). Smad3 regulates senescence and malignant conversion in a mouse multistage skin carcinogenesis model. Cancer Res *63*, 3447-3452.

Vineis, P., Airoldi, L., Veglia, F., Olgiati, L., Pastorelli, R., Autrup, H., Dunning, A., Garte, S., Gormally, E., Hainaut, P*., et al.* (2005). Environmental tobacco smoke and risk of respiratory cancer and chronic obstructive pulmonary disease in former smokers and never smokers in the EPIC prospective study. BMJ *330*, 277.

Visel, A., Zhu, Y., May, D., Afzal, V., Gong, E., Attanasio, C., Blow, M.J., Cohen, J.C., Rubin, E.M., and Pennacchio, L.A. (2010). Targeted deletion of the 9p21 non-coding coronary artery disease risk interval in mice. Nature *464*, 409-412.

Vogelstein, B., and Kinzler, K.W. (1993). The multistep nature of cancer. Trends Genet *9*, 138-141.

Vousden, K.H., and Lane, D.P. (2007). p53 in health and disease. Nat Rev Mol Cell Biol *8*, 275-283.

Wang, B., Hendricks, D.T., Wamunyokoli, F., and Parker, M.I. (2006). A growth-related oncogene/CXC chemokine receptor 2 autocrine loop contributes to cellular proliferation in esophageal cancer. Cancer Res *66*, 3071-3077.

Wang, C., Zhou, Q., Wang, X., Wu, X., Chen, X., Li, J., Zhu, Z., Liu, B., and Su, L. (2015). The TLR7 agonist induces tumor regression both by promoting CD4(+)T cells proliferation and by reversing T regulatory cell-mediated suppression via dendritic cells. Oncotarget *6*, 1779-1789.

Wang, D., Precopio, M., Lan, T., Yu, D., Tang, J.X., Kandimalla, E.R., and Agrawal, S. (2010). Antitumor activity and immune response induction of a dual agonist of Toll-like receptors 7 and 8. Mol Cancer Ther *9*, 1788-1797.

Wang, J.C., and Bennett, M. (2012). Aging and atherosclerosis: mechanisms, functional consequences, and potential therapeutics for cellular senescence. Circ Res *111*, 245-259.

Wang, Y., Liu, J., Ma, X., Cui, C., Deenik, P.R., Henderson, P.K.P., Sigler, A.L., and Cui, L. (2019). Real-time imaging of senescence in tumors with DNA damage. Sci Rep *9*, 2102.

Wang, Y., Zhang, Z., Yan, Y., Lemon, W.J., LaRegina, M., Morrison, C., Lubet, R., and You, M. (2004). A chemically induced model for squamous cell carcinoma of the lung in mice: histopathology and strain susceptibility. Cancer Res *64*, 1647-1654.

Wang, Z., Moro, E., Kovacs, K., Yu, R., and Melmed, S. (2003). Pituitary tumor transforming gene-null male mice exhibit impaired pancreatic beta cell proliferation and diabetes. Proc Natl Acad Sci U S A *100*, 3428-3432.

Webley, K., Bond, J.A., Jones, C.J., Blaydes, J.P., Craig, A., Hupp, T., and Wynford-Thomas, D. (2000). Posttranslational modifications of p53 in replicative senescence overlapping but distinct from those induced by DNA damage. Mol Cell Biol *20*, 2803-2808.

Weihrauch, M.R., Richly, H., von Bergwelt-Baildon, M.S., Becker, H.J., Schmidt, M., Hacker, U.T., Shimabukuro-Vornhagen, A., Holtick, U., Nokay, B., Schroff, M.*, et al.* (2015). Phase I clinical study of the toll-like receptor 9 agonist MGN1703 in patients with metastatic solid tumours. Eur J Cancer *51*, 146-156.

Wells, C., and Mannino, D.M. (1996). Pulmonary fibrosis and lung cancer in the United States: analysis of the multiple cause of death mortality data, 1979 through 1991. South Med J *89*, 505-510.

Welsh, T.J., Green, R.H., Richardson, D., Waller, D.A., O'Byrne, K.J., and Bradding, P. (2005). Macrophage and mast-cell invasion of tumor cell islets confers a marked survival advantage in non-small-cell lung cancer. J Clin Oncol *23*, 8959-8967.

Wennerberg, K., Rossman, K.L., and Der, C.J. (2005). The Ras superfamily at a glance. J Cell Sci *118*, 843-846.

West, A.P., Khoury-Hanold, W., Staron, M., Tal, M.C., Pineda, C.M., Lang, S.M., Bestwick, M., Duguay, B.A., Raimundo, N., MacDuff, D.A.*, et al.* (2015). Mitochondrial DNA stress primes the antiviral innate immune response. Nature *520*, 553-557.

Wieland, E., Rodriguez-Vita, J., Liebler, S.S., Mogler, C., Moll, I., Herberich, S.E., Espinet, E., Herpel, E., Menuchin, A., Chang-Claude, J.*, et al.* (2017). Endothelial Notch1 Activity Facilitates Metastasis. Cancer Cell *31*, 355-367.

Wiemann, S.U., Satyanarayana, A., Tsahuridu, M., Tillmann, H.L., Zender, L., Klempnauer, J., Flemming, P., Franco, S., Blasco, M.A., Manns, M.P.*, et al.* (2002). Hepatocyte telomere shortening and senescence are general markers of human liver cirrhosis. FASEB J *16*, 935-942.

Wiggins, K.A., Parry, A.J., Cassidy, L.D., Humphry, M., Webster, S.J., Goodall, J.C., Narita, M., and Clarke, M.C.H. (2019). IL-1alpha cleavage by inflammatory caspases of the noncanonical inflammasome controls the senescence-associated secretory phenotype. Aging Cell *18*, e12946.

Wolstein, J.M., Lee, D.H., Michaud, J., Buot, V., Stefanchik, B., and Plotkin, M.D. (2010). INK4a knockout mice exhibit increased fibrosis under normal conditions and in response to unilateral ureteral obstruction. Am J Physiol Renal Physiol *299*, F1486-1495.

Woo, R.A., and Poon, R.Y. (2004). Activated oncogenes promote and cooperate with chromosomal instability for neoplastic transformation. Genes Dev *18*, 1317-1330.

Wu, G.X., Goldstein, L., Kim, J.Y., and Raz, D.J. (2016). Proportion of Non-Small-Cell Lung Cancer Patients that Would Have Been Eligible for Lung Cancer Screening. Clin Lung Cancer *17*, e131-e139.

Xiao, Z., Jiang, Q., Willette-Brown, J., Xi, S., Zhu, F., Burkett, S., Back, T., Song, N.Y., Datla, M., Sun, Z.*, et al.* (2013). The pivotal role of IKKalpha in the development of spontaneous lung squamous cell carcinomas. Cancer Cell *23*, 527-540.

Xu, Y., Yang, E.M., Brugarolas, J., Jacks, T., and Baltimore, D. (1998). Involvement of p53 and p21 in cellular defects and tumorigenesis in Atm-/- mice. Mol Cell Biol *18*, 4385-4390.

Xue, W., Zender, L., Miething, C., Dickins, R.A., Hernando, E., Krizhanovsky, V., Cordon-Cardo, C., and Lowe, S.W. (2007). Senescence and tumour clearance is triggered by p53 restoration in murine liver carcinomas. Nature *445*, 656-660.

Yanagi, S., Kishimoto, H., Kawahara, K., Sasaki, T., Sasaki, M., Nishio, M., Yajima, N., Hamada, K., Horie, Y., Kubo, H.*, et al.* (2007). Pten controls lung morphogenesis, bronchioalveolar stem cells, and onset of lung adenocarcinomas in mice. J Clin Invest *117*, 2929-2940.

Yang, F., Tuxhorn, J.A., Ressler, S.J., McAlhany, S.J., Dang, T.D., and Rowley, D.R. (2005). Stromal expression of connective tissue growth factor promotes angiogenesis and prostate cancer tumorigenesis. Cancer Res *65*, 8887-8895.

Yang, L.S., Wu, W.S., Zhang, F., Jiang, Y., Fan, Y., Fang, H.X., and Long, J. (2014). Role of toll-like receptors in lung cancer. J Recept Signal Transduct Res *34*, 342-344.

Yang, X., Chang, H.Y., and Baltimore, D. (1998). Autoproteolytic activation of pro-caspases by oligomerization. Mol Cell *1*, 319-325.

Yosef, R., Pilpel, N., Tokarsky-Amiel, R., Biran, A., Ovadya, Y., Cohen, S., Vadai, E., Dassa, L., Shahar, E., Condiotti, R.*, et al.* (2016). Directed elimination of senescent cells by inhibition of BCL-W and BCL-XL. Nat Commun *7*, 11190.

Young, A.P., Schlisio, S., Minamishima, Y.A., Zhang, Q., Li, L., Grisanzio, C., Signoretti, S., and Kaelin, W.G., Jr. (2008). VHL loss actuates a HIF-independent senescence programme mediated by Rb and p400. Nat Cell Biol *10*, 361-369.

Zhang, C., Zhang, J., Xu, F.P., Wang, Y.G., Xie, Z., Su, J., Dong, S., Nie, Q., Shao, Y., Zhou, Q.*, et al.* (2019). Genomic Landscape and Immune Microenvironment Features of Preinvasive and Early Invasive Lung Adenocarcinoma. J Thorac Oncol *14*, 1912-1923.

Zhang, H., and Cohen, S.N. (2004). Smurf2 up-regulation activates telomere-dependent senescence. Genes Dev *18*, 3028-3040.

Zhang, J., Fujimoto, J., Zhang, J., Wedge, D.C., Song, X., Zhang, J., Seth, S., Chow, C.W., Cao, Y., Gumbs, C.*, et al.* (2014). Intratumor heterogeneity in localized lung adenocarcinomas delineated by multiregion sequencing. Science *346*, 256-259.

Zhang, X., Li, J., Sejas, D.P., and Pang, Q. (2005). The ATM/p53/p21 pathway influences cell fate decision between apoptosis and senescence in reoxygenated hematopoietic progenitor cells. J Biol Chem *280*, 19635-19640.

Zhang, Y., Gao, Y., Zhang, G., Huang, S., Dong, Z., Kong, C., Su, D., Du, J., Zhu, S., Liang, Q.*, et al.* (2011a). DNMT3a plays a role in switches between doxorubicin-induced senescence and apoptosis of colorectal cancer cells. Int J Cancer *128*, 551-561.

Zhang, Y., Luo, F., Cai, Y., Liu, N., Wang, L., Xu, D., and Chu, Y. (2011b). TLR1/TLR2 agonist induces tumor regression by reciprocal modulation of effector and regulatory T cells. J Immunol *186*, 1963-1969.

Zhang, Y., Xiong, Y., and Yarbrough, W.G. (1998). ARF promotes MDM2 degradation and stabilizes p53: ARF-INK4a locus deletion impairs both the Rb and p53 tumor suppression pathways. Cell *92*, 725-734.

Zhao, B., Liu, P., Fukumoto, T., Nacarelli, T., Fatkhutdinov, N., Wu, S., Lin, J., Aird, K.M., Tang, H.Y., Liu, Q.*, et al.* (2020). Topoisomerase 1 cleavage complex enables pattern recognition and inflammation during senescence. Nat Commun *11*, 908.

Zhao, Z.R., Lau, R.W.H., and Ng, C.S.H. (2018). Catheter-based alternative treatment for early-stage lung cancer with a high-risk for morbidity. J Thorac Dis *10*, S1864-S1870.

Zhu, D., Wu, J., Spee, C., Ryan, S.J., and Hinton, D.R. (2009). BMP4 mediates oxidative stress-induced retinal pigment epithelial cell senescence and is overexpressed in age-related macular degeneration. J Biol Chem *284*, 9529-9539.

Zhu, F., Li, Y., Zhang, J., Piao, C., Liu, T., Li, H.H., and Du, J. (2013). Senescent cardiac fibroblast is critical for cardiac fibrosis after myocardial infarction. PLoS One *8*, e74535.

Zhu, J., Woods, D., McMahon, M., and Bishop, J.M. (1998). Senescence of human fibroblasts induced by oncogenic Raf. Genes Dev *12*, 2997-3007.

Zhu, Y., Tchkonia, T., Fuhrmann-Stroissnigg, H., Dai, H.M., Ling, Y.Y., Stout, M.B., Pirtskhalava, T., Giorgadze, N., Johnson, K.O., Giles, C.B.*, et al.* (2016). Identification of a novel senolytic agent, navitoclax, targeting the Bcl-2 family of anti-apoptotic factors. Aging Cell *15*, 428-435.

Zhu, Y., Tchkonia, T., Pirtskhalava, T., Gower, A.C., Ding, H., Giorgadze, N., Palmer, A.K., Ikeno, Y., Hubbard, G.B., Lenburg, M.*, et al.* (2015). The

Achilles' heel of senescent cells: from transcriptome to senolytic drugs. Aging Cell *14*, 644-658.